Study of the parameters for optimisation of the design and performance of Bio-electrochemical systems for energy/hydrogen generation and resource recovery

By

Abdullah Almatouq

B.Sc., M.Sc.

Thesis submitted in partial fulfilment of the requirement for the degree of Doctor of Philosophy (PhD)

School of Engineering - Cardiff University

UK

2017

DECLARATION AND STATEMENTS

DECLARATION

This work has not previously been accepted in substance for any degree and is not

concurrently submitted in candidature for any degree.

Signed …………………….….. (**Student name**) Date……………….

STATEMENT 1

This thesis is being submitted in partial fulfilment of the requirements for the degree of

Doctor of Philosophy (PhD).

Signed ………………………. (**Student name**) Date……….……….

STATEMENT 2

This thesis is the result of my own independent work/investigation, except where otherwise

stated. Other sources are acknowledged by explicit references.

Signed ……………………… (**Student name**) Date……….……….

STATEMENT 3

I hereby give consent for my thesis, if accepted, to be available for photocopying and inter-

library loan, and for the title and summary to be made available to outside organisations.

Signed …………………….…. (**Student name**) Date……….……….

ABSTRACT

This study focused on the exploration, assessment and experimental investigation of bio-electrochemical systems (BES) for concurrent phosphorus (P) recovery and energy generation/hydrogen (H_2) production. The main aim was to study and understand the parameters for optimisation of the design and the performance of BESs for concurrent phosphorus recovery and energy generation/hydrogen production. In total, four dual chamber bio-electrochemical systems (Microbial Fuel Cells (MFCs) and Microbial Electrolysis Cells (MECs)) were used to investigate the impacts of key design and operational conditions on BES performance.

P was precipitated successfully as struvite in both MFCs and MECs. The MFCs and MECs achieved a maximum P precipitation efficiency of 90% and 95% with a maximum columbic efficiency of 10% and 51% respectively. The MFCs and MECs achieved an average of 80 % and 70 % COD removal efficiency respectively, which confirms the ability of these systems to be used in wastewater treatment. Deterioration in both reactors occurred due to P precipitation on the cathode surface and the membrane. The three operational parameters (influent COD, cathode aeration flow rate, and external resistance) were found to have significant impacts on MFC performance and P recovery. In addition, applied voltage and influent COD had significant effects on MEC performance and P recovery. Results were supported through statistical analysis and optimisation modelling using full factorial design, central composite design, and response surface methodology. Generally, results have shown that MFCs and MECs have the potential to concurrently recover P, treat wastewater, and generate electricity/produce H_2. Further research is needed to enhance the performance of MFCs for energy generation and MECs for H_2 production in addition to P recovery and minimising scaling on electrodes. The results of this study increase the understanding of P recovery mechanisms in MFCs and MECs and can contribute to future BES research. Moreover, the results will help in selecting the optimum operational parameters of BESs depending on the applications and process requirements. Applying BESs in wastewater treatment plants will reduce energy consumption and, at the same time, find an alternative source of P.

DEDICATION

Dedicated to my lovely family
For their unconditional love and support

ACKNOWLEDGEMENTS

LIST OF PUBLICATIONS, CONFERENCES AND AWARDS

- **Publications**

1. Almatouq, A. and Babatunde A.O. (2016). Concurrent Phosphorus Recovery and Energy Generation in Mediator-Less Dual Chamber Microbial Fuel Cells: Mechanisms and Influencing Factors. International Journal of Environmental Research and Public Health, 13(4), 375.

2. Almatouq, A. and Babatunde A.O. (2017). Concurrent Hydrogen Production and Phosphorus Recovery in Dual Chamber Microbial Electrolysis Cell. Bioresource Technology (2017).
   http://dx.doi.org/10.1016/j.biortech.2017.02.043

- **Publications in Preparation**

1. Almatouq, A. and Babatunde A.O. (2017). Energy generation and P recovery in a mediator-less dual chamber microbial fuel cell: An optimization study. Intended journal: Water Research journal

2. Almatouq, A. and Babatunde A.O. (2017). Bacterial community structure, compartmentalization and activity in bio-electrochemical system (microbial fuel cell and microbial electrolysis cell). Intended journal: Journal of Applied Microbiology

- **Conferences**

1. Almatouq, A. and Babatunde A.O. (2016). Mechanisms and influencing factors for Phosphorus recovery as struvite in dual chamber microbial electrolysis cell. Presented at the 1st International Conference on Sustainable Water Processing; 11-14 September 2016, Sitges, Barcelona, Spain.

2. Almatouq, A. and Babatunde A.O. (2016). Optimisation of phosphorus recovery in mediator-less dual chamber microbial fuel cells. Presented at the 1st International Conference on Sustainable Water Processing; 11-14 September 2016, Sitges, Barcelona, Spain.

3. Almatouq, A. and Babatunde A.O. (2016). Concurrent Phosphorus Recovery And Energy Generation In Mediator-less Dual Chamber MFC: Mechanisms

& Influencing Factors. Accepted at the WA World Water Congress & Exhibition 2016; 9-13 October 2016, Brisbane, Queensland, Australia.

4. Almatouq, A. and Babatunde A.O. (2016). Hydrogen production and phosphorus recovery in microbial electrolysis cell: the influence of COD concentration and applied voltage. Presented at the 1st International Conference on Bioresource Technology for Bioenergy, Bioproducts & Environmental Sustainability; 23-26 October 2016, Sitges, Barcelona, Spain.

5. Almatouq, A. and Babatunde A.O. (2016). Hydrogen production and phosphorus recovery optimisation in bio-electrochemical system. Presented at the International Conference on Gas, Oil and Petroleum Engineering; 14-16 November 2016, Las Vegas, USA.

- **Awards**

1st place (out of 66 researchers) in poster presentation award at the International Conference for Sustainable Water Processing held in Spain from 11-14 Sept 2016.

Table of Contents

List of Figures

List of Tables

LIST OF ABBREVIATIONS

PG	Population growth
BES	Bio-electrochemical system
PBS	phosphate buffer solution
MFC	Microbial fuel cell
MEC	Microbial electrolysis cell
H_2	Hydrogen
COD	Chemical oxygen demand
N	Nitrogen
TN	Total nitrogen
NH_3	Ammonia
NH_4	Ammonium
TP	Total phosphorus
PO_3	Ortho-phosphate
EU ETS	EU Emissions Trading System
OCV	Open circuit voltage
REDOX	Reduction-oxidation
ORP	Oxidation-reduction potential
DO	Dissolved oxygen
SEM	Scanning electron microscopy
XRD	X-ray diffraction
RSM	Response surface methodology
FFD	Full factorial design
CCD	Central composite design
AEM	Anion exchange membrane
CEM	Cation exchange membrane
PEM	Proton exchange membrane
BOD	Biological oxygen demand
CE	Coulombic efficiency
Ean	Anodic potential
E°an	Standard Electrode Potential
E°cat	Standard Electrode Potential for Hydrogen

Ecat	Cathodic Potential
emf	Electromotive Force
EU	European Union
F	Faraday constant
R	Universal gas constant
Vapp	Applied Voltage
T	Temperature
UWWTD	Urban Waste Water Treatment Directive
OFAT	One-factor-at-a-time
ANOVA	Analysis of variance
R^2	Coefficient of determination
Pt	Platinum
NMDS	Non metric multidimensional scaling
NH_4Cl	Ammonium chloride
MgCl	Magnesium chloride
CO_2	Carbon dioxide
N	Nitrogen
NO^{3-}	Nitrate
NO^{2-}	Nitrite
OTUs	Operational taxonomic units
PCR	Polymerase chain reactions
PCoA	Principal coordinates analysis
UK	United Kingdom
USA	United State of America

Chapter 1

Introduction

1.1 Background

1.1.1. Population Growth and Global Energy Demand

Due to the rapid and uncontrolled growth of the global population, the demand for food, water, and energy has reached a critical point (Figure 1.1). Currently, more than 7 billion people live on the earth, and this number is estimated to reach 9.6 billion by 2050 (Miles, 2009). The massive population growth is causing significant damage to humanity and the environment. The world total primary energy supply increased from 6,101 Mtoe (million tonnes of oil equivalent) in 1973 to 13,699 Mtoe in 2014 (IEA, 2016). Fossil fuels, such as oil, coal, and natural gas, are an unsustainable natural resource, yet more than 80% of the supplied energy comes from fossil fuels (IEA, 2016). Besides the risk of fossil fuel depletion in the future, fossil fuel consumption also has a negative impact on the environment. Fossil fuel consumption as a source of energy has grown from insignificant levels in 1800 to nearly 10,000 Mtoe in 2012 (Höök et al., 2012); this has increased the emission of greenhouse gases, which negatively affect the environment (air, water and aquatic organisms).
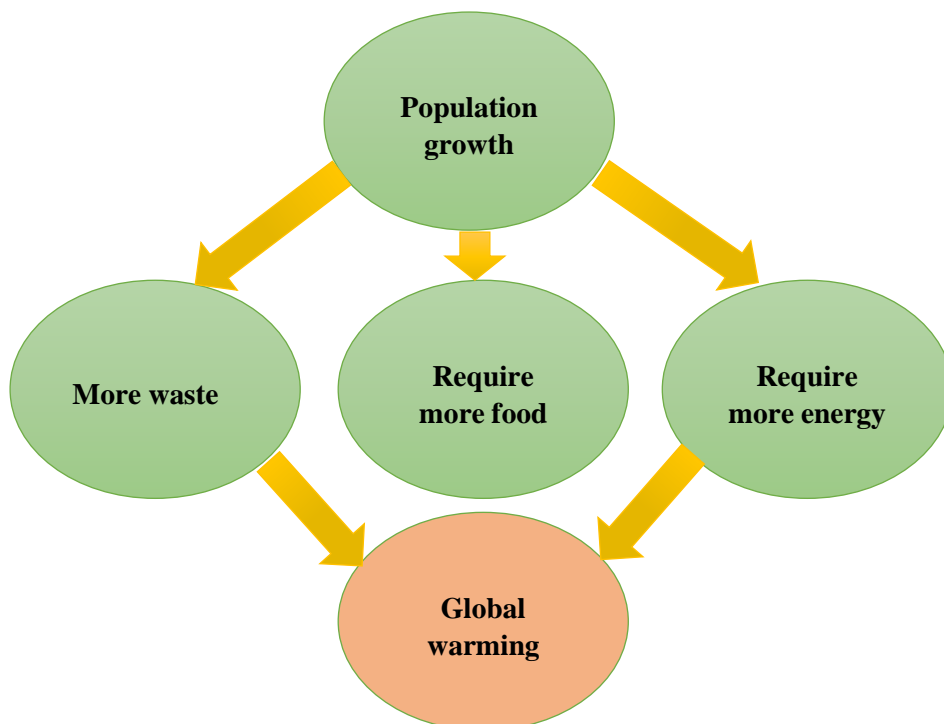
Figure 1.1 The impacts of population growth

1.1.2 Energy from wastewater

The generation of wastewater is increasing due to the continuous population growth, requiring more energy and new treatment plants. Conventional wastewater treatment processes are expensive and consume huge amounts of energy especially with the restrictive regulations prior to discharge. It has been estimated that European countries consume 1% of the total electricity consumption on wastewater treatment plants (Longo et al., 2016), where most of the energy is used for aeration and recirculation. Increasing the usage of energy from the conventional energy source has increased the concerns regarding energy source depletion and climate change effect.

Wastewater contains 3 to 10 times more energy than the energy required for treating the wastewater, so if each g of chemical oxygen demand (COD) contains 14.7 kJ, the total energy that could be made available around the world for 6.8 billion people is $2.2 - 4.4 \times 10^{18}$ J/year. This amount of energy is equivalent to burning 52-104 million tons of oil in a power station (Gude, 2016).

1.1.3 Phosphorus in wastewater

In terms of food security, population growth is linked to food demand, as increases in the world population have led to an increased demand for food. Phosphate rocks are the main source of phosphorus (P), which is an essential substance (fertiliser) for the agricultural production of food (Neset et al., 2008). However, phosphate rocks are a non-renewable and limited resource, and it is estimated that sources will be depleted in less than 100 years due to the need to meet the food demand of the world population (Cooper et al., 2011). Therefore, alternative sources of P need to be found. Wastewater is considered a rich source of nutrients (nitrogen and phosphorus) since the Urban Waste Water Treatment Directive (UWWTD) decreased the concentration of P in the effluent in order to reduce the eutrophication of water bodies (Doyle and Parsons, 2002). Approximately 16% of the total mined phosphorus is digested by humans and discharged into waste streams (Fig. 1.2) (Mulchandani and Westerhoff, 2016). The phosphorus concentration in wastewater varies between 4 and 16 mg/L. P can be removed via chemical precipitation or biological phosphorus removal. In both approaches, P is removed from the wastewater and retained in the sludge. The phosphorus in the sludge can be released

via the anaerobic digester process and P concentration at anaerobic digester stream ranged between 10 to 1000 mg/L (Pastor et al., 2008; Blöcher et al., 2012). Streams with a high concentration of P are optimal for P recovery.
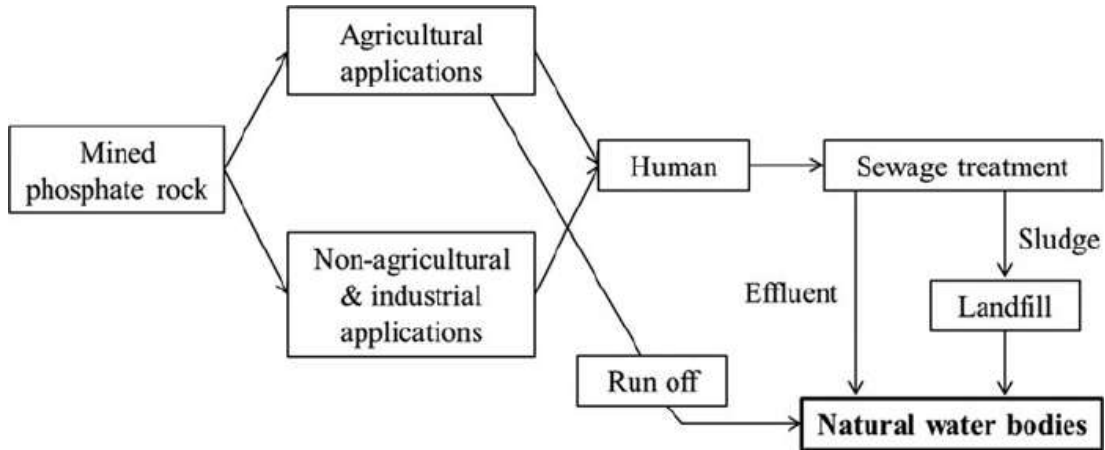
Figure 1.2 Phosphorus cycle in modern society (adapted from Desmidt et al. (2015))

Thus, instead of consuming more energy from fossil fuels and depleting more sources of phosphate rocks, efforts for finding and developing new alternatives as energy and nutrient sustainable sources should be increased. Utilising renewable energy sources, such as wind, solar, and biomass, is crucial in energy structure and future projects. Renewable energy involves using sustainable resources and is totally different from fossil fuels, the use of which is unsustainable and which may be exhausted in the near future. Minimising the usage of fossil fuels and maximising the usage of renewable energy will reduce the cost and environmental impact.

1.2 Bio-electrochemical system for energy generation and phosphorus recovery

Due to several concerns about population growth and the impacts on the environment, there is a need to find and develop new technologies to treat generated wastewater, reduce energy usage for wastewater treatment, and at the same time, have the potential to recover nutrients. Bio-electrochemical systems (BES) represent an emerging clean technology that can concurrently generate electricity (Microbial Fuel Cell-MFC) or produce hydrogen (Microbial Electrolysis Cell-MEC) and can treat wastewater by oxidising organic matter and converting the chemical energy into electricity or hydrogen.

Treating wastewater through a BES has many advantages:

- It can generate electricity or produce hydrogen, which can be used as a source of energy.
- It can reduce the treatment cost.
- It can reduce the generated sludge.
- It provides a sustainable source of nutrients and minimises the P losses to water bodies.

P is commonly recovered as magnesium ammonium phosphate or struvite ($MgNH_4PO_4.6H_2O$), which is a slow release fertiliser that is generated from the combination of ammonium (NH_4), magnesium (Mg), and phosphate in equal molar concentration (1:1:1) (Doyle and Parsons, 2002). Struvite is an efficient alternative to phosphate rocks which are used as a fertiliser. Many methods have been used for recovering P as struvite, such as chemical addition and carbon dioxide stripping through aeration; however, those methods are expensive and, indeed, the costs of the recovered phosphate exceeds the cost of phosphate rocks (Morales et al., 2013). Fortunately, an alkaline environment, which is required for P recovery, can be achieved during energy generation in BES. Therefore, the cost of struvite can be reduced using BES. Recently, BESs have been used successfully to concurrently generate energy and recover nutrients (Hirooka and Ichihashi, 2013; Cusick et al., 2014). However, most of the studies achieved low P recovery due to using single-chamber BES, which negatively affects solution pH and minimises P precipitation.

This thesis presents the investigation of dual-chamber (MFCs and MECs) systems for energy generation, hydrogen production, and P recovery as struvite: it is designed to concurrently generate energy and recover P as struvite. The performance of the BES to generate electricity (MFC), produce hydrogen (MEC), and recover P as struvite (MFC and MEC) were investigated to determine the overall effectiveness of the system. Furthermore, microorganism community and structure were investigated to identify the dominant species and their role in energy generation and H_2 production.

1.3 Aims and objectives

The overall aim of the current study was to study and understand the parameters for the optimisation of the design and performance of BES for concurrent phosphorus recovery, and energy generation/hydrogen production. The specific objectives were:

Objectives:

1. To carry out a comprehensive literature review to identify the gaps in knowledge regarding energy generation/hydrogen production and phosphorus recovery in BES.

2. To understand the mechanisms of P recovery as struvite in dual-chamber MFC and MEC, and to investigate the impacts of different operational conditions on P recovery and energy generation in MFC.

3. To investigate the effect of influent COD and cathode aeration flow rate on power output, coulombic efficiency, COD removal, cathode pH, and precipitation efficiency in MFC using full factorial design and central composite design statistical tools.

4. To formulate statistical models to predict power density and P recovery, and explore the impacts of key parameters on the size, shape and purity of struvite crystals.

5. To investigate the role of applied voltage and influent COD in P recovery as struvite and hydrogen production using a dual-chamber MEC.

6. To improve and optimise struvite precipitation and hydrogen production under different operational conditions (applied voltage and COD), using a response surface methodology (RSM) optimisation statistical model.

7. To investigate the microbial community and structure that develop in the anode compartment of MFCs and MECs.

1.4 Outline thesis

Chapter 1 provides a brief background and highlights the aims and objectives of the study. Chapter 2 provides a comprehensive literature review of the bio-electrochemical system (MFC and MEC), BES principles, BES applications, and recent researches on P recovery using BES.

The research presented in this thesis was carried out using four H-type lab scale cells in Cardiff University School of Engineering. The study and analysis were carried out over a period of 400 days to obtain comprehensive results concerning P recovery and the impact of different operational conditions on BES performance. Each chapter contains the experimental set-up, procedure and calculation used in the chapter to achieve the abovementioned objectives.

Chapter 3 provides the general performance results of MFCs and the impact of different operational conditions (COD, electrolyte volume, cathode aeration flow rate, and external resistance) on energy generation and P recovery in MFCs. (Chapter 3 - published: Almatouq, A. and Babatunde A.O. (2016). Concurrent Phosphorus Recovery and Energy Generation in Mediator-Less Dual Chamber Microbial Fuel Cells: Mechanisms and Influencing Factors. International Journal of Environmental Research and Public Health, 13(4), 375)

The results of Chapter 3 were used in Chapter 4 to optimise energy generation and P recovery in MFCs using full factorial design, central composite design and surface response methodology statistical tools. Statistical analysis was applied to enhance the understanding of the role of key parameters on MFC performance.

The impact of applied voltage and COD on hydrogen production and P recovery in MECs was investigated in Chapter 5. In addition, central composite design and surface response methodology statistical tools were applied to optimise hydrogen production and P recovery in MECs. (Chapter 5 - published: Almatouq, A. and Babatunde A.O. (2017). Concurrent Hydrogen Production and Phosphorus Recovery in Dual Chamber Microbial Electrolysis Cell. Bioresource Technology. http://dx.doi.org/10.1016/j.biortech.2017.02.043)

Chapter 6 explores bacteria communities and structure in MFC and MEC, and identifies the main species in both systems. The main conclusion of the study is presented in Chapter 7. Finally, Chapter 8 presents recommendations for future research.

Chapter2

Literature Review

2. Literature Review

2.1. Introduction

This chapter provides a literature review of BES principles, materials, components, and applications and the most recent research regarding energy generation, H_2 production, and nutrient recovery. The objectives of the review are as follows:

- To collect information on recent studies of bio-electrochemical systems design, performance, optimisation, and problems.
- To review the research and different state of art applications on bio-electrochemical systems.
- To identify gaps in the knowledge and consider how bio-electrochemical systems can be improved in terms of performance and applications.

2.2 Renewable Energy

Renewable energy can be defined as energy generated from sustainable natural resources, for example, wind, solar, hydropower, and bioenergy. Due to fossil fuel depletion and the huge impacts of conventional sources of energy on our planet, many studies have focused on finding new and sustainable sources of energy that can substitute the current resources. Using sustainable natural resources as a source of energy can minimise the impacts of climate change on our planet and secure the planet's resources from depletion. Biomass is considered one of the renewable energy resources with the potential to be converted into an energy carrier and used for power generation (Mohammed et al., 2014). Around 10% of the total global energy is derived from biomass (Hamzeh et al., 2011), as biomass contains organic carbon, which allows it to be an energy source.

2.3 Hydrogen

Recently, the attention paid to the use of hydrogen as a fuel has increased due the high energy density of H_2. Hydrogen has been used as a fuel in transportation and for backup power. In addition, H_2 is used in many industries, such as the petrochemical and food industries. More than 65 million tonnes of hydrogen is produced every year, and H_2 is produced mainly from fossil fuels (48% from natural gas, 30% from refinery/chemical off-gases, 18% from coal, the rest from electrolysis) (IEA, 2007).

As H_2 production is mainly from fossil fuels, which are an unsustainable resource, therefore, many studies have focused on finding new technologies for H_2 production from renewable sources. In fact, many technologies are currently available for H_2 production, such as electrolysis, biological production methods, and algae and photosynthetic bacteria (Hallenbeck and Benemann, 2002; Zeng and Zhang, 2010; Xia et al., 2015). The most common and efficient technology for hydrogen production is electrolysis; however, the required energy input for electrolysis is high (4.5-5 kWh/m^3)(Liu et al., 2005b). Indeed, all the aforementioned technologies either require a high input of energy or are not efficient technologies. Thus, an efficient and cost effective technology is required for H_2 production.

2.4 Bio-electrochemical systems (BESs)

During 1911, the concept of current generation from live microorganisms was found by Potter (Pant et al., 2010), but in the 1970s and 1980s, real interest in this concept started to grow, and since then, the number of studies regarding bio-electrochemical systems has increased. Bio-electrochemical systems (BESs), such as microbial fuel cells (MFCs) and microbial electrolysis cells (MECs), can be defined as a promising technology that can produce electricity or H_2 from the organic material present in wastewater using microbial biocatalysts (Rozendal et al., 2008). In other words, BESs can convert the chemical energy in the chemical compounds into electricity (MFC) or H_2 gas (MEC) (Figure 2.1). Thus, these systems have the ability to produce clean and sustainable energy from different waste sources. In a BES, electrochemically active microorganisms are attached to one or both electrodes to catalyse the redox reactions in cells. In MFC, electrical energy is produced, whereas in MEC, H_2 gas is produced.

In both MFCs and MECs, bacteria is used in the anaerobic anode chamber to oxidise and transfer the chemical energy in the organic matter into electricity or H_2. In the MFC cathode chamber, various elements (oxygen, nitrate, and ferricyanide) can be used as an electron acceptor. In an MEC, an anaerobic cathode is used to reduce the electrons and protons to produce H_2. Recently, many studies have focused on developing BES to be used in real life situations (Heidrich et al., 2014).
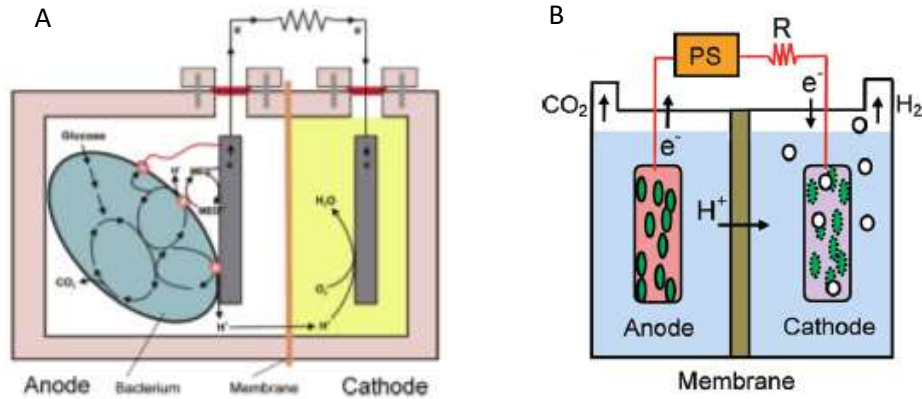
Figure 2.1 Schematics of dual chamber (a) MFC and (b) MEC (adapted from (Logan et al., 2006) and (Logan et al., 2008))

Treating wastewater in the conventional wastewater processes require 0.3 – 0.6 KWh/m^3, but wastewater can be considered a valuable resource of energy, as it contains an energy content equivalent to 10 times the amount required for conventional treatment (Heidrich et al., 2010). Therefore, utilising wastewater in such a way that the energy in the wastewater can be extracted is essential. Furthermore, BESs have demonstrated the ability to treat efficiently different types of wastewater, such as low strength domestic wastewater (Yu et al., 2012), industrial wastewater (Zhang et al., 2014), swine wastewater (Kim et al., 2016), digestion sludge (Abourached et al., 2014). Beside energy generation and H$_2$ production, BESs have been used for different applications, such as methane production (Ding et al., 2016), nitrogen removal (Hussain et al., 2016), sulphate removal (Lee et al., 2014), hydrogen peroxide (Rozendal et al., 2009), nickel removal (Qin et al., 2012), metal recovery (Wang et al., 2016b), and nutrient recovery (Ichihashi and Hirooka, 2012).

2.5 Principle of MFC and MEC

Microbial fuel cells (MFCs) are defined as devices that use bacteria as the catalysts to oxidise organic and inorganic matter and generate current (Logan et al., 2006). A standard MFC contains two main chambers: an anode and a cathode. The two chambers are separated by an anion or cation exchange membrane. Electrons, protons and carbon dioxide are released into the solution by oxidising the organic matter using the bacteria in the anaerobic anode chamber. Electrons are transferred to the anode (negative terminal) and flow to the cathode (positive terminal) through an external resistor. Electrons are transferred to the anode electrode either directly, indirectly, or by a mediator, such as methylene blue. During the movement of the

electrons through the resistor, current is generated. Protons are transferred to the cathode side through the membrane and combined with an electron acceptor (oxygen) in the cathode to complete the circuit (Figure 2.2).

Electromotive force (emf) is defined as the potential difference between the anode and the cathode (Logan et al., 2006). Theoretically, the maximum electromotive force attainable in MFC is 1.1 V with acetate oxidation and oxygen reduction using half-cell reaction, but due to the different losses in the system, the emf is lower than 1.0 V (Logan et al., 2006; Rozendal et al., 2007). The open circuit voltage (OCV) is the voltage when no current is flowing between the anode and the cathode. Cell emf should be close to the OCV; however, in practice, emf is greater than OCV due to the losses in the system.

Microbial electrolysis cell (MEC) is a system that is able to produce hydrogen from biomass. MECs are similar to MFCs but with some changes, as a power source is connected to the anode and cathode to apply a small amount of voltage to the circuit (Rozendal et al., 2006b). An MEC was designed recently by two research groups (Kadier et al., 2016), and it is similar to the MFC concept, where in the anode chamber, the electrochemically active bacteria oxidise the organic matter and transfer the electrons to the electrode. In an MEC, a power source is used to apply the relatively small amount of energy to overcome the thermodynamic limit for hydrogen evolution (Logan et al., 2008). In addition, the cathode chamber in an MEC is operated under anaerobic conditions to produce H_2. The anode reactions in both MFCs and MECs are the same if acetate is the carbon source (Table 2.1). Hydrogen production rate and current density have been used to evaluate MEC performance (Logan et al., 2008).

$$CH_3COO^- + 4\,H_2O \rightarrow 2\,HCO_3^- + 9\,H^+ + 8\,e^-$$

$$O_2 + 4H^+ + 4\,e^- \rightarrow 2H_2O$$

$$CH_3COO^- + 4\,H_2O \rightarrow 2\,HCO_3^- + 9\,H^+ + 8\,e^-$$

$$8H^+ + 8\,e^- \rightarrow 4H_2$$
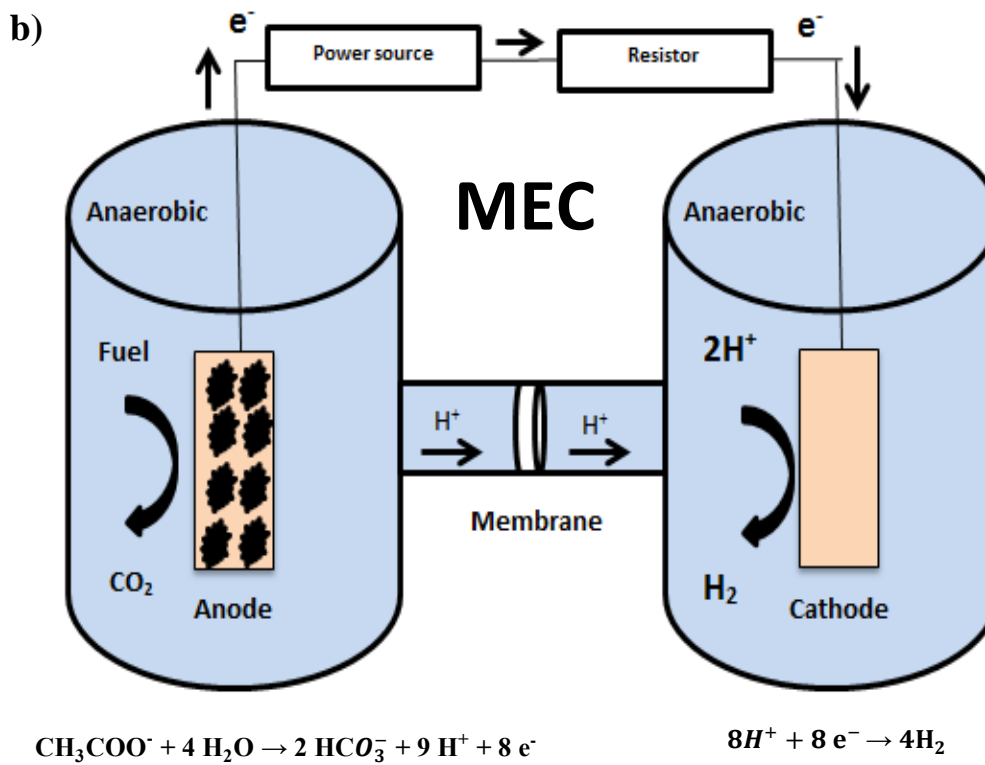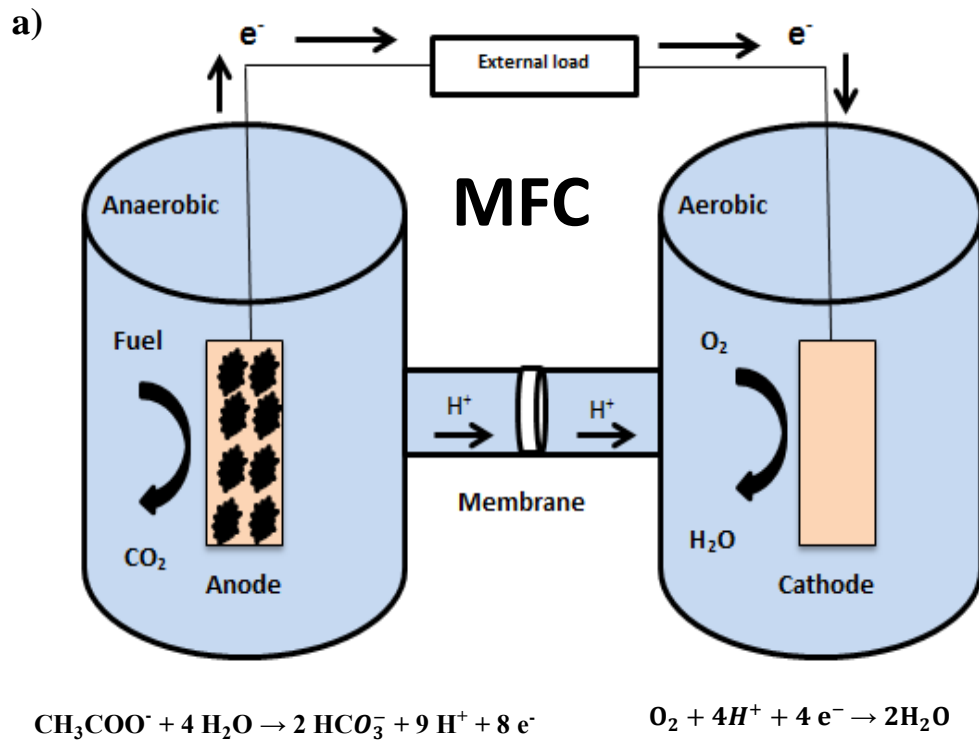
Figure 2.2 a) Microbial fuel cell and b) microbial electrolysis cell (equations adopted from Logan et al. (2006))

13

Electrons can be transferred to the anode by different methods: electron mediators or shuttles, bacteria nanowires, and indirect transfer. Chemical mediators can enhance the movement of the electrons, but they are expensive and harmful to the environment. If no mediators are used, then the system can be classified as a "mediator-less system".

Table 2.1 Electrode reactions and potentials of MEC, MFC, and water electrolysis systems under standard conditions (pH=7).

System	Anode reaction	Cathode reaction	Δ Potential
MFC	$CH_3COO^-+4H_2O\rightarrow2HCO_3^-$ $+9H^++8e^-$	$O_2+4H++4e^-$ $\rightarrow2H_2O$	1.085 V
MEC	$CH_3COO^-+4H_2O\rightarrow2HCO_3^-$ $+9H^++8e^-$	$2H++2e^-\rightarrow H_2$	-0.135 V
Water electrolysis	$2H_2O\rightarrow O_2+4H^++4e^-$	$2H++2e^-\rightarrow H_2$	-1.22 V

To generate high cell potential from the reaction, the anode chamber in the MFC should be operated at very low potential (anaerobic) and at the same time, the cathode chamber should be operated at very high potential (aerobic) (Logan et al., 2006).

For instance, in an MEC, the theoretical anode potentials can be calculated in terms of half-cell reactions (acetate is the carbon source) (Logan et al., 2008):

$$E_a = E_a^\circ - \frac{RT}{8F}\left(\frac{[CH_3COO^-]}{[HCO_3^-]^2[H^+]^9}\right) \quad (2\text{-}1)$$

where $E_a^\circ(0.187)$ V is the standard potential for acetate oxidation, R (8.314 J/K/mol) is the universal gas constant, T (K) is the absolute temperature, and F (96485 C/mol e$^-$) is the Faraday's constant. The anode potential is = - 0.279 V

The theoretical cathode reaction can be calculated as follows (Logan et al., 2008):

$$E_{cat} = E_{cat}^0 - \frac{RT}{2F}\ln\frac{P_{H2}}{[H^+]^2} \quad (2\text{-}2)$$

where E_{cat}^0 (0) V is the standard electrode potential for hydrogen, and P_{H2} is the hydrogen partial pressure under standard biological conditions. The cathode potential is = - 0.414 V; therefore, the equilibrium voltage is

E_{eq}= E_{cat} – E_a= (- 0.414 V) – (- 0.279 V) = - 0.135 V

The negative equilibrium voltage means that additional voltage (at least 0.14 V) is required to produce hydrogen from acetate. In practical terms, the applied voltage should be more than 0.2 V due to the losses in the system. According to Logan et al. (2008), at least 0.2 V is needed to produce H_2 in an MEC, and that amount of energy is much lower than that required for water electrolysis. The energy input in MEC and water electrolysis is 1 kWh/m^3H_2 and 4-5.5 kWh/m^3H_2 respectively (Rozendal et al., 2008).

2.6 BES design

BES can be designed in different shapes and structures based on their applications. During the last decade, many studies have focused on improving the design and the cell materials to optimise energy generation, H_2 production and reduce the losses in BESs (Ishii et al., 2013; Ahn et al., 2014; Yahya et al., 2015). BES performance is dependent on physical, chemical, and biological parameters including external resistance, substrate oxidation by bacteria, cathode reduction, protons and electrons movement (Rahimnejad et al., 2015). Therefore, all of these parameters should be considered during the designing process to optimise the performance.

2.6.1 Dual chamber BES

The dual chamber cell is the most common type of BES, which is mainly used in laboratory studies. A dual chamber BES contains two main chambers (anode and cathode), and these are separated by an ion exchange membrane. Each chamber contains an electrode, which is connected to a wire and linked to an external load. Electron acceptors, such as oxygen, ferricyanide, are used in the MFC cathode for cathodic reduction reaction. Phosphate buffer solution (PBS) is commonly used in the MFC and MEC cathode to maintain a constant pH, as the reduction of oxygen (MFC) and the consumption of protons (MEC) results in a pH increase. High catholyte pH has a negative influence on BES performance and causes a significant potential loss of the cathode (Logan et al., 2006; Logan et al., 2008). Therefore, in

most BES studies, PBS is commonly used as a catholyte due to the excellent performance in maintaining the pH balance during system operation. However, PBS is not suitable for practical applications of the MEC due to its high cost and the need to avoid phosphate release into the environment.

In MFC, using a chemical such as a ferricyanide as a catholyte can be expensive and it presents a hazard to the environment (Forrestal et al., 2014). The advantage of dual chamber BES is that anode and cathode reactions (oxidation and reduction) are separated, which makes it possible to extract useful products. The main disadvantage of dual-chamber BESs is the high internal resistance due to the distance between the electrodes. In addition, using a cation exchange membrane in some applications can be challenging due to the transportation of cations (i.e. NH^+_4, Na^+, K^+, $Mg^{2+,}$ and Ca^{2+}) from the anode to the cathode, which leads to a pH gradient and reduces the performance of the BES (Rozendal et al., 2006a).

2.6.2 Single chamber BES

Due to the high internal resistance and high designing cost for scaling-up a dual chamber BES, the single chamber was developed to enhance BES performance. In a single chamber MFC, both anode and cathode share the same chamber (anode chamber), where the anode is immersed in the anolyte, and the cathode is exposed to the air (Logan et al., 2006), where in a single-chamber MEC, both anode and cathode are immersed in the electrolyte. The distance between the electrodes in single chamber MFC is small compared to in a dual-chamber MFC, and this enhances the MFC's performance (Cheng et al., 2006; Cheng and Logan, 2011a). Furthermore, using a single chamber is an energy and cost effective system where no aeration or any other chemicals should be used at the cathode (Logan et al., 2015).

In MEC studies, using a single chamber MEC for hydrogen production has shown a negative effect on MEC performance because the hydrogen was consumed by hydrogenotrophic methanogens (Gil-Carrera et al., 2011). Therefore, a dual-chamber MEC was suggested to prevent methane production (Nam and Logan, 2012)

2.6.3 Others

Cylindrical, tubular and stacked MFC are different types of MFC that are designed to improve MFC performance (Aelterman et al., 2006; Zuo and Logan, 2011). It is not

clear which design is the best; however, selecting the design is totally dependent on the application.

2.7 Losses in bio-electrochemical system

In a BES, many losses can occur during system operation, which reduces BES performance (Fig. 2.3). The losses can be classified into activation losses, bacterial metabolic losses, mass transport or concentration losses, and ohmic losses (proton diffusion resistance and charge transfer resistance) (Logan et al., 2006). The internal losses in the MFC can be calculated using Equation 2-3 (Logan et al., 2006):

$$E_{cell} = OCV - IR_{int} \tag{2-3}$$

where E_{cell} is the cell voltage, OCV is the open circuit voltage, I is the generated current and R_{int} is the total internal losses in the system.
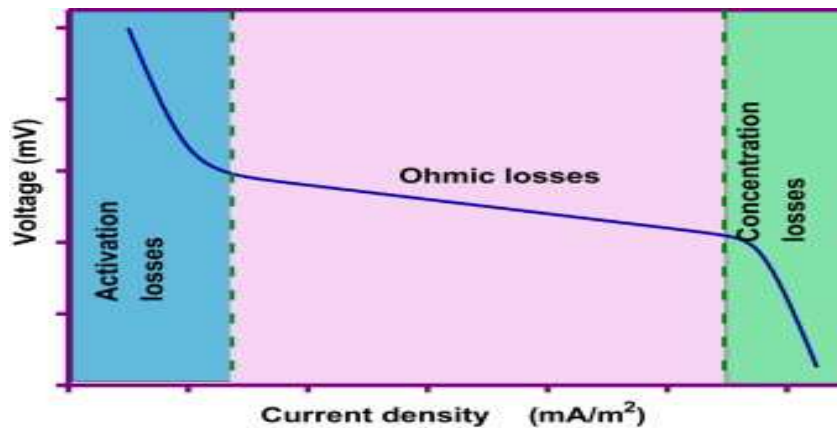
Figure 2.3 Voltage Vs current density curve showing the losses during electron transfer(adopted from Venkata Mohan et al. (2014))

Activation losses can be described as the activation energy needed for oxidation/reduction reactions, and such losses occur during the transfer of electrons from or to a compound reacting at the electrode surface (Logan et al., 2006). Activation losses can be affected by different anode and cathode parameters (area, roughness, electrochemical characteristic of the material, anode potential and kinetics of electron transfer) (Rabaey and Verstraete, 2005). In addition, activation losses can be reduced by decreasing the distance between the anode and cathode electrodes, increasing the electrode surface area, increasing the operating temperature, and improving electrode catalysis (Gil et al., 2003; Cheng et al., 2006; Logan et al.,

2006). Furthermore, enhancing electron transfer strategies in an electrogenic microorganism can reduce the activation loss (Pham et al., 2009).

Ohmic loss or ohmic polarisation refers to the losses that occur due to transferring the electron and proton processes through electrodes, electrolytes, and membranes and across the distance between the anode and the cathode (Rismani-Yazdi et al., 2008).

Bacterial losses can be described as the energy that is used by microorganisms (for growth) instead of them using it for the current generation. The microorganism oxidises the organic matter at a low potential and transfers the electron to an electron acceptor at a high potential such as oxygen, in the case of MFCs. Anode potential should be low to optimise the MFC voltage and minimise metabolic losses. However, maintaining a very low potential at the anode can negatively inhibit electron transfer mechanisms (Pham et al., 2009). Different losses may occur during electron transfer, including bacterial electron transfer losses, electrolyte resistance losses, anode losses, MFC resistance and membrane resistance losses, cathode losses, and electron acceptor reduction losses (Figure 2.4).

Mass transport losses occur when the rate of mass transport of a species to or from the electrode limits current production, and it mainly occurs at high current density (Logan et al., 2006). The magnitude of the loss increases with the increase of current density, and the mass transport losses can be reduced by maintaining a high concentration of oxidant, optimising cathode electrode and compartment design, and optimising operational conditions (Rismani-Yazdi et al., 2008). The same losses (Ohmic losses, bacterial metabolic losses, and mass transport losses) can be found in MECs (Logan et al., 2008).
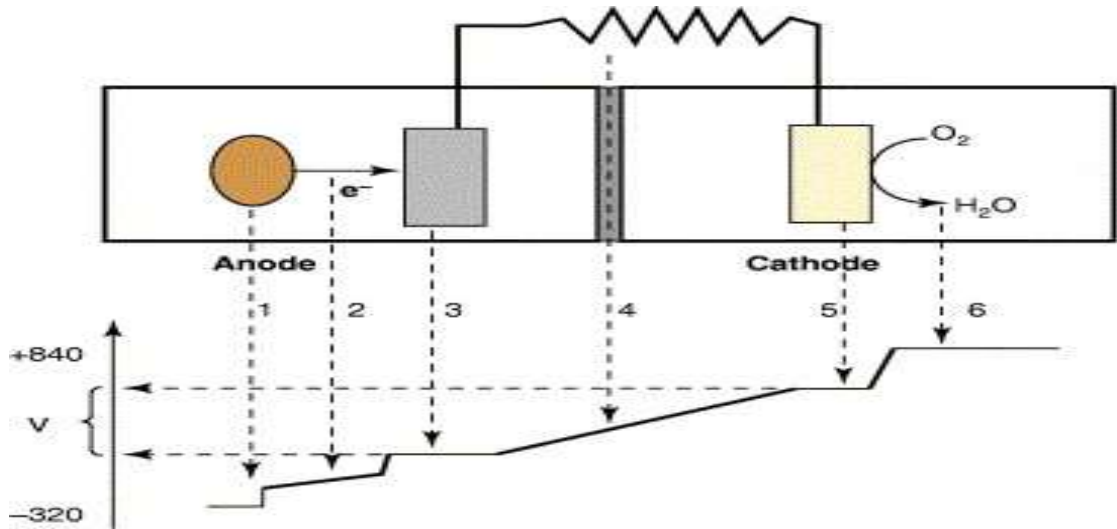
Figure 2.4 Potential losses during electron transfer in MFC: 1) bacterial electron transfer losses, 2) electrolyte resistance losses, 3) anode losses, 4) MFC resistance and membrane resistance losses, 5) cathode losses, 6) electron acceptor reduction losses (adopted from Rabaey and Verstraete (2005))

2.8 BES components

2.8.1 Anode and cathodes

Energy generation and H_2 production in BES can be affected by many factors, such as BES design and electrode materials; therefore, selecting the material for the electrodes is crucial for enhancing BES performance. Thus, different electrode materials have been studied in BES research. The ideal electrode material should have (1) good electrical conductivity and low resistance, (2) chemical stability and anti-corrosion, (3) a large surface area, and (4) appropriate mechanical strength (Logan et al., 2006; Rahimnejad et al., 2015). Many electrode materials have been used in MFC and MEC studies, and the most common material is carbon material, which includes carbon cloth, carbon paper, reticulated vitreous carbon (RVC) and carbon felt. These materials were selected for their stability in microbial cultures, high electric conductivity, and large surface area (Rahimnejad et al., 2015). Furthermore, many techniques, such as electrode heat pre-treatment (Wang et al., 2009), ammonia electrode treatment (Cheng and Logan, 2007), and electrode catalysts (Ramachandran et al., 2015), have been employed to enhance anode performance. However, using these methods could increase the cost of the reactor.

Cathode electrode and catalyst performance have a great impact on the reduction reactions in the cathode chamber. Most of the cathode electrodes are coated with

precious metals, such as platinum, which are used as catalysts. Selecting an appropriate catalyst on the electrode surface can lower the activation energy and enhance the reaction rate (Rahimnejad et al., 2015). Furthermore, biocathodes were suggested by Huang et al. (2011) to overcome the high cost of the catalysis. In biocathode systems, microorganisms are used as a catalyst on the cathode surface to enhance the MFC performance instead of artificial mediators or catalysts using nitrate, sulphate, tetrachloroethene, fumarate, perchlorate, and trichloroethene, CO_2, H^+, Fe(III), Cr(VI), U(VI) and Mn(IV) as electron acceptors and without the help of exogenous (Chen et al., 2008; Huang et al., 2011; Najafpour et al., 2011).

Recently, inexpensive and durable electrode materials have been used to reduce the cost of MFC materials. For example, corrugated cardboard has been used as an inexpensive and high-performance electrode material in MFCs (Chen et al., 2012). In addition, Offei et al. (2016) used palm kernel shell activated carbon as an anode and cathode in an MFC. The MFC achieved 86% of the value obtained by the MFC that used a carbon paper anode.

2.8.2 Ion Exchange Membrane

The ion exchange membrane is another important part that has a significant impact on BES performance. The membrane separates the anodic and cathodic reactions. Many types of membrane have been used in BES studies (cation exchange membrane, anion exchange membrane, membrane-less BES, polymer membrane, and porous membranes); the usage of these membranes is dependent on the system applications. The presence of an ion exchange membrane between the anode and the cathode prevents substrate crossover and leads to the production of a pure product, which is pure hydrogen gas (MEC), and nutrient or metal recovery (Sleutels et al., 2010). Unfortunately, the membrane also increases the resistance of the system, resulting in an increased specific energy consumption per m^3 of produced hydrogen. Some disadvantages were observed when separators were used in BES studies: (1) oxygen diffusion from the cathode to the anaerobic anode in the MFC, which lowered the coulombic efficiency and microorganism activity (Oh et al., 2009; Leong et al., 2013), (2) pH splitting between the anode and the cathode especially when a cation membrane was used (high pH at the cathode and low pH at the anode), which resulted in low system performance (Pandit et al., 2012), (3) membrane resistance,

which is influenced by the electrolyte, pH and electrolyte concentration (Harnisch et al., 2008). Thus, selecting the appropriate membrane is crucial in a BES.

2.9 Electrochemically active microorganisms

The role of microorganisms in MFCs and MECs is very important, as it is responsible for oxidising the organic matter and transferring the electrons from the substrate to the electrode. Microorganisms such as *Aeromonas*, *Geobacter* and *Shewanella* have shown their ability to generate current, and these genera are able to transfer electrons to the outer membrane without the assistance of electron carriers (Logan et al., 2008; Sharma et al., 2008). Anaerobic respiration is the main process for the electrochemical active bacteria to transfer electrons from organic compounds to an electrode (Moon et al., 2006). Thus, understanding bacteria structure and community can enhance BES performance by selecting the inoculation source and appropriate operational conditions. In MFC, *Shewanella* and *E.Coli* were found to generate electricity (Rathmell and Wiley, 2011), whereas in an MEC, *Geobacter* is used to create a proton gradient across the cell membrane to generate hydrogen (Call et al., 2009a).

Diverse microbial communities can be found in wastewater, and the presence of these communities is essential for energy generation in BESs (Kiely et al., 2011). Electrochemical active bacteria can be obtained from wastewater, anaerobic digested sludge, and sediments. Wastewater is commonly used for MFC and MEC inoculation, so it is expected that multiple microbial communities can be established in these systems. However, the microbial communities and community structure in MFCs and MECs can be different due to operational conditions. In an MFC, oxygen is used as an electron acceptor in the cathode, whereas in an MEC, the system is operated completely under anaerobic conditions. The operation of an MEC under anaerobic conditions can help the anaerobic bacteria (exoelectrogen *Geobacter* and methanogenic bacteria) to grow, whereas in an MFC, the microbial structure and the performance can be affected by oxygen diffusion (Call et al., 2009b; Zhang et al., 2009b).

The microorganism structure and communities vary depending on different operational conditions and system architectures, and on the electron donors and acceptors in each system (Logan and Regan, 2006; Sun et al., 2012). To a certain

extent, the microbial communities in the BES show an indication of the situation of microbial activity in the system, and any change in environmental conditions can lead to changes in microbial communities. In addition to the role of the major microorganism communities in BES, minor communities can contribute significantly in BES performance (Zhi et al., 2014).

Three main transfer mechanisms have been discussed in previous studies, namely, direct electron transfer via outer membrane c-type cytochromes, direct electron transfer via conductive pili (microbial nanowires), and indirect electron transfer via endogenous metabolites (Wrana et al., 2010; Huang et al., 2011; Zhi et al., 2014).

2.9.1 Direct electron transfer (outer membrane c-type cytochromes and nanowires)

In direct electron transfer, electrons transfer when there is direct contact between the anode electrode and the bacteria cell membrane or a membrane organelle, and this transfer occurs without any soluble redox-active metabolites. Electrochemically active bacteria, anode respiring bacteria, and exoelectrogenic bacteria, have shown their ability to transfer electrons from substrates to the electrode without the need for any mediator (Figure 2.5). In membrane electron transfer, the redox active proteins, such as c-type cytochromes, are localised at the outer membrane and can act as direct channels for the electron flow to the solid phase electron acceptor. Microorganisms, such as *Geobacter metallireducens*, *Aeromonas hydrophilia*, *Shewanella spp*, and *Rhodoferax ferrireducens*, use this transfer mechanism (Chaudhuri and Lovley, 2003; Pham et al., 2003; Rabaey and Verstraete, 2005; Newton et al., 2009).

The nanowires electron transfer mechanism is used when the cells are not in direct contact with the surface, where highly conductive nanowires are used to transfer the electrons from the cells to the surface (Gorby et al., 2006). Microorganisms, such as *Shewanella* and *Geobacter*, have shown their ability to produce nanowires for electron transfer (Logan and Regan, 2006).
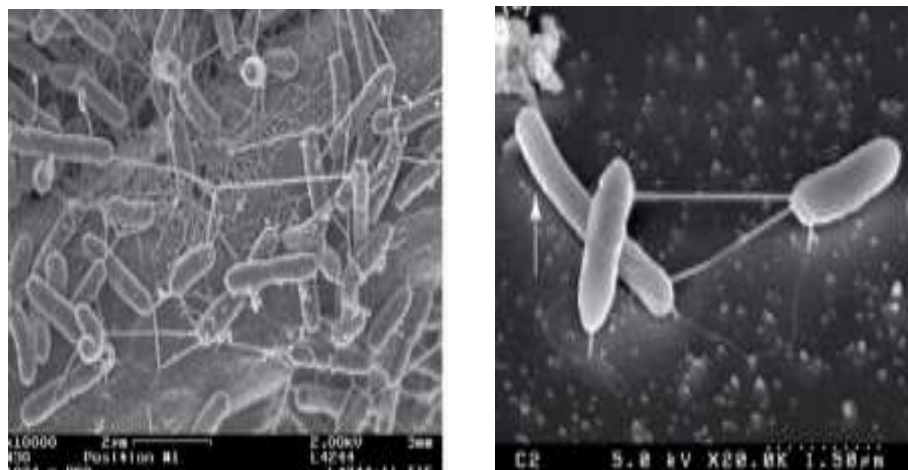
Figure 2.5 SEM image of MFC anode colonized by S. oneidensis MR-1 and Pelotomaculum thermopropionicum and Methanothermobacter thermautotrophicus. (Image extracted from Logan and Regan (2006))

On the other hand, artificial mediators, such as methylene blue (MB), neutral red (NR) and 2-hydroxy-1,4-naphthoquinone (HNQ) are different mediators that are used to enhance the power generation in an MFC (Ho et al., 2011; Rahimnejad et al., 2011). These mediators can accept electrons from electron carriers and transfer these electrons to the electrode (Lovley, 2006). In other words, these mediators are used as an electron shuttle between the bacteria and the electrode in a mediated electron transfer. However, these mediators are costly and toxic, and so cannot be considered for large-scale operations (Zhi et al., 2014). Nonetheless, using these mediators in an MFC that uses microorganisms such as *Escherichia coli*, *Proteus* and *Bacillus* is essential because these microorganisms are not able to transfer the electrons (Reddy et al., 2010).

2.9.2 Indirect electron transfer by reduced metabolic products

In indirect electron transfer, metabolic products, such as hydrogen and alcohol, are the result of glucose conversion on the anode surface by a fermentative microorganism (Lovley, 2006). Electricity production in these systems is inefficient due to the slow reaction of fermentation products with electrodes, and only a few electrons are utilised for electricity production (Schröder et al., 2003; Lovley, 2006). Several microorganisms, such as *Clostiridium*, *Alcaligenes*, or *Enterococcus*, have shown their ability to generate current using this mechanism (Karube et al., 1977; Rabaey and Verstraete, 2005).

2.10 The impact of operational conditions and components on BES performance

The operational conditions and components of BESs have a great impact on electricity generation (MFC) and H_2 production (MEC). Thus, BESs are influenced by operational conditions and reactor components, such as substrate concentration, electrolyte volume, cathode aeration flow rate, pH, and external resistance.

2.10.1 Substrate

The substrate is an important parameter for BES performance, as it provides the organic matter (carbon source) for the microorganisms in the anode chamber. The efficiency of the BES to convert the organic waste into bioenergy depends on the characterization of the waste material (Nam et al., 2010; Pant et al., 2010). The microorganisms oxidise and degrade the organic matter to produce electrons and protons. Then, the electrons are transferred through the resistor to the cathode chamber. In the cathode, protons, electrons, and electron acceptor are combined together to produce water. BESs have been used for different types of substrate, including synthetic wastewater (He et al., 2005; Hirooka and Ichihashi, 2013; Luo et al., 2014), domestic wastewater (Yu et al., 2012; Ahn et al., 2014), and industrial wastewater (Velasquez-Orta et al., 2011; Abbasi et al., 2016).

The synthetic substrate (acetate and glucose) is the common type of substrate that is being used in laboratory-scale BESs due to their simplicity. However, a complex substrate that is rich in complex organic matter helps in the growth of many active microbes (Das and Mangwani, 2010).

The concentration of the substrate is a key factor in BES performance. For example, COD has a great impact on BES performance, where increasing COD increases the current density and the generated power (Gil et al., 2003; Jadhav and Ghangrekar, 2009). However, overdosing the BES with a substrate leads to saturation and decreases the amount of power generated (Juang et al., 2011; Juang et al., 2012). Martin et al. (2010) studied the impact of COD on power generation. In their study, an air cathode MFC was fed with COD ranging from 200 to 8000 mg/L. Power generation increased with the increase in COD up to 4000 mg/L, then started to decrease. With regard to COD removal efficiency, the efficiency decreased with the increase in COD.

Similarly, Li et al. (2011) investigated the effect of hydraulic retention time and COD on MFC performance. The study showed that increasing COD increased the power and decreased COD removal efficiency. Therefore, the substrate concentration should be controlled in such a way that a balance is found between the removal efficiency of the substrate and the production of current.

2.10.2 External resistance

External resistance is the link between the anode and the cathode electrodes, where the electrons transfer through it. External resistance in a BES controls the ratio between the generated current and the voltage. Based on Ohm's law, the generated current in a BES is totally dependent on the external resistance (Logan et al., 2006; Pinto et al., 2011), and to obtain the highest power in the BES, the external resistance value should be equal or close to the internal resistance (Molognoni et al., 2014). Large losses in BES performance may occur if the incorrect external load is selected. Using low external resistance leads to a decrease in the voltage and an increase in the current and vice versa. COD removal is influenced by the value of external resistance, where at low external resistance, COD removal is higher than high external resistance (Jadhav and Ghangrekar, 2009).

Furthermore, studies have shown that external resistance has a significant effect on biofilm diversity and formation in the anode chamber (Rismani-Yazdi et al., 2011; Liu et al., 2016). Therefore, selecting the optimum external resistance helps to enhance BES performance.

2.10.3 Cathode aeration

In a dual chamber MFC, oxygen is commonly used as an electron acceptor due to the high potential. Therefore, providing the optimum amount of oxygen in the cathode chamber is essential to optimise MFC performance. Researchers have obtained a variety of results cathode aeration flow rate in a dual chamber MFC varied from 10-200 mL/min (Gil et al., 2003; Amari et al., 2015). A linear correlation was found between the generated current and cathode aeration flow rate (lower or equal to 100 mL/min). In contrast, Zhang et al. (2008) achieved a maximum volumetric power density at a high cathode aeration rate (300 mL/min). All of these studies confirmed that cathode aeration is the major limiting factor for the operation of an MFC, thus

identifying that the optimum cathode aeration flow rate is crucial to optimise MFC performance.

2.10.4 Anolyte and catholyte volumes

MFCs have been designed with different structures and scales, some in lab scales (micrometres to litres) and some in pilot scales (120 L) (Heidrich et al., 2014; Wang et al., 2015; Kim et al., 2016). However, the impact of anolyte and catholyte volumes on MFC performance has not been studied in depth. Logan et al. (2015) studied the impact of the volume of the anode and cathode chambers on the current and showed that increased chambers volume and maintained electrode surface area in the anodes and cathodes decreased the generated energy because of an insufficient electrode surface area for capturing all the substrate as electrical current.

2.10.5 Applied voltage in MEC

Theoretically, an MEC requires a low voltage (0.2 V) to produce H_2 (Logan et al., 2008), but in practice and due to potential losses, it requires $>= 0.4$ V for H_2 production (Logan et al., 2008; Kadier et al., 2016). Studies have confirmed that there is a linear correlation between the applied voltage, H_2 production rate, and substrate removal (Escapa et al., 2013; Rivera et al., 2015; Ding et al., 2016). An applied voltage of 0.8 V was determined to be the optimum applied voltage for hydrogen production (Call and Logan, 2008; Kyazze et al., 2010; Kim and Logan, 2013). Ye et al. (2010a) studied the impact of applied voltage on a single chamber MFC. The study showed that applying 1 V in an MEC was optimum for H_2 production while applying a high voltage (>1.2 V) had a negative impact on H_2 production and substrate removal. In addition, a high voltage could inhibit the activity of microorganisms in the MEC and reduce the treatment efficiency (Valle et al., 2007; Ding et al., 2016).

2.10.6 pH

The pH is another important factor that has an influence on BES performance, especially on the life and growth of microorganisms. The pH difference between the anode and the cathode occurred when proton transport through the Nafion is slower than the proton production rate in the anode chamber (pH decreased) and the proton consumption rate in the cathode chamber (pH increased) (Rozendal et al., 2006a).

The pH buffer is commonly used in dual-chamber BESs to maintain the solution pH and increase the solution conductivity, as the pH buffer plays an important role in facilitating proton transfer and reducing internal resistance in MFCs. Studies have found that the microbial activity is very active at a neutral pH, while it is slower at a pH less than 6 and higher than 7.5 (He et al., 2008; Jadhav and Ghangrekar, 2009). A pH >7.5 is favourable for methanogenesis, which contributes to COD removal and results in a low value of current. Thus, the performance of the MFC decreases when the pH gradients occurs. Zhang et al. (2011a) studied the impact of pH on dual-chamber MFC performance and anodic biofilm. The study demonstrated that operating the MFC under acidic pH conditions led to a reduction in the output voltage and power. In addition, acidic conditions accelerated COD removal. The same observation was found for MECs, where increasing the pH difference led to a decrease in H_2 production in the system (Luo et al., 2010). Furthermore, some studies found that MFC internal resistance decreased when the pH difference between the anode and the cathode was increased, as the higher pH difference increases the proton flux rate through the PEM (Jadhav and Ghangrekar, 2009). In contrast, increasing the cathode pH negatively affects BES performance; based on the Nernst equation, a unit of pH difference between the anode and the cathode means an extra potential loss of about 0.06 V will occur in the system (Aboutalebi et al., 2011).

2.10.7 Temperature

Temperature is a critical factor that influences BES performance, as it has a significant impact on the growth and reproduction of microorganisms, which can affect both intracellular biochemical processes and extracellular chemical or biochemical processes (Wei et al., 2013). Many researchers have studied the impact of temperature on BES performance, and it has been demonstrated that the generated current increased by 80% when the temperature was increased from 30 to 40 C° (Liu et al., 2011). Similarly, Min et al. (2008) showed that increasing the temperature from 22 to 33 C° increased the power density by 62%, while Wei et al. (2013) demonstrated that increasing the environmental temperature from 25 to 45 C° enhanced the microbial activity in the system and that the activity decreased significantly when the temperature was increased to 50 C°. In contrast, other studies showed that the performance of BES was better at low temperatures (8-22 C°) than at high temperatures (20-35C°) (Jadhav and Ghangrekar, 2009). Therefore, further

studies are needed to fully understand the impact of temperature on BES performance.

2.11 BES for wastewater treatment

Staying within effluent discharge limits requires intensive treatment processes, which leads to the use of more energy to achieve those limits. Currently, wastewater treatment industry goals are to minimise energy consumption, maximise energy recovery and recover nutrients (instead of removing nutrients) (Gude, 2016). In a BES, the microorganisms oxidise the organic matter (measured as COD) in the wastewater and convert the chemical energy into electricity or other useful products (hydrogen, methane, ethanol and hydrogen peroxide). BESs have shown they have the ability to treat different types of substrates, such as municipal, agricultural, industrial, dairy and food waste (Figure 2.6) (Gude, 2016). Therefore, BESs can be used in wastewater treatment instead of using the traditional high energy demanding processes.
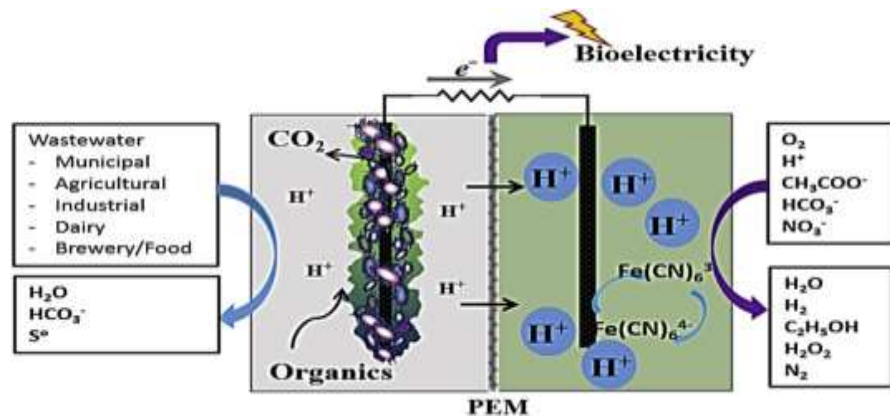
Figure 2.6 MFC for treatment using different wastewater types (adopted from (Gude, 2016))

There are several advantages for using a BES as a tool for wastewater treatment (Kelly and He, 2014):

1. Environmental advantages:
   a. low carbon footprint.
   b. lower sludge volumes.
   c. nutrient recovery (save natural resource).
2. Energy advantages:
   a. lower energy consumption (anaerobic treatment).

       b. source of energy.

  3. Operational advantages:

       a. potential use under different environmental conditions.

       b. real-time monitoring and control.

       c. low operational cost (energy generation can be used to reduce the operational cost).

However, same as other technologies BES has some disadvantages:

- The requirement of expensive materials, such as platinum, as cathodic catalysts.

- Relatively low output voltage.

The conventional wastewater treatment processes (such as aerobic process) produce a high amount of sludge (approximately 0.53 g biomass-COD g/COD), whereas in MFCs, the system produces a lower amount of sludge, for example, 0.02-0.22 g biomass- COD g/COD (Clauwaert et al., 2008).

2.12 Struvite

Magnesium ammonium phosphate hexahydrate or struvite ($MgNH_4PO_4.6H_2O$) is a slow release fertiliser that is generated from the combination of ammonium (NH_4), magnesium (Mg) and phosphate in equal molar concentrations (1:1:1) (Doyle and Parsons, 2002). Struvite precipitates in the form of white crystals and in an alkaline environment (pH>8), according to the reaction shown below:

$$Mg^{+2} + NH^{4+} + PO_4^{3-} + 6H_2O \rightarrow MgNH_4PO_4\ 6(H_2O) \hspace{3cm} (2\text{-}4)$$

Mg^{+2}, NH^{4+} and PO_4^{3-} can be found in wastewater, which makes wastewater a potential source of struvite. Struvite was first observed in 1973 as a crust of crystalline material in a multiple-stage digestion system (Le Corre et al., 2009). Struvite can be found in pipes, equipment surfaces, pumps, aerators, and post-digestion processes. While struvite precipitation in wastewater treatment plants can be a problem, studies have shown that it can be used as a high-quality fertiliser (Doyle and Parsons, 2002; Jaffer et al., 2002).

2.13 Struvite Morphology

Struvite can be precipitated in different shapes (needle, cube, rod, X shape, irregular; Fig. 2.7), and colours (white, yellowish, or brownish-white) (Lee et al., 2009; Zhang et al., 2009a; Rahman et al., 2014). Struvite crystal shape and size may vary depending on the precipitation process. Many parameters have an influence on crystal sizes, such as differences in operating conditions, crystal retention time, and variations in quantities of impurities in liquors (Le Corre et al., 2007; Rahman et al., 2014). In addition, pH has an influence on crystal growth and morphology, where a lower pH produces small-sized crystals (Prywer et al., 2012).
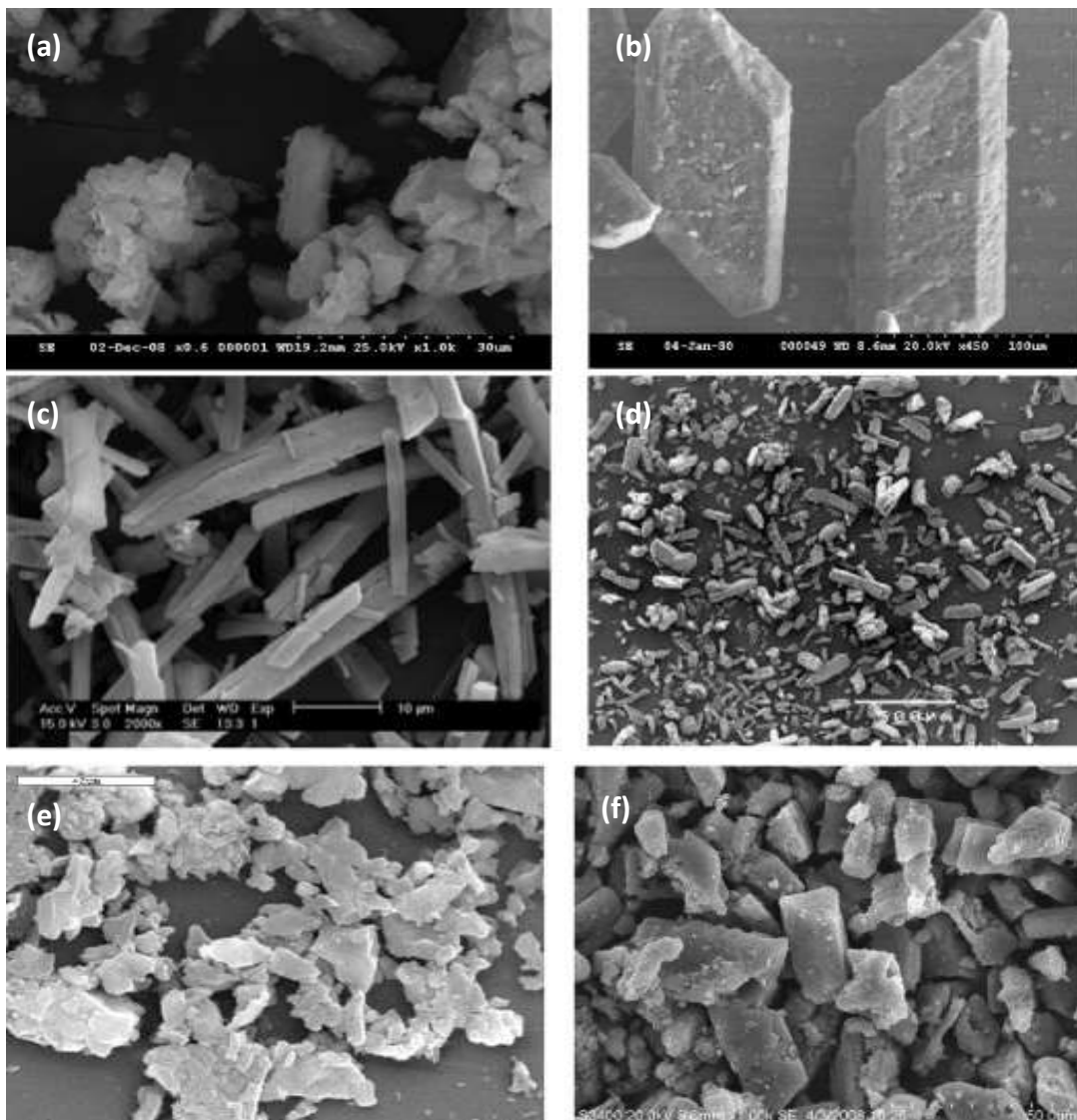
Figure 2.7 SEM of struvite crystals, (a) irregular crystals, (b) cube, (c) rod irregular crystals, (d) irregular crystals, (e) irregular crystals, and (f) cube irregular crystals (Rahman et al., 2014)

Two main stages control the development of struvite crystals: nucleation (crystal birth) and crystal growth (Rahman et al., 2014). In the nucleation stage, ions (P, NH_4, Mg) combine together to form crystals, and this mechanism is controlled by the kinetics of the reaction. Crystal growth can be defined as the development of the crystals until the equilibrium is reached (Le Corre et al., 2009). In other words, crystal growth shows the size the crystal will reach at the final stage. Many parameters and factors control struvite precipitation, such as the thermodynamics of liquid-solid equilibrium, kinetics of the reaction, state of crystals' initial condition, and physical-chemical parameters (pH, supersaturation, mixing energy, temperature, and presence of foreign ions) (Le Corre et al., 2009).

2.14 Struvite precipitation

Predicting the mechanisms of struvite crystals is difficult and complex because many parameters can influence these mechanisms. However, understanding the factors that affect the mechanisms can help to optimise and enhance struvite crystallisation. Different physical and chemical parameters can influence struvite precipitation in the solution, such as pH, molar ratio, mixing energy, aeration rate, temperature, supersaturation and foreign ions.

2.14.1 pH

Solution pH is the most important parameter in struvite precipitation, and it is correlated to solubility and supersaturation. Struvite solubility decreases with increasing pH; it precipitates in a pH range of between 7 and 11 (Nelson et al., 2003), and different studies have shown that the optimal pH range for struvite precipitation is 7.5- 9 (Hao et al., 2008; Wang et al., 2010). Indeed, Adnan et al. (2003) showed that more than 90% of P can be removed at pH=8.3.

Solution pH is also an important parameter to maintain NH_4^+ in the solution, as at high pH, ammonium ions are transferred into gaseous ammonia. Sánchez-Monedero et al. (2001) stated that at pH > 8, NH_4^+ can be lost through volatilization; that reduces the concentration of NH_4, and as a result, the molar ratio of struvite (1:1:1) will be affected. Moreover, aeration plays an important role in ammonium concentration; high aeration in the solution increases the ammonia volatilization (Rahman et al., 2014).

The quality and the size of struvite crystals can also be affected by solution pH. A high pH can affect struvite purity as impurities such as calcium can attach to and merge with the pure struvite (Wang et al., 2005; Merino-Jimenez et al., 2017). Thus, precipitating P at a controlled pH can enhance struvite purity. In addition, an increase in solution pH has a negative impact on crystal size; increasing solution pH decreases crystals size, whereas increasing the pH from 9 to 11 decreases the crystal mean size by three times (Kozik et al., 2013).

Furthermore, in struvite precipitation, a steady operation condition can be achieved if the pH, molar ratios, influent flow rate, and temperature are maintained at their optimal conditions.

2.14.2 Molar ratio

The molar ratio of P: NH_4: Mg in a solution is crucial for struvite precipitation; many studies have studied the optimal ratio of P: NH_4:Mg for struvite precipitation. Such studies have confirmed that a P: NH_4:Mg molar ratio of 1:1:1 would be sufficient to precipitate struvite (Yetilmezsoy and Sapci-Zengin, 2009; Rahman et al., 2011). In addition, struvite crystallisation can be improved by increasing the molar ratio of Mg:P to 1.15:1 (Zhang et al., 2009a). The molar ratio also has an influence on struvite crystals, where crystal size increased from 42 μm to 58 μm when the molar ratio of Mg: P was increased from 1:1 to 1.2:1 (Kozik et al., 2011). Thus, the optimum ratio of P:Mg is between 1:1 and 1:1.2 (Hirooka and Ichihashi, 2013; Kozik et al., 2013).

2.14.3 Mixing energy

Struvite crystals were found in locations with high turbulence in wastewater treatment plants, which shows the importance of turbulence in struvite crystallisation. In addition, Ohlinger et al. (1999) showed that struvite size and shape were affected by mixing energy, where growth kinetics was strongly dependent on mixing energy. Furthermore, high mixing energy was shown to accelerate the nucleation rate, limit crystal growth, and increase crystal breakage (Durrant et al., 1999).

2.14.4 Temperature

Temperature is another factor that can influence struvite solubility; however, the impact of the temperature is lower than the impact of pH and supersaturation (Durrant et al., 1999). It has been shown that increasing the temperature from 10 to 50 C° increases struvite solubility products (K_{sp}) from 0.3×10^{-14} to 3.73×10^{-14} (Aage et al., 1997). The optimal temperature for struvite precipitation is between 25 to 35 C° (Le Corre et al., 2009). Moreover, crystal growth and shape are affected by high temperatures, as at a high temperature, crystal growth increases and the nature of the crystals is affected (Babić-Ivančić et al., 2002).

2.14.5 Presence of foreign ions

The presence of foreign ions in struvite can negatively affect the purity of the struvite. Struvite crystallisation with foreign ions (such as Ca) leads to the formation of amorphous precipitate rather than crystalline struvite (Le Corre et al., 2005; Ye et al., 2010b). Therefore, pure struvite should be formed without any traces of other compounds.

On the other hand, struvite crystallisation with the presence of foreign ions inhibits the increase of crystal size, as Le Corre et al. (2005) found that increased Ca concentration reduces crystal size and inhibits struvite growth. In a different study, Kabdaşlı et al. (2006) found that for struvite crystallisation, the presence of sodium, calcium, sulphate, and carbonate-bio carbonate ions affects induction time and struvite morphology and size.

2.15 Nutrients removal and recovery in BES

Most of the organic matter (COD) is removed efficiently in BESs (MFC or MEC; Fig 2.8); however, the anaerobic environment in the anode chamber makes these systems inefficient for nutrient removal (Gude, 2016). The concept of photosynthetic with algal growth was used to remove phosphorus from wastewater. A sediment photo microbial fuel cell combined with algal growth achieved 69% of phosphorus removal, and algae biomass uptake was the main removal mechanism (Zhang et al., 2011c). A photo-bioreactor with microbial fuel cell concept was suggested to enhance N and P removal from wastewater (Jiang et al., 2012). MFC effluent was

transferred to an external photo-bioreactor for N and P removal. The novel system increased phosphorus removal from 58 to 92 %.
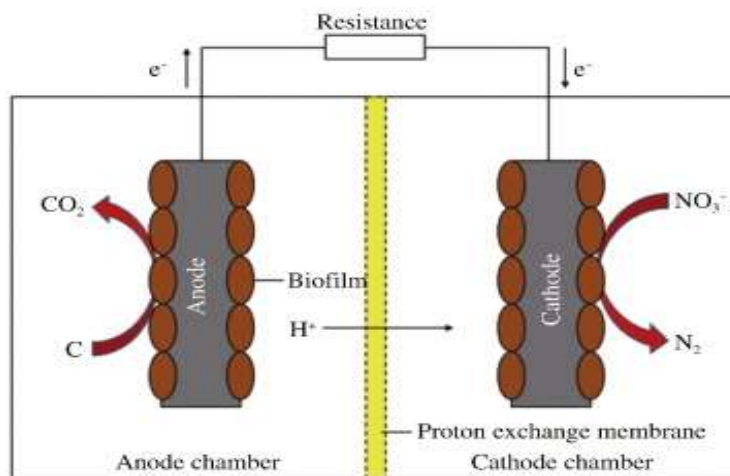
Figure 2.8 Schematic of simultaneous carbon and nitrogen removal in a typical two-chamber microbial fuel cell (Sun et al., 2016)

Recently, many studies have focused on nutrient recovery in BES. Nitrogen and phosphorus are the main nutrients that are harmful to the environment if they are discharged to water bodies in high concentrations. Therefore, all discharge regulations and rules have been adjusted to restrict the discharge concentration. The P recovery process in a BES is different from that for other nutrients, as P recovery in BES occurs via precipitation only, and P compounds are not involved in electron transfers via REDOX reactions like nitrogen (Kelly and He, 2014).

The impact of pH on power generation and P removal was first studied using a single-chamber MFC (Puig et al., 2010). Phosphate was removed through precipitation at pH>8.5 as calcium or potassium phosphate. P solubility was strongly influenced by the pH, and a chemical addition was needed to precipitate P. Solution pH was controlled by dosing with base or acid in the solution, and the impact of REDOX reactions on pH was neglected.

The first study for P recovery was conducted on a dual chamber MFC using digested sludge as a source of P. Methylene blue mediator was used in the cathode chamber with digested sludge to reduce $FePO_4$ and convert it to a soluble form. The reduction of $FePO_4$ liberates orthophosphate as phosphoric acid. Then, ammonium and magnesium were added to precipitate P as struvite (Fischer et al., 2011). The system achieved orthophosphate recovery of 82% from the digested sludge. In this study, the

main purpose of using MFCs was only to release orthophosphate, and ammonium and magnesium were added to the solution to precipitate P. In addition, pH adjustment via chemical addition was used to increase the pH for P recovery as struvite. The addition of methylene blue mediator and pH adjustment to precipitate P as struvite is not economical and increases the cost of struvite.

A single-chamber microbial electrolysis cell was used for the first time for struvite precipitation with the presence of a high carbonate concentration (Cusick and Logan, 2012). Both H_2 production and P recovery were studied, and the system achieved P removal ranging from 18 to 40%. Due to proton consumption for H_2 production in the cathode chamber, the cathode pH increased (pH>8). The rate of struvite accumulation was affected by batch time and applied voltage. Studies have shown that using a single chamber MEC negatively affects H_2 production due to H_2 consumption by methanogens (Gil-Carrera et al., 2011). In addition, using a single chamber MEC negatively affects P recovery, where producing and consuming protons at the same chamber led to pH buffering, which negatively affects P precipitation, and separate anode and cathode reactions promote the precipitation.

A similar concept was applied in an air-cathode single chamber MFC with real swine wastewater (Ichihashi and Hirooka, 2012). In this study, the system achieved a maximum P removal of 82% due to the high P concentration in the solution (influent TP concentration = 780 mg/L). The struvite was precipitated on the cathode surface only, which confirms that the pH around the cathode is higher than in the entire chamber. The system achieved a maximum effluent pH of 8.23, and this pH is relatively lower than the optimal pH for struvite precipitation pH>8.5(Cusick et al., 2014). Using a single chamber design limits increases in pH and P precipitation.

The previous study was expanded to examine the impact of different ammonium and magnesium concentrations on P recovery and the impact of P precipitation on the cathode electrode performance (Hirooka and Ichihashi, 2013). No precipitates were found when only NH_4 was added to the solution, while cattiite was precipitated when only Mg was added to the solution. Increasing the concentration of NH_4 and Mg increased P precipitation. Lastly, struvite precipitation on the cathode decreased electricity generation and electrode dissolution in Milli-Q water, and the MES buffer was very helpful to increase electrode performance and restore the initial

performance. Struvite purity must be determined in this study because different NH_4 and Mg concentrations were used, and P precipitates as struvite at equal molar ratios of NH_4:Mg:P. Furthermore, COD concertation and COD removal efficiency were not identified, which means the performance of the MFC in COD removal is unknown.

In all the previous studies, single-chamber BESs were adapted to recover P as struvite. Using a single chamber BES, in which anode and cathode electrodes are sharing the electrolyte, leads to pH buffering because the accumulation of the protons (at the anode) and generation of hydroxide ions (at the cathode) occur in the same electrolyte. This configuration buffers the pH and prevents the pH in the cathode from rising, and as a result, little P is precipitated (Kelly and He, 2014). Therefore, a dual-chamber MEC was designed with a fluidised bed reactor cathode to recover P as struvite from anaerobic digester effluent (Cusick et al., 2014). It was suggested that a fluidised bed reactor might enhance P recovery and minimise cathode scaling. The MEC achieved a maximum P removal of 85%, and no scaling on the cathode was observed. However, in this study, the MEC was used only for P recovery, and H_2 production was not studied. Using MEC for concurrent P recovery and H_2 production can reduce the operating costs and the cost of the struvite by using H_2 as a source of energy.

Furthermore, a three-stage MFC/struvite precipitation process was designed to generate electricity and recover P from urine (You et al., 2015). In the first stage, urine was introduced to the MFC to generate electricity and raise the urine pH. In the second stage, struvite was precipitated by adding magnesium to the urine. Struvite was collected in the precipitation tank, and the supernatant was used in the third stage for energy generation and enhanced COD removal. Such a design is suitable for urine only as a substrate, and P recovery might be affected if a different substrate is used. Urine hydrolysis increased urine pH and that enhanced P recovery in the second stage.

Recently, a 3-litre volume BES was designed with three chambers to extract phosphate from sewage sludge (Happe et al., 2016). The study focused on phosphate remobilized from iron phosphate and fluid particle kinetics. The system was operated as an MFC and an MEC and achieved a maximum P recovery of 67%. Applying voltage to the system (MEC) enhanced and accelerated P recovery from sewage

sludge. Methylene blue was used to enhance electron transfer, but applying such a mediator negatively affects the environment. All of these studies confirmed the potential of BESs to concurrently generate energy/produce H_2 and recover P as struvite.

The literature review found that BESs have the potential to be used for concurrent energy generation / H_2 production and P recovery. However, there are still some gaps need to be addressed to improve BES performance. In relate to design configuration, using single chamber BES limits P recovery process due to pH buffering. Therefore, using dual chamber BES will improve P recovery due to the better separation between the anode and cathode. In relate to P recovery, the lack of understanding of the impacts of different operational conditions on energy generation (MFC)/H_2 production (MEC) and P recovery. Understanding these impacts will help to design the system to achieve the optimum P recovery. In relate to struvite crystal size, the lack of understanding of the impacts of the key parameters on struvite size, purity and morphology. Understanding these impacts will help to produce struvite crystals that can be used as an efficient fertiliser. In doing so, this study will contribute in enhancing our understanding of concurrent energy generation / H_2 production and P recovery through BES.

Chapter3

Performance Assessment of Dual-chamber Microbial Fuel Cells

3.0 Performance Assessment of Dual-chamber Microbial Fuel Cells

3.1. Introduction

This chapter presents the general performance analysis of dual-chamber microbial fuel cells for energy generation and P recovery. In addition, different operational conditions were investigated to identify the impact of the operational conditions on MFC performance. The objectives of this chapter are as follows:

- To assess P recovery as struvite in a dual-chamber MFC.

- To understand the mechanisms of P recovery as struvite in a dual-chamber MFC.

- To investigate and evaluate the impacts of different operational conditions on P recovery and energy generation in MFCs and identify the influencing factors.

Wastewater is a rich source of nutrients, such as nitrogen (N) and P, which can be used as an alternative for non-sustainable sources of nutrients. In wastewater treatment, P can be recovered from different waste streams that contain high concentrations of P, such as reject wastewater, digester effluent, and swine wastewater. P recovery can be achieved using several methods, including chemical addition, carbon dioxide stripping, or electrolysis (Jaffer et al., 2002; Cusick et al., 2014; You et al., 2015). Magnesium ammonium phosphate hexahydrate (MAP or struvite) is an efficient slow release fertiliser that is applied on a large scale for crop growth (Güney et al., 2008). The mechanism of struvite precipitation is highly dependent on solution pH (pH > 8). The precipitation occurs in an equimolecular concentration of magnesium (Mg), ammonium (NH_4) and phosphorus (P); and these combine with water to form struvite (Doyle and Parsons, 2002). Generally, P is recovered as struvite using the chemical addition method. However, the chemical addition is a costly process, and the chemicals used to raise the pH can account for up to 97% of the cost of the struvite (Jaffer et al., 2002; Cusick and Logan, 2012). MFCs are an emerging technology; bacteria oxidises the organic matter at the anode (eq. 3.1) and releases electrons and protons. The electrons transfer to the cathode

through the external load and are reduced by the electron acceptor (oxygen) while the protons transfer through the solution. The reduction of oxygen in the cathode chamber results in the production of hydroxide (eq. 3.2), which increases the pH. Recent research findings on MFCs have demonstrated their potential to recover P as struvite (Cusick and Logan, 2012; Ichihashi and Hirooka, 2012; Hirooka and Ichihashi, 2013). P can be recovered exclusively through precipitation in MFCs because P compounds are not involved in electron transfer via reduction—oxidation (REDOX) reactions (Kelly and He, 2014). P recovery as struvite using MFCs involves cathode reactions, whereby water is consumed and hydroxide is generated due to electrons being transferred from the anode to the cathode.

Anode chamber: $CH_3COO^- + 4\,H_2O \rightarrow 2\,HCO_3^- + 9\,H^+ + 8\,e^-$ (3.1)

Cathode chamber: $2H_2O + O_2 + 4\,e^- \rightarrow 4\,OH^-$ (3.2)
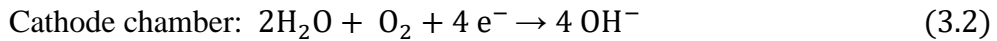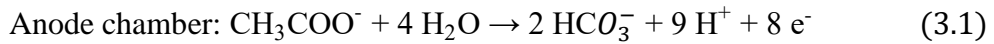
The generation of hydroxide leads to an increase in the pH around the cathode, and P starts to precipitate. P recovery from different wastewater sources has been studied using single-chamber MFCs (Ichihashi and Hirooka, 2012; Hirooka and Ichihashi, 2013; Cusick et al., 2014). Ichihashi and Hirooka (2012) reported that 27% of P was recovered as struvite from swine wastewater in a single-chamber MFC. It was noted that precipitates formed around the cathode, which indicates that the pH around the cathode is higher than at any other point in the MFC. In another study, synthetic wastewater was used in a single-chamber MFC to identify the effect of Mg and NH_4 concentration on P recovery as struvite (Hirooka and Ichihashi, 2013). Dosing ammonium and magnesium for precipitation is essential to form struvite; as the concentrations of NH_4 and Mg increase, more P is precipitated. A 3-stage single-chamber MFC was used to enhance P recovery and COD removal from human urine. P recovery reached 78% and the precipitation was confirmed as struvite (You et al., 2015). Using urine as a substrate enhanced and accelerated the P recovery process due to urea hydrolysis, which increased the pH and created an alkaline environment. From these studies, it has been shown that MFCs have the potential to recover P as struvite from different wastewater sources. However, most of these studies were conducted in single-chamber MFCs, where pH buffering may occur due to the accumulation of protons and hydroxide ions in the same electrolyte; this could limit the P recovery. To overcome this limitation, dual-chamber MFCs are increasingly being used. They have better separation between the anode and cathode chambers,

and this leads to pH splitting, which creates an alkaline environment around the cathode to improve the P recovery process (Kelly and He, 2014). 2-stage dual chamber MFC was operated in the current study to recover P in the form of struvite. In addition, the impacts of different operational conditions on cathode pH are investigated, since P solubility decreases as pH increases. To achieve a steady operation condition for struvite crystallisation, molar ratios, batch duration, and temperature were maintained constant through the study duration.

3.2. Materials and Methods

3.2.1. Reactor Set-up

Two sets of dual-chamber H-type bottles (Adams & Chittenden Scientific Glass, Berkeley, CA, USA) were used to construct the MFCs, with a height of 105 mm and an outer diameter of 95 mm (see Figure 3.1 & 3.2). Each set contained two identical bottles with a volume of 300 mL for each chamber. Both bottles were connected at the middle by a clamp and a sealing ring with an outer diameter of 45 mm. Each chamber contained two ports (each port measured 14 mm in diameter), one at the bottom and one at the top. These ports were fitted with sealing rings for the pH and oxidation-reduction potential (ORP) probes. The anode and cathode electrodes were made of carbon cloth (2.5×5 cm) with a projected area of 25 cm^2 (Fuel Cells Etc, Texas, USA). The cathode contained a Pt catalyst (0.5 mg/cm^2 10% Pt on Carbon Cloth Electrode) to improve cathode performance whilst the anode was plain carbon cloth. Both electrodes were connected with a titanium wire (0.5 mm, purity > 99.98%, Alfa Aesar, Heysham, UK). A Nafion membrane (Nafion 117#, Sigma-Aldrich, London, UK) was placed in the middle of the anode and the cathode chambers. The membrane was pretreated by boiling in H_2O_2 (30%) and deionized water, followed by 0.5 M H_2SO_4 and deionized water, each for 1 h, and thereafter it was stored in deionized water prior to being used. The electrodes were positioned 8 cm apart. The components of the reactor were cleaned before use and the MFCs were maintained at 20 °C in a temperature-controlled room.
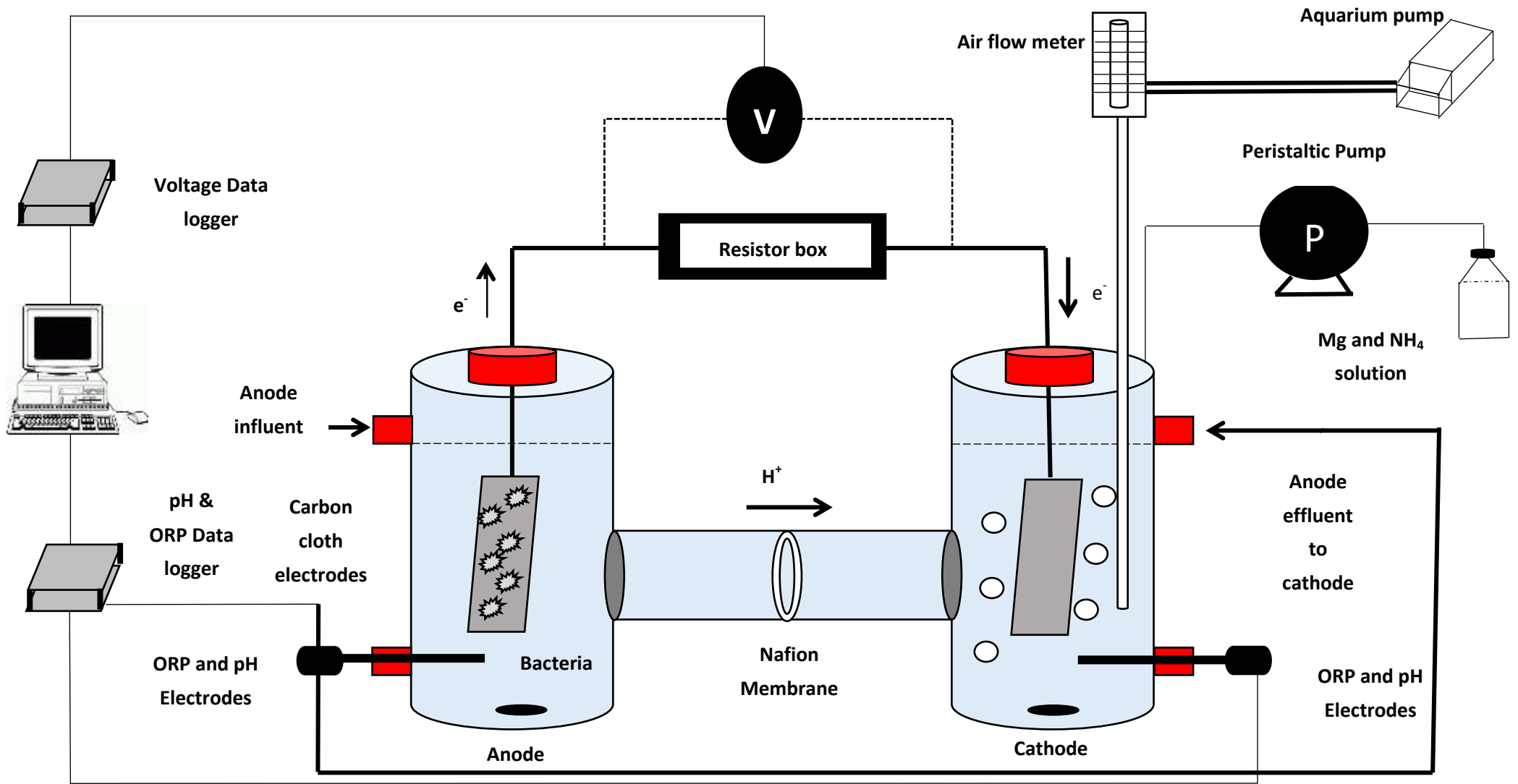
Figure 3.1 Experimental set-up of the dual chamber MFC

3.2.2. Inoculation

Activated sludge flocs and anaerobic digester sludge were collected from the Cardiff wastewater treatment plant (Cardiff, UK). The wastewater treatment is operated by Dwr Cymru Welsh Water Ltd, and it treats domestic wastewater. Samples were collected in 1 L containers and transferred directly to the lab. They were used directly for the inoculation process, during which pure nitrogen gas was used (Logan, 2011). The anode chamber was inoculated with a 1:1 mixture of activated sludge and anolyte medium (containing in (g/L): sodium acetate 3.28 + ammonium chloride 0.31+ potassium chloride 0.13 + sodium phosphate anhydrous monobasic 2.69 + disodium hydrogen phosphate 4.33 + 10 ml of vitamins solution (Ingredient Concentration (per litre): biotin, 0.2 g; folic acid, 0.2 g; pyridoxine HCl, 1 g; riboflavin, 0.5 g; thiamin, 0.5 g; nicotinic acid, 0.5 g; pantothenic acid, 0.5 g; B-12, 0.01 g; p-aminobenzoic acid, 0.5 g; thioctic acid, 0.5 g) + 10 ml of a trace element solution containing (per litre): iron(II) sulfate heptahydrate ($FeSO_4 \cdot 7H_2O$), 1 g; zinc chloride ($ZnCl_2$), 0.07 g; manganese(II) chloride tetrahydrate ($MnCl_2 \cdot 4H_2O$), 0.1 g; boric acid (H_3BO_3), 0.006 g; calcium chloride hexahydrate ($CaCl_2 \cdot 6H_2O$), 0.13 g; copper (II) chloride dihydrate ($CuCl_2 \cdot 2H_2O$), 0.002 g; nickel (II) chloride ($NiCl_2 \cdot 6H_2O$), 0.024 g; sodium molybdate ($Na_2MoO_4 \cdot 2H_2O$), 0.036 g; cobalt(II) chloride ($CoCl_2 \cdot 6H_2O$), 0.238 g). The inoculum was introduced to the cell through the upper sampling port using a syringe. During the inoculation process, a small syringe was used to sparge the media and the headspace with nitrogen.

3.2.3 Sterilisation

All the MFC parts were cleaned properly with soap, rinsed with distilled water three times, and finally dried and wiped. Anodes were left in dionised water for 1 day prior to use. In addition, a sterilisation stage was conducted using autoclave at 121 C° for 30 minutes for any equipment that was used in the MFCs. In addition, the cathode chamber was washed and cleaned after each batch to remove any precipitate and any attached particles.
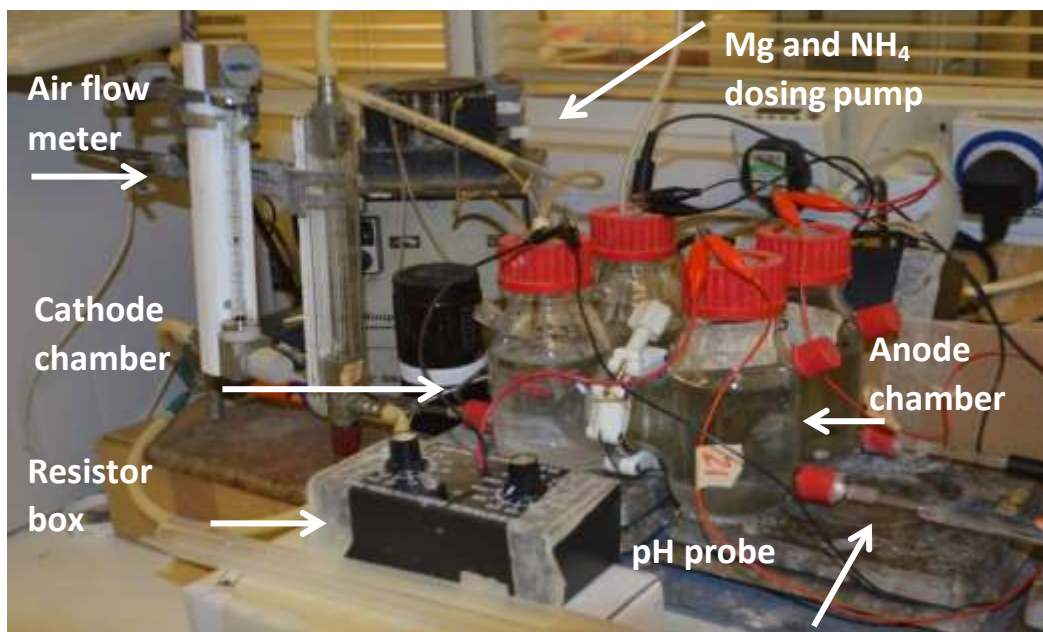
Figure 3.2 Lab experimental set-up of the dual-chamber MFC

3.2.4 Degassing

Pure nitrogen gas (99.9%, BOC Ltd, Cardiff, UK) was used to remove the dissolved oxygen from the media. A small syringe was fitted in the anode chamber, and nitrogen gas was sparged through the solution for 20 minutes.

3.2.5 Start-up

The anode chambers were inoculated with a 1:1 mixture of activated sludge and anolyte medium (containing: acetate, phosphate buffer). A small syringe was used to sparge the media and the headspace with nitrogen during the inoculation and media replacement. The cathode chamber was filled with 50 mM phosphorus buffer, and it was continuously aerated using an aquarium pump. Both electrodes were connected to a 1000 Ω external resistance at the initial stage of the operation. A fresh medium combined with inoculum mixture was used to replace the anolyte when the voltage dropped (Logan, 2011). The replacement procedure was carefully conducted to avoid any distribution of the biofilm.

Once the MFC had achieved stable electricity production for at least three cycles, the phosphorus buffer was discarded, and both chambers were fed with synthetic wastewater. After each cycle, the anode effluent was directed to the cathode chamber, and a new substrate was introduced to the anode. The resistance was

reduced to 470 Ω, where the system produced the maximum power in the polarisation test.

3.2.6 MFC Experimental Design

The MFCs were operated in a 2-stage feed-batch mode at room temperature. In the first stage, the synthetic wastewater was fed to the anode chamber for COD removal. At the end of each cycle (cycle duration = 48 hours), the effluent from the anode chamber was filtered (0.2 um filter, Fisher Scientific, UK) and directed into the cathode chamber (second stage) for P recovery (see Figure 3.1). Anode influent pH was adjusted to pH = 7, and an aquarium pump was used to supply air continuously (50 mL/min) to the cathode chamber in order to provide oxygen as an electron acceptor. Media replacement was carried out in an anaerobic environment to maintain the anaerobic environment for the anode biofilms. The synthetic wastewater contained (0.5-2 g/L depending on the operation condition) sodium acetate; KH_2PO_4, 0.65 g/L; K_2HPO_4, 0.65 g/L; KCl, 0.74 g/L; NaCl, 0.58 g/L; NH_4Cl, 0.375 g/L; $MgSO_4 \cdot 7H_2O$, 0.1 g/L; $CaCl_2 \cdot 2H_2O$, 0.1 g/L; and 0.1 mL/L of a trace element mixture and vitamins.

3.2.7 Anode and cathode sampling

At the end of each batch, anolyte and catholyte were removed from the MFC. Approximately 20 ml of the anolyte and catholyte were collected in small vials and analysed directly.

3.2.8 Analytical Methods

3.2.8.1 Water analysis

All results reported are the average of the two duplicate reactors ± SD. Chemical oxygen demand (COD) analysis was carried out using a Hach Lange kit LCI 400 (HACH, UK). To determine COD concentration, 2 mL of the sample was added to the COD cuvette and digested at 148 C° for two hours. Then, COD values were determined using a DR3900 spectrophotometer (HACH, UK) in accordance with its operating procedures.

COD removal efficiency was calculated using Equation (3.3):

$$\text{COD removal efficiency} = \frac{\text{anode COD influent} - \text{anode COD effluent}}{\text{anode COD influent}} \times 100 \qquad (3.3)$$

Ammonium (NH_4-N) and Orthophosphate concentration were measured using a Hach Lange kit LCK 303 and LCK 049 (HACH, UK). Total phosphorus (TP), magnesium (Mg), calcium (Ca), potassium (K), and sodium (Na) concentration were measured using inductively coupled plasma optical emission spectrometry (ICP-OES), type Perkin Elmer Optima 2100DV apparatus. In addition, anion concentrations were determined using an ion chromatograph (Dinonx ICS-2000 IC).

3.2.8.2. pH and ORP

Anolyte and catholyte pH and ORP were measured continuously every 15 mins during each batch using a 12-channel measuring and monitoring data logger (EA Instruments, London, UK). pH electrodes (refillable glass body, shaft diameter 4.3 mm, 90 mm long) (EA Instruments, London, UK) were fixed in the bottom port of both chambers. ORP electrodes (refillable glass body, diameter 4.3 mm, 90 mm long) (EA Instruments, London, UK) were fixed in the bottom port of both chambers. The pH probes were calibrated before each run. Monitoring the pH will help to monitor the microbial environment and, at the same time, explain the oxidation-reduction reactions and their effect on energy generation and P recovery. Furthermore, ORP was monitored to understand oxidation-reduction reactions in the anolyte and catholyte. ORP readings can be used as an indicator of the reactor's anaerobicity, where negative ORP (-100 to -400 mV) indicates an anaerobic range where no oxygen is present, and positive ORP (+50 mV) indicates the presence of free oxygen (Torres et al., 2008).

3.2.8.3 Polarisation

The MFC was studied under different conditions; at each condition, a polarisation test was conducted manually by varying the external resistance from 10,000 to 10 Ω. At each resistance, the MFC was allowed to adapt to the new resistance for 15 min to obtain a stable voltage reading. The voltage and the current were recorded at each resistance to obtain the polarisation curve.

3.2.9. Phosphorus Precipitation in MFC

The theoretical P concentration in the synthetic wastewater was approximately 8 mM at pH 7. For P precipitation, ammonium chloride and magnesium chloride solutions with the theoretical concentration of 8 mM were pumped into the cathode chamber using a peristaltic pump (Gilson, Middleton, USA). The ammonium and magnesium solution was pumped with a flow rate of 6 mL/day. The flow rate was chosen to achieve a 1:1:1 molar ratio of struvite precipitation NH_4:Mg:P. Before and after each cycle, the cathode chamber was washed with deionised water 3 times, and then cleaned and dried to remove any precipitates attached to the chamber walls. After each precipitation cycle, the used cathode was removed for maintenance and replaced with a new one. Cathode maintenance is essential to remove P precipitates from the cathode surface, as the precipitates reduce cathode performance, and dissolution treatment increases cathode performance to the initial level. At the end of each cycle, the catholyte was filtered using a 0.2 um filter membrane (Fisher Scientific, UK). The precipitate was collected, weighed, and analysed by X-ray diffraction (XRD) and scanning electron microscopy coupled with energy dispersive X-ray spectroscopy (SEM-EDS). The precipitated P in the cathode was calculated using Equation (3.4):

$$\text{Precipitation efficiency } (\%) = \frac{P_{in} - P_{out}}{P_{in}} \times 100 \tag{3.4}$$

where P_{in} is the P concentration in the catholyte influent, P_{out} is the P concentration in the catholyte effluent. In addition, P precipitation rate (g-P/$m^3_{cathode}$-d) was calculated using Equation (Cusick et al., 2014) (3.5):

$$P \text{ precipitation rate } (g\text{-}P/m^3_{cathode}\text{-}d) = P_{\text{filter precipitates}} + P_{\text{attached to cathode}} =$$

$$\frac{P_{\text{weight in the filter}}}{V_{cathode} \times \Delta t} + \frac{\Delta TP_{\text{dissoultion solution}} \times V_{\text{dissoultion solution}}}{V_{cathode} \times \Delta t} \tag{3.5}$$

where $P_{\text{filter precipitates}}$ is the P which is collected through catholyte filtration, and $P_{\text{attached to cathode}}$ is the P that is attached to the electrode, $P_{\text{weight in the filter}}$ is the mass of P in the captured struvite in the filter (g), $V_{cathode}$ is the volume of cathode chamber (m^3), $\Delta TP_{\text{dissolution solution}}$ is the difference in P concentration (before adding the electrode and after adding the electrode) of the dissolution solution (g/m^3),

$V_{dissoultion\ solution}$ is the volume of dissolution solution (m^3), and Δt is the batch duration (d).

3.2.10 Precipitation test without MFC operation

Prior to the start of the experiment, checks were conducted to confirm that P cannot be precipitated without an MFC. A small beaker filled with the same synthetic wastewater (pH = 7 and 8 mM of P) and the same concentration of ammonium chloride and magnesium chloride was pumped into the beaker at the same rate (6 mL/day) to achieve a molar ratio of (1:1:1). No precipitates were observed anywhere in the beaker during the operation time, and the pH remained constant. Thereafter, solution pH was gradually increased using 1 M NaOH. Precipitation started to occur when the pH reached 7.58.

3.2.11 Scanning electron microscopy (SEM) and energy dispersive X-ray spectrometry (EDX) analysis

For SEM analysis, precipitates that had accumulated on the cathodes and had been captured in the filter were analysed to examine the crystals' morphology as well as the elemental composition. In addition, the used proton exchange membrane (PEM) was cut into pieces, carefully rinsed with deionized water, and finally dried completely at ambient temperature. The microscopic structure and elemental components of the PEM surface were analysed using FEI-XL30 Environmental SEM equipped with an EDX.

3.2.12 Crystal quality, composition, and purity

The quality of the collected crystals was determined by analysing the crystals' composition and purity. Approximately 0.05 g of crystals were dissolved in 50 mL of a 0.5% nitric acid solution. In order to accelerate the dissolution, the samples were stirred with a magnetic stirrer for 24 hours, after which, samples were analysed for magnesium, ammonia, ortho-phosphate, calcium, aluminium and iron using inductive coupled plasma (ICP) (Fattah et al., 2008).

3.2.13 Cathode maintenance

After each batch, the cathode electrode was removed from the MFC for maintenance and replaced with a new electrode. P precipitation on the cathode was removed by immersion in the dissolution solution. The electrode was immersed 3 times in deionised water (pH=7) each time for 2 days. After the deionised water dissolution, the electrode was immersed again 3 times in an MES buffer ($C_6H_{13}NO_4S$ [MES]:10 mM, adjusted to pH 5.5 with NaOH) each time for 30 hours. Finally, the electrode was rinsed and dried before use (Hirooka and Ichihashi, 2013).

3.2.14 Voltage data loggers

The voltage across the external resistance was recorded every 15 min using an ADC-20 data logger system (Pico Technology, UK), which was connected to a computer using a BS32 high-resolution analogue cable (Pico Technology, UK). Based on the recorded voltage, the current and power were calculated using the following equations:

- Current

Current was calculated using Ohms law:

$$E = IR_{ext} \tag{3.6}$$

Current density:

$$I_{anode} = \frac{E}{A_{anode} * R} \tag{3.7}$$

where I_{anode} is the current density (A/m^2), E is the cell potential in volts (V), R is the external load in ohms (Ω), and A_{anode} (m^2) is the projected anode surface area (25 cm^2).

- Power

The power was calculated using the equation:

$$P = \frac{E^2}{R} \tag{3.8}$$

49

Power density

$$P_{anode} = \frac{E^2}{A_{anode} * R} \qquad (3.9)$$

Volumetric power density can be calculated by:

$$P = \frac{E^2}{V_{cell} * R} \qquad (3.10)$$

where E is the cell potential in volts (V), R is the extrnal load in ohms, and V_{cell} is the anode volume (m^3).

- Coulombic efficiency (CE)

CE was calculated by integrating the measured current relative to the theoretical current.

$$CE = \frac{M_s \int_0^t I \, dt}{F \, b_{es} V_{anode} \, \Delta COD} \qquad (3.11)$$

where M_s is the molecular mass of substrate, I is the current in amperes, F is Faraday's constant, b_{es} is a number of electrons exchanged per mole of reactant, V_{anode} is the volume of anode chamber in litres, and ΔCOD is the change in COD concentration over the time t.

3.2.15 Statistical Analyses

Statistical analyses were performed using Spearman's rank correlation coefficient analysis to determine any correlation between the different operational conditions and the monitored parameters (Coulombic efficiency, average current density, precipitation efficiency, and cathode pH). Spearman's rank correlation coefficient analysis was used because the data set was not normally distributed. All statistical analyses were performed using SPSS Software. In particular, understanding the correlation between the operational parameters and the MFC performance (coulombic efficiency, average current density, precipitation efficiency and cathode pH) will help to enhance our understanding of maximising P recovery and energy generation in MFCs.

3. 3 Results and Discussion

3.3.1 MFC general performance

During the start-up period for approximately 23 days, stable electricity production was achieved in the MFC (Figure 3.3). After the start-up period, the MFC was operated without any dosing of Mg and NH_4 in the cathode chamber, to let the MFC adapt to the conditions. The resistance was reduced to 470 Ω where the system produced the maximum power in the polarisation test. At the beginning of each batch (batch duration = 48 h), electricity production peaked with a current density and decreased with time until the end of each batch. The maximum output voltage of the MFC at the beginning of each batch under different COD (0.3, 0.7, 1, 1.5 and 1.7 g/L) was 244, 266, 316, 361, and 380 mV respectively. As the COD (acetate) increased from 0.7 g/L to 1.5 g/l, the output voltage increased from 266 mV to 361 mV. The electricity was generated due to the consumption of the acetate in the substrate; therefore, low substrate concentration in the anode results in poor current density. A positive correlation was observed between COD and the generated voltage in the MFC.
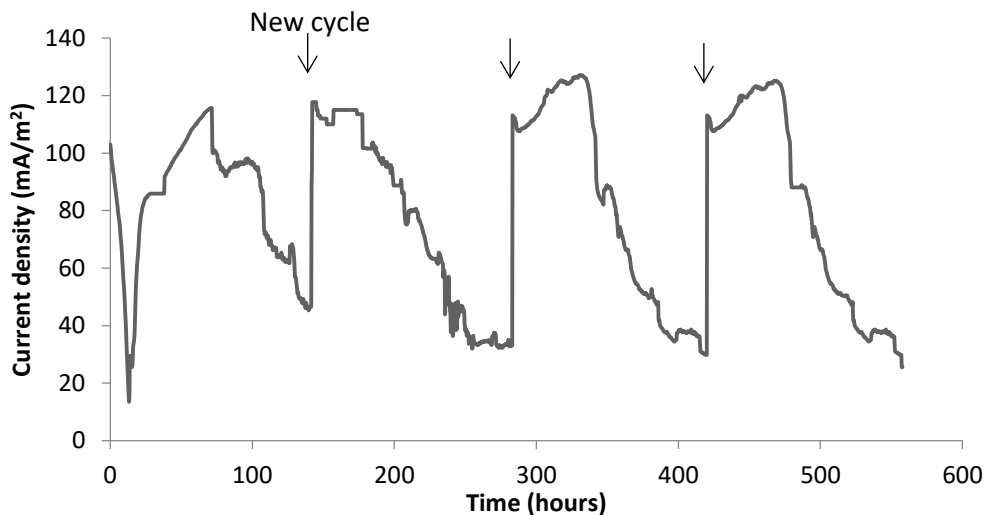
Figure 3.3 Electricity production at the start-up period (arrow for new cycle)

3.3.2. COD Removal and Coulombic Efficiency

The system was operated at five different COD (0.3, 0.7, 1.0, 1.5 and 1.7 g/L). Samples were collected from the influent and anode effluent during each batch for

COD analysis. The COD removal process occurred in the anode chamber, and COD removal efficiency ranging from 70% to 90% was achieved. At low COD, the average removal efficiency was 90%, and at high COD, the average removal efficiency was 70% (Figure 3.4). The electroactive bacteria degraded and consumed the COD (organic matter) to generate energy.

Some of the anaerobic treatment technologies are considered ineffective in treating low strength wastewater, but based on these results, the MFCs showed their ability to treat low strength wastewater (Katuri et al., 2011). Similar results were reported by Zhang et al. (2015) where an MFC was able to treat low strength wastewater. Furthermore, it was observed that increasing influent COD decreased COD removal efficiency; the higher the COD (substrate concentration), the longer the period of time needed to fully degrade the substrate, and in this study, the batch cycle duration was fixed (48 hrs), which might affect the COD removal efficiency. To obtain good removal efficiency in the MFC, cycle duration should be reasonable to reduce the COD level < 0.1-0.2 g/L. Furthermore, linear regression analysis was conducted to identify the correlation between COD removal and the coulomb (quantity of electrons; calculated by integrating the current over the time from the beginning till the end of each batch). The result showed that there was no clear correlation between COD removal and coulomb (R^2 for linear regression = 0.157). There are many reasons behind this, as COD could be removed via different reactions, such as aerobic oxidation due to air diffusion and methanogenesis. The results showed that MFCs are able to reduce COD (as acetate) and generate electricity.
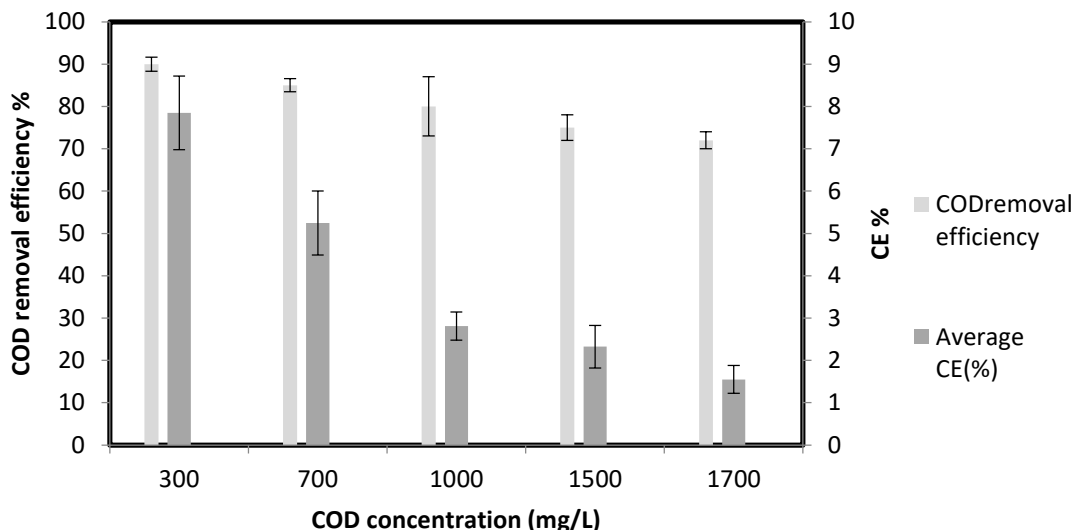
Figure 3.4 The impact of COD concentration on COD removal efficiency and CE.

In terms of coulombic efficiency, CE was calculated based on the COD concentration using eq (3.11). The MFC coulombic efficiency ranged from 1.1% at (COD = 1.7 g/L) to 10% at (COD = 0.3 g/L). Thus, the coulombic efficiency during the study period was low. Low coulombic efficiency showed that the electron transfer bacteria was not able to convert all the available organics into electricity. Most of the substrate was consumed either by aerobic digestion due to oxygen diffusion through the membrane or by methanogenesis (He et al., 2005). Similar findings were reported by Katuri et al. (2011), where a dual chamber MFC was operated and a very low CE ($<$1%) was obtained.

Furthermore, increases in the cathode pH due to hydroxide generation lead to a decrease in electricity generation, which then reduces the coulombic efficiency (Cheng and Logan, 2011b). The coulombic efficiency can be improved by using a better configuration of the dual chamber MFC, where H-shape type BES is known to be a low-efficiency system due to the limited surface area for ion exchange membranes and the long distance between electrodes (Zhang and He, 2012). In addition, the diffusion of oxygen from the cathode chamber could decrease the coulombic efficiency where oxygen could work as an electron acceptor in the anode chamber. A negative correlation was observed between coulombic efficiency and COD. Similar findings were reported by Sleutels et al. (2011), where it was noted that increasing the substrate concentration leads to a reduction in the coulombic

efficiency. This result demonstrates that COD is an important factor for obtaining high coulombic efficiency and energy generation in MFCs.

3.3.3. Water analysis in the anode chamber

Water quality parameters (NH_4^+, NO_3^-, NO_2^- and TP) were analysed in the influent and effluent of the anode chamber. The concentration of TP in the anode effluent did not decrease and was similar to or slightly higher than the concentration of TP in the synthetic wastewater (influent), since the anode chamber was operated under an anaerobic environment and as a result of low reduction-oxidation reactions in the MFC, which would motivate the release of the stored phosphate in the bacteria (Kim, 2006; Tao et al., 2014). The removal of P in the cathode chamber is discussed in section 3.3.4.

Ammonium concentration in anode influent was 1.2 mM of NH_4^+- N. Generally in a dual-chamber MFC, ammonium concentration in the anode chamber decreases due to microbial consumption and ammonium diffusion to the cathode chamber through Nafion 117 to compensate for charge balances between the anode and cathode chambers (concentration gradient) (Cord-Ruwisch et al., 2011). However, in this study, ammonium concentration in the effluent was similar or slightly higher than the influent concentration, and this increment was due to ammonium chloride dosing in the cathode chamber. In the cathode chamber, 8 mM of ammonium chloride and magnesium chloride were dosed to achieve a molar ratio of P:Mg:NH_4 (1:1:1) for P recovery and a high concentration in the cathode chamber led to the diffusion of ammonium from the cathode to the anode, which was induced by a concentration gradient. Similar phenomena occurred in a dual-chamber MFC that was designed for the removal of ammonium and odour from swine wastewater (Kim et al., 2008).

On the other hand, nitrate (NO_3^-) and nitrite (NO_2^-) concentrations in the anode influent were 0 and 0.01 mg/L respectively. The concentrations of nitrate and nitrite in the anode effluent were nearly the same as those of the anode influent. However, at a high aeration flow rate, nitrate and nitrite concentrations increased from 0 to 14 ± 4 mg/L and $0.01\pm$ to 0.03 ± 0.01 mg/L respectively, and this increase occurred due to oxygen diffusion to the anode chamber through the cathode.

3.3.4. Phosphorus Recovery in Dual Chamber MFC

When the synthetic wastewater is introduced into the anode chamber, the bacteria starts to degrade the organic matter. As a result, electrons and protons are released, and electroactive bacteria transfer the electrons to the anode and then to the cathode through the external resistance. Current is generated during the transfer of electrons from the anode to the cathode. The effluent from the anode chamber was filtered and directed to the cathode chamber.

Phosphorus can be removed via two main mechanisms: biological removal or physical-chemical removal. In this study, P was removed and recovered only via chemical precipitation in the cathode chamber, and the biological mechanism was eliminated because bacteria exist in the anode chamber, but not in the cathode chamber. In the cathode, water is consumed, and hydroxide is generated; this increases the pH around the cathode electrode (pH > 8). Since the solubility of P is strongly influenced by solution pH, therefore, the solubility of P decreased when the pH increased; then, precipitates around the cathode were observed after a short period of adding Mg and NH_4 solution to the cathode chamber. The cathode effluent was filtered at the end of each batch, and the precipitations were collected, weighed, and analysed using XRD and SEM.

P precipitates were found on the inner wall of the cathode chamber, on the cathode electrode surface, suspended in the solution, and at the bottom of the chamber. To identify the morphology and the composition of the precipitates, XRD and SEM-EDS were used. XRD analysis showed that the precipitation had a similar pattern to the pattern of struvite (Figure 3.5), where it was found that most of the peaks matched with the model for struvite standard. In addition, SEM analysis showed that the recovered particles had tubular-shaped crystals (Figure 3.6) and by comparing the morphology of the precipitates and struvite standard, it was observed that both samples have similar morphology. The majority of the precipitates was formed of fine, white particles. EDX analysis showed that the main components of the analysis were P, O, and Mg, which are the main components of struvite. Furthermore, the composition of the precipitates as identified through the dissolution method showed that the molar ratio of Mg:P was approximately 1:1. This can confirm that the precipitated struvite had a similar molar ratio to that of the struvite standard.
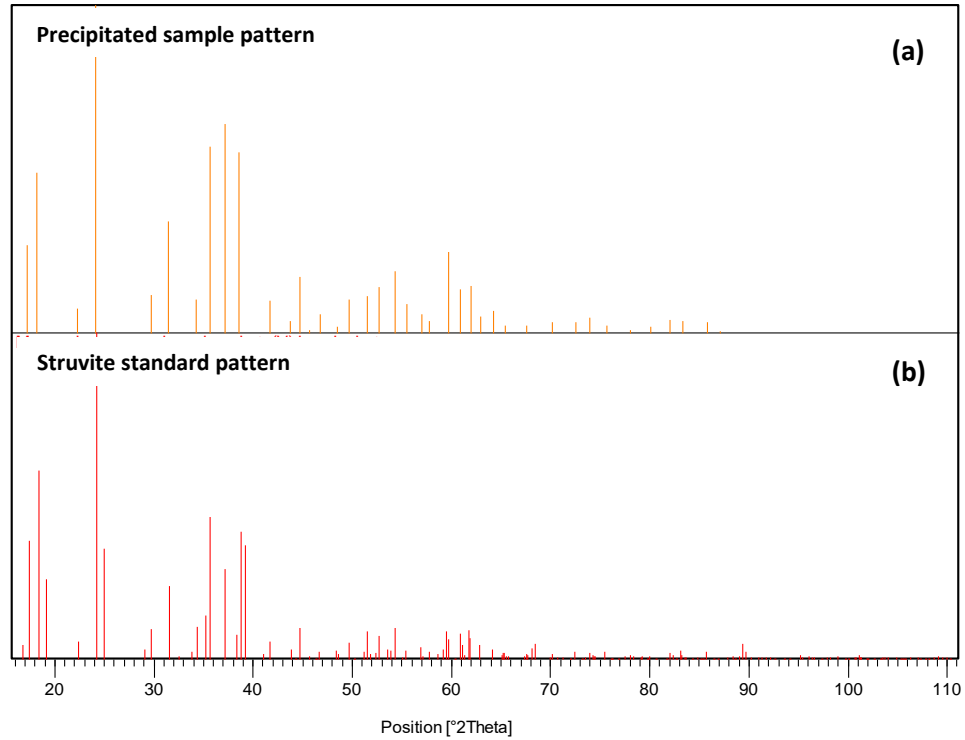
Figure 3.5 XRD patterns of precipitates in the cathode chamber, (**a**) precipitated sample and (**b**) magnesium ammonium phosphate standard.

When the anode effluent was directed to the cathode chamber, P recovery process occurred, and P started to precipitate. It was found that P started to precipitate in the catholyte and on the cathode surface. The current density was negatively affected by P precipitates at the cathode chamber, where low current density (62 mA/m^2) was observed with high P precipitates. The high P precipitates on the cathode electrode obstructed the mass transfer of ions and oxygen, and as a result, low current was observed (Hirooka and Ichihashi, 2013).

P was recovered in the dual chamber MFC as magnesium ammonium phosphate hexahydrate (struvite) at the cathode chamber, by dosing 8 mM of NH$_4$Cl and MgCl$_2$ (0.76 g/L and 0.42 g/L, respectively) to achieve a molar ratio (Mg: NH$_4$: P: 1:1:1).
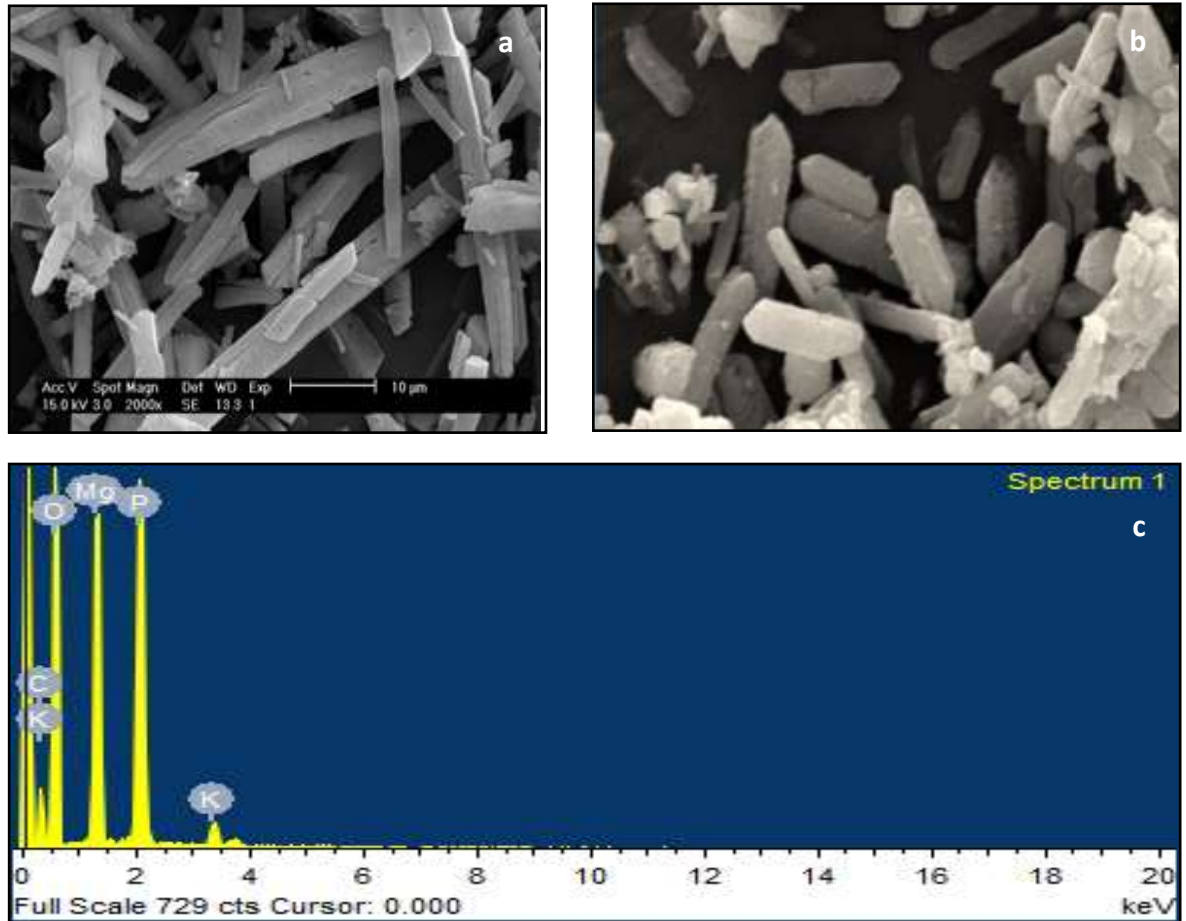
Figure 3.6 (a) SEM images of the of typical struvite crystals (Le Corre et al, 2007), (b) precipitates recovered at the MFC, and (c) EDS analysis of the precipitates' components.

3.3.5. Electricity generation and the effect of struvite precipitation on the MFC performance.

The effect of struvite precipitation on the MFC performance was monitored through the generated energy and through P concentration during cathode maintenance. After each cycle, the cathode electrode was removed from the MFC and immersed in the dissolution solutions to remove any P precipitates on the surface. Throughout the dissolution processes, P concentration was measured at each stage to quantify the concentration of P on the cathode electrode. Increased precipitation of P caused a reduction in the generated energy and a decrease in the average current density (Figure 3.7).

The results showed that due to the high pH around the cathode electrode at high COD, more P was precipitated (Figure 3.7). Table 3.1 shows the mass and the percentage of P in each part of the MFC at COD= 1 g/L. The results showed that the majority of struvite was attached to the electrode due to the high pH around the

electrode. Similar results were found by Ichihashi and Hirooka (2012) where 30% of P was precipitated on the cathode electrode.
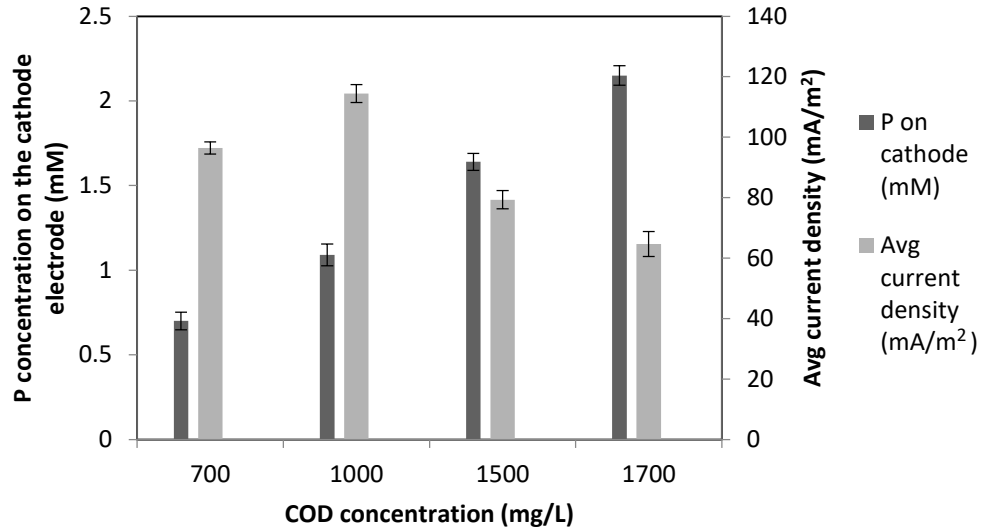
Figure 3.7 The effect of P precipitation on the cathode surface

On the other hand, after a long-term operation, the PEM in MFCs was affected by the precipitates. PEM is another important factor that has an impact on MFC performance, where the membrane resistance makes a contribution to the total internal resistance of the MFC. Therefore, membrane fouling and increased membrane resistance can lead also to a deterioration of the MFC performance (Xu et al., 2012).

Table 3.1 Cathode mass balance of P in MFC 1 and MFC 2

			Accumulation		
Unit	Influent	Effluent	Cathode chamber	Cathode electrode	Cell wall & membrane
	mg (%)	mg (%)	mg (%)	mg (%)	mg (%)
MFC 1 P	44.9 (100)	10.6 (22.6)	15.3(33)	20.2(41.4)	1.3(3)
MFC 2 P	47.3(100)	12.7(25.8)	11.7(24.7)	22(47.5)	1(2)

SEM and EDS analysis were used to identify the differences in the morphology and components between a new PEM and the used PEM in the MFC. SEM pictures

(Figure 3.8) showed that the surface of the new PEM was smooth and clear without any particles on the surface, and the main components of the new PEM were oxygen, carbon, fluoride, and sulphur. In contrast, the SEM image of the used PEM contained many small particles with different shapes on the surface. The EDX analysis showed that the PEM contained phosphorus, magnesium, and calcium precipitations, which were mainly precipitated during the operation time. These results confirmed that some of the struvite particles were attached to the PEM surface. The precipitation of these particles and salts during the long-term operation of the MFC would lead to a deterioration in the MFC performance. In addition, these particles on the PEM surface will lead to the blockage of cations transfer through the membrane and subsequently cause the decay of the current (Xu et al., 2012).
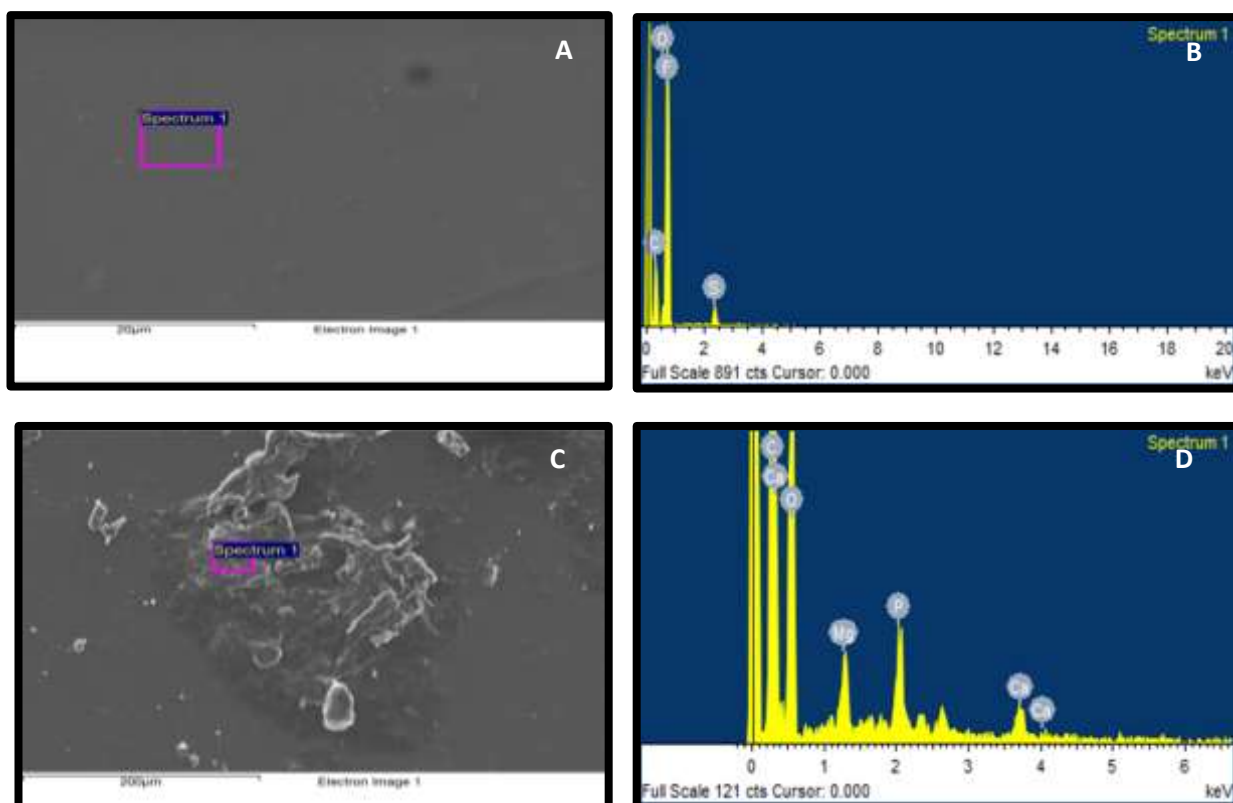
Figure 3.8 (A&B) SEM image and EDX spectrum for the new PEM, and (C&D) the used PEM.

3.3.6. Performance of the MFC in recovering P under various conditions

The performance of MFCs can be influenced by different operational parameters, such as COD concentration, solution volume, catholyte aeration flow rate, and external resistance. It is therefore very important to understand the impact of these parameters on MFC performance and cathode pH. The influence of COD, electrolyte

volume, cathode aeration flow rate and external resistance on MFCs for electricity generation, has been studied (Aelterman et al., 2008; Jadhav and Ghangrekar, 2009; Nam et al., 2010; Cheng and Logan, 2011b). In general, the studies show that increasing COD, anolyte volume, and cathode aeration leads to increase energy generation. Furthermore, increasing external resistance leads to a reduction in the generated current in the system; however, the influence of these parameters on P recovery has not been investigated. As P solubility is dependent on solution pH, therefore, the focus in the following section will be the impact of the operational condition on cathode pH and P recovery. Each mode of operation was maintained long enough to ensure a steady state performance.

3.3.6.1 P recovery at different substrate concentrations

Different COD were used to identify the impacts of COD on P recovery and energy generation. The COD at the anode chamber varied from 0.3 to 1.7 g/L (organic loading rate = 0.15 to 0.85 g COD/L/day). It was observed that increasing the substrate COD leads to increased precipitation efficiency at the cathode chamber (Figure 3.9A). As the COD increased from 0.3 g/L to 1.7 g/L, precipitation efficiency increased from 9% to 90%. Increasing COD leads to an increase in the transfer of electrons from the anode to the cathode chamber. This implies that more electrons are available at the cathode for oxygen reduction reactions; this, in turn, facilitates struvite formation. Increased oxygen reduction reactions at the cathode led to increases in the generation of hydroxide ions, which increased the pH to >8 at the cathode (Figure 3.9B). It was noted that cathode pH increased as COD increased. The average cathode pH increased from 7.3 at COD = 0.3 g/L to 8.9 at COD = 1.7 g/L. Energy generation was negatively affected by P precipitation in the cathode chamber.

As COD increased, more precipitates on the cathode were observed. The average current density decreased with increasing COD, and this reduction probably due to the precipitate on the cathode surface (Figure 3.10A). The precipitate on the cathode covered the surface area of the cathode, and this might obstruct the mass transfer of ions and oxygen. This finding is consistent with the finding of Hirooka and Ichihashi (2013), which showed that the electricity generated by MFCs with precipitate was lower than that of MFCs without precipitate. However, the average current density of

COD = 0.3 g/L was smaller than the average of the current density of COD=0.7 g/L, because at both COD concentrations, the amount of P precipitate was small compared to the other concentrations; therefore, MFC performance at COD= 0.7 g/L was better than at COD=0.3 g/L.

Similarly, as influent COD increased at the anode, anode oxidation reactions increased (Figure 3.10B). This implies that organic matter degradation increases due to substrate availability for the microorganism. As a result of the organic matter degradation, electrons are liberated and transferred from the anode to the cathode (Logan et al., 2006)
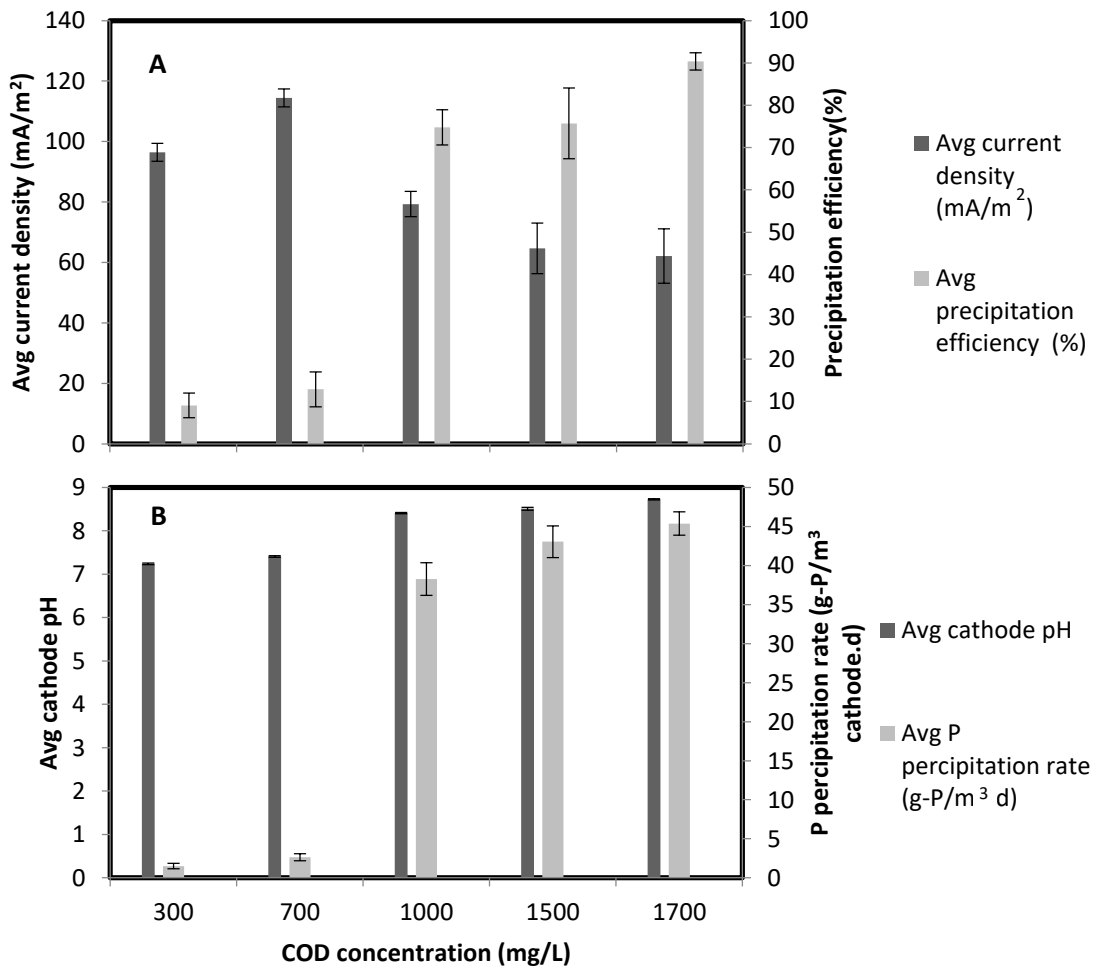
Figure 3.9 (a) The impact of COD on average current density and precipitation efficiency,
(b) the impact of COD on average cathode pH and precipitation rate.

Figure (3.10) shows the difference in average current density, ORP, and cathode pH between three different COD. During substrate concentration of (COD = 0.7 g/L), the average current density achieved was 115 mA/m^2, and the average cathode pH was

7.4. A small amount of struvite was precipitated in the cathode chamber (2.64±0.4 g-P/m³.d). During substrate concentration of (COD = 1 g/L), the average current density decreased significantly compared to (COD = 0.7 g/L), where average cathode pH increased to 8.41, and the struvite precipitate rate increased to 38±2 g-P/m³.d. During substrate concentration of (COD = 1.5 g/L), the decrease in current density was significantly greater and this probably due to the increased amount of precipitate on the cathode electrode, where the average cathode pH increased and peaked at 8.7 (Figure 3.9B).
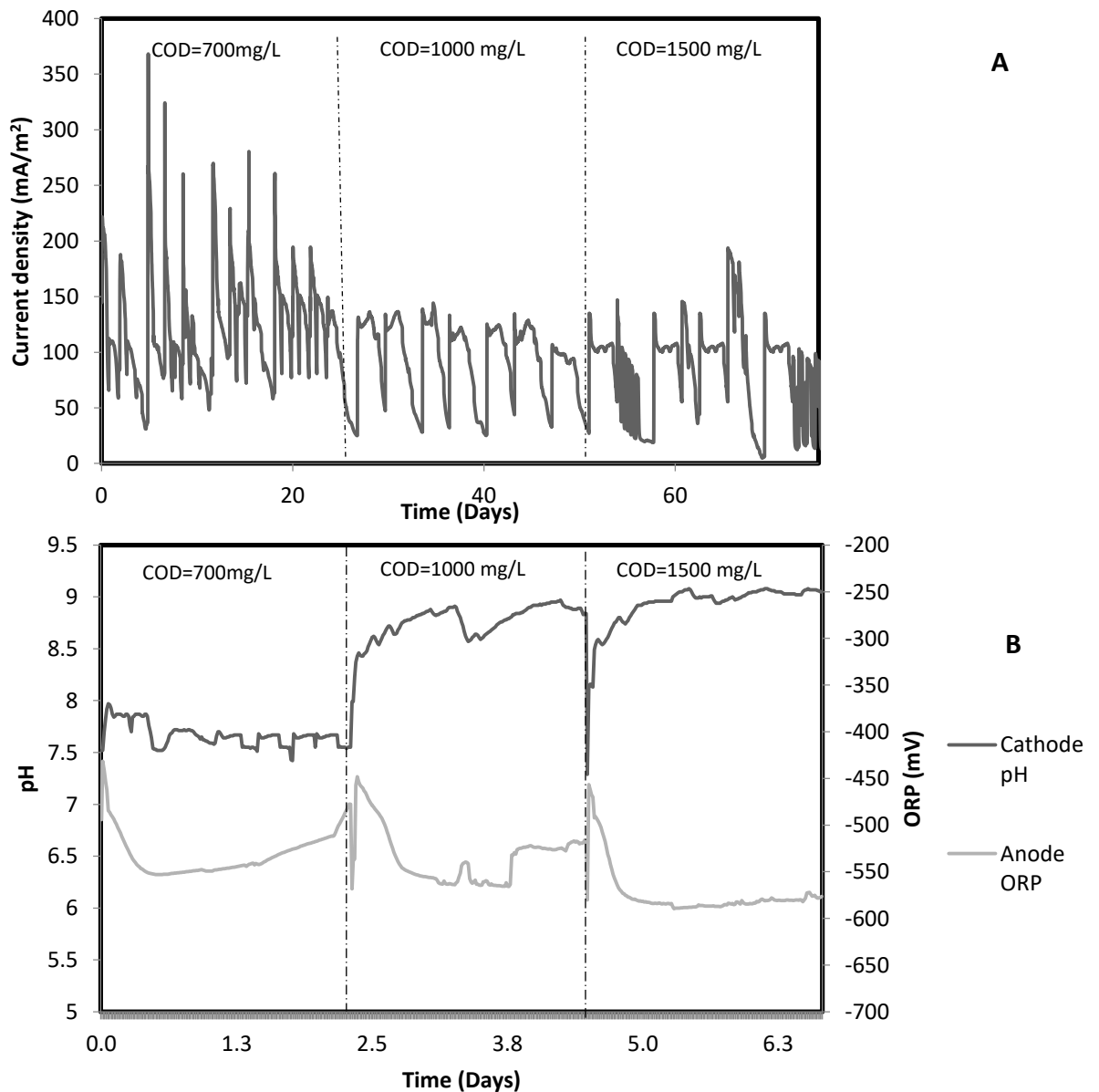
Figure 3.10 The impact of COD on (A) current density, (B) cathode pH and anode ORP (a representative cycle of each COD concentration).

The MFC achieved a maximum struvite precipitate rate of 43 ± 2 g-P/m^3.d. These results imply that the greater the amount of precipitate at the cathode, the less energy that is generated by the MFC.

In addition, increasing the COD concertation led to increases in the oxidation reaction in the anode, and as a result, low (pH 5-6) was observed at the anode chamber. Low anode pH is accompanied by low electricity generation. This result is in agreement with the results reported by Behera and Ghangrekar (2016), where low current was observed at a low pH environment (pH=5-6).

3.3.6.2. P recovery at different anode and cathode volumes

Electrolyte volume is another important parameter for P recovery. Three different volumes (180, 225, and 270 mL) were used to investigate the impact of anode and cathode volumes on P recovery and energy generation (operational condition: COD= 700 mg/L, aeration flow rate = 50 mL/min and resistor = 470 Ω). The volumes were chosen based on the volume of the chamber and the electrode surface area.

Increasing the electrolyte volume leads to increases in the amount of P precipitated. The greater the volume of synthetic wastewater available at the anode, the more substrate that there is available for the bacteria to be oxidised. By increasing the anode chamber volume, more organic matter is offered for the organism at the anode for oxidation, and consequently; more reduction reactions occur at the cathode. In addition, the greater the volume of synthetic wastewater available at the cathode, the more P that can be recovered from the solution. However, the impact of electrolyte volume on cathode pH was not significant, as cathode pH at all volumes was very similar.

The average current density output of the MFC under three different volumes (180, 225, 270 mL) was 113, 110 and 100 mA/m^2 respectively. Increasing the anode chamber volume from 180 mL to 270 mL led to a reduction in the average current density from 113 mA/m^2 to 100 mA/m^2. The reduction in current density probably occurred due to the amount of P precipitate in 270 mL, which was greater than 180 mL. Furthermore, increasing in the electrolyte volumes and maintaining anodes and cathodes electrode surface area led to a decrease in the generated energy because there was insufficient electrode surface area for capturing all the substrate as electrical current (Logan et al., 2015). The anode and cathode volumes have an

impact on energy generation, as increasing the volume leads to a reduction in the average current density (Figure 3.11).
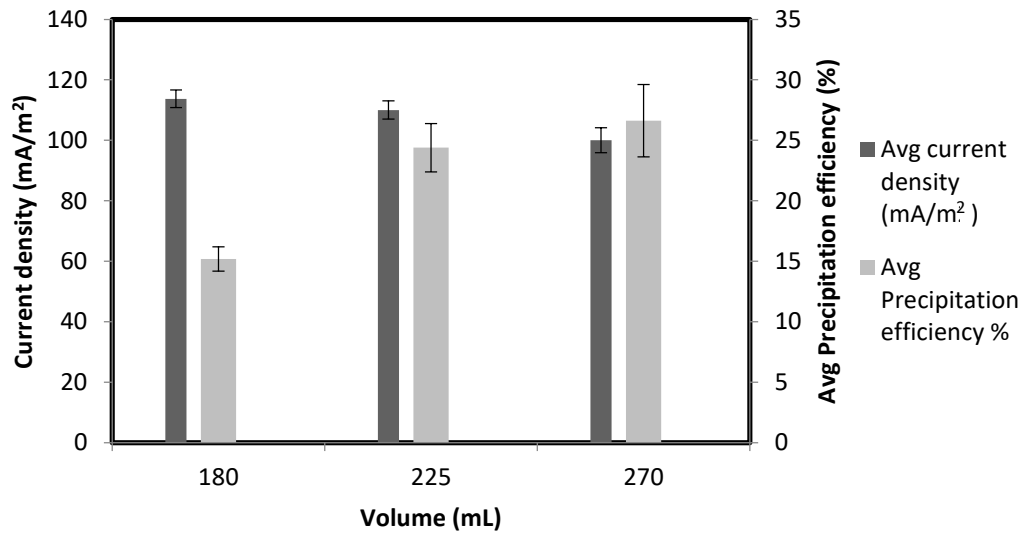
Figure 3.11 Maximum current density and precipitation efficiency % at different electrolyte volumes.

In terms of COD removal efficiency, the impact of anode and cathode volume on COD removal efficiency was not significant, and the removal efficiency of the MFC at all electrolyte volumes was almost the same.

3.3.6.3. P Recovery at different aeration flow rates at the cathode

Cathode aeration is an important parameter for system optimisation. The MFCs were operated under different controlled aeration flow rates, and these rates were used to examine the impact of aeration flow rate on both energy generation and P recovery (COD= 1000 mg/L and resistor = 470 Ω). Identifying the impacts of aeration flow rates on MFC performance is important for scaling up the system and assessing the operational cost. Previous studies have shown that cathode aeration has a great impact on energy generation, where the current increased as the cathode dissolved oxygen (DO) concentration increased. These results show the importance of supplying the optimal amount of oxygen to obtain the optimal performance of the MFC (Mashkour and Rahimnejad, 2015). The average current density of the MFC under five different aeration flow rates (no aeration, 10, 50, 150, and 250 mL/min) was 92, 110, 127, 155, and 160 mA/m^2 respectively (Figure 3.12). The result showed that there was a significant ($P < 0.05$) correlation between aeration flow rate and

average current density (R^2 for linear regression = 0.86). Applying aeration in the cathode chamber with a flow rate of (150 mL/min) increased the average current density by more than 40% (from 92 at no aeration to 155 mA/m^2) (Figure 3.12); as a result, the generated power was increased. These findings were in agreement with similar findings by Mashkour and Rahimnejad (2015).
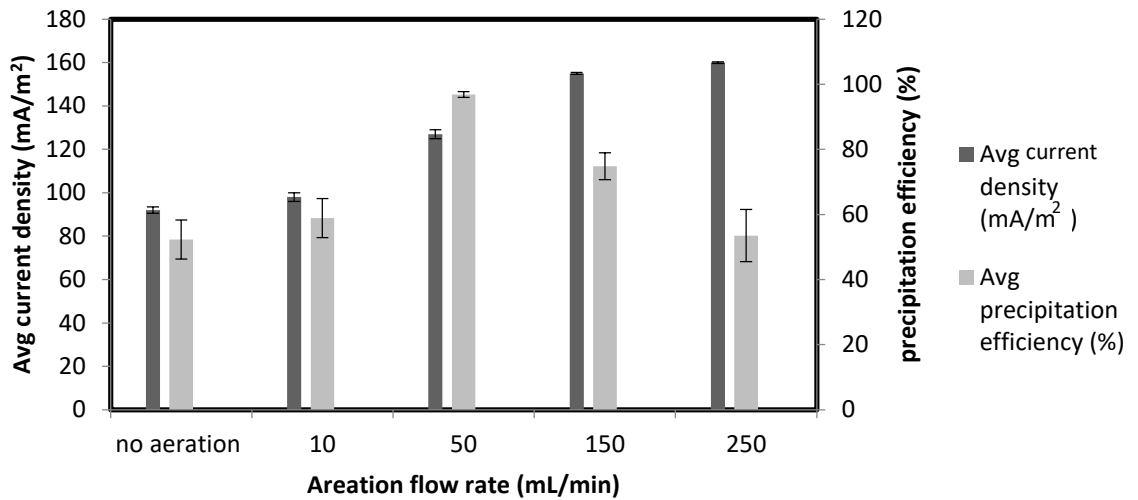
Figure 3.12 The impact of aeration flow rate on energy generation and P recovery.

With regard to P recovery, it was found that increasing the aeration flow rate at the cathode leads to an increase in cathode pH, where oxygen is being used as an electron acceptor and hydroxide ions are produced (Kelly and He, 2014). With 50 mL/min aeration flow rate, cathode pH reached 8.5, which was optimal for P recovery as struvite; whereas with no aeration, cathode pH reached 7.5 (Figure 3.13). However, increasing the cathode aeration flow rate to 150 mL/min leads to a reduction in precipitation efficiency. At a continuous high aeration flow rate, ammonia concentration might be affected and reduced due to ammonium volatilization, which leads to a reduction in the molar ratio between NH_4:P:Mg; as a result, there is a reduction in P recovery (Rahman et al., 2014). However, there was an increase of 25% in power density when the aeration flow rate was increased from 50 to 150 mL/min. These results show that passive or low aeration cannot supply enough oxygen for the protons that had been transferred from the anode chamber. These findings also show that cathode aeration is an influencing factor for energy generation and P recovery.

On the other hand, aeration flow rate had a significant effect on CE ($P < 0.05$), where increasing the aeration flow rate decreased the CE (R^2 for linear regression = 0.75). However, there was no clear correlation between aeration flow rate and COD removal efficiency. Nonetheless, when comparing COD removal efficiency between the aerated cathode and the nonaerated cathode, the COD removal efficiency of the aerated cathode was better than that of the nonaerated cathode. Due to the insufficient aeration in the cathode chamber, an accumulation of protons (H^+) occurred, which could affect the consumption of acetate in the anode chamber. In addition, sufficient aeration in the cathode chamber promotes the reduction reaction by consuming the protons, which enhances the MFC performance (Rahimnejad et al., 2015).
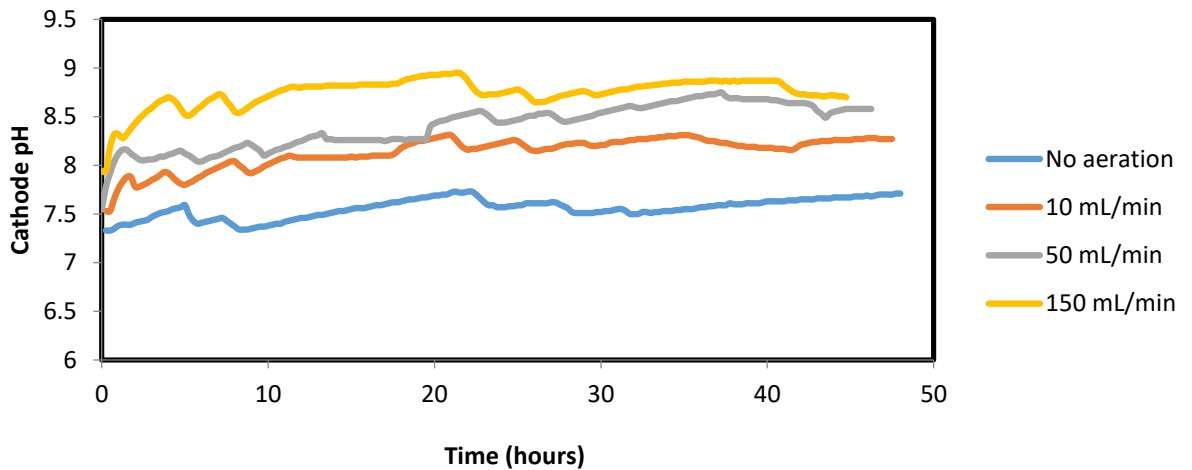
Figure 3.13 The impact of aeration flow rate on cathode pH.

3.3.6.4. P recovery at different external resistance

The MFCs were operated with different external resistance across the anode and cathode using synthetic wastewater with COD of 1000 mg/L. Each mode of operation was maintained long enough to ensure a steady state performance, which was evaluated based on MFC output voltage. It was noticed that increasing external resistance led to a reduction in the generated current (Figure 3.14). When external resistance was increased from 100 Ω to 470 Ω, a sudden drop in the current occurred, and then the current stabilised after some time. The same trend occurred again when the resistance was increased from 470 Ω to 1000 Ω. In addition, CE was affected by external resistance, as increases in external resistance reduce the rate of electron transfer to the anode, resulting in a decrease in current. This result showed that there

66

was a significant (P < 0.05) negative correlation between external resistance and coulombic efficiency (R^2 for linear regression = 0.74).

On the other hand, the effect on P precipitation of increasing external resistance from 100 Ω to 470 Ω was not significant; at both resistances, the precipitation efficiency was above 80%. In addition, average cathode pH at both resistances was 8.5 and 8.7 respectively. However, increasing the resistance from 470 Ω to 1000 Ω led to a reduction in the precipitation efficiency from 80% to 70%, and the average cathode pH was 8.2. A reduction in precipitation efficiency and average cathode pH at high external resistance occurred, where some electrons might be consumed in the anode to reduce other electron acceptors, such as sulphate and nitrate, or oxygen diffused through the membrane and the sampling ports, and that leads to a reduction in the current and cathode pH (Gil et al., 2003).
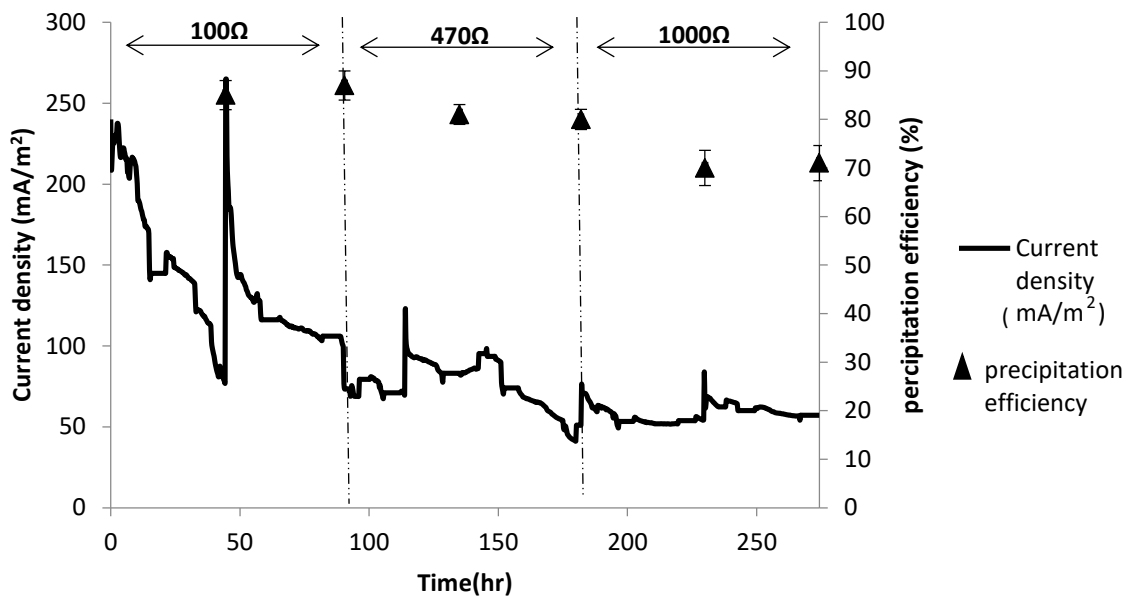
Figure 3.14 The impact of external resistance on current density and precipitation efficiency

Moreover, COD removal efficiency improved when low external resistance was used, and increasing the resistance decreased the removal efficiency. In all resistance, the removal efficiency was above 70%, and the difference between the three resistances was statistically insignificant. When 100 Ω was used as external resistance, the MFC achieved 85% COD removal efficiency, whereas the MFC achieved 70% COD removal efficiency when external resistance was 1000 Ω. However, the difference in removal efficiency between the MFC

operated at open circuit and operated under external load was significant (P<0.05). At open circuit, oxygen diffusion from the membrane might contribute in COD reduction, where COD removal was not caused by the current generation. Similar findings were reported by Katuri et al. (2011). Therefore, to achieve high COD removal efficiency in the MFC, low external load should be used.

3.3.7. Statistical Analyses

The key goal of the statistical analysis was to understand and identify the parameters that contributed to pH increases and enhanced energy generation. MFC performance was evaluated by coulombic efficiency, average current density, cathode pH, and precipitation efficiency. Understanding the main parameters that contributed to energy generation and cathode pH elevation would help to optimise MFC performance. Spearman's correlation coefficients are presented in Table 3.2, and Spearman's coefficients are presented as values between -1 and 1. A strong negative correlation (-0.875, P < 0.01) was observed between COD and CE. Increases in COD led to a reduction in CE, as most of the substrate at high COD was not involved in current generation. Furthermore, a strong positive correlation (0.88 and 0.864 respectively, P < 0.01) was observed between COD, cathode pH, and precipitation efficiency. The availability of the substrate in the anode chamber led to an increase in cathode pH. As a result of high pH at the cathode, the solubility of P decreased and more P was precipitated.

On the other hand, there was no significant correlation between anolyte and catholyte volumes with any of the monitored parameters, and that migh be due to the small volume of the BES chambers. This means the impact on MFC performance of changing anode and cathode volume in this study was not significant, however the impact of volume on BES performance might be significant if bigger volumes were used. With regard to the cathode aeration flow rate, the result showed a significant negative correlation (-0.42, P < 0.05) between cathode aeration and CE. Most of the substrate might be degraded by aerobic oxidation due to the high oxygen transfer rate through the Nafion membrane (Rahimnejad et al., 2014). At high aeration flow rate at the cathode, oxygen can be diffused to the anode chamber, and that accelerates COD removal and reduces CE. In addition, a significant positive correlation (0.356, 0.3, P < 0.05) was found between cathode aeration, average current density, and

cathode pH respectively. Increasing cathode aeration led to an increased supply of oxygen in the cathode, which works as an electron acceptor, and as a result, current density increased (Amari et al., 2015). External load plays an important role in the current density, where a significant negative correlation (-0.65, P < 0.01) was observed between external load and the current density. An increase in external load led to a reduction in number of electrons that are transferred from the anode to the cathode. No significant correlation was found between external resistance and P precipitation.

More importantly, a strong positive correlation (0.873, P < 0.01) was observed between P precipitation efficiency and cathode pH. This correlation confirms that P precipitation was dependent on solution pH, as an increase in solution pH led to a reduction in P solubility. CE was affected by precipitation efficiency and cathode pH. A strong negative correlation (-0. 617, P < 0.01) was found between CE and precipitation efficiency. Furthermore, a similar correlation was found between CE and cathode pH. An increase in cathode pH generates a large membrane pH gradient between the anode and the cathode, which causes a significant potential loss (Zhang et al., 2010). In addition, high pH is accompanied by P precipitation on the cathode electrodes, which potentially obstruct the mass transfer of ions and oxygen, and as a result, CE was decreased.

Spearman's correlation analysis suggests that COD, cathode aeration rate, and external load are the key influencing factors for P recovery and energy generation. COD showed that it had a great impact on CE, cathode pH, and precipitation efficiency. In addition, cathode aeration showed that it had a great impact CE, average current density, and cathode pH. Therefore, focusing on these two parameters (COD and cathode aeration flow rate) during the design stage would help to optimise the MFC performance and reduce the operational cost. Based on these findings, concurrent energy generation, and phosphorus recovery optimisation is carried out in the next chapter. Central composite design and surface response methodology were conducted to optimise MFC performance using the following parameters: COD and cathode aeration rate.

Table 3.2 Correlation analysis for the MFC performance

Variable	COD	Volume	Cath. aeration	Ext. load	CE	Avg I Density	Precipitation efficiency
COD	1	-	-	-	-	-	-
Volume	-	1	-	-	-	-	-
Cath. aeration	0.38	-0.01	1	-	-	-	-
External Load	0.06	-0.001	-0.03	1	-	-	-
CE	-0.875**	0.17	-0.42*	-0.33	1	-	-
Avg I density	0.2	-0.32	0.35*	-0.65**	0.03	1	-
Precip. eff.	0.864**	0.173	0.176	-0.28	-0.61**	0.206	1
Cathode pH	0.88**	0.016	0.3*	-0.067	-0.7**	0.31	0.873**

** Correlation is significant at the 0.01 level (2-tailed).

* Correlation is significant at the 0.05 level (2-tailed).

3.4. Summary

- This chapter has discussed the overall performance and the set-up of the experiment using a dual-chamber MFC for concurrent energy generation and phosphorus recovery as struvite and their operational conditions.

- Phosphorus was recovered in the dual-chamber MFC as magnesium ammonium phosphate hexahydrate (struvite) at the cathode chamber, by dosing NH_4Cl and $MgCl_2$ to achieve a molar ratio (Mg: NH_4: P: 1:1:1).

- XRD and SEM-EDS analysis showed that the precipitated particles were struvite with tubular-shaped crystals and had a similar pattern to the pattern of struvite.

- The precipitation of struvite particles on the electrode and membrane during the long-term operation of MFC leads to deterioration of the MFC performance.

- COD concentration had a great impact on CE, cathode pH, and precipitation efficiency. A negative correlation was found between COD concentration and CE. In addition, a positive correlation was found between COD concentration, cathode pH, and precipitation efficiency.

- The impact of anolyte and catholyte volumes on the MFC performance was not significant, probably due to the small volume of the MFC.

- The impact of cathode aeration flow rate on CE, cathode pH, and average current density was significant. A positive correlation was observed between cathode aeration flow rate, cathode pH, and average current density. A negative correlation was found between cathode pH and CE.

- The external load had an impact on the current density and COD removal efficiency.

- The results outlined within this chapter have improved the current scientific understanding of phosphorus recovery in a dual chamber MFC and the impact of the recovery on MFC performance.

3.5. Conclusions

The results in this chapter assess concurrent P recovery and energy generation achieved by dual-chamber MFCs. A mediator-less dual-chamber MFC was used to investigate and understand concurrent P recovery and energy generation. Due to the high pH around the cathode, which resulted from oxidation-reduction reactions, the MFC forms precipitates containing phosphorus in the catholyte and on the cathode surface. The main component of the precipitate was determined by XRD and SEM-EDS to be magnesium ammonium phosphate hexahydrate (struvite). P precipitation efficiency at the cathode ranged from 9% to 90% was achieved and the MFC coulombic efficiency ranged from 1 to 10%. The precipitation of P on the cathode surface and the membrane led to deterioration of the MFC performance. Different operational parameters, such as COD concentration, anolyte and catholyte volumes, cathode aeration flow rates and external resistance, were tested to understand the impact of different operational parameters on MFC performance. Spearman's correlation coefficients analysis indicated that COD had a great impact on CE, cathode pH, and P precipitation efficiency. On the other hand, aeration flow rate had a great effect on the CE, average current density, and cathode pH in the MFC. In addition, external resistance had an impact on current density. COD concentration, cathode aeration flow rate, and external resistance are the key factors influencing P recovery and energy generation. Achieving high current density and high P recovery concurrently in the system would require further research and development, as P precipitation on the cathode leads to deteriorating electricity production in the MFC, and this reduces the generated power. Based on these findings and the nonlinearity of the current density and precipitation efficiency, further work was carried out, as is discussed in Chapter 4, to improve and optimise MFC performance. The key factors that influence energy generation and P recovery were chosen for the MFC optimisation. COD concentration and cathode aeration flow rate were studied in depth using full factorial design, central composite design, and surface response methodology to understand the role of each parameter on energy generation and P recovery.

Chapter4

Concurrent energy generation and P recovery optimisation in a mediator-less dual chamber microbial fuel cell

4.0 Concurrent energy generation and P recovery optimisation in a mediator-less dual chamber microbial fuel cell

4.1 Introduction

This chapter focuses on MFC optimisation for energy generation and P recovery. Two factors (influent COD and cathode aeration flow rate) were chosen based on their impacts on the MFC performance in the performance assessment of the dual-chamber MFC (Chapter 3). In this chapter, a full factorial design (FFD) and a central composite design (CCD) were conducted using dual-chamber MFCs to investigate and understand the effect of influent COD and cathode aeration flow rate. Most importantly, the interaction effect of those parameters on MFC performance can be identified for system optimisation. The performance of the MFCs was evaluated based on power output, CE, COD removal efficiency, cathode pH, and precipitation efficiency (%).

The objectives of this chapter are as follows:

- To investigate the impacts of influent COD and cathode aeration flow rate on power output, CE, COD removal efficiency, cathode pH, and precipitation efficiency (%).
- To optimise power density and P recovery in the MFC.
- To explore the impacts of influent COD and cathode aeration flow rate on crystal size and purity.

System modelling is an efficient technique that helps in understanding the system while at the same time identifying the most important parameters that have an impact on system performance. Recently, many studies have focused on optimising the performance of MFCs for wastewater treatment and energy generation (Fang et al., 2013; Madani et al., 2015; Yahya et al., 2015). Different approaches have been employed to improve the performance of MFCs, for example, modifying cell design and materials (Liu et al., 2005a; Ahn et al., 2014), increasing buffer capacity (Hosseinpour et al., 2014), and modifying the operational conditions that have a significant impact on system performance (Sleutels et al., 2011; Ishii et al., 2013;

Hosseinpour et al., 2014). Operating conditions, such as influent COD, pH, external load and cathode aeration flow rate, are important factors that influence system performance and microbial community in MFC (Ishii et al., 2013).

Influent COD and aeration flow rate have been shown to be important factors limiting energy generation and P recovery in MFCs (Zhang et al., 2015; Abbasi et al., 2016; Almatouq and Babatunde, 2016). Organic matter measured in terms of COD plays an important role in providing the bacteria with the required carbon source for electricity generation (Zhang et al., 2015; Abbasi et al., 2016); increasing the influent COD concentrations leads to an increase in the generated voltage. Furthermore, it has been found that increasing the COD concentration leads to an increase in cathode pH due to the oxygen reduction reaction; as a result, P was precipitated (Jadhav and Ghangrekar, 2009; Zhang et al., 2015; Almatouq and Babatunde, 2016). On the other hand, dissolved oxygen concentration in the cathode chamber, which can be controlled via cathode aeration flow rate, plays an important role in energy generation, as oxygen acts as an electron acceptor for the transferred electron (Gil et al., 2003). Choosing the optimum aeration flow rate in the cathode compartment can be challenging especially in dual-chamber MFCs.

Concurrent energy generation and P recovery in MFC has been studied using different cell designs (Ichihashi and Hirooka, 2012; Hirooka and Ichihashi, 2013; Almatouq and Babatunde, 2016). Understanding the effect of different operational conditions on energy generation and P recovery will help to improve the overall performance of MFCs and, at the same time, reduce the operational costs. Furthermore, identifying those effects will help to optimise energy generation and P recovery. System modelling optimisation can be achieved using two main approaches: engineering approaches and statistical approaches. In the engineering approaches, physical-chemical-microbiology and electrochemical equations are used to model the system process. Most of the engineering models are deterministic models because the output of the model is determined by the parameter values and the initial conditions (Luo et al., 2016). In addition, the parameters in the engineering models need to be adjusted to predict the output accurately. In contrast, in the statistical approaches, the model is constructed based on the measured data from the system. Using the statistical optimisation approach can be helpful in understanding the effect of different parameters within a wide experimental domain with a

minimum number of runs. Furthermore, applying this approach will help to identify the joint effect between different parameters. Eventually, the effect of each factor can be evaluated at different levels of the other factors (Montgomery, 2001).

Therefore, response surface methodology (RSM) and central composite design (CCD) were used in the experiments discussed in this chapter. RSM and CCD are powerful statistical methods that have been widely used in different applications and industries, such as biology (Zheng et al., 2008), chemistry (Asghar et al., 2014), and the petroleum industries (Rastegar et al., 2011). These methods can be used for designing experiments, developing statistical models, evaluating the effects of several factors, and finding the optimum conditions for a certain response (Kim, 2016). This is the first time that FFD and response surface methodology are being used to study the effect of influent COD concentration and cathode aeration flow rate on several parameters in a mediator-less dual-chamber MFC.

4.2 Materials and methods

The experimental procedures for this chapter are summarised below and can be found in more detail in sections 3.2.1–3.2.14

4.2.1 MFC setup

Two sets of dual-chamber H-type bottles (Adams & Chittenden Scientific Glass, Berkeley, CA, USA) were used to construct the MFCs. Anode and cathode electrodes were made of carbon cloth 2.5 × 5 cm (projected area of 25 cm^2) with a volume of 300 mL for each chamber (see Figure 3.1). In order to monitor anode and cathode pH, two openings were considered on the side of the compartment. The unused holes of the anode chamber were firmly sealed to prevent oxygen diffusion to the anodic chamber. The cathode contained a Pt catalyst (0.5 mg/cm^2 10% Pt on Carbon Cloth Electrode) to improve cathode performance, whilst the anode was plain carbon cloth. Both electrodes were connected with a titanium wire (0.5 mm, purity > 99.98%, Alfa Aesar, Heysham, UK). A Nafion membrane (Nafion 117#, Sigma-Aldrich, London, UK) was placed in the middle of the anode and the cathode. The membrane was pre-treated by boiling in H_2O_2 (30%) and deionized water, followed by 0.5 M H_2SO_4 and deionized water, each for 1 h, and thereafter, it was stored in deionized water prior to being used. The MFCs were maintained at 20 °C in a temperature-controlled room.

4.2.2 Inoculation and operating conditions

The anode chambers were inoculated with a 1:1 mixture of activated sludge and anaerobic digester sludge obtained from a wastewater treatment plant in Cardiff (section 3.2.2), and anolyte medium (mainly containing acetate). The external resistance was 1000 Ω at the initial stage of the operation, and it was reduced to 470 Ω, which is where the system produced the maximum power in the polarisation test. During the start-up period, the cathode chamber was filled with 50 mM phosphorus buffer, and it was continuously aerated using an aquarium pump. Once the MFCs achieved stable electricity production for at least three cycles, the phosphorus buffer was replaced with anolyte effluent.

The MFCs were operated in 2-stage feed-batch mode at room temperature. In the first stage, the synthetic wastewater was fed to the anode chamber for organic matter removal. The organic matter was measured as COD. The concentration of COD was measured using a COD kit (Hach lange, UK). At the end of each cycle, the effluent from the anode chamber was filtered using a 0.2 um filter membrane (Fisher Scientific, Pittsburgh, UK) and directed into the cathode chamber (second stage) for P recovery, and a new synthetic wastewater batch was introduced into the anode chamber. Anode influent pH was adjusted to pH = 7, and an aquarium pump with an air flowmeter was used to supply air continuously to the cathode chamber in order to provide oxygen as the electron acceptor. Media replacement was carried out in an anaerobic environment, and the synthetic wastewater contained 0.6-2 g/L (depending on COD concentration) sodium acetate; KH_2PO_4, 0.45 g/L; K_2HPO_4, 0.45 g/L; KCl, 0.74 g/L; NaCl, 0.58 g/L; NH_4Cl, 0.25 g/L; $MgSO_4.7H_2O$, 0.1 g/L; $CaCl_2 .2H_2O$, 0.1 g/L; 0.1 mL/L of a trace element mixture containing (per litre): iron(II) sulphate heptahydrate ($FeSO_4.7H_2O$), 1 g; zinc chloride ($ZnCl_2$), 0.07 g; manganese(II) chloride tetrahydrate ($MnCl_2.4H_2O$), 0.1 g; boric acid (H_3BO_3), 0.006 g; calcium chloride hexahydrate ($CaCl_2.6H_2O$), 0.13 g; copper (II) chloride dihydrate ($CuCl_2.2H_2O$), 0.002 g; nickel (II) chloride ($NiCl_2.6H_2O$), 0.024 g; sodium molybdate ($Na_2MoO_4.2H_2O$), 0.03 g; cobalt(II) chloride ($CoCl_2.6H_2O$), 0.238 g and vitamins.

4.2.3 Analytical Methods

The voltage across the external resistance was recorded every 15 min using an ADC-20 data logger system (Pico Technology, Saint Neots, UK), which was connected to a computer. Based on the recorded voltage, current (I) and power (P = IV) were calculated according to

Ohm's law. The current density and power density were calculated by dividing the current and the power by the anode area (25 cm^2). CE was calculated by integrating the measured current relative to the theoretical current previously described by Equation (4-1) (Logan et al., 2006). Polarisation curves were obtained only after adoption of the MFCs to the applied experimental conditions according to each run (at least after three complete operating cycles) by varying the external resistance systematically in the range of 10,000 to 10 Ω with an interval of 15 min to obtain a stable voltage reading:

$$CE \ (\%) = \frac{M \int_0^t I \, dt}{Fbv_{An}\Delta COD} \tag{4-1}$$

where M is the molecular weight of oxygen (M=32), F is Faraday's constant, b is the 4 is the number of electrons exchanged per mole of oxygen, v_{An} is the volume of liquid in the anode compartment, and ΔCOD is the difference between anode COD influent and anode COD effluent over time t_b (cycle duration). COD removal efficiency was calculated using Equation (4-2):

$$COD \ removal \ efficiency = \frac{anode \ COD \ influent - anode \ COD \ effluent}{anode \ COD \ influent} \times 100 \tag{4-2}$$

The COD, TN, NH$_4$-N, NO$_3$, NO$_2$ and TP were measured using a HACH DR3900 spectrophotometer in accordance with its operating procedures. Other cation concentrations (Na$^+$, K$^+$, Ca^{2+} and Mg^{2+}) were determined using inductively coupled plasma-optical emission spectroscopy (ICP-OES; Perkin-Elmer Optima 3000XL). Water quality analyses were conducted to assess the wastewater treatment efficiency of the MFCs. The pH was recorded and monitored in real time using a multi-channel parameter data recorder (EA Instruments, London, UK). Probes for measuring the pH were connected to the data logger, which was connected to a personal computer.

4.2.4 Phosphorus precipitation in MFC

The theoretical P concentration in the synthetic wastewater was approximately 6 mM at pH 7. For P precipitation, ammonium chloride and magnesium chloride solutions with the theoretical concentration of 6 mM were pumped into the cathode chamber using a peristaltic pump. The ammonium and magnesium solution was pumped with a flow rate of 6 mL/day. The flow rate was chosen to achieve a 1:1:1 molar ratio of struvite precipitation NH$_4$:Mg:P.

Before and after each cycle, the cathode chamber was washed with deionised water 3 times, and then cleansed and dried to remove any precipitate attached to the chamber walls. After each precipitation cycle, the used cathode was removed for maintenance and replaced with a new one. Cathode maintenance is essential to remove P precipitates from cathode surface, as the precipitates reduce cathode performance and dissolution treatment increases cathode performance to the initial level. The used cathodes were firstly soaked in deionised water, and thereafter, in 10 mM MES buffer adjusted to pH 5.5 with NaOH, and then finally rinsed with deionised water. At the end of each cycle, the catholyte was filtered using a 0.2 µm filter membrane (Fisher Scientific, Pittsburgh, UK). The precipitate was collected, weighed, and analysed by XRD and SEM equipped with an EDX. The precipitation efficiency and precipitation rate of P were calculated using Equation (3-4) and (3-5), respectively.

4.2.5 Particle size distribution

After each batch, the catholyte was filtered to collect the precipitated particles. These were then analysed using an SEM to determine the morphology and the size of the crystals. The size distribution of the precipitated crystals was determined by analysis of the SEM images, and the sizes of more than 1000 particles were calculated using the method of linear sections (Ivakin et al., 2015). In this case, several images were used to determine the average size. Based on the SEM size data, a distribution diagram was constructed as the dependence of the percentage of total particles volume (frequency ratio) that fall into a group interval on the size of crystals. To minimise errors, additional SEM images were used to increase the number of calculated particles and improve statistics in the group intervals. Crystal size and morphology were also analysed to determine the impact of operational conditions on the crystals.

4.2.6 Experimental design and data analysis

Regression analysis was used to determine the effect of each variable and the interaction effect on the responses. This helps in understanding and optimising the system. In developing the regression equation, the actual values were coded to define the levels in the design and make the analysis easier by removing the non-significant terms without changing the estimates for the terms. The relationship between the coded values and the actual values was described by the following equation:

$$X_i = \frac{(X_i - X_i^*)}{\Delta X_i}$$

(4-3)

where x_i is the coded value of the *i*th independent variable, X_i is the uncoded value of the ith independent variable, X_i^* is the uncoded value of the ith independent variable at the centre point, and ΔX_i is the step change value. The coded values are shown in Table 4.1.

Table 4.1 Level of independent variables in FFD and CCD.

Variable	Design	Factor	Applied levels				
			--	-	Centre	+	++
Full factorial design	X_1	COD (mg/L)	-	500	1000	1500	-
	X_2	Aeration flow rate (mL/min)	-	50	150	250	-
Central composite design	X_1	COD (mg/L)	300	-	1000	-	1700
	X_2	Aeration flow rate (mL/min)	10	-	150	-	290

4.2.7 Full factorial design (FFD)

Full factorial design (FFD) is a powerful tool that is used to identify the effect of the independent variables at different levels on the responses. Moreover, using FFD helps to identify the interaction effect between variables on the response, which is ignored in many statistical approaches (DouglasC, 2009). In this study, FFD with two replicates at each factor combination was employed. At the beginning of each factor combination, the system was running for at least two batches to let the system adapt to the new conditions. In addition, three experiments at the centre of the design for the analysis of curvature were performed.

4.2.8 Central composite design (CCD)

In CCD, the effects of influent COD concentration (X_1) and cathode aeration flow rate (X_2) on power output, coulombic efficiency (CE), COD removal efficiency, cathode pH, and precipitation efficiency were determined. The nonlinear behaviour of the response is explained by the following quadratic and cubic model (DouglasC, 2009):

$$y = \beta_o + \sum_{I=1}^{n} \beta_i X_i + \sum_{i=1}^{n} \beta_{ii} X_i^2 + \sum_{i=1}^{n-1} \sum_{j=1+i}^{n} \beta_{ij} X_i X_j + E \qquad (4\text{-}4)$$

$$y = \beta_o + \sum_{I=1}^{n} \beta_i X_i + \sum_{i=1}^{n} \beta_{ii} X_i^2 + \sum_{i=1}^{n-1} \sum_{j=1+i}^{n} \beta_{ij} X_i X_j + \sum_{i=1}^{n} \beta_{iii} X_i^3 + \sum_{i=1}^{n-2} \sum_{j=i+1}^{n-1} \sum_{k=j+1}^{n} \beta_{ijk} X_i X_j X_k + E \qquad (4\text{-}5)$$

where y is the response, β_i is the coefficient of the *i*th main effect, β_{ii} is the coefficient of the *i*th quadratic term, β_{ij} is the coefficient of the interaction between the *i*th and *j*th terms, β_{iii} is the coefficient of the cubic single term, β_{ijk} is the coefficient of the cubic three cross product terms, and E is the error term. CCD is the most frequently used technique in RSM design, where chosen points are selected to obtain several properties, such as orthogonality. In addition, the CCD method was chosen because it is able to capture the nonlinear behaviour of the response and fit quadratic models. Furthermore, CCD reduces operation time and cost by estimating the second order coefficients with the minimum number of runs. Adding axil (with a distance α from the centre) and centre point runs to 2^k FDD helps to understand the whole design of the experiment (spherical, orthogonal, rotatable, or face centred).

4.2.9 Statistical analysis

Design expert version 10.0.3 (Stat-Ease Inc., Minneapolis, MN, USA) was used for the design, analysis, and optimisation. The variables used were influent COD (X1) and cathode aeration flow rate (X2). The responses were power density (Y1), CE (Y2), COD removal efficiency (Y3), cathode pH (Y4), and precipitation efficiency (Y5). Analysis of variance (ANOVA) provided the statistical results and diagnostic check tests to evaluate the adequacy of the models. The quality of the fitted models was evaluated by the coefficient of determination R^2, and its statistical significance was checked using the Fisher F-test. To obtain a good fit of mode, R^2 should be at least 0.8 (Myers et al., 2016). Model terms were evaluated by the P-value (probability of error) with a 95% confidence level. Three-dimensional plots and their respective contour plots were obtained based on the effects of the two factors (COD and aeration flow rate). In total, 22 experiments were conducted with 8 factorial points, 8 axial points, and 6 centre points; replicates of the centre points were added to the design to examine the adequacy of the model and to obtain a good estimate of the experimental error.

4.3 Results and discussion

Magnesium ammonium phosphate hexahydrate (struvite) was precipitated in the cathode chamber by dosing with a NH_4 and Mg solution to achieve a molar ratio (Mg: NH_4: P: 1:1:1). Due to the degradation of organic matter at the anode and the release of electrons to the cathode, water is consumed and hydroxide is generated, and this leads to an increase in pH (pH>8) around the cathode. The system achieved a maximum precipitation rate of 95 % and a maximum power density of 185 mW/m^2. In wastewater treatment plants, reject wastewater with high ammonium (10-600mg/L) and phosphorus concentration (10-1000 mg/L) is produced from anaerobically digested sludge (Pastor et al., 2008; Blöcher et al., 2012). Since the reject water has a high P concentration, it can be an optimal stream for P recovery from wastewater. Therefore, reject wastewater was simulated and used for this study. The low (COD=300 mg/L) and high (COD=1700 mg/L) levels of influent COD concentration were chosen based on the concentration of COD in reject wastewater (Thorndahl, 1993; Hu et al., 2017). Oxygen in MFCs is used as a final electron acceptor. Similarly, the flow rate levels of air have varied in MFC research; the range in this study was selected based on the range of the flow rates that have been commonly used in previous studies to provide a sufficient amount of oxygen (Freguia et al., 2008; Cercado-Quezada et al., 2010; Kalathil et al., 2011).

In this study, the range of the cathode aeration flow rate was between 10 to 290 mL/min, as that range is widely used in MFC studies.

As a first step for the analysis, FFD was employed to identify the contribution of each factor and identify the interaction effect on each response. If FFD was not able to explain the response behaviour, CCD was used to fit a quadratic model to the data. Four axial points with $\alpha = \pm 1.4$ and six centre points were performed to have a rotatable design. The levels of variables for FFD and CCD are given in Table 4.1.

The performance of the MFCs was investigated in terms of maximum power density, CE, COD removal efficiency, cathode pH, and precipitation efficiency. The performance of the MFCs in terms of energy generation was evaluated by maximum power density, while coulombic efficiency measured the recovered electrons as current. COD removal efficiency shows MFC as a treatment tool for wastewater. Cathode pH is the most important factor for P recovery, where P solubility is dependent on solution pH. Furthermore, precipitation efficiency was used to evaluate P recovery as struvite in the cathode chamber. The experimental design and the results are summarised in Table 4.2.

Table 4.2 Experimental design and the responses of the duplicates of FFD and CCD.

No of run	Block	X_1: COD (mg/L)	X_2: aeration flow rate (mL/min)	Y_1:Max power density (mW/m^2)	Y_2: CE (%)	Y_3: COD removal efficiency (%)	Y_4: cathode pH	Y_5: Precipitation efficiency (%)
1	Block 1	500	250	48	5.6	90	7.43	6.95
2	Block 1	500	250	32	4.9	88	7.4	2.7
3	Block 1	1000	150	38	2.69	78.4	8.98	76.17
4	Block 1	500	50	25.7	4.94	87.1	7.7	6.56
5	Block 1	500	50	26.3	4.61	84.2	7.34	6.5
6	Block 1	1500	250	137	2.3	71	8.9	77.7
7	Block 1	1500	50	80.3	4.25	60	8.4	95.9
8	Block 1	1000	150	32	2.74	87.4	8.76	62.7
9	Block 1	1500	250	125	1.93	70	9.08	80
10	Block 1	1500	50	78	3	65	8.42	95
11	Block 1	1000	150	30	2.89	70.9	8.5	69.5
12	Block 2	1700	150	185	1.6	68.8	8.88	90.2
13	Block 2	1000	10	19	1.73	73.4	8.13	88.2
14	Block 2	1000	290	53	2.13	76.5	8.12	48.6
15	Block 2	300	150	40	7.77	71.37	7.63	4
16	Block 2	1000	150	27	2.97	84	8.7	86.7
17	Block 2	1000	150	64.8	3.24	74.81	8.29	68.68
18	Block 2	1700	150	120	1.76	61.9	8.92	93.2
19	Block 2	300	150	43	8.51	72.7	7.2	5
20	Block 2	1000	10	16	1.95	79.6	8.18	75
21	Block 2	1000	150	40	2.9	85	8.69	87
22	Block 2	1000	290	60	2.58	74.7	8.3	70

4.3.1 Power density

Maximum power density was obtained from the polarisation curves, which were conducted only after the MFCs had been adapted to the applied experimental conditions. The figures of power density versus current density of factorial and axial runs are shown in Fig. 4.1 (a and b).
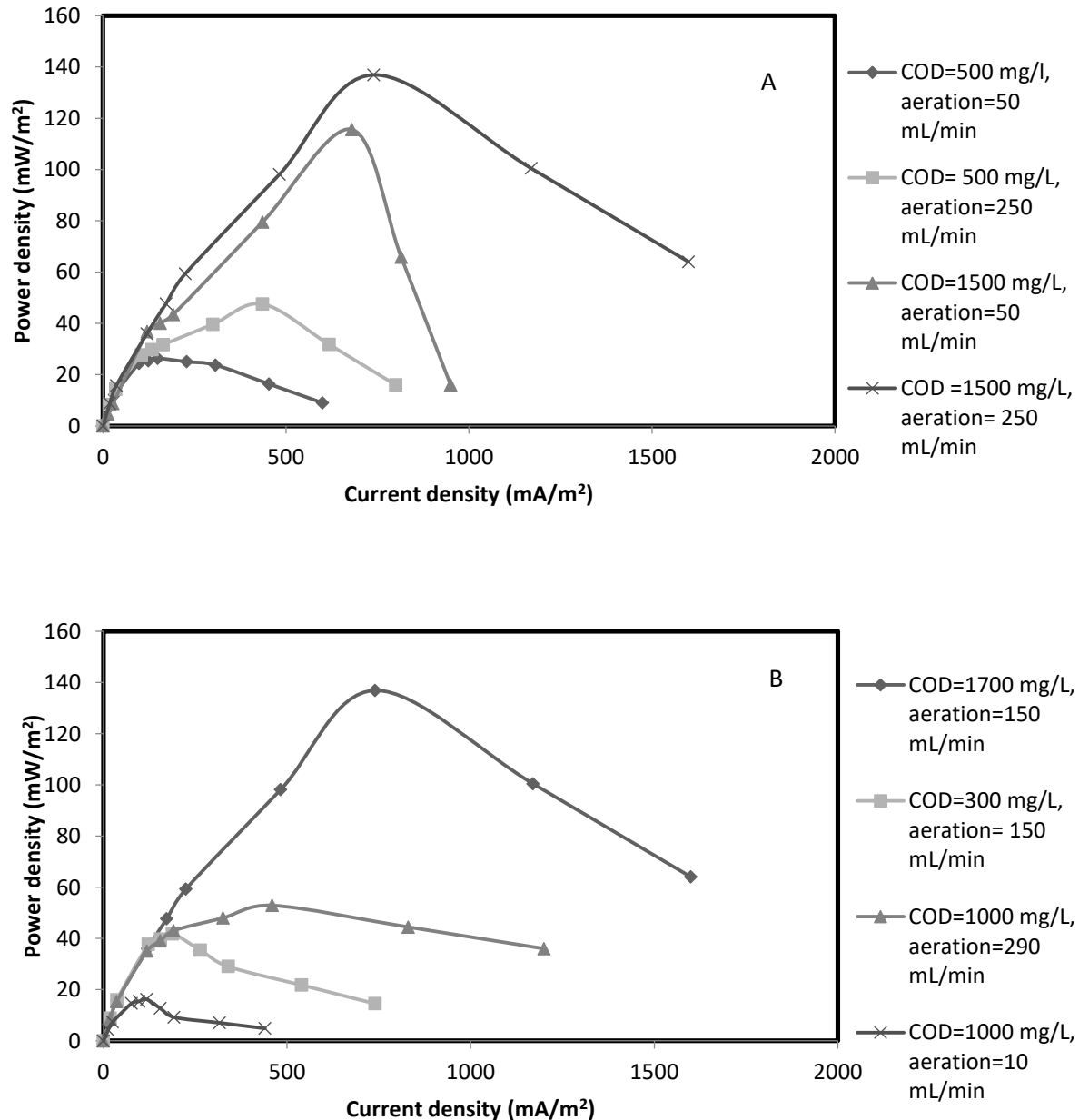
Figure 4.1 Effect of influent COD concentration and cathode aeration flow rate levels on power density (A) factorial runs and (B) axial runs.

The experimental data of the maximum power density was used for statistical analysis. In FFD, ANOVA showed that the model was significant with a P-value of 0.0001; similarly, the model F-value of 100.19 implies the model is significant, as there is only a 0.01% chance that a model F-value this large could occur due to noise. The P-value of 0.0013 shows that the curvature is significant. The curvature was measured by the difference between the average of the centre points and the average of the factorial points. First order model cannot explain the twisted plane and the interaction term in the power density behaviour. Therefore, as a second step, CCD was employed by adding four axial points to explain the response curvature.

Before finalising any model or graph, diagnostic plots should be examined to check if this model provides a good representation of the actual data. Firstly, it is important to verify if the standard deviation between the actual and the predicted response values follow a normal distribution. Secondly, the studentized residuals versus predicted values showed that there was no evidence of violation of constant or independence assumptions throughout the response space. Thirdly, the data were checked for outliers if any (influential values). In this analysis, Cook's distance was used to check if any influential values were available. The maximum value of Cook's distance was 0.25, which was far from unity. Lastly, the Box-Cox plot for power transformation was checked to see if the data required any transformation. In this case, square root with Lambda= 0.5 was used to transform the data. The ANOVA table for the final model is given in Table 4.3.

Table 4.3 ANOVA for the quadratic model of power density

Source	Sum of Squares	DF	Mean Square	F-Value	Prob > F
Block	0.03598	1	0.03598		
Model	137.439	5	27.4879	52.2185	< 0.0001
X_1	79.413	1	79.413	150.86	< 0.0001
X_2	17.8681	1	17.8681	33.9438	< 0.0001
X_1^2	34.2158	1	34.2158	64.9995	< 0.0001
X_2^2	0.17867	1	0.17867	0.33943	0.5688
X_1X_2	0.91467	1	0.91467	1.73759	0.2072
Residual	7.89602	15	0.5264		
Lack of Fit	1.56676	3	0.52225	0.99017	0.4303
Pure Error	6.32926	12	0.52744		
Total	145.371	21			

Eventually, the following second order model was considered satisfactory in representing power density:

$$(Power\ Density)^{1/2} = 6.21 + (2.23 * X_1) + (1.06 * X_2) + (1.74 * X_1^2) - (0.13 * X_2^2) + (0.34 * X_1 * X_2) \quad (4\text{-}6)$$

The model and the terms X_1, X_2, X_1^2 have a P-value of less than 0.0001. The concentration of COD showed that it had the greatest effect on the power density. The effects of COD concentration and cathode aeration flow rate were quadratic and linear on the power density, respectively. The terms X_2^2 and X_1X_2 as the interaction terms between COD concentration and cathode aeration had a minor and statistically insignificant effect on power density. The R^2 of 0.9457 and adjusted R^2 of 0.9276 implied that the model was able to express approximately 94% of the variability in the response. The response surface of the power density is shown in Fig. 4.2. The quadratic model (4-6) was used to identify the optimal value of power density (192 mW/m^2), which was obtained at COD =1700 mg/L and aeration flow rate= 240 mL/min.
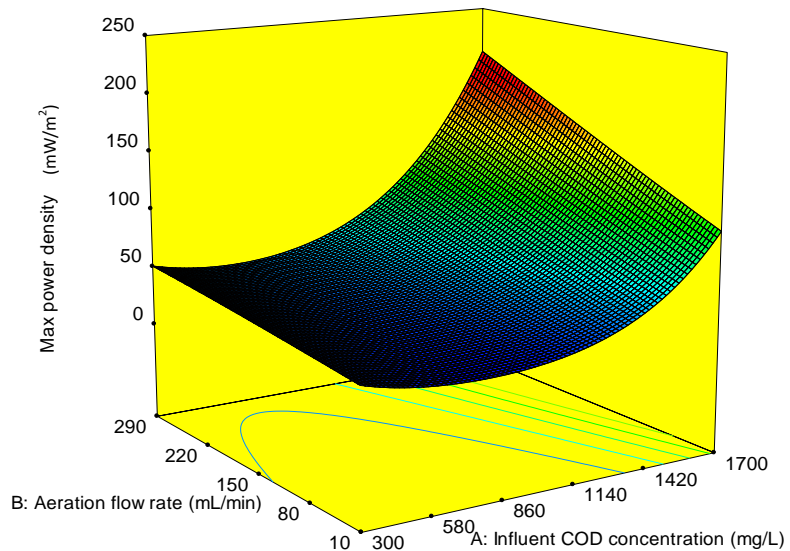
Figure 4.2 Response surface of power density as a function of COD concentration and cathode aeration flow rate.

4.3.2 Coulombic efficiency

Coulombic efficiency was used to determine the amount of the substrate that was converted to electrical current. The coulombic efficiency of each run was calculated using Eq. (4-1). The same analysis procedure was followed for analysing CE. In FFD, ANOVA results showed that the model was significant with a P-value of <0.0001. In addition, the main effect of COD and aeration flow rate was significant and greatly influenced the CE. Moreover, a curvature P-value of <0.0001 indicated that there was a significant curvature in the design space. The first order model cannot explain the twisted plane and the interaction term in the Coulombic efficiency behaviour. In the CCD method, ANOVA results showed that the quadratic model with an F-value of 110.4 and P-value of <0.0001 was significant. The lack of fit with a P-value of 0.0001 showed that the lack of fit was significant. In a case of significant lack of fit, the response needs to be transformed, or the model requires the use of cubic terms to achieve an adequate fit. In this case, a cubic term was added to the model to obtain a non-significant lack of fit and obtain high model accuracy. The ANOVA table for the final model is given in Table 4.4.

Table 4.4 ANOVA for the cubic model of coulombic efficiency

Source	Sum of Squares	DF	Mean Square	F-Value	Prob > F
Block	0.009618	1	0.009618		
Model	104.344	6	17.39067	1030.202	< 0.0001
X_1	0.397764	1	0.397764	23.56308	0.0003
X_2	3.611158	1	3.611158	213.9206	< 0.0001
X_1^2	17.86538	1	17.86538	1058.323	< 0.0001
X_2^2	0.932177	1	0.932177	55.22102	< 0.0001
X_1X_2	0.06125	1	0.06125	3.628375	0.0776
X_1^3	4.742806	1	4.742806	280.958	< 0.0001
Residual	0.236332	14	0.016881		
Lack of Fit	0.023865	2	0.011933	0.673942	0.5280
Pure Error	0.212467	12	0.017706		
Total	104.59	21			

The model was significant with an F-value of 1030.2 and a P-value of <0.0001. There was only a 0.01% chance that this level of fit could occur due to noise. The lack of fit was not significant with a P-value of 0.5280. The normal probability plot of the studentized residuals was normally distributed. The studentized residuals versus predicted values plot showed that there was no evidence of any violation of the constant or independence assumptions throughout the response space. In addition, Cook's distance had a maximum value of 0.386, which was far from unity. As a result, all the plots showed that this model was adequate to explain the behaviour of the CE.

Therefore, the following model was considered satisfactory in representing coulombic efficiency:

$$CE = 3.03 - (0.50 * X_1) + (0.48 * X_2) + (1.26 * X_1^2) - (0.29 * X_2^2) - (0.087 * X_1 * X_2) - (1.09 * X_1^3) \tag{4-7}$$

Eq. 4-7 shows that the main terms X_1, X_2, X_1^2, X_2^2, and X_1^3 are significant and important terms in the response. The effects of COD concentration and cathode aeration flow rate were quadratic on the CE. The interaction term between COD concentration and cathode aeration had a minor and statistically insignificant effect on CE. Moreover, the effect of COD was more significant than aeration flow rate. The coefficient of determination of 0.9977 and the adjusted R^2 of 0.9968 implied that the model was able to express approximately 99% of the variability in the response. The response surface of the coulombic efficiency is shown in Fig. 4.3.

The range of CE was between 1 to 8.5 %. Fig. 4.3 shows that at low influent COD concentration (300 mg/L), CE was at the maximum 8.5%, and it reached 2% when the COD was increased (1500 mg/L). At high COD concentration, just a small amount of COD was being used for current generation, and the rest might be consumed by methanogens. Increasing the aeration flow rate had a small effect on CE in all COD concentrations. In addition, there was no significant difference in the resultant CE if aeration flow rate was increased from 150 to 250 mL/min, which means using aeration flow rate in the range of 150 mL/min is sufficient.
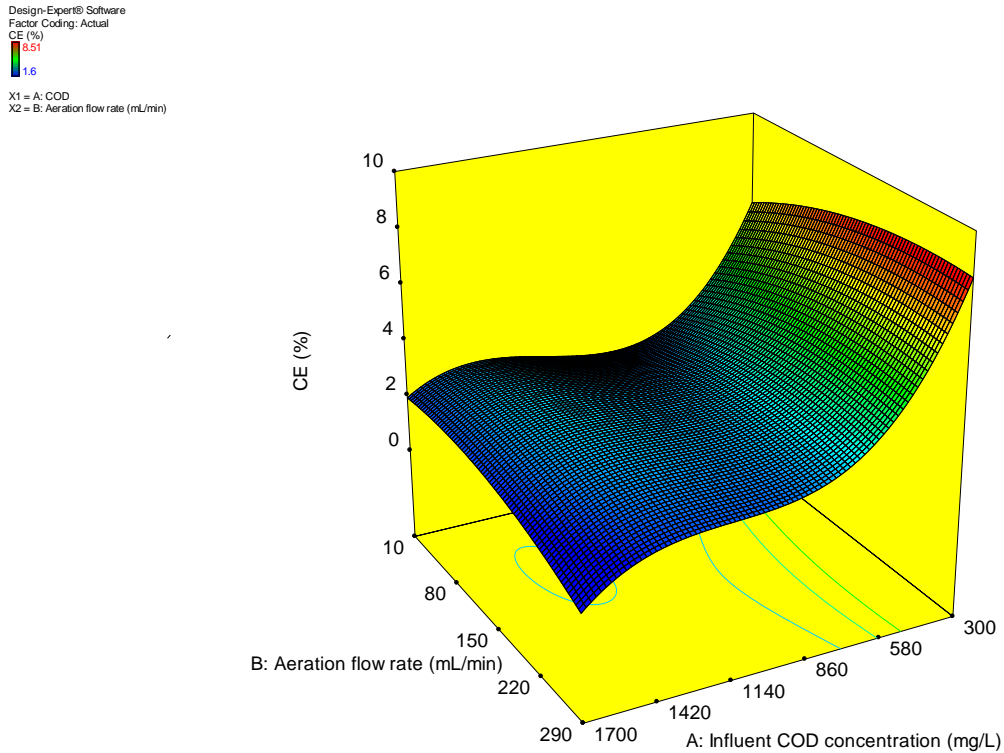
Figure 4.3 Response surface of coulombic efficiency as a function of COD concentration and cathode aeration flow rate

This low CE might be due to the following reasons:

- High cathode aeration flow rate led to an increase in oxygen diffusion to the anode chamber through the membrane, and that accelerated the degradation of the organic matter.

- High internal resistance due to the MFC design and struvite crystallisation in the solution decreased the overall performance, and that led to a reduction in CE.

- Struvite precipitation on the cathode electrode covered the Pt layer on the cathode surface and that led to a deterioration in electricity production in the MFC; this reduced the CE as well (Ichihashi and Hirooka, 2012; Hirooka and Ichihashi, 2013; Almatouq and Babatunde, 2016)

- High COD concentration can be more than the biocatalytic capabilities of the anode, which leads to a decrease in CE (Velasquez-Orta et al., 2011).

The CE model was able to predict a maximum value of 9.4% at COD 300 mg/L and a cathode aeration flow rate of 230 mL/min. Three experimental runs were conducted

using the previous values to check model adequacy. A CE average of 9 ± 1 % was achieved, which proved that the model has high accuracy for prediction purposes.

4.3.3 COD reduction efficiency

COD removal efficiency was studied to investigate the ability of MFCs to treat wastewater with different influent COD concentrations. COD removal was calculated using Eq. (4.2). In the FFD method, the analysis of variance showed that a linear model was able to represent the COD removal efficiency:

COD removal efficiency = 78.11–(10.41 * X_1)+(2.84 * X_2)+(1.16 * X_1* X_2)   (4-8)

The model was significant with a p-value of 0.0061. In addition, the model curvature was not significant and the coefficient of determination (R^2) was 0.808 and adjusted R^2 was 0.71, which means the model was able to explain 80% of the variability in the response. Eq. (4-8) shows that COD had a significant effect on COD removal. The results showed that increasing influent COD concentration led to a decrease in the removal efficiency, and the maximum COD removal efficiency that the MFC achieved was 90% at low COD concentration (500 mg/L). Increasing COD concentration and maintaining the same batch cycle duration (hydraulic retention time) led to a reduction in the COD removal efficiency. In MFCs, COD removal is achieved through substrate uptake by fermentative, exoelectrogenic, and methanogenic bacteria (Behera and Ghangrekar, 2016). Therefore, the microorganism requires more time (long cycle duration) to biodegrade and oxidise the organic matter in the wastewater. In addition, it was observed that cathode aeration flow rate had a impact on COD removal efficiency at the anode, and increasing aeration rate slightly increased the removal efficiency. Increasing aeration rate increases the reduction reaction at the cathode, and as a result, more protons are generated at the anode. However, increasing aeration rate will also increase the possibility of oxygen diffusion to the anode and accelerate the removal.

4.3.4 Cathode pH

The pH is a crucial parameter in MFCs, especially for P recovery. Therefore, cathode pH was studied to understand the effect of influent COD concentration and cathode

aeration flow rate on power output and P recovery, as P recovery as struvite is highly dependent on pH solution (pH>8). On the other hand, the generated power can be affected significantly by changes in the pH.

The ANOVA for FFD showed that the model was highly significant with a model F-value of 52.91. There is only a 0.03% chance that a model F-value this large could occur due to noise (P-value of 0.0003). Furthermore, a curvature P-value of 0.001 showed that the curvature was significant, which means that the first order model was not adequate to explain cathode pH behaviour. Therefore, CCD was employed as a second phase to explain that behaviour. Table 4.5 shows the ANOVA result.

Table 4.5 ANOVA for the quadratic model of cathode pH.

Source	Sum of squares	DF	Mean Square	F-Value	Prob > F
Block	0.0004729	1	0.0004729		
Model	6.6845083	5	1.336902	35.34142	< 0.0001
X_1	5.1758687	1	5.175869	136.8258	< 0.0001
X_2	0.080594	1	0.080594	2.130529	0.1650
X_1^2	0.8154824	1	0.815482	21.55754	0.0003
X_2^2	0.7413765	1	0.741376	19.59853	0.0005
X_1X_2	0.22445	1	0.22445	5.933408	0.0278
Residual	0.5674226	15	0.037828		
Lack of Fit	0.1517333	3	0.050578	1.460065	0.2747
Pure Error	0.4156893	12	0.034641		
Total	7.2524038	21			

The Model F-value of 35.34 implies the model was significant, and there is only a 0.01% chance that a model F-value this large could occur due to noise. The lack of fit P-value of 0.2747 showed that the source of variability was not significant. All the terms are significant except the aeration flow rate (X_2). The normal probability plot of the studentized residuals was normally distributed. In addition, the plot of studentized residuals versus predicted values showed constant errors over the variable range. Furthermore, Cook's distance showed a maximum value of 0.322, which was far from unity. Finally, the Box-Cox plot for power transformations showed that no transformation was required. Based on these checks, it can be concluded that the model is adequate to represent cathode pH behaviour.

The following second order model was chosen for cathode pH:

pH cathode = $8.65 + (0.57 * X_1) + (0.071 * X_2) - (0.27 * X_1^2) - (0.26 * X_2^2) +$

$\quad (0.17 * X_1 * X_2)$ (4-9)

A P-value less than 0.05 showed that all the terms were significant except aeration flow rate (X_2), which was not significant. The effects of COD concentration and the cathode aeration flow rate were quadratic on the cathode pH (Figure 4.4). The coefficient of determination of 0.9218 implied that the model was able to express approximately 92% of the variability in the response, and the adjusted R^2 was 0.8957. Cathode pH was highly influenced by COD concentration and the second order terms of both factors. Moreover, the interaction term was significant as well, which means the effect of COD concentration on cathode pH is dependent on the level of cathode aeration flow rate.
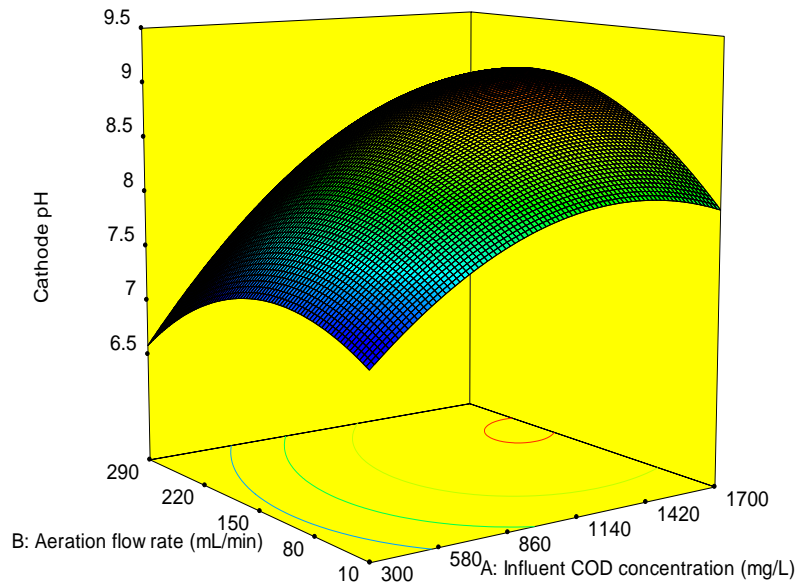
Figure 4.4 Response surface of cathode pH as a function of COD concentration and cathode aeration flow rate

The maximum pH value the system achieved in the cathode was 9.5, and this was obtained at COD = 1500 mg/L and an aeration flow rate of 250 mL/min. At low COD concentration, increasing the cathode aeration flow rate from 50 to 250 mL/min led to an increase in the average pH from 7.4 to 7.5, whereas at high COD concentration, increasing aeration flow rate led to an increase in average cathode pH from 8.5 to 9. However, high aeration flow rate might lead to a reduction in cathode pH, and cathode pH started to fluctuate. This pH drop can be explained by ammonia volatilization and protons being left behind (Cord-Ruwisch et al., 2011).

4.3.5 Precipitation efficiency (%)

Precipitation efficiency and P precipitation rate on the cathode electrode were calculated using Eqs.(3-4 & 3-5), where precipitation efficiency is the amount of P that is precipitated in the cathode chamber, and it is the difference in P concentration between the cathode influent and the cathode effluent, whereas P precipitation rate on the cathode electrode is the amount of P that is attached to the cathode electrode. The ANOVA for FFD showed that the model was highly significant with a model F-value of 1345.9. There is only a 0.01% chance that a "Model F-Value" this large could occur due to noise (P-value of< 0.0001). Furthermore, the curvature P-value of 0.0002 showed that the curvature was significant, which means that the first order model was not adequate to explain the precipitation efficiency behaviour. Therefore, CCD was employed as a second phase to explain the behaviour. Table 4.6 shows the ANOVA result.

Table 4.6 ANOVA for the quadratic model of precipitation efficiency

Source	Sum of Squares	DF	Mean Square	F-Value	Prob > F
Block	817.4	1	817.4		
Model	24608.277	5	4921.655	66.94739	< 0.0001
X_1	20687.705	1	20687.71	281.4069	< 0.0001
X_2	656.43468	1	656.4347	8.929229	0.0092
X_1^2	3127.3412	1	3127.341	42.54002	< 0.0001
X_2^2	337.35124	1	337.3512	4.58886	0.0490
X_1X_2	132.76351	1	132.7635	1.805931	0.1990
Residual	1102.729	15	73.51527		
Lack of Fit	457.2784	3	152.4261	2.833855	0.0830
Pure Error	645.45058	12	53.78755		
Total	26528.406	21			

The Model F-value of 66.95 implies that the model was highly significant, and there is only a 0.01% chance that a model F-value this large could occur due to noise. The model showed a non-significant lack of fit with a P-value of 0.083. All the terms are significant except the interaction term $(X_1 X_2)$ between COD concentration and cathode aeration, which had a minor and statistically insignificant effect on precipitation efficiency. The effects of COD concentration and cathode aeration flow rate were quadratic on the precipitation efficiency. All the diagnostic plots and checks showed that there was no violation of the assumptions, and it can be concluded that the model is adequate to represent P precipitation efficiency behaviour.

The following second order model was chosen for precipitation efficiency:

Precipitation efficiency $= 75.13 + (35.96^* X_1) - (6.41^* X_2) - (16.64^* X_1^2) - (5.47^* X_2^2) - (4.07^* X_1 * X_2)$ (4-10)

A model P-value less than 0.0001 showed that the model was highly significant. The coefficient of determination of 0.9517 implied that the model was able to express approximately 95% of the variability in the response, and the adjusted R^2 was 0.9428. The response surface of the precipitation efficiency is shown in Fig. 4.5. Influent COD concentration had the greatest effect on precipitation efficiency.
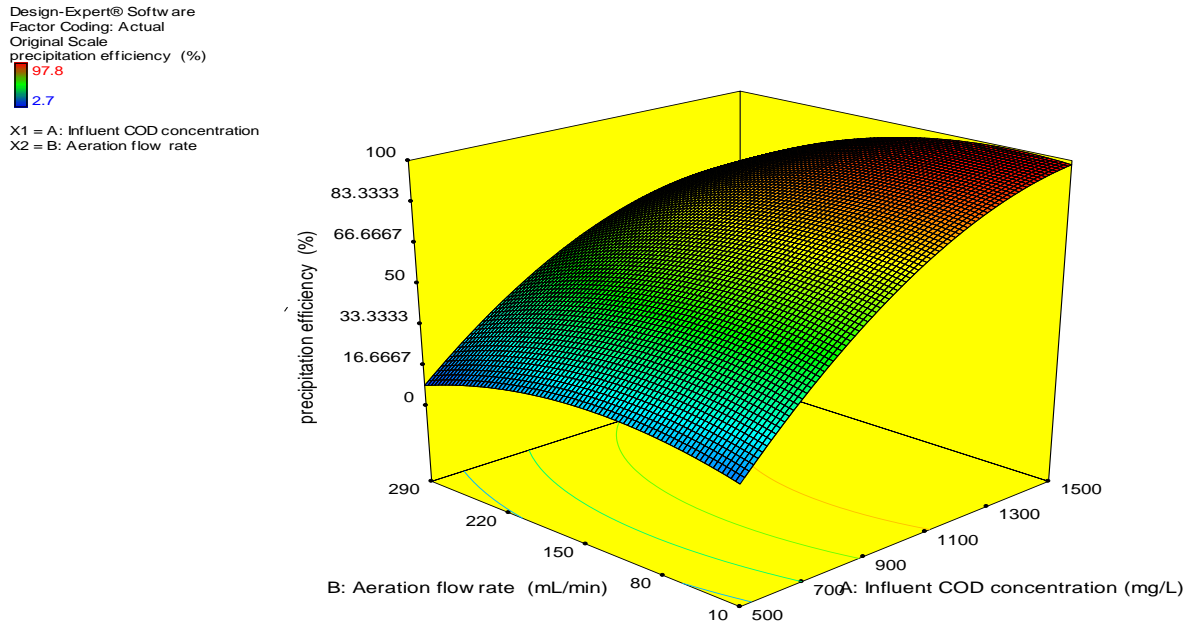
Figure 4.5 Response surface of precipitation efficiency as a function of COD concentration and cathode aeration flow rate

4.4 Discussion

4.4.1 The effect of influent COD concentration and aeration flow rate on power density and P recovery

4.4.1.1 The effect of influent COD at a constant aeration flow rate

The effect of influent COD on power generation has been studied previously (Zhang et al., 2015; Abbasi et al., 2016; Almatouq and Babatunde, 2016). Increasing influent COD from (500 mg/L) to (1500 mg/L) at a low cathode aeration flow rate of 50 mL/min resulted in about a three-fold power increase (from 26 to 80 mW/m^2). At high COD concentration, more protons are available for the reduction reaction at the cathode, which resulted in a higher power density, whereas at low COD concentration, fewer protons are available, and the system suffers from the lack of protons. In addition, increasing COD concentration had an impact on pH difference between the anode and the cathode. Increasing COD concentration in the anode chamber will increase the pH difference between the anode and the cathode, as more oxidation will occur at the anode due to the availability of the substrate, and that will reduce the anode pH. At the same time, more reduction reactions will occur at the cathode, and these will increase the pH at the cathode; as a result, a high pH

96

difference between the two chambers was observed. The internal resistance decreases with an increasing pH difference between the anode and cathode solutions. Increasing the pH difference increases the proton flux rate through the cation exchange membrane, and that increases MFC performance (Jadhav and Ghangrekar, 2009).

On the other hand, P precipitation was negatively affected by the generated current during the batch duration. The generated energy was reduced due to struvite being precipitated on the cathode surface, which might obstructe the mass transfer of ions and oxygen (Hirooka and Ichihashi, 2013; Almatouq and Babatunde, 2016).

Increasing influent COD from low to high resulted in an increment of the P precipitation efficiency (from 2.7 to 95 %). Due to the availability of substrate for the microorganism at high COD concentration, more organic matter degradation occurred at the anode chamber. Therefore, more electrons were transferred from the anode to cathode. As a result, more electrons were available in the cathode chamber for oxygen reduction reactions. An increase in the oxygen reduction reactions at the cathode led to an increase in the generation of hydroxide ions. As a result, average cathode pH increased from 7.4 (at COD=500 mg/L) to 9 (at COD=1500 mg/L)

At high cathode aeration flow rate (250 mL/min), the MFC system followed the same behaviour. Increasing the influent COD increased power density from 32 (at COD=500 mg/L) to 137 mW/m^2 (at COD=1500 mg/L). Furthermore, the difference of pH between anode and cathode increased at high COD, as a result the power output of the MFC increased. The improvement of power at high COD concentration was due to low internal resistance which enhanced the movement of protons (He et al., 2008). Beside power enhancement, P precipitation efficiency was increased also from 3% (at COD=500 mg/L) to 80% (at COD=1500 mg/L).

4.4.1.2 The effect of aeration flow rate at constant influent COD.

Increasing cathode aeration flow rate (from 50 to 250 mL/min) at low COD concentration led to an increase in the maximum power density from 26 to 48 mW/m^2. The enhancement of the generated power was relatively small at low COD concentration. Moreover, increasing aeration flow rate had no effect on P recovery. However, at high influent COD concentration, the effect of increasing cathode aeration flow rate from low to high on power density and P recovery was different. A

power enhancement of nearly two-fold (from 78 to 137 mW/m^2) was observed. Increasing aeration flow rate led to an increase in the amount of oxygen which is used as an electron acceptor; as a result, more power was generated at high aeration flow rate. Furthermore, increasing aeration flow at high COD concentration led to an increase in average cathode pH from 8.5 at low aeration flow rate to 9 at high aeration flow rate, but the P precipitation efficiency was reduced with an increase in aeration flow rate.

High aeration flow rate at the cathode chamber plays an important role in decreasing precipitation efficiency in the MFC. At a high aeration flow rate, it was noted that the concentration of NH$_4$ at the cathode effluent was lower than for cathode effluent with a low aeration flow rate. Increasing the aeration flow rate led to an increase in ammonia volatilization from the solution and that led to a reduction in the concentration of ammonium in the cathode chamber and, as a result, less P was precipitated as struvite (Yetilmezsoy and Sapci-Zengin, 2009; Rahman et al., 2014).

4.4.1.3 Optimisation and verification

The generated models were used to predict the optimal conditions for power density and P precipitation efficiency. The following operational conditions were obtained: influent COD of 1700 mg/L and cathode aeration flow rate of 210 mL/min. The optimal predicted values of power density and P precipitation efficiency were 184 mW/m^2 and 84% respectively.

Based on the statistical models, these operational conditions are the optimal conditions for maximum power density and P recovery. More experiments were carried out to validate the model predictions. The validation experiments were carried out near the optimum values, and the lab results showed that a maximum power density of 180 ± 15 mW/m^2 and P precipitation efficiency of 84 ± 6 % were achieved (Table 4.7). Finally, the lab results confirmed that the predicted values were in close agreement with the observed values and fell well within the 95% prediction interval.

Table 4.7 Validation of model predictions using experimental results

Operational condition	Actual and predicted variable	Limit of prediction interval	Power density (mW/m^2)	P precipitation (%)
COD= 1700 mg/l; cathode aeration= 210 mL/min	Actual value		180 ± 15	84 ± 6
	Predicted value (95% prediction interval)	Low	159	73
		High	211	96

4.5 The effect of pH on precipitation efficiency, struvite morphology, and crystal size
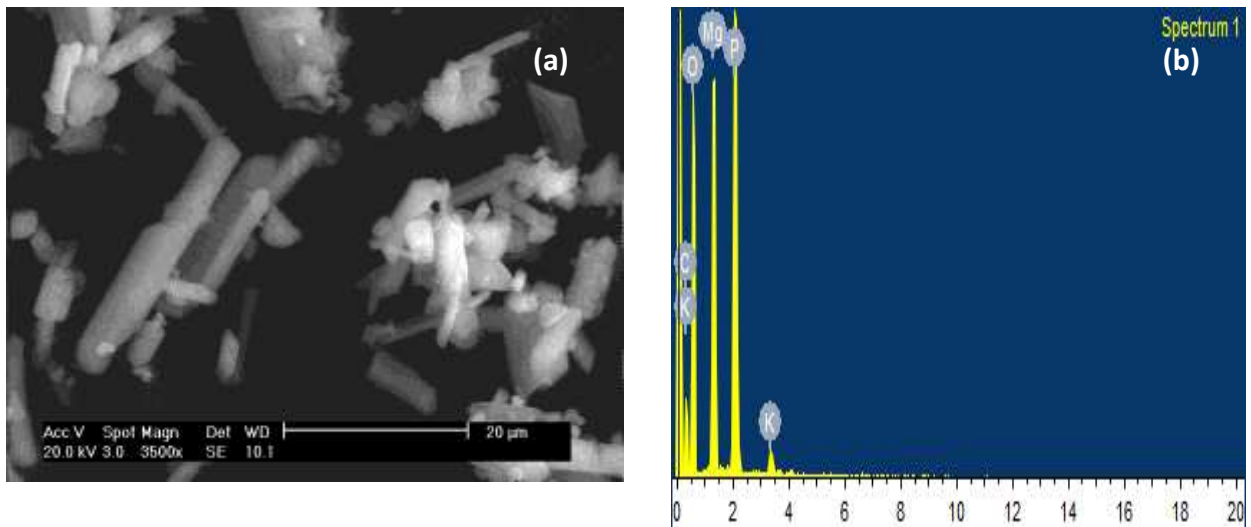
Figure 4.6 (a) Scanning electron microscopy image of struvite crystals and (b) EDX of the precipitates

Phosphorus recovery is highly dependent on pH, as P is highly insoluble in alkaline solutions. The results showed that P precipitation was increased when pH increased. Increasing cathode pH from 7.5 to 9 led to an increase in precipitation efficiency from 9 to 82%. Struvite can be formed in different shapes and sizes. In crystal formation, many parameters can affect the formation process, such as solubility, mixing effect, nucleation, mass transfer phenomena between the liquid phase and the surface, mechanical stability of the crystal, and crystallisation kinetics (Ronteltap et

al., 2010). In these conditions, struvite was formed with needle- and tubular-shaped crystals (Fig.4.6-a). Crystal shape was similar in all influent COD levels. Crystal morphology can be improved by increasing the concentration of Mg, as increasing the Mg molar ratio to 1.64 mM can improve crystal morphology and increase crystal size (Le Corre et al., 2005). Crystal size varied between 5 to 48 um. The recovered precipitate was analysed using the EDS spectrum, and the results showed that Mg, P, and O were the main elements of the precipitates. Indeed, these three elements (Mg, P, and O) are the main elements of the pure struvite standard (Cusick and Logan, 2012). As Mg, P, and O are the highest peaks in the EDS; this can confirm the purity of struvite where no other compounds have been found. In addition, struvite crystal size was investigated to identify the impact of operational conditions on struvite crystal size (Table 4.8). The results showed that increasing influent COD from 500 to 1500 mg/L led to an increase in average cathode pH from 7.4 to 9; as a result, the average struvite particle size increased from 9 to 14 µm. Changes in the solution pH led to a change in the degree of supersaturation during the operational time. An increase in pH caused an increase in supersaturation and a resultant increase in the growth rate (Le Corre et al., 2009).

Table 4.8 Operational conditions, average pH, crystal size, and removal efficiency

Operational conditions (COD)	Average pH	Temperature (°C)	Crystal size (Average µm)	P precipitation efficiency (%)
500	7.5	25	9	9
1000	8.4	25	17	74
1500	9	25	14	82

However, a smaller crystal size was noticed when COD was increased from 1000 mg/L to 1500 mg/L (Fig. 4.7). This phenomenon occurred at high supersaturation and can be explained by the competition between nucleation rate and crystal growth. At high supersaturation, the crystal growth process is lower than the nucleation rate and that's why more precipitates were found with smaller size (Ronteltap et al., 2010). In addition, high mixing speeds, which occurred during high aeration flow, can accelerate the nucleation rate and, at the same time, limit crystal growth, which is indicated by crystal breakage (Le Corre et al., 2009). On the other hand, any further

increase in cathode pH (pH> 9) might disturb the purity of the struvite, as some impurities, such as $Mg(OH)_2$ and Mg_3PO_4, probably emerged in the precipitations (Rahman et al., 2014).
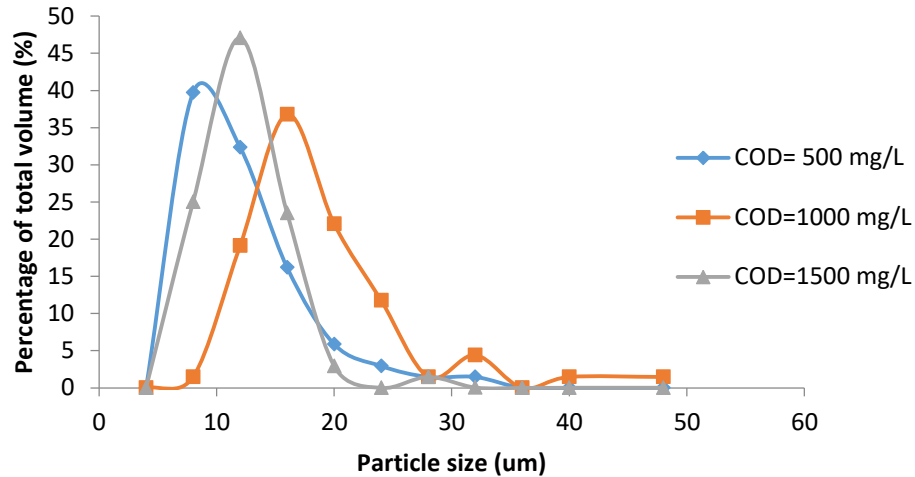
Figure 4.7 The impact of COD on particle size distribution

4.6 Summary

- This chapter has investigated the impact of COD levels and cathode aeration flow rate on energy generation and phosphorus recovery for MFC optimisation.

- Applying FFD was not adequate to explain the behaviours of the responses, except for COD removal efficiency.

- CCD was used to explain the behaviours of the responses and to find any interaction between the parameters; quadratic equations were used to find representative models.

- The effect of COD was greater than that of cathode aeration flow rate on the responses (power density, CE, COD removal efficiency, cathode pH, and precipitation efficiency).

- The statistical significance of COD and cathode aeration varied depending on the response. COD had a significant effect on all the responses, whereas cathode aeration had a significant effect on power density, CE, and

precipitation efficiency. The interaction effect between COD and cathode aeration was significant for cathode pH.

- The precipitates on the cathode surface and on the cation exchange membrane had a negative impact on the electricity generated, as deterioration was observed with high precipitates.

- Crystal size was affected by solution pH and supersaturation, as bigger crystal size was observed at high pH.

- The results outlined within this chapter have improved the current scientific understanding and can be used to optimise the system for P recovery and energy generation in dual-chamber MFCs.

4.7 Conclusion

The results in this chapter have investigated the impacts of the key parameters (COD and cathode aeration flow rate) as well as their interactive effects on dual-chamber MFC performance: power density, CE, COD removal efficiency, cathode pH, and precipitation efficiency. An FFD and a CCD were conducted to find the optimum condition for energy generation and P recovery. Both energy generation and P recovery were highly affected by COD and aeration flow rate. Cathode pH increases with increases in influent COD, and this results in increases in P precipitation. In addition, power generation increases with increases in COD. COD has mixed effects on cathode pH at different levels of cathode aeration flow rate. System optimisation of energy generation and P recovery demonstrates that optimum energy generation and P recovery can be obtained when the MFC is operated at COD =1700 mg/L and a cathode aeration flow rate of 210mL/min. Moreover, cathode pH has an impact on crystal size, as bigger crystals were found at pH between 8 and 9. The information in this chapter can be used in developing a full understanding of the MFC system under a range of conditions. It will also help to operate the system under optimal conditions, which could help to reduce the operational costs and optimise the responses.

Chapter 5

Concurrent Hydrogen Production and Phosphorus Recovery in Dual Chamber Microbial Electrolysis Cell

5.0 Concurrent Hydrogen Production and Phosphorus Recovery in Dual Chamber Microbial Electrolysis Cell

5.1 Introduction

This chapter presents the general performance analysis of the dual chamber microbial electrolysis cell (MEC) for concurrent hydrogen production and P recovery. In addition, this chapter investigates the influence of applied voltage and COD concentration on hydrogen production and struvite crystallisation in MEC. The specific objectives of the study were:

- To assess P recovery as struvite in dual chamber MEC.

- To understand the role of applied voltage and COD concentration in P recovery as struvite and in H_2 production using a dual-chamber MEC.

- To improve and optimize struvite precipitation and hydrogen production under different operational conditions (applied voltage and COD concentration), using a response surface methodology (RSM) optimization statistical model.

Microbial electrolysis cells (MECs) are a new and promising approach for hydrogen (H_2) production from organic matter, including wastewater and other renewable resources. In MECs, electrochemically active bacteria oxidise organic matter and generate CO_2, electrons and protons. The bacteria transfer the electrons to the anode and the protons are released into the solution. The electrons then travel through a wire to a cathode and combine with the free protons in the solution to produce hydrogen gas (Equations (5.1) and (5.2)) (Logan et al., 2008).

Anode chamber: $CH_3COO- + 4\ H_2O \rightarrow 2\ HCO^{3-} + 9\ H^+ + 8\ e^-$ \hspace{1cm} (5.1)

Cathode chamber: $8\ H^+ + 8\ e^- \rightarrow 4\ H_2$ \hspace{2cm} (5.2)
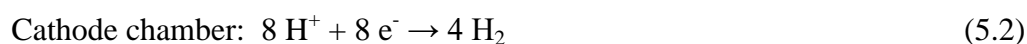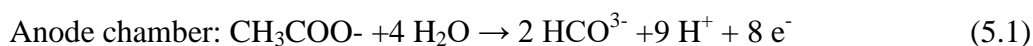
Due to the oxidation of the organic matter at the anode electrons and protons are released. An external power supply is used to overcome the thermodynamic limit for hydrogen evolution. The electrons are transferred through the resistor to the cathode chamber, where protons are transferred through the solution to the cathode chamber.

Protons and electrons are combined together to produce hydrogen gas (equation 5.2). The consumption of protons at the cathode chamber increases solution pH (Moussa et al., 2006). Based on this hypothesis, the cathode chamber in the MEC can be used to precipitate P as struvite. In this chapter, a dual chamber MEC was used to overcome the pH buffering between the anode and the cathode, and improve P recovery.

5.2. Materials and Methods

5.2.1 Reactor Set-up

Two sets of dual chamber H-type bottles (Adams & Chittenden Scientific Glass, Berkeley, CA, USA), were used to construct the MECs. Each had a height of 105 mm and an outer diameter of 95 mm (see Figure 5.1 & 5.2). Each set contained two identical bottles, with a volume of 300 mL for each chamber. Both bottles were connected at the middle by a clamp and a sealing ring with an outer diameter of 45 mm. Each chamber contained two ports, one at the bottom and one at the top (each port was 14 mm in diameter). These ports were fitted with sealing rings for the pH and ORP probes. The anode and cathode electrodes were made of carbon cloth measuring 2.5×5 cm, with a projected area of 25 cm^2 (Fuel Cells Etc., Texas, USA). The cathode contained a Pt catalyst (0.5 mg/cm^2 10% Pt on carbon cloth electrode) to improve cathode performance, whilst the anode was plain carbon cloth. Both electrodes were connected with a titanium wire (0.5 mm, purity > 99.98%, Alfa Aesar, Heysham, UK). A Nafion membrane (Nafion 117#, Sigma-Aldrich, London, UK), with an area of 12.57 cm^2, was placed in the middle of the anode and the cathode chambers. The membrane was pretreated by boiling in H_2O_2 (30%) and deionized water, followed by 0.5 M H_2SO_4 and deionized water, each for one hour. It was then stored in deionized water prior to being used. A DC power supply, PSD 30/3B (CALTEK, Hong Kong), was used to apply voltage for the MEC. The voltage was added by connecting the positive pole of the power source to the anodes, while the negative pole led to a high precision resistor (10 Ω) and the cathodes. The electrodes were positioned 8 cm apart. The components of the reactor were cleaned before use, and the MECs were maintained at 20 °C in a temperature-controlled room.
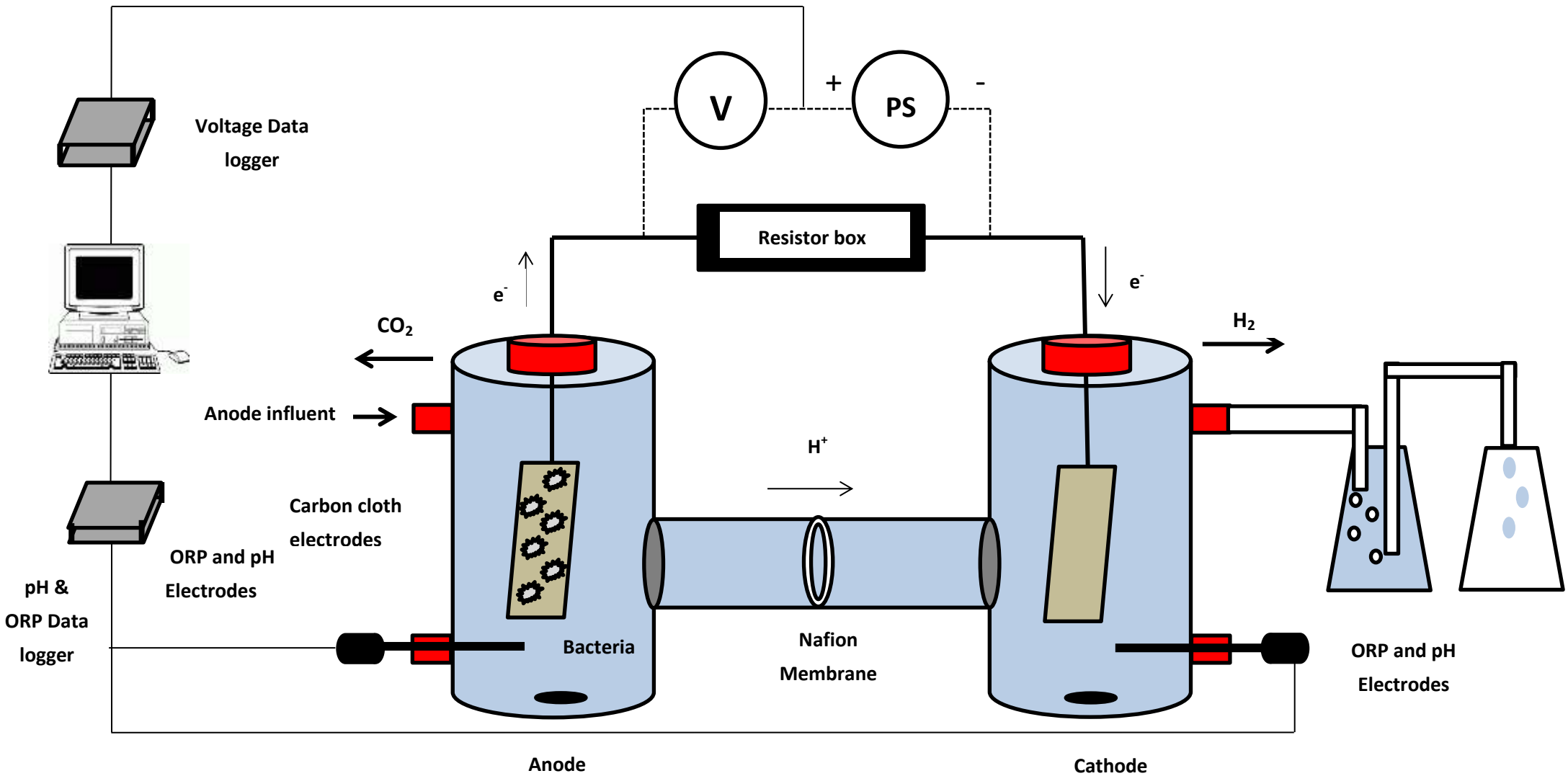
Figure 5.1 Experimental set-up of the dual chamber MEC

5.2.2 Inoculation

Activated sludge flocs and anaerobic digester sludge were collected from Cardiff Wastewater Treatment Plant (Cardiff, UK). The wastewater treatment sites are operated by Dwr Cymru Welsh Water, Ltd, and are used to treat domestic wastewater. Samples were collected in 1 L containers and transferred directly to the lab. They were used directly for the inoculation, and pure nitrogen gas was used during the inoculation process. The anode chamber was inoculated with a 1:1 mixture of activated sludge and anolyte medium (containing, in g/L: Sodium acetate 3.28 + ammonium chloride 0.31 + potassium chloride 0.13 + sodium phosphate anhydrous monobasic 2.69 + disodium hydrogen phosphate 4.33 + 10 mL of vitamin solution + 10 mL of a trace element solution). The inoculum was introduced into the cell through the upper sampling port, using a syringe. During the inoculation process, a small syringe was used to sparge the media and the headspace with nitrogen.
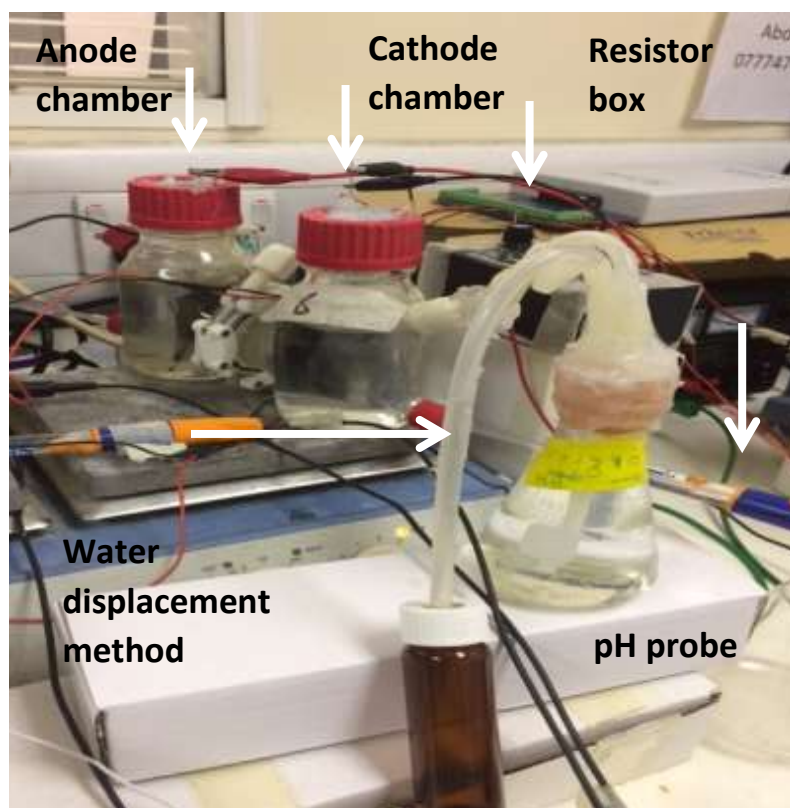
Figure 5.2 Lab experimental set-up of the dual-chamber MEC

5.2.3 Sterilisation

All the MEC parts were cleaned with soap; rinsed with distilled water three times; and, finally, dried and wiped. Anodes were left in dionised water for one day prior to use. In addition, a sterilization stage was conducted, using autoclave at 121 °C for 30 minutes, for any equipment that was used in the MEC. In addition, the cathode chamber was washed and cleaned after each batch to remove any precipitate and attached particles.

5.2.4 Degassing

Pure nitrogen gas (99.9%, BOC, Ltd., Cardiff, UK) was used to remove the dissolved oxygen in the media. Small syringes were fitted in the anode and cathode chambers, and nitrogen gas was sparged through the solution for 20 minutes.

5.2.5 Start-up

The anode chambers were inoculated with a 1:1 mixture of activated sludge and anolyte medium (containing acetate, in a phosphate buffer). A small syringe was used to sparge the media and the headspace with nitrogen during the inoculation and media replacement. The cathode chamber was filled with 50 mm phosphorus buffer, and it was continuously aerated using an aquarium pump. Both electrodes were connected to 1000 Ω of external resistance at the initial stage of the operation; this was changed to 10 Ω after the inoculation process. A fresh medium, combined with inoculum mixture, was used to replace the anolyte when the voltage dropped. The replacement procedure was carefully conducted to avoid any distribution of the biofilm. Once the system achieved stable electricity production for at least three cycles, the phosphorus buffer was disposed of and both chambers were fed with synthetic wastewater.

5.2.6 MEC Experimental Design

Anode and cathode influent pH was adjusted to pH = 7 and media replacement was carried out in an anaerobic environment, to maintain the anaerobic environment for the anode biofilms. Anode synthetic wastewater contained (0.6-2 g/L depends on the operation condition) sodium acetate; KH_2PO_4, 0.65 g/L; K_2HPO_4, 0.65 g/L; KCl, 0.74 g/L; NaCl, 0.58 g/L; NH_4Cl, 0.375 g/L; $MgSO_4 \cdot 7H_2O$, 0.1 g/L; $CaCl_2 \cdot 2H_2O$, 0.1 g/L; 0.1 mL/L of a trace element mixture and vitamins. The cathode synthetic wastewater contained (0.5 g/L sodium acetate; KH_2PO_4, 0.25 g/L; K_2HPO_4, 0.25 g/L; KCl, 0.74 g/L; NaCl, 0.58 g/L; NH_4Cl, 0.375

g/L; $MgCl_2$, 0.32 g/L; $MgSO_4 \cdot 7H_2O$, 0.1 g/L; $CaCl_2 \cdot 2H_2O$, 0.1 g/L). After each MEC cycle, both chambers were drained, and anode chamber was exposed to air for 30-45 minutes to inhibit methanogen growth (Call and Logan, 2008). It was then refilled with synthetic wastewater solution, and both anode and cathode chambers were sparged for 20 minutes with pure N_2. The MECs were run at applied voltages of (0.4, 0.5, 0.8, 1.1 and 1.2 V) for at least three batch cycles at each voltage. In addition, five COD levels were used in the artificial feed solution, as follows: 1700, 1500, 1000, 500 and 300 mg/L. The current densities and operation time of a cycle varied with the change of the anolyte compositions. The COD reduction was calculated at the end of each cycle. The volume of the produced gas in the cathode chamber was measured via the displacement method. The produced gases in the MEC were collected into an air tight gas collecting a glass flask filled with water (saturated NaCl) via a silicone tube. The data presented are the average values ± SD.

5.2.7 Anode and Cathode sampling

At the end of each batch, the anolyte and catholyte were removed from the MEC. Approximately 20 mL of each (anolyte and catholyte) were collected in small vials and analysed directly.

5.2.8 Analytical Methods

5.2.8.1 Water analysis

All results reported are the average of at least six independent trials (three cycles for each cell). Chemical oxygen demand (COD) analysis was carried out using a Hach Lange kit LCI 400 (HACH, UK). To determine the COD concentration, 2 mL of the sample was added to the COD cuvette and digested at 148 °C for two hours. COD values were then determined using a DR3900 spectrophotometer (HACH, UK), according to its operating procedures.

COD removal efficiency was calculated using Equation (5.3):

$$\text{COD removal efficiency} = \frac{\text{anode COD influent} - \text{anode COD effluent}}{\text{anode COD influent}} \times 100 \qquad (5.3)$$

Ammonium (NH_4-N) and Orthophosphate concentration were measured using Hach Lange kit LCK 303 and LCK 049 (HACH, UK). Total phosphorus (TP), magnesium (Mg), calcium

(Ca), potassium (K), and sodium (Na) concentration were measured using inductively coupled plasma optical emission spectrometry (ICP-OES), type Perkin Elmer Optima 2100DV apparatus. In addition, anion concentrations were determined using an ion chromatograph (Dinonx ICS-2000 IC).

5.2.8.2 pH and ORP

Anolyte and catholyte pH and oxidation-reduction potential (ORP) were measured continuously every 15 mins during each batch, using 12-Channel measuring and monitoring data logger (EA Instruments, London, UK). pH Electrodes (Shaft diameter 4.3 mm, 90 mm long) in a refillable glass body (EA Instruments, London, UK) were fixed in the bottom port of both chambers. ORP electrodes (diameter 4.3 mm, 90 mm long) in a refillable glass body (EA Instruments, London, UK) were fixed in the bottom port of both chambers.

5.2.8.3 Gas analysis

The total volume of the gas produced was measured using the water displacement method (Logan et al., 2008). A gas-tight flask was connected to the cathode chamber with silicon tubing. A gas chromatograph (compact GC, CE Instruments Ltd, UK) was used to analyse the produced gas in the cathode chamber during each batch, but anode gases were analysed periodically. The compact GC was equipped with a thermal conductivity detector (TCD) and flame ionization detector (FID). Argon gas was used as a carrier gas for the GC, and was run at a flow rate of 2 mL/min. A gas-tight lock syringe (1 mL, Hamilton lock syringe, Sigma-Aldrich, UK) was used to sample the gases from the headspace of the anode and cathode chambers and from the air-tight flask. The volume of each gas was calculated as Equation 5.4:

$$V_i = (V_t + V_h) * X_i \tag{5.4}$$

where V_t is the measured gas volume (mL) using the displacement method, V_h is the headspace volume of the chamber (mL) and of the gas collection tube at sample time (t), and X_i is the gas fraction (%). Since nitrogen gas was used to create an anaerobic environment in the MEC, it was removed from the calculation in order to find the concentration of the other gases.

5.2.9 Phosphorus Precipitation in MEC

The theoretical P, Mg, and NH_4 concentration in the cathode solution was approximately 3 mM at pH 7. For P precipitation as struvite a 1:1:1 molar ratio of NH_4:Mg:P should be achieved. Before and after each cycle, the cathode chamber was washed with deionised water three times, and then cleaned and dried properly to remove any attached precipitates on the chamber walls. After each precipitation cycle, the used cathode was removed for maintenance and replaced with a new one (Section 3.2.13). At the end of each cycle, the catholyte was filtered using a 0.2 um filter membrane (Fisher Scientific, UK). The precipitate was collected, weighted and analysed by X-ray diffraction (XRD) and by scanning electron microscopy coupled with energy dispersive X-ray spectroscopy (SEM-EDS). The recovered P was calculated using Equation (5.5):

$$\text{Precipitation efficiency (\%)} = \frac{P_{in} - P_{out}}{P_{in}} \times 100 \qquad (5.5)$$

where P_{in} is the P concentration in the catholyte influent, P_{out} is the P concentration in the catholyte effluent. In addition, P precipitation rate (g-P/$m^3_{cathode}$-d) was calculated using Equation (5.6):

$$\text{P precipitation rate (g-P/}m^3_{cathode}\text{-d)} = \frac{(TP_{in} - TP_{out}) \times V_{catholyte}}{V_{cathode} \times \Delta t} \qquad (5.6)$$

where TP_{in} is the total phosphorus influent cathode concentration, TP_{out} is the total phosphorus effluent cathode concentration, $V_{catholyte}$ is the volume of catholyte solution (m^3), $V_{cathode}$ is the volume of cathode chamber (m^3), and Δt is the batch duration (d).

5.2.10 Scanning electron microscopy (SEM) and energy dispersive X-ray spectrometry (EDX) analysis

For SEM analysis, the precipitates that accumulated on the cathodes and in the cathode chamber were analysed to examine the morphology of the crystal as well as its elemental composition. In addition, the used proton exchange membrane (PEM) was cut into pieces, carefully rinsed with deionized water and finally dried completely at ambient temperature. The microscopic structure and elemental components of the PEM surface were analysed using a FEI-XL30 Environmental SEM equipped with an EDX.

5.2.11 Crystals quality, composition, and purity

The quality of the collected crystals was determined by analysing their composition. Struvite purity was determined using SEM-EDS and the dissolution method to identify the composition of the crystals. Approximately 0.05 g of crystals were dissolved in 50 mL of 0.5% nitric acid solution. In order to accelerate dissolution, the samples were stirred with a magnetic stirrer for 24 hours, after which samples were analysed for magnesium, ammonia, orthophosphate, calcium, aluminium and iron using inductive coupled plasma (ICP) (Fattah et al., 2008).

5.2.12 Cathode maintenance

After each batch, the cathode electrode was removed from the MEC for maintenance, and was replaced with a new electrode. P precipitation on the cathode was removed via immersion in a dissolution solution. The electrode was immersed 3 times in deionised water (pH = 7), for 2 days each time. After deionized water dissolution, the electrode was immersed again 3 times in MES buffer ($C_6H_{13}NO_4S$ [MES]:10 mM, adjusted to pH 5.5 with NaOH) each for 30 hours. Finally, the electrode was rinsed and dried before use (Hirooka and Ichihashi, 2013).

5.2.13 Visual Minteq software

Visual Minteq modeling software (Visual MINTEQ 3.1) is a chemical equilibrium computer programme that allows for the calculation of speciation, solubility and equilibrium in both solid and dissolved phases of minerals in an aqueous solution (Çelen et al., 2007). Minteq model default values were used in this study. Minteq was used to predict the saturation index of the soluble salts, and oversaturated solids were allowed to precipitate.

5.2.14 Voltage data loggers

The voltage across the external resistance was recorded every 15 minutes using the ADC-20 data logger system (Pico Technology, UK). Based on the recorded voltage, different parameters were calculated using the following equations (Logan et al., 2008):

- Current and current density were calculated using equations 3.6 and 3.7.

- The total theoretical number of moles of hydrogen produced based on COD removal

$$n_{th} = \frac{b_{H2/S} v_L \Delta S}{M_s} \tag{5.7}$$

$b_{H2/S}$ is the maximum stoichiometric hydrogen production possible from the substrate (4 mol-H_2/mol-$C_2H_4O_2$), V_L is the volume of liquid in the reactor (250 mL), ΔS (g-COD/L) is the change in substrate concentration over a batch cycle, and Ms is sodium acetate molecular weight (82 g/mol).

- The moles of hydrogen that can be recovered based on the measured current (n_{CE})

$$n_{CE} = \frac{\int_{t=0}^{t} I \, dt}{2 \, F} \tag{5.8}$$

where I is the current (A) calculated from the voltage across the resistor (10 Ω), 2 is used to convert moles of electron to moles of hydrogen, F is Faraday's constant (96,485 C/mole-e^-), and dt (s) is the interval (15 minutes) over which data were collected.

- Coulombic efficency (CE)

$$r_{CE} = \frac{n_{CE}}{n_{th}} = CE \tag{5.9}$$

where CE is the coulombic efficiency or the moles of electrons recovered as current versus the total amount of electrons consumed as substrate.

- Cathodic hydrogen recovery (r $_{Cat}$)

$$r_{Cat} = \frac{n_{H2}}{n_{CE}} \tag{5.10}$$

r_{Cat} is the moles of hydrogen recovery, relative to that possible based on the measured current, where n_{H2} is the number of moles of hydrogen recovered during a batch cycle.

- Hydrogen recovery (r $_{H2}$)

$$r_{H2} = r_{CE} * r_{Cat} \tag{5.11}$$

- Maximum volumetric hydrogen production rate (m^3-H_2/m^3-d)

$$Q = \frac{43.2 \, I_v r_{Cat}}{F c_g(T)} \tag{5.12}$$

where I_v (A/m^3) is volumetric current density averaged over a 4-hour period of maximum current production for each batch cycle normalized by the liquid volume, c_g is the concentration of gas at a temperature T calculated using the ideal gas law, and 43.2 is for unit conversion. All of the experiments were performed using duplicate cells, and the reported data are the average of at least six independent trials (three cycles for each cell).

- Energy recovery

The amount of energy added to the MEC by the power source was calculated,

$$W_E = \sum_1^n (I\, E_{app}\, \Delta t - I^2 R_{ex}\, \Delta t) \tag{5.13}$$

where I is the current, E_{app} is the voltage applied in the circuit using the power source (V), Δt is the time increment for n data points measured during a batch cycle (s), and R_{ex} is the external resistor (10 Ω). Heats of combustion equations are commonly used in MEC studies to calculate the energy balance and estimate the energy content of organic matter (Logan et al., 2008)

- The amount of energy added by the substrate.

$$W_s = \Delta H_s n_s \tag{5.14}$$

where ΔH_s is the heat of combustion of the substrate (870.28 KJ/mol), and n_s is the number of mole of substrate consumed during batch cycle based on COD removal.

- The energy efficiency relative to the electrical input, η_E

$$\eta_E = \frac{n_{H2} \Delta H_{H2}}{W_E} \tag{5.15}$$

where η_E is the ratio of the energy content of the hydrogen produced, to the input electrical energy consumed, ΔH_{H2} is the energy content of hydrogen based on the heat combustion value (285.83 KJ/mol) and $W_{H2} = n_{H2} \Delta H_{H2}$.

- The efficiency relative to the consumed substrate, η_S

$$\eta_S = \frac{W_{H2}}{W_S} \tag{5.16}$$

- The overall energy recovery based on both the electricity and substrate inputs, η_{E+S}

$$\eta_{E+S} = \frac{W_{H2}}{W_E + W_S} \tag{5.17}$$

- The electrical energy input per kg of COD removed (Whin/kg-COD)

$$Wh_{in} = \frac{\int_2^t W_{in} dt}{\Delta COD.\dot{V}} \tag{5.18}$$

where W_{in} is the electrical input, ΔCOD the change in solution COD, and V the reactor liquid volume.

- The energy recovered as hydrogen per kg of COD (Wh_{H2}, kWh/kg-COD)

$$Wh_{H2} = Y_{H2}.HHV_{H2} \tag{5.19}$$

where Y_{H2} (kg H_2/kg-COD) is the hydrogen yield, HHV_{H2} is the higher heating value of hydrogen (39.4 kWh/kg-H_2)

Finally, pH gradient loss over the membrane was calculated (Sleutels et al., 2009),

$$E_{\Delta pH} = \frac{RT}{F}\ln(10^{(pH\ cathode - pH\ anode)}) \tag{5.20}$$

where R is the universal gas constant (8.3145 J mol−1 K−1) and T is the temperature (293 K).

5.2.15 Statistical analysis

Regression analysis was used to determine the effect of each variable and the interaction's effect on the performance of the system. This aids in understanding and optimising the system by identifying the impact of different parameters on MEC performance. In developing the regression equation, the actual values were coded to define the levels in the design, and to make the analysis easier by removing the non-significant terms without changing the estimates for the terms. The relationship between the coded values and the actual values was described by equation 4-3.The coded values are shown in Table 5.1.

Design Expert Version 10.0.3 (Stat-Ease Inc., Minneapolis, MN, USA) was used for the design, analysis, and optimisation. The variables used were: applied voltage (X1) and influent COD concentration (X2). The responses were: CE (Y1), COD removal efficiency (Y2), cathode pH (Y3), Precipitation efficiency (Y4), and maximum volumetric hydrogen production (Y5). Analysis of variance (ANOVA) provided the statistical results and the diagnostic check tests to evaluate the adequacy of the models. The quality of the fitted models was evaluated using the coefficient of determination R^2, and its statistical significance was checked by the Fisher F-test. Model terms were evaluated by the P-value (probability of error) with a 95% confidence level.

Table 5.1 Level of independent variables in CCD

Variable	Design	Factor	Applied levels				
			--	-	Centre	+	++
Central composite design	X_1	Applied voltage (V)	0.4	0.5	0.8	1.1	1.2
	X_2	COD (mg/L))	300	500	1000	1500	1700

Three-dimensional plots and their respective contour plots were obtained based on the effects of the two factors (applied voltage and COD). In total, 19 experiments were conducted with 8 factorial points, 8 axial points and 3 center points. Replicates of the center points were added to the design to examine the adequacy of the model and to get a good estimate of the experimental error.

5.2.15.1 Central composite design (CCD)

The study determined the effects of applied voltage (X_1) and influent COD concentration (X_2) on coulombic efficiency (CE), COD removal efficiency, cathode pH, precipitation efficiency and maximum volumetric hydrogen production. The nonlinear behaviour of the response is explained by the following quadratic model:

$$y = \beta_o + \sum_{I=1}^{n} \beta_i X_i + \sum_{i=1}^{n} \beta_{ii} X_i^2 + \sum_{i=1}^{n-1} \sum_{j=1+i}^{n} \beta ij\, X_i X_j + E \qquad (5.21)$$

where y is the response, βi is the coefficient of the ith main effect, β_{ii} is the coefficient of the ith quadratic term, βij is the coefficient of the interaction between the ith and jth terms and E is the error term. Two replicates were employed at each factor combination. At the beginning

of each factor combination, the system was run for at least 2 batches to let the system adapt to the new conditions.

5.3 Results and discussion

5.3.1 MEC general performance

During the inoculation period, the system was operated as an MFC and transformed to an MEC when it achieved a stable electricity production. During the start-up period, 50 mM of phosphate buffer solution (PBS) was used as a catholyte and the external load was changed from 1000Ω to 10Ω. Since the cathode chamber in an MEC operates under an anaerobic environment, pure nitrogen gas was used to flush the chamber and the headspace for 20 minutes to remove the oxygen. Finally, a DC power source was used to apply 0.8 V to the circuit for hydrogen production, unless stated otherwise.

All of the experiments were performed using duplicate cells, and the reported data are the average of at least six independent trials (three cycles for each cell unless stated otherwise). After the start-up period, PBS was replaced with a synthetic cathode solution (Section 5.2.6) for P recovery and H_2 production. Both anolyte and catholyte were replaced when the voltage decreased below 2 mV, and the anode chamber was left exposed to air for 20 minutes to inhibit the growth of methanogens (Yossan et al., 2013). At the anode chamber, the microorganism consumes the organic matter and releases electrons and protons. At the cathode, hydrogen gas is produced by the combination of protons (which are transferred from the anode to the cathode through the membrane) and electrons. Reduction-oxidation reactions (REDOX) in both the anode and the cathode chambers affected the solution's pH, where anolyte pH decreased and catholyte pH increased due to proton consumption.

5.3.2 COD removal efficiency in the anode

The impact of applied voltage and influent COD were studied to understand the impact of these parameters on P recovery and hydrogen production. COD removal is an important parameter to assess the ability of MECs to treat wastewater and to find any correlation between applied voltage and COD removal. MECs were operated under different applied voltages (0.4, 0.5, 0.8, 1.1, and 1.2 V) at COD =1000 mg/L. The achieved COD removal efficiency ranged from 59 to 92% (Figure 5.3). COD removal efficiency increased when the applied voltage was increased from 0.4 to 0.8 V, where the system achieved the maximum removal efficiency. The removal efficiency then decreased when the applied voltage rose

above 0.8 V. Increasing the applied voltage from 0.4 V to 0.8 V increased the removal efficiency by 30%. Increasing the applied voltage above 0.8 V had a negative impact on COD removal, where high voltage could inhibit bacteria activity (Luo et al., 2005; Ding et al., 2016). As a result, low COD removal was observed. Similar results, with high COD removal efficiency, were found in dual chamber MEC (Ditzig et al., 2007; Ding et al., 2016). It was shown that the voltage applied had a great impact on COD removal, and that applying the optimal value can improve COD removal and reduce the operational cost.

On the other hand, MECs also were operated under different COD concentrations (300, 500, 1000, 1500 and 1700 mg/L) at applied voltage = 0.8 V. The achieved COD removal efficiency ranged from 50 to 90%. High COD removal was achieved with low influent COD concentration. The results showed that COD removal was clearly affected by current generation and by the period of a batch cycle. Therefore, choosing the optimal applied voltage and COD concentration is crucial to obtain high removal efficiency of the substrate.
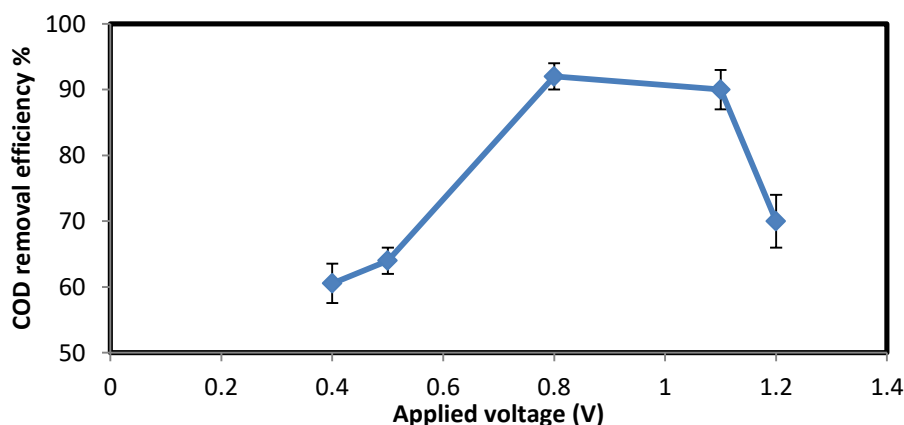
Figure 5.3 COD removal efficiency as a function of applied energy

5.3.3 Coulombic efficiency (CE)

CE was calculated based on the COD concentration and the generated current, using Equation (5.9). Coulombic efficiency was affected by the applied voltage and by COD influent concentration, where increasing the applied voltage from 0.4 to 1.2 V at COD = 1000 mg/L, increased the CE from 9.5 ± 0.5 % to 21 ± 0.5 %. Moreover, increasing COD concentration from 300 mg/L to 1700 mg/L, at an applied voltage of 0.8 V, led to a decrease in coulombic efficiency from $51 \pm 2.7\%$ to $13.3 \pm 0.9\%$. This means that a small part of the substrate was

used for current generation and the rest was used for methane production (Sleutels et al., 2011). The availability of excess substrate in the anode chamber might lead the methanogens to consume it, instead of using it in current production. Influent COD should be controlled to achieve the balance between high CE and high COD removal efficiency.

5.3.4 Water analysis in the anode chamber

Water quality parameters (NH_4^+, NO_3^-, NO_2^- and TP) were analysed in the influent and effluent of the anode chamber. The concentration of $N-NH^{4+}$ and TP in the anode influent were 94.5 $\pm$ 2.9 and 100 $\pm$ 7 mg/L, respectively. The concentration of TP in the anode effluent was 102 $\pm$ 2.7 mg/L. TP concentration in the anode effluent was equal to or slightly higher than that in the anode influent, due to the release of stored phosphate in the bacteria under an anaerobic environment (Kim, 2006; Tao et al., 2014). The concentration of $N-NH^{4+}$ in the anode effluent was 65 $\pm$ 10 mg/L. The reduction of ammonium concentration in the anolyte occurred due to microbial consumption and ammonium diffusion to the cathode chamber through Nafion 117, to compensate charge balances between the anode and cathode chambers (concentration gradient) (Cord-Ruwisch et al., 2011). Moreover, the concentrations of nitrate and nitrite in the anode effluent were low and nearly the same as those in the anode influent, due to the anaerobic environment.

5.3.5 Hydrogen production

Hydrogen production rate was analysed to evaluate the performance of the MECs. The gases produced in the cathode chamber were analysed using compact GC; they were found to contain mainly hydrogen in all cases, and methane was detected in the anode chamber. The hydrogen production rate in the dual chamber MEC ranged from 0.06 to 0.28 $m^3.H_2/m^3$.d. The volume of the produced gas was variable and dependent on the applied voltage. Increasing the applied voltage led to an increase in the current density. As a result, an increase in the production of hydrogen gas ($P < 0.05$) was observed (Figure 5.4). An increase in applied voltage from 0.4 to 1.2 V led to a more than four-fold increase in hydrogen production. The system achieved a maximum volumetric hydrogen production rate of 0.22 m^3-H_2/m^3.d at (COD=1000 mg/L, applied voltage =1.2).
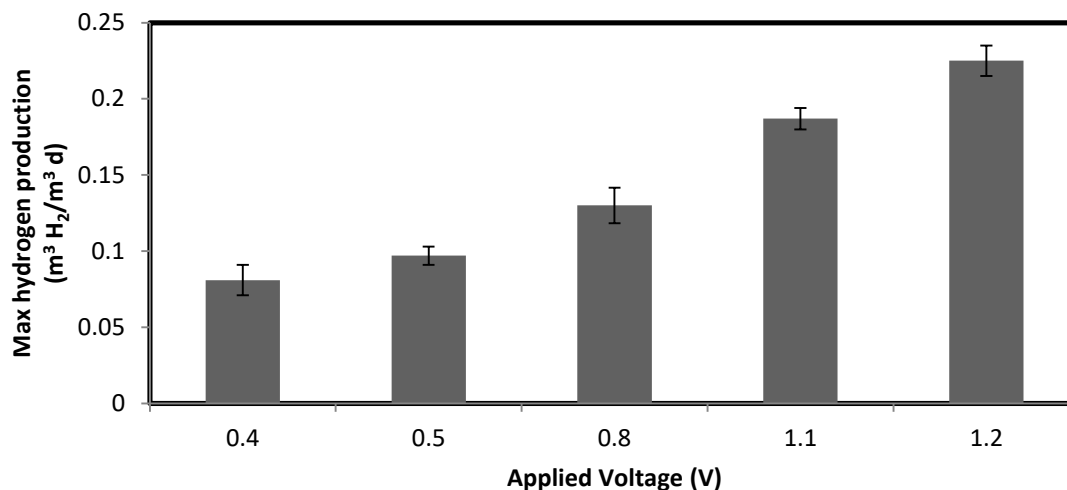
Figure 5.4 Hydrogen production rate as a function of applied voltage

In addition, different COD concentrations were used to identify the impact of COD concentration on hydrogen production. The cycle duration and the current densities varied when anolyte COD concentrations were changed. Figure 5.5 shows that there was no correlation between COD concentration and hydrogen production rate, where increasing COD concentration from 300 to 1700 mg/L had no impact on hydrogen production (P > 0.05). This means that changing the anolyte COD concentration did not affect the H_2 production rate in the MEC. The maximum hydrogen production rate (0.18 $m^3.H_2/m^3.d$) was achieved at COD= 500 mg/L, and the H_2 production rate varied at different COD concentrations. The low hydrogen production rate in this study was similar to previous studies (Rozendal et al., 2007; Yossan et al., 2013).

The overall energy recovery rates in the MEC ranged from η_{E+S}= 25 ± 1 % to 37 ± 1.7 %. Overall energy recovery was calculated under different applied voltages. The results showed that there is no correlation between applied voltage and overall energy recovery (P > 0.05).

The electrical consumption in the MEC was higher than the energy production in all tests. An increase in applied voltage in the circuit, from 0.4 to 1.2 V, increased electrical energy input Wh_{in} from 0.5 ± 0.05 to 1.9 ± 0.2 kWh/kg-COD. The low strength of the wastewater required the use of relatively high added voltages, and the reactor had high internal resistance leading to low hydrogen recoveries and the H_2 production in the MEC was not enough to recover the electrical consumption. However, the recovered energy and struvite can be used to reduce the operational cost.
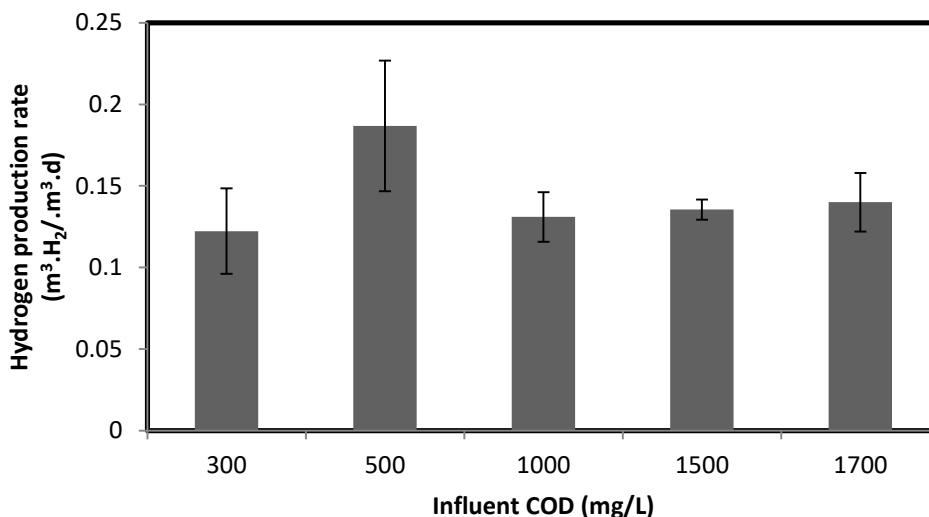
Figure 5.5 Hydrogen production rate as a function of influent COD concentration

5.3.6 Phosphorus recovery in MEC

Phosphorus started to precipitate as struvite when the cathode pH reached 8. The system achieved a maximum precipitation efficiency of $95 \pm 2.13\%$. P was recovered in the cathode chamber, where proton consumption converts the neutral solution to alkaline. Figure 5.6 shows the influence of applied voltage on cathode pH. An increase in applied voltage from 0.4 to 0.8 V increased the average cathode pH from 8 to 9.1. However, increasing the applied voltage to 1.2 led to a decrease in the average cathode pH, down to 8.5. Using high voltage may inhibit bacteria activity and affect the oxidation process in the anode chamber, with the result that low protons are released and cathode pH is affected.

To understand the role of the current on P recovery and cathode pH, the system was shifted to an open circuit system (OCV), where no resistance was used in the circuit, and MECs were operated for at least three cycles. Cathode pH did not increase and remained at 7 (Figure 5.6). These findings show the importance of determining the ideal applied voltage to obtain high pH in the cathode.
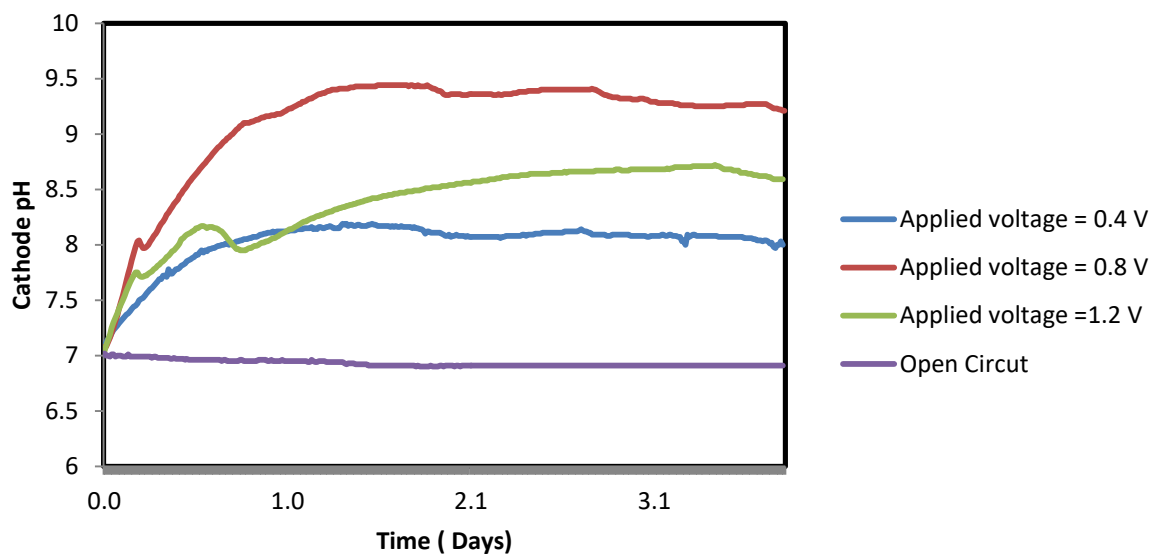
Figure 5.6 The impact of applied voltage on cathode pH

Precipitation efficiency (in OCV) was less than 1%, but when the circuit closed and 0.4 V was applied, the MEC achieved $45 \pm 5\%$ precipitation efficiency (Figure 5.7). Furthermore, precipitation efficiency improved and reached $90 \pm 7\%$ when the applied voltage increased to 0.8 V. At 1.2 V, precipitation efficiency reached $92 \pm 5\%$. Similar results were observed with CE, where an increase in the applied voltage increased CE.

The precipitated P was found on the cathode electrode, suspended on the catholyte and on the chamber walls. The precipitation rate achieved in the MECs ranged from 1.4 to 20 g-P/m^3.d. The highest precipitation rate was achieved at 0.8 V. An increase in the applied voltage to 1.2 V decreased the precipitation rate. Increasing the applied voltage to 1.2 V inhibits microorganism activity and increases the cycle duration. The precipitation rate was affected by cycle duration, which decreased with applied voltage (Cusick and Logan, 2012). Operating MECs with long cycle duration is favourable for H$_2$ production and COD removal (Escapa et al., 2013).

122
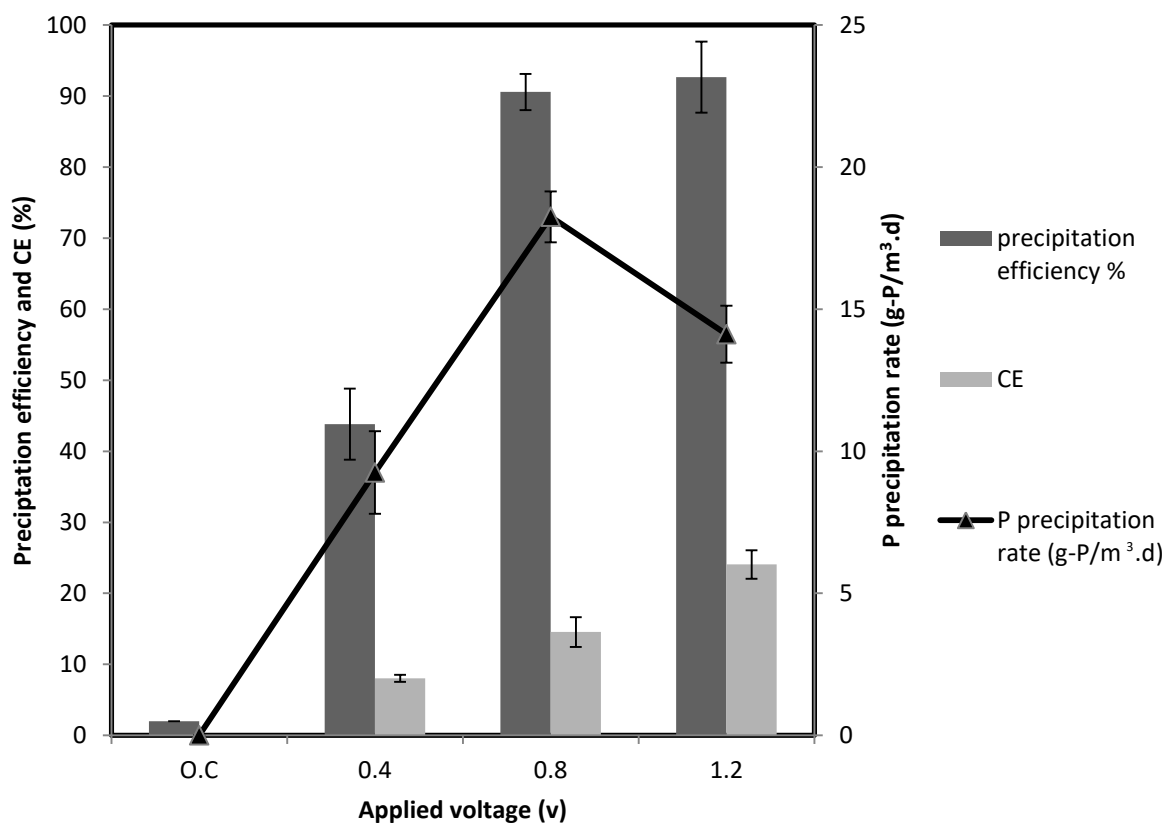
Figure 5.7 The impact of applied voltage on precipitation efficiency, precipitation rate, and CE

To understand struvite recovery in dual chamber MECs, the concentrations of P, Mg, NH_4 and Ca were measured in the influent and effluent of both the anode and cathode chambers. The concentrations of P and Mg in cathode influent were approximately 3 mM, and struvite precipitates when the molar ratio of NH_4:Mg:P in the solution is 1:1:1 at an alkaline environment (pH > 8). Figures 5.7 & 5.8 show that (in OCV) there was no P removed from the cathode due to a neutral environment (pH=7). This confirms that P was removed only by precipitation. However, more than 1 ± 0.2 mm of Mg was transferred from the cathode chamber to the anode chamber through Nafion membrane exchange, due to the concentration gradient.
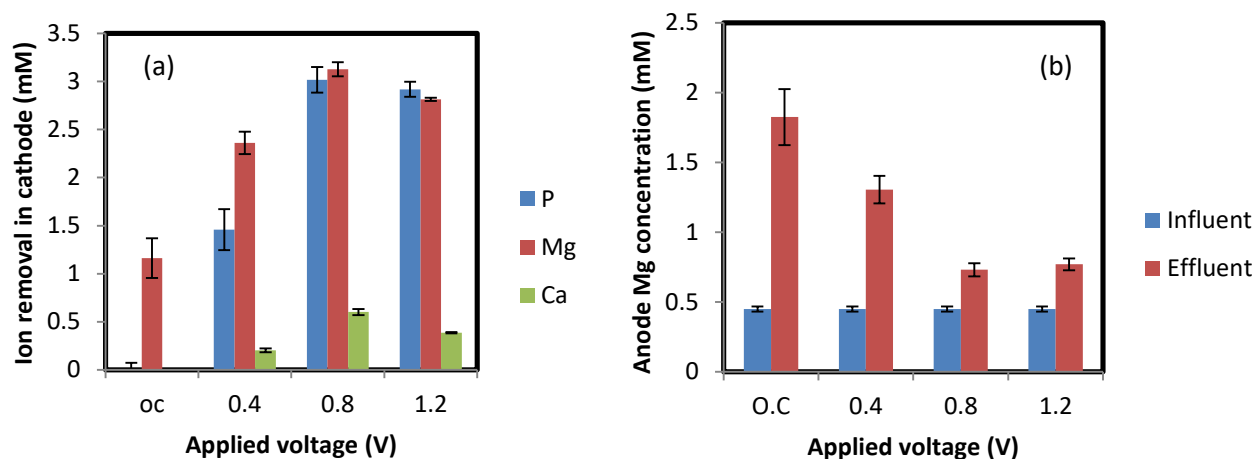
Figure 5.8 (a) Molar ionic removal in the cathode chamber and (b) Mg concentration in the anode chamber

When 0.4 V was applied to the circuit, catholyte pH increased to 8, and around 1.45 ± 0.2 mM of P and approximately 2.3 ± 0.2 mM of Mg were removed from the cathode chamber. Around 1.45 ± 0.2 mM of P and 1.3 ± 0.2 mM of Mg were precipitated as struvite and an additional 1 ± 0.1 mM of Mg was transferred from the cathode to the anode. Increasing the applied voltage increased the pH. As a result, the precipitated P and Mg increased. This reduced the Mg transferred to the anode, because most of the Mg was precipitated as struvite. Creating the optimal pH in the cathode chamber is very important, to minimise the diffusion of cations to the anode chamber.

On the other hand, NH_4 concentration in the anode chamber decreased in all cycles due to NH_4 diffusion and microorganism consumption. In addition, NH_4 removal was observed to increase when applied voltage was increased, ranging from 0.7 ± 0.1 mM at 0.4 V to 2.25 ± 0.2 mM at 1.2 V. However, calculating NH_4 concentration in the cathode effluent was challenging. The concentration of NH_4 in the cathode effluent varied and fluctuated in each cycle, due to ammonia volatilization caused by the high pH (Cusick et al., 2014; Rahman et al., 2014).

5.3.7 Crystals analysis

After each batch, the catholyte was filtered and the precipitated crystals were weighted and analysed. In addition, the cathode electrode was treated, using the dissolution method, and replaced with a new cathode electrode for the next cycle. The XRD pattern showed that the precipitated crystals matched the standard pattern. The SEM images (Figure 5.9-a) showed

that the crystals had a tubular morphology with sharp edges (needle), which confirms that the precipitated crystals had struvite morphology (Hutnik et al., 2011). Furthermore, EDS analysis showed that the main peaks of the crystals (from all cycles) were Mg, O and P, which is similar to the peaks of standard struvite (Ronteltap et al., 2010).

The dissolution treatment for the cathode showed that the molar ratio of Mg:P in the solution was approximately 1:1. This can also confirm that the precipitated crystals had a similar molar ratio to the struvite standard.
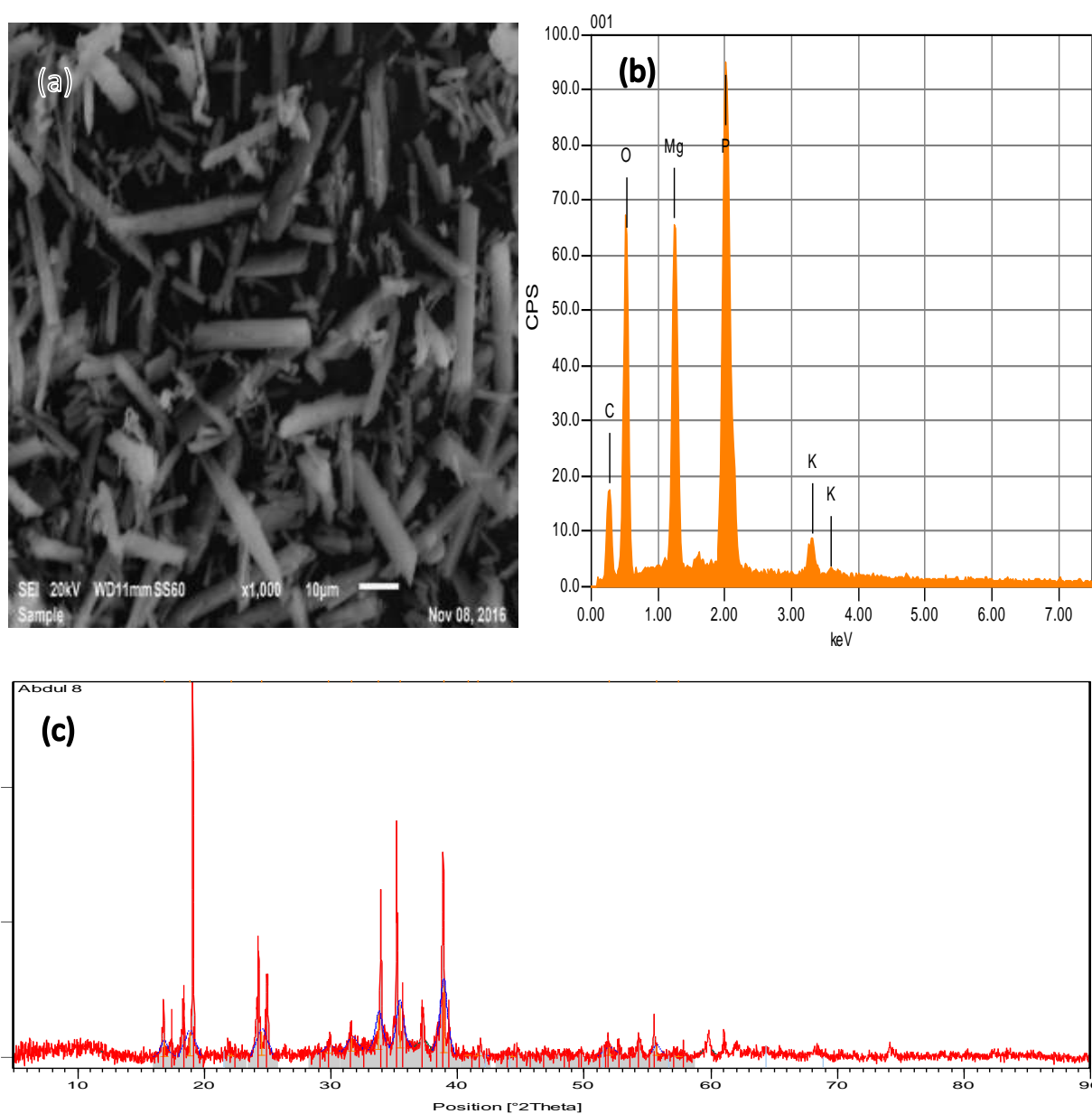
Figure 5.9 (a) Scanning electron microscopy image of struvite crystals, (b) EDX of the precipitates, and (c) XRD patterns of precipitates on the cathode

5.3.8 Cathode and membrane scaling

A deterioration in the current was observed during the time of operation. The more precipitates on the cathode surface, the more fluctuation in the current was noticed. At 1.2 V, the electrode was completely covered with struvite (Figure 5.10). The current started to drop after one day of operation, and this continued until the end of the batch duration. No deterioration in current in OCV was noticed, which confirms the effect of P recovery on the current. Similar findings were observed in previous studies (Cusick et al., 2014).

Figure 5.10 Precipitates covered cathode surface

After each cycle, the cathode electrode was replaced with a new electrode and the used electrode was removed for maintenance. The electrode was immersed in the MES buffer to remove any P precipitates on its surface. Through dissolution processes, the P concentration was measured to quantify the concentration of P on the cathode electrode. Due to the high pH around the cathode electrode, more than 50% of P was precipitated on the electrode surface. Furthermore, after a long-term operation, the PEM in MECs was affected by the precipitates. PEM is another important factor that has an impact on MEC performance, where the membrane resistance contributes to the total internal resistance of MEC. Therefore, membrane fouling and an increase in membrane resistance can also lead to deteriorated MEC performance (Xu et al., 2012).

SEM and EDS analysis were used to identify the impact of P precipitation on the membrane. SEM pictures showed that the surface of the new PEM was smooth and clear, without any particles on the surface, and that the main components of the new PEM were oxygen, carbon, fluoride and sulphur (Çetinkaya et al., 2015). In contrast, the SEM image of the used PEM contained many small particles with different shapes on the surface. The EDX analysis showed that the PEM contains phosphorus, magnesium and calcium precipitations, which

were mainly precipitated during the operation time (Figure 5.11). These results confirmed that some of the struvite particles were attached to the PEM surface. The precipitation of these particles and salts during the long-term operation of MECs would deteriorate the MECs' performance and increase internal resistance.
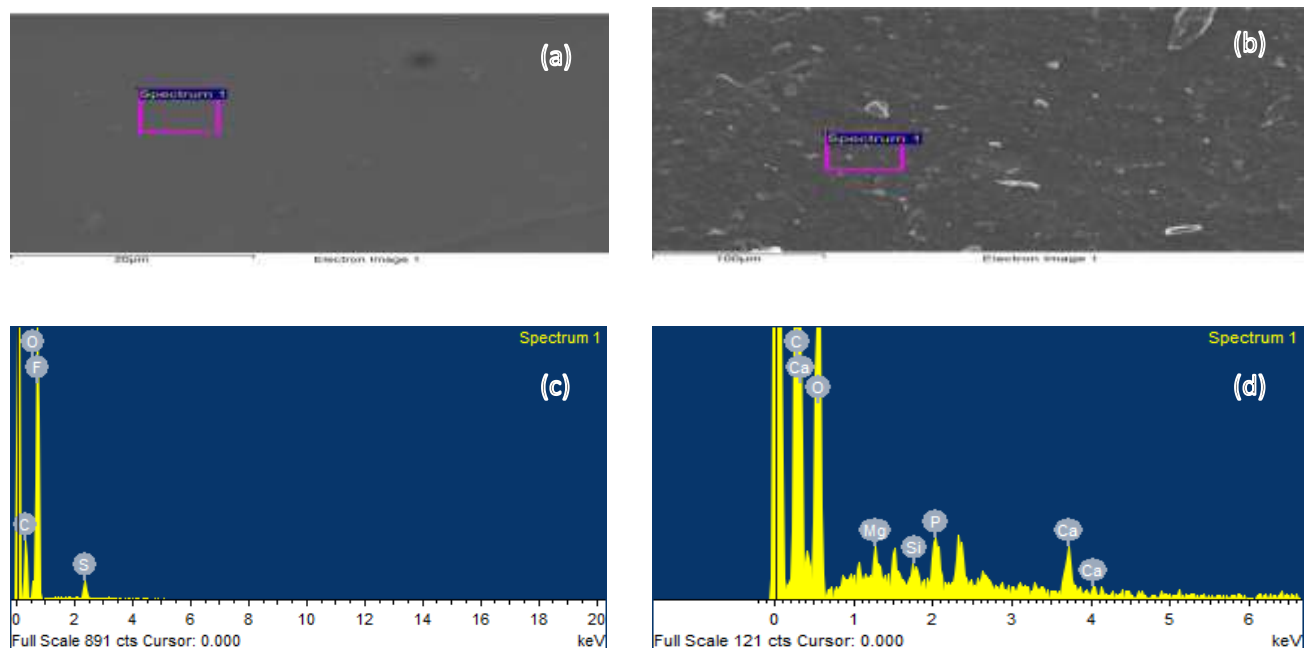
Figure 5.11 (A & C) SEM image and EDX spectrum for the new PEM and (B & D) for the used PEM.

5.3.9 Visual Minteq modeling

Visual Minteq software was used to gain a better understanding of P precipitation in MECs. The concentration of each element in the cathode synthetic influent solution was added to the software. The software result showed that 5 different minerals were formed: Hydroxyapatite, tricalcium phosphate, octacalcium phosphate, bobierrite and struvite. However, Hydroxyapatite was eliminated because magnesium ions in the solution kinetically obstruct the nucleation and formation of this species. In addition, octacalcium was eliminated because it formed at low pH (5-6) (Çelen et al., 2007).

The SEM and XRD analysis showed that only struvite was precipitated in the cathode chamber. The model showed that struvite started to be supersaturated when the cathode pH reached 8.1 (Figure 5.12). In the supersaturated solution, P started to precipitate as struvite. The model supports the experimental results; struvite started to precipitate when the cathode pH reached 8.

127
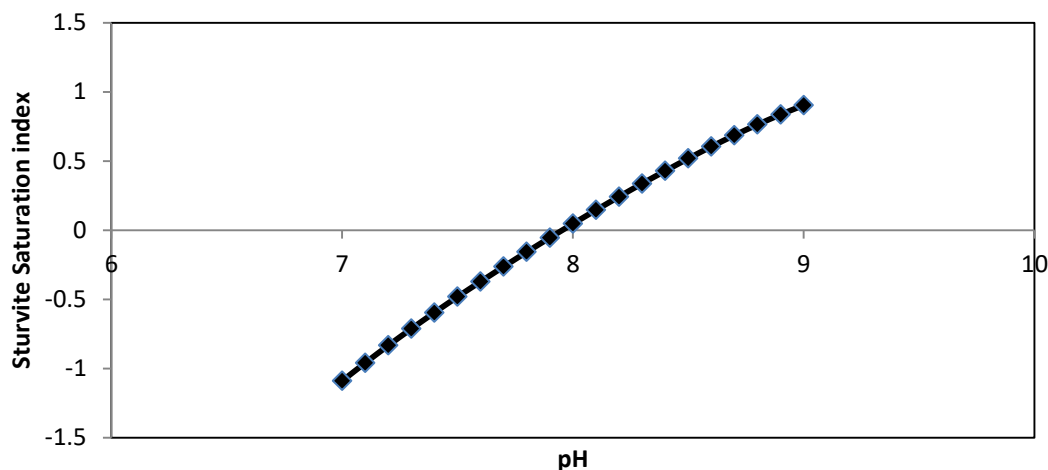
Figure 5.12 Saturation index of struvite as a function of pH

.

5.3.10 Statistical analysis

The synthetic wastewater in this study was used to simulate reject wastewater, since reject water contains a high P concentration and can be an optimal stream for P recovery from wastewater (Wu and Modin, 2013). As discussed in Section (5.3.6), the applied voltage had a great influence on P recovery and hydrogen production. However, the impact of COD concentration on P recovery and hydrogen production was not clear. Therefore, CCD was used to find the impact of each parameter, as well as the interaction impact on MEC performance, and to identify the optimum operating conditions for the dual chamber MEC.

Theoretically, MEC requires 0.2 V to produce hydrogen gas, but in practice, MEC requires >0.2 V to produce hydrogen due to the losses (Logan et al., 2008). Furthermore, water electrolysis requires >1.2 V (in theory) to produce hydrogen (Logan et al., 2015). Therefore, the applied voltage range in this study was selected between 0.4 V (low voltage) and 1.2 V (high voltage). Moreover, the low (COD=500 mg/L) and high (COD=1500 mg/L) levels of influent COD concentration were chosen, based on the concentration of COD in reject wastewater (Thorndahl, 1993; Hu et al., 2017)**.**

CCD and response surface methodology (RSM) were used to identify the impact of applied voltage (X1) and COD concentration (X2) on MEC performance, and to determine the optimum operating conditions. CCD was used to fit a quadratic model to the data. Four axials with $\alpha = \pm 1.4$ and three center points were performed to have a rotatable design. The levels of variables for CCD are given in Table 5.1.

128

The performance of the MEC was investigated in terms of coulombic efficiency, COD removal efficiency, cathode pH, precipitation efficiency and maximum volumetric hydrogen production rate. The performance of the MEC as a treatment tool for wastewater was evaluated by the COD removal. Furthermore, cathode pH is the most important factor for P recovery, where P solubility is dependent on solution pH. Precipitation efficiency was used to evaluate P recovery as struvite in the cathode chamber. Finally, the maximum volumetric hydrogen production rate was used to assess hydrogen production in the MEC. The experimental design and the results are summarised in Table 5.2.

Table 5.2 Experimental design and the responses of the duplicates of CCD runs

No of run	Block	X_1: Applied voltage (V)	X_2: COD (mg/L)	Y_1: CE (%)	Y_2: COD removal efficiency (%)	Y_3: cathode pH	Y_4: Precipitation efficiency (%)	Y_5: Max volumetric H_2 production ($m^3.H_2/m^3.d$)
1	Block 1	0.5	500	27	70	7.43	50	0.06025
2	Block 1	0.5	1500	8.75	83	8.25	70	0.08514
3	Block 1	1.1	1500	16.68	89	8.47	91	0.1318
4	Block 1	1.1	500	36	80	7.95	62	0.28057
5	Block 1	0.5	500	25	65	7.4	44	0.061
6	Block 1	1.1	1500	17.9	86	8.67	95	0.13987
7	Block 1	0.8	1000	16.9	90	8.25	90	0.10052
8	Block 1	1.1	500	41.8	83	8.06	60	0.2674
9	Block 1	0.8	1000	13.1	92	8.24	88	0.13101
10	Block 1	0.5	1500	9.1	79	8.18	72	0.09755
11	Block 2	0.4	1000	11	53	7.7	57	0.076
12	Block 2	0.8	300	41	95	7.44	68	0.15939
13	Block 2	1.2	1000	22	59	8.49	87	0.20943
14	Block 2	0.8	1700	16	87	8.4	91	0.06564
15	Block 2	1.2	1000	24	62	8.4	85	0.22482
16	Block 2	0.8	1000	13.61	92	8.1	90	0.11677
17	Block 2	0.8	1700	10	85	8.35	90	0.09103
18	Block 2	0.4	1000	10	59	7.6	59	0.08678
19	Block 2	0.8	300	42	92	7.5	66	0.1223

5.3.10.1 Coulombic efficiency

The coulombic efficiency of each run was calculated using Equation (5.9). Before finalising any model (in all responses), tests of assumptions were conducted to confirm that none of these conditions were violated. First, the standard deviations between the actual and the predicted response values followed a normal distribution. Second, the studentized residuals, versus predicted values, showed that there was no evidence for the violation of constant or independence assumptions throughout the response space. Third, checking for outliers if any influential values are available. In these statistics, Cook's distance was used to check if there were any influential values. Lastly, the Box-Cox plot for power transformation was checked, to see if the data required any transformation. After all these checks, the models were finalised and the RSM was drawn up. The Analysis of Variance (ANOVA) results showed that the quadratic model, with an F-value of 107.63 and a P-value of <0.0001, was significant (Table 5.3). There was only a 0.01% chance that this level of fit could occur due to noise. The lack of fit was not significant, with a P-value of 0.8551. The coefficient of determination (R^2) of 0.9782 and adjusted (R^2) of 0.9691 implied that the model was able to express approximately 97.8% of the variability in the response and that, to obtain a good fit of mode, R^2 should be at least 0.8 (Myers et al., 2016). The response surface of the coulombic efficiency is shown in Fig. 5.13.

Table 5.3 ANOVA for the quadratic model of coulombic efficiency

Source	Sum of Squares	DF	Mean Square	F-Value	P-value
Block	0.11	1	0.11		
Model	2328.95	5	465.79	107.63	< 0.0001
X_1	379.13	1	379.13	87.61	< 0.0001
X_2	1559.86	1	1559.86	360.44	< 0.0001
X_1X_2	10.28	1	10.28	2.38	0.1492
X_1^2	14.33	1	14.33	3.31	0.0939
X_2^2	333.12	1	333.12	76.97	< 0.0001
Residual	51.93	12	4.33		
Lack of Fit	4.09	3	1.36	0.26	0.8551
Pure Error	47.85	9	5.32		
Total	2380.99	18			

The following model was considered satisfactory in representing coulombic efficiency:

$$CE = 14.39 + 4.87\,X_1 - 9.87\,X_2 - 1.13\,X_1X_2 + 1.37\,X_1^2 + 6.62\,X_2^2 \qquad (5.22)$$

Table 5.3 shows that the effects of X_1, X_2, and X_2^2 were significant on the coulombic efficiency, and that X_1^2 and the interaction term were statistically insignificant. In addition, from Equation 5.22 it was determined that the effect of COD concentration was greater than applied voltage.

The RSM graph in Figure 5.13 shows that applied voltage had a linear effect on coulombic efficiency, and that the CE increased with an increase in applied voltage. However, COD concentration had a quadratic effect on the response, and increased COD concentration decreased the coulombic efficiency. Decreasing COD concentration from 1500 mg/L to 500 mg/L at 1.1 V, increased the CE by two-fold. Using a high COD concentration in batch mode requires a long cycle duration, which increases methane formation. Similar findings were reported by (Rivera et al., 2015), where reducing the cycle time from 120 hours to 48 hours successively inhibited methane formation. Therefore, most of the COD was consumed by methanogens in the long cycle duration, leading to a decrease in CE. In addition, current deterioration occurred, due to struvite precipitation on the cathode surface, which decreased CE as well. Finally, the catholyte, which was used instead of phosphate buffer solution, had a negative impact on CE.

Equation 5.22 was able to predict a maximum CE of 37% at an applied voltage of 1.1 V and a COD concentration of 500 mg/L. Three experimental runs were conducted to check model adequacy. A CE average of 39±3% was achieved, confirming the accuracy of the model.
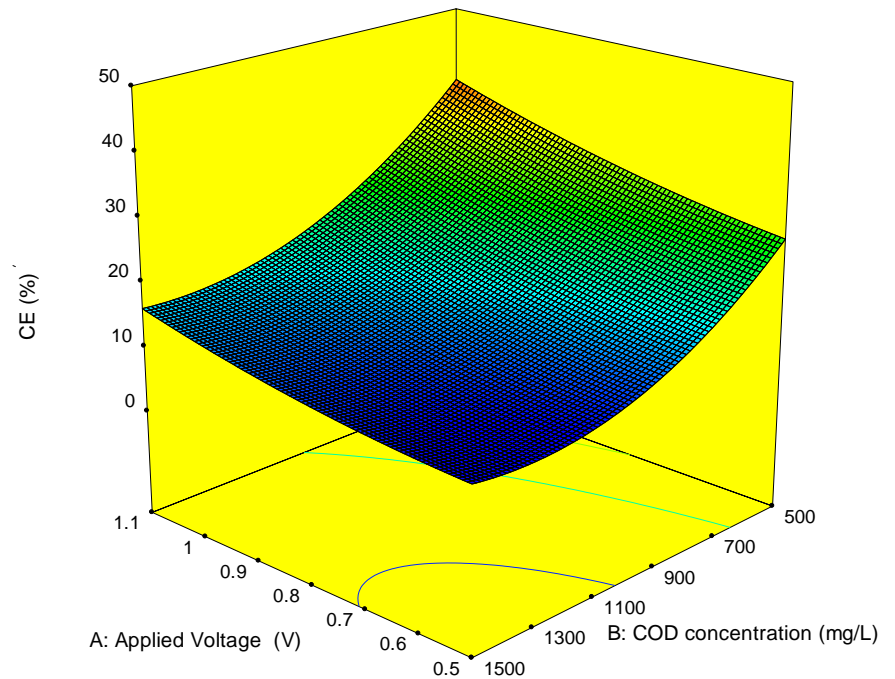
Figure 5.13 Response surface of coulombic efficiency as a function of applied voltage and COD concentration

5.3.10.2 COD removal efficiency

COD removal efficiency was studied to assess MEC as a wastewater treatment tool. The COD removal efficiency was calculated using Equation 5.3. The Analysis of Variance (ANOVA) results showed that a quadratic model with an F-value of 50.68 and a P-value of <0.0001 was significant. There was only a 0.01% chance that this level of fit could occur due to noise. The lack of fit was not significant with a P-value of 0.096. The coefficient of determination (R^2) of 0.9726 and adjusted (R^2) of 0.9534 implied that the model was able to express approximately 97.26 % of the variability in the response. The response surface of the COD removal is shown in Figure 5.14.

Table 5.4 ANOVA for the quadratic model of COD removal efficiency

Source	Sum of Squares	DF	Mean Square	F-Value	P-value
Block	153.90	1	153.90		
Model	2970.38	7	424.34	50.68	< 0.0001
X_1	20.25	1	20.25	2.42	0.1509
X_2	56.25	1	56.25	6.72	0.0269
X_1X_2	28.12	1	28.12	3.36	0.0967
X_1^2	1669.04	1	1669.04	199.35	< 0.0001
X_2^2	6.48	1	6.48	0.77	0.3995
$X_1^2X_2$	226.60	1	226.60	27.07	0.0004
$X_1X_2^2$	49.96	1	49.96	5.97	0.0347
Residual	83.72	10	8.37		
Lack of Fit	23.22	1	23.22	3.45	0.0960
Pure Error	60.50	9	6.72		
Total	3208.00	18			

The following model was considered satisfactory in representing COD removal:

$$\text{COD removal} = 90.59 + 1.59\ X_1 - 2.65\ X_2 - 1.87\ X_1X_2 - 14.83\ X_1^2 + 0.92\ X_2^2 + 7.53\ X_1^2X_2 + 3.53\ X_1X_2^2 \tag{5.23}$$

Table 5.4 shows that the effects of X_2, X_1^2, $X_1^2X_2$ and $X_1X_2^2$ were significant on COD removal. The terms X_1, X_1X_2, and X_2^2 were statistically insignficant. In addition, Equation 5.23 showed that COD concentration had the greatest effect on the response.

The RSM graph in Figure 5.14 shows that both applied voltage and COD concentration had a quadratic effect on COD removal. The system achieved > 50% COD removal efficiency in all COD concentrations. The RSM shows that COD removal efficiency increased when the applied voltage was increased, and that maximum COD removal efficiency was achieved at 0.8 V. Increasing applied voltage over 0.8 V decreased the removal efficiency. Applying high voltage may affect microorganism activity. Studies have shown that high voltage can be harmful to living organisms and inhibit their existence (Valle et al., 2007; Ding et al., 2016)

Equation 5.23 was able to predict a maximum COD removal efficiency of 95% at the applied voltage of 0.8 V and at a COD concentration of 500 mg/L. Three experimental runs were conducted to check model adequacy. A COD removal efficiency average of 91±4% was achieved, confirming the accuracy of the model.
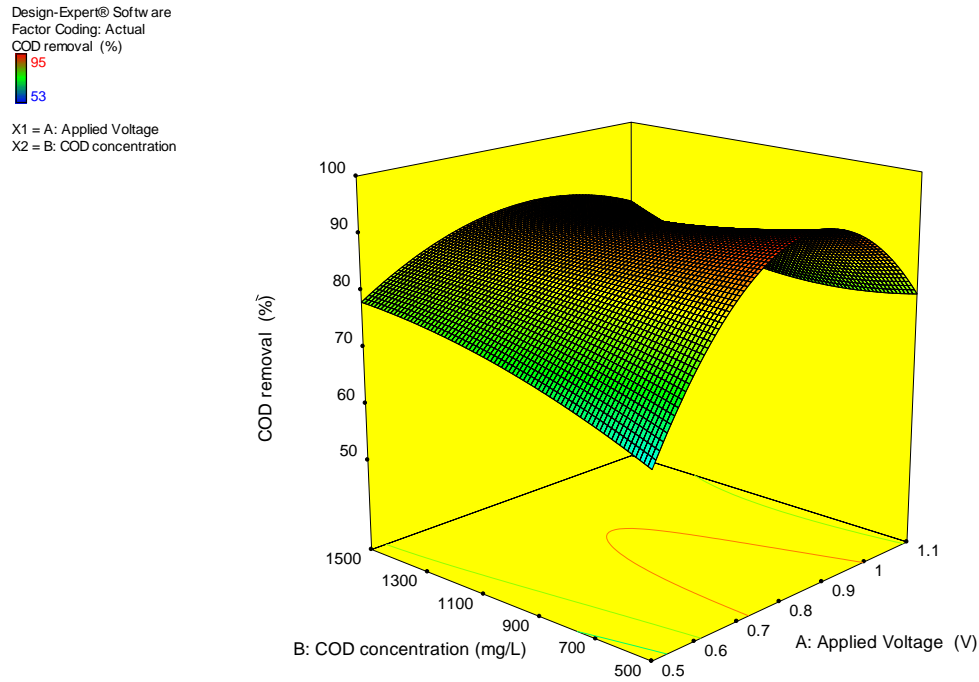
Figure 5.14 Response surface of COD removal efficiency as a function of applied voltage and COD concentration

5.3.10.3 Cathode pH

Cathode pH is the most important parameter for P recovery. Cathode pH was studied to identify the impact of applied voltage and COD concentration on MEC performance. The Analysis of Variance (ANOVA) results showed that a quadratic model with an F-value of 129.44 and a P-value of <0.0001 was significant. There was only a 0.01% chance that this level of fit could occur due to noise. The lack of fit was not significant, with a P-value of 0.4487. The coefficient of determination (R^2) of 0.9818 and adjusted (R^2) of 0.9724 implied that the model was able to express approximately 98.18% of the variability in the response. The response surface of the cathode pH is shown in Fig. 5.15

Table 5.5 ANOVA for the quadratic model of cathode pH

Source	Sum of Squares	DF	Mean Square	F-Value	P-value
Block	0.042	1	0.042		
Model	2.95	5	0.59	129.44	< 0.0001
X_1	1.07	1	1.07	234.82	< 0.0001
X_2	1.75	1	1.75	384.28	< 0.0001
X_1X_2	0.030	1	0.030	6.48	0.0256
X_1^2	0.020	1	0.020	4.32	0.0597
X_2^2	0.098	1	0.098	21.45	0.0006
Residual	0.055	12	4.554E-003		
Lack of Fit	0.013	3	4.449E-003	0.97	0.4487
Pure Error	0.041	9	4.589E-003		
Total	3.04	18			

The following model was considered satisfactory in representing cathode pH:

$$\text{Cathode pH} = 8.18 + 0.26\,X_1 + 0.33\,X_2 - 0.061\,X_1X_2 - 0.051\,X_1^2 - 0.11\,X_2^2 \quad (5.24)$$

Table 5.5 shows that the effects of all terms were significant on cathode pH, except X_1^2, which was statistically insignificant. More importantly, the interaction term was significant, which means that the effect of applied voltage on cathode pH is dependent on the level of COD concentration. In addition, Equation 5.24 showed that COD concentration had the greatest effect on response. The RSM graph in Figure 5.15 shows that the effect of applied voltage was linear on cathode pH, and that cathode pH increased with an increase in applied voltage. However, the effect of COD concentration was quadratic on the response, and increased COD concentration increased cathode pH.

Proton consumption in the cathode chamber for hydrogen production in the MEC resulted in a pH increase. Therefore, increased COD concentration from 500 to 1500 at 1.1 V led to an increase in average cathode pH from 7.9 to 8.5. The availability of the substrate in the anode chamber led to the release of more protons, due to the oxidation of organic matter. As a result, more protons were consumed at the cathode chamber and a high pH was achieved. Since P solubility is dependent on solution pH, the optimal pH for struvite crystallisation is 8.5 (Cusick et al., 2014). Furthermore,

increasing the cathode pH to (PH > 10) led to decreased struvite precipitation and struvite purity, due to: (1) a decrease in ammonium ion concentration, (2) formation of $Mg(OH)_2$, which reduced Mg^{2+} availability for struvite crystallisation (Zhou and Wu, 2012). Thus, the optimum pH from struvite precipitation is 8.5. Equation 5.24 was able to predict an average cathode pH of 8.5 at applied voltage of 1.1 V and COD concentration of 1500 mg/L. Three experimental runs were conducted to check model adequacy. A cathode pH average of 8.6±0.1 was achieved, confirming the accuracy of the model.
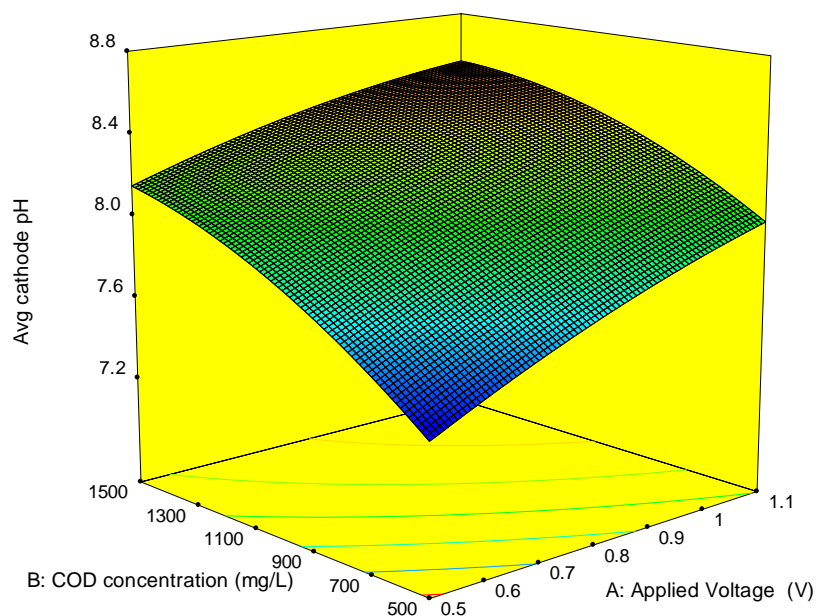
Figure 5.15 Response surface of cathode pH as a function of applied voltage and COD concentration

5.3.10.4 Precipitation efficiency

Precipitation efficiency was measured to assess the P recovery efficiency of the MEC. Equation 5.5 was used to calculate the precipitation efficiency. The Analysis of Variance (ANOVA) results showed that a quadratic model with an F-value of 128.26 and a P-value of < 0.0001 was significant. There was only a 0.01% chance that this level of fit could occur due to noise. The lack of fit was not significant, with a P-value of 0.095. The coefficient of determination (R^2) of 0.9859 and adjusted (R^2)

of 0.9782 implied that the model was able to express approximately 98.59% of the variability in the response. The response surface of the precipitation efficiency is shown in Fig. 5.16.

Table 5.6 ANOVA for the quadratic model of precipitation efficiency

Source	Sum of Squares	DF	Mean Square	F-Value	P-value
Block	109.14	1	109.14		
Model	4544.64	6	757.44	128.26	< 0.0001
X_1	1428.76	1	1428.76	241.94	< 0.0001
X_2	552.25	1	552.25	93.52	< 0.0001
X_1X_2	32.00	1	32.00	5.42	0.0400
X_1^2	927.00	1	927.00	156.97	< 0.0001
X_2^2	447.18	1	447.18	75.72	< 0.0001
$X_1^2 X_2$	129.57	1	129.57	21.94	0.0007
Residual	64.96	11	5.91		
Lack of Fit	26.46	2	13.23	3.09	0.0950
Pure Error	38.50	9	4.28		
Total	4718.74	18			

The following model was considered satisfactory in representing precipitation efficiency:

Precipitation efficiency = $90.41 + 9.45\ X_1 + 8.31\ X_2 + 2\ X_1X_2 - 11.05\ X_1^2 - 7.67\ X_2^2 + 5.69\ X_1^2X_2$
(5.25)

Table 5.6 shows that all terms were significant on precipitation efficiency, and that applied voltage had the greatest effect on precipitation efficiency. The RSM in Figure 5.16 shows that the applied voltage and COD concentration had a quadratic effect on precipitation efficiency. At low applied voltage (0.5 V) increased the COD concentration from 500 mg/L to 1500 mg/L, increased the precipitation efficiency from 50 to 72%. The same trend was observed at high applied voltage (1.1 V), where the precipitation efficiency increased from 62 to 95% when COD concentration increased from 500 to 1500 mg/L. Increased COD concentration increased the electrons and protons that transferred to the cathode. This, in turn, increased the catholyte pH due to proton consumption. At high pH (>8), P reached the

supersaturation point. More than 90% of P can be precipitated when pH reaches 8.3 (Adnan et al., 2003).

Furthermore, an increase in the applied voltage led to increased current and, as a result, to an increase in precipitation efficiency. At a low COD concentration (500 mg/L), an increase in applied voltage from 0.5 to 0.8 V increased the precipitation efficiency from 42 to 70%. However, precipitation efficiency started to decrease when applied voltage increased above 0.8 V. Increased applied voltage increased the cathode pH. By changing the applied voltage from 0.5 V to 1.1 V, the pH increased from 7.5 to 8.1, leading to an increase in ammonia volatilization and diffusion to the anode chamber (Stratful et al., 2001; Zhou and Wu, 2012; Rahman et al., 2014).
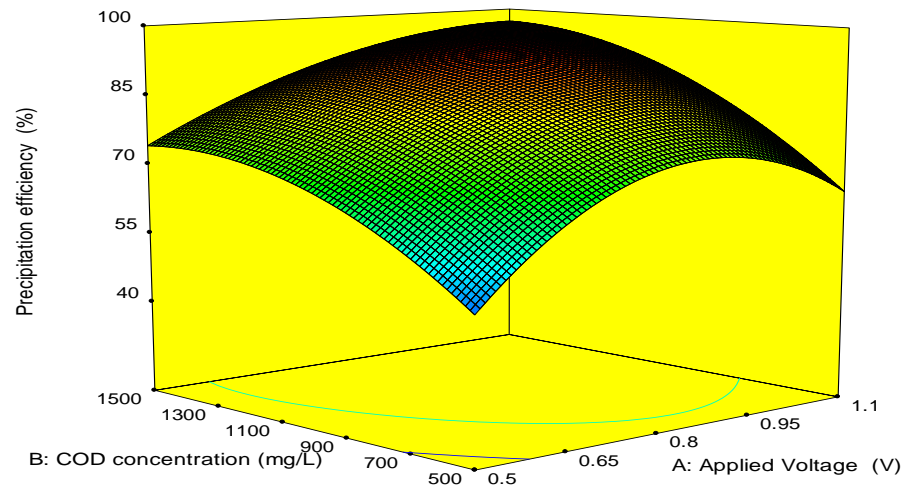
Figure 5.16Response surface of precipitation efficiency as a function of applied voltage and COD concentration

5.3.10.5 Hydrogen production rate

The hydrogen production rate was studied to assess the ability of MEC to recover P and produce H_2. The Analysis of Variance (ANOVA) results showed that a quadratic model with an F-value of 72.28 and a P-value of < 0.0001 was significant. There was just a 0.01% chance that this level of fit could occur due to noise. The lack of fit was not significant, with a P-value of 0.6682. The coefficient of determination (R^2) of 0.9753 and adjusted (R^2) of 0.9618 implied that the model was able to express

approximately 97.53% of the variability in the response. The response surface of the H_2 production rate is shown in Figure 5.17.

Table 5.7 ANOVA for the quadratic model of H_2 production rate

Source	Sum of Squares	DF	Mean Square	F-Value	P-value
Block	2.660E-004	1	2.660E-004		
Model	0.080	6	0.013	72.28	< 0.0001
X_1	0.018	1	0.018	100.27	< 0.0001
X_2	9.588E-003	1	9.588E-003	52.18	< 0.0001
X_1X_2	0.014	1	0.014	77.60	< 0.0001
X_1^2	3.071E-003	1	3.071E-003	16.71	0.0018
X_2^2	5.800E-007	1	5.800E-007	3.157E-003	0.9562
$X_1 X_2^2$	1.085E-003	1	1.085E-003	5.91	0.0334
Residual	2.021E-003	11	1.838E-004		
Lack of Fit	1.732E-004	2	8.660E-005	0.42	0.6682
Pure Error	1.848E-003	9	2.053E-004		
Total	0.082	18			

The following model was considered satisfactory in representing the hydrogen production rate:

H_2 production rate $= 0.11 + 0.048\ X_1 - 0.024\ X_2 - 0.042\ X_1X_2 + 0.02\ X_1^2 +$
$2.764\times10^{-4}\ X_2^2 + 0.016\ X_1X_2^2$ (5.26)

Table 5.7 shows that the effects of all terms were significant on H_2 production rate, except X_2^2, which was statistically insignificant. More importantly, the interaction term was significant. Equation 5.26 shows that the effect of applied voltage had twice the effect of COD concentration on the response.

The RSM graph in Figure 5.17 shows that the effects of applied voltage and COD concentration were linear and quadratic on the H_2 production rate, respectively. H_2 production increased linearly along with the applied voltage. An increase in applied voltage from 0.5 to 1.1 V increased H_2 production rate from 0.06 to 0.267 $m^3.H_2/m^3/d$. However, at high COD concentration (1500 mg/L) the effect of increasing applied voltage on H_2 production rate was smaller. Generally, dual chamber MECs are operated with a phosphate buffer solution (PBS) to maintain pH

balance in the cathode chamber, because high cathode pH causes many losses in the system. The hydrogen production rate in this study was low, due to: (1) high internal resistance, caused by the distance between anode and cathode (8 cm). H_2 can be improved by reducing this distance (Rozendal et al., 2007; Hu et al., 2008), (2) substrate consumption by methanogens in high COD concentration, due to the long cycle duration, and (3) using synthetic wastewater as a catholyte instead of PBS. Using a low buffer solution as a catholyte resulted in a low current, due to a limited supply of protons and high catholyte pH. Operating MEC with a high cathode pH will deteriorate the MEC performance (Nam and Logan, 2012).

The production of H_2 in the low COD concentration (500 mg/L) was better than in the high COD concentration. Hydrogen production was negatively affected by the absence of a high concentration of PBS in the cathode. Due to substrate oxidation and proton consumption, the change of anode and cathode pH at high COD concentration was greater than the low COD concentration. Table 5.8 shows that the higher the COD concentration, the higher the pH difference between anode and cathode chambers, and the less H_2 production in the MEC. This explains why the production of H_2 was low (Luo et al., 2010; Yossan et al., 2013; Rivera et al., 2015).

Table 5.8 The pH values of the anodic and cathodic chambers

COD concentration (mg/L)	Cathode pH	Anode pH	ΔpH	Membrane potential loss (V)
500	7.98 ± 0.11	6.84 ± 0.04	1.1 ± 0.1	0.06
1000	8.17 ± 0.09	6.34 ± 0.06	1.8 ± 0.2	0.10
1500	8.43 ± 0.12	6.35 ± 0.03	2.1 ± 0.2	0.12

Furthermore, a high pH difference between anode and cathode chambers led to high cell potential losses and membrane potential loss, which negatively affecting MEC performance. Thus, PBS was used in most of the dual chamber MECs to maintain the pH balance during the operation of the system (Luo et al., 2014).
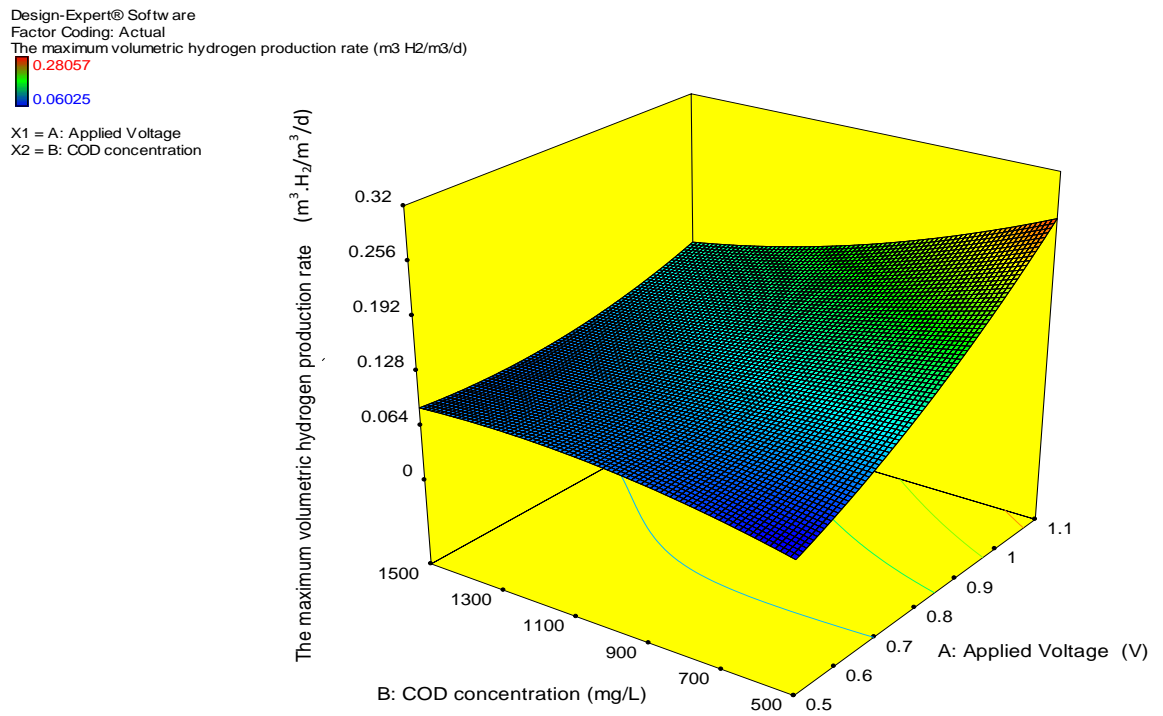
Figure 5.17Response surface of H_2 production rate as a function of applied voltage and COD concentration.

5.3.10.6 Optimisation and verification

The generated models were used to predict the optimal conditions for H_2 production and P precipitation efficiency. The following operational conditions are obtained, applied voltage 1.2 V and influent COD concentration of 1000 mg/L. The optimal predicted values of H_2 production rate and P precipitation efficiency were 0.214 $m^3.H_2/m^3/d$ and 83%, respectively.

Based on the statistical models, these operational conditions are the optimal conditions for H_2 production and P recovery. Three experiments were carried out to validate the model predictions. The validation experiments were carried out near the optimum values and the lab results showed that a maximum H_2 production rate of 0.2 ± 0.01 $m^3.H_2/m^3/d$ and P precipitation efficiency of 82 ± 5 % were achieved (Table 5.9). Finally, the lab results can confirm that the predicted values were in close agreement with the observed values fall well within 95% prediction interval.

Table 5.9 Validation of model predictions using experimental results

Operational condition	Actual and predicted variable	Limit of prediction interval	max H_2 production rate $m^3.H_2/m^3/d$	P precipitation (%)
Applied voltage =1.2 V; COD= 1000 mg/l	Actual value		0.2 ± 0.01	82 ± 5
	Predicted value (95% prediction interval)	Low	0.19	80
		High	0.23	86

5.4 Summary

- This chapter discussed the overall performance and the set-up of experiments on the use of a dual chamber MEC for concurrent H_2 production and P recovery as struvite.

- Phosphorus was recovered in the cathode chamber of the MEC, due to the high catholyte pH. XRD and SEM-EDS analysis showed that the precipitates are struvite with tubular shaped particles.

- The applied voltage had a great influence on H_2 production rate and P recovery. However, COD concentration had an influence on P recovery.

- The MEC achieved a maximum H_2 production rate of 0.28 $m^3.H_2/m^3/d$. and a maximum precipitation efficiency of 95%.

- The overall energy recovery in the MEC ranged from η_{E+S}= 25 ± 1% to 37 ± 1.7%, and the H_2 production was not high enough to recover the electrical consumption.

- A central composite design was conducted to understand the effect of applied voltage and COD concentration on coulombic efficiency, COD removal efficiency, cathode pH, precipitation efficiency and H_2 production rate.

- Applied voltage had a positive linear effect on coulombic efficiency, cathode pH and H_2 production rate. It had a quadratic effect on COD removal and precipitation efficiency.

- COD concentration had a quadratic effect on all responses.

- The results outlined within this chapter have improved the current scientific understanding of phosphorus recovery and H_2 production in a dual chamber MEC.

5.5 Conclusion

The results in this chapter assess concurrently H_2 production and P recovery in dual chamber MEC. In addition, the impacts of applied voltage and COD concentration, as well as their interactive effects on H_2 production and P recovery on MEC performance were investigated. A mediator-less dual chamber microbial electrolysis cell was used to concurrently produce H_2, recover phosphorus and treat wastewater. Phosphorus was precipitated in the cathode chamber, and the main components of the precipitate were determined by XRD and SEM-EDS to be struvite. The MEC achieved a maximum H_2 production rate of 0.28 m^3-H_2/m^3/d (at applied voltage = 1.1 V, COD = 500 mg/L) and a maximum precipitate efficiency of 95% (at applied voltage =1.1 V, COD =1500 mg/L). The overall energy recovery in the MEC ranged from η = 25 ± 1 % to 37 ± 1.7 %. The response surface methodology demonstrated the impact of each factor (applied voltage and COD concentration) on H_2 production and P recovery. Identifying the interaction effect between these factors would also be useful to optimise MEC performance. Statistical analysis of the data obtained from the lab-scale MECs was used to develop predictive models for H_2 production and P recovery. High applied voltage would result in higher H_2 production and high precipitation efficiency. It is important to consider the initial COD concentration, if the system is to be used for H_2 production and P recovery. More importantly, this model can help in achieving the balance between P recovery and H_2 production.

Chapter 6

Microbial community structure and activity in a dual chamber bio-electrochemical system for electricity generation/H$_2$ production and P recovery

6.0 Microbial community structure and activity in a dual chamber bio-electrochemical system for electricity generation/H$_2$ production and P recovery

6.1 Introduction

This chapter presents the microbial community structure analysis of the dual-chamber MFC and MEC that were designed for concurrent P recovery and energy generation / H$_2$ production. The objectives of this chapter are as follows:

- To identify and understand the microbial communities and structure that developed in MFCs and MECs operated under different operational conditions, during 400 days of operation using next generation sequencing on the Illumina MiSeq platform.
- To link the relative abundance of known exoelectrogenic microorganism species with BES performance.

In a BES, microorganisms convert the chemical energy in organic matter to electrical energy or hydrogen gas. The operation of BESs is influenced by different parameters, such as microorganism activity, cell design, and materials. Bacteria community and electron transfer in BESs are important parameters that have an impact on energy generation and hydrogen production. Bacteria, such as anode respiring bacteria and electrochemically active bacteria, have demonstrated their ability to transfer electrons from the substrate to the electrodes without the aid of any external mediator, that is, "mediator-less BES" (Logan and Regan, 2006). In contrast, mediators are used in the presence of electrochemically inactive bacteria in BESs to facilitate electron transfer between the electrode and the bacteria (Ho et al., 2011; Najafpour et al., 2011).

The anaerobic electrochemically active biofilm that develops on the anode plays an important role in BES performance, and most recent studies have focused on improving BES design and materials but have paid less attention to the microbial community aspects in the system. Thus, microbial communities and their effect on BES operation and performance remain unknown as a "black box system".

Different communities of microorganism can be found in MFCs and MECs, as operational and environmental conditions can change the microbial communities in

the system (Yanuka-Golub et al., 2016). In other words, the changes in microbial communities are linked to the system's environmental and operational conditions. The MFC comprised an anaerobic anode chamber and aerobic cathode chamber separated by a cation exchanger membrane, whereas the MEC comprised an anaerobic anode chamber and anaerobic cathode chamber. The anode chambers of both systems contained exoelectrogenic bacteria, which are the bacteria responsible for transferring electrons to the anode electrode either through direct contact or using an electron soluble shuttle. In BESs, microbial species, such as *Geobacter spp.*, *Shewanella spp.*, and phototrophic bacteria, can be found in the anode electrode; as in MECs, the growth of anaerobic bacteria, such as methanogenic microorganisms can be promoted due to the anaerobic condition in both the anode and cathode chambers (Logan et al., 2008). Most BESs use wastewater as an inoculum, which contains different bacteria communities, and these communities can deal with different types of wastewater. Thus, the microorganism community is expected to change when the wastewater is changed to adapt to the new environment. In addition, bacteria community and composition can be affected by solution pH (Patil et al., 2011). Due to organic matter oxidation at the anode chamber, anode pH decreases, and that could harm the bacteria community.

A few studies have focused on P recovery in bio-electrochemical systems; however, none of these studies has focused on identifying and understanding the bacterial structure in these systems. Hence, it is essential to identify the community, structure, and composition of the biofilm in the anode chambers to achieve a better performance of BESs and increase our understanding how different microbes affect BES performance. Therefore, the main aim of this chapter is to better understand the microbial community and structure in both MFCs and MECs that designed for P recovery. In addition, identify the similarities and differences of microbial communities in MFCs and MECs.

6.2 Material and Methods

6.2.1 Mediator-less BES construction

The BES configurations for this chapter are summarised below and can be found in more detail in sections 3.2.1 and 5.2.1. Four sets of dual-chamber H-type bottles (Adams & Chittenden Scientific Glass, Berkeley, CA, USA), were used to construct

two MFCs and two MECs. Anode and cathode electrodes were made of carbon cloth 2.5 × 5 cm (projected area of 25 cm^2) with a volume of 300 mL for each chamber (see Figures 3.1 and 5.1). The cathode contained a Pt catalyst (0.5 mg/cm^2 10% Pt on Carbon Cloth Electrode) whilst the anode was plain carbon cloth. Both electrodes were connected with a titanium wire (0.5 mm, purity > 99.98%, Alfa Aesar, Heysham, UK). A Nafion membrane (Nafion 117#, Sigma-Aldrich, London, UK) was placed in the middle of the anode and the cathode.

6.2.2 BES inoculation and operation condition

The inoculation and operating conditions have already been discussed in detail (sections 3.2.1-3.2.6 MFC, sections 5.2.1-5.2.6 MEC) and are summarised below.

The anode chamber was inoculated with a 1:1 mixture of activated sludge and anolyte medium (containing in (g/L): Sodium acetate 3.28 + ammonium chloride 0.31+ potassium chloride 0.13 + sodium phosphate anhydrous monobasic 2.69 + disodium hydrogen phosphate 4.33+ 10 mL vitamins solution + 10 mL trace element solution. The BESs were operated in feed-batch mode at room temperature. Anode influent pH was adjusted to pH = 7. Media replacement was carried out in an anaerobic environment to maintain the anaerobic environment for the anode biofilms. The synthetic wastewater contained mainly sodium acetate, trace element mixture, and vitamins.

6.2.3 Analytical Methods

The voltage across the external resistance (470 Ω MFC and 10 Ω MEC) was recorded every 15 minutes using the ADC-20 data logger system (Pico Technology, Saint Neots, UK), which was connected to a computer. Based on the recorded voltage, current (I) and power (P = IV) were calculated according to Ohm's law. The current density and power density were calculated by dividing the current and the power by the anode area (25 cm^2). Coulombic efficiency (CE) was calculated by integrating the measured current relative to the theoretical current (Logan et al., 2006).

6.2.4 Bacteria sampling

All the anode electrodes were removed from the anode chambers, which had been in stable operation for more than 400 days. All electrodes were first rinsed with

deionized water to remove any residue from the synthetic wastewater, and then were divided into two pieces. For biofilm collection, each piece of electrode was transferred to a sterile 20 mL universal tube containing 1 ml of wash buffer containing (0.2% Tween 20). The tube was shaken vigorously to wash off the microbes trapped on the electrode. The resulting cell suspension was transferred to a clean micro-centrifuge tube, then the cells were pelleted at 14,000 x g and the supernatant discarded (Kim et al. 2006).

6.2.5 DNA extraction

Genomic DNA was extracted using a Metagenomic DNA Isolation Kit (Cambio Ltd, Cambridge, UK) according to the manufacturer's instructions. Briefly, the cell pellet was re-suspended in 300 μl of Tris-EDTA (10 mM Tris-HCl (pH 7.5), and 1 mM EDTA) buffer; 2 μl of Ready-Lyse Lysozyme solution and 1 μl of RNase-A were added to the cell suspension. The tube was mixed by vortexing and then incubated at 37 °C for 30 minutes. Next, 300 μl of Meta-Lysis solution (2X) and 1 μl of Proteinase K were added to the tube and mixed by vortexing. The tube was then incubated at 65 °C for 15 minutes to lyse the cells, and was subsequently cooled to room temperature and placed on ice for 3-5 minutes. Then, 350 μl of MPC Protein Precipitation Reagent was added to the tube and mixed by vortexing vigorously for 10 seconds. The tube was centrifuged at 14,000 x g for 10 minutes at 4 °C. The supernatant was transferred to a clean 1.5 ml microcentrifuge tube. Following that, 570 μl of isopropanol was added to the supernatant and mixed by inverting the tube multiple times. The DNA was pelleted by centrifugation at 14,000 x g for 10 minutes at 4 °C. A pipet tip was used to remove the isopropanol without dislodging the DNA pellet. The tube was centrifuged and then any residual liquid was removed with a pipet tip, without disturbing the pellet. To wash, 500 μl of 70% ethanol was added to the pellet without disturbing the pellet. Then, the tube was centrifuged for 10 minutes at 14,000 x g in a microcentrifuge at 4 °C. Again, a pipet tip was used to remove the ethanol without dislodging the DNA pellet. The tube was centrifuged, after which any residual liquid was removed with a pipet tip, without disturbing the pellet. The pellet was air dried for 8 minutes at room temperature to evaporate any residual ethanol. The DNA pellet was re-suspended in 50 μl of TE buffer. The isolated DNA was validated by comparing the size and concentration of the isolated DNA with the Fosmid Control DNA.

6.2.6 PCR amplification and 16S rRNA sequencing with the Illumina MiSeq

The size and quantity of the extracted DNA fragments were examined using an Agilent Tape Station (Genomic DNA ScreenTape –HSD-1000 and Genomic DNA Reagents, Agilent, Santa Clara CA, USA) and a Qubit assay machine (Qubit assays, Life technologies, Sweden), respectively. Following the DNA extraction, a single-step amplification and sequencing library creation PCR was performed for bacterial 16S rRNA genes using primers targeting the V4 variable region, in a 96-well PCR plate. The forward and reverse primers were designed following Kozich et al. (2013), and consisted of the Illumina adapter sequence (F: 5'-AATGATACGGCGACCACCGAGATCTACAC-3'; R: 5'-CAAGCAGAAGACGGCATACGAGAT-3'), 8-bp i5 and i7 index sequences (Table 6.1), a pad sequence to boost the sequencing primer melting temperatures ((F: 5'-TATGGTAATT-3'; R: 5'-AGTCAGTCAG-3'), and a 2-bp sequence that is anti-complementary to the known sequences (F: 5'-GT-3'; R: 5'-CC-3'). Finally, the 16S V4 specific sequences (F: 5'-GTGCCAGCMGCCGCGGTAA-3'; R: 5'-GGACTACHVGGGTWTCTAAT-3') were included at the 3' end, resulting in an overall generic PCR primer sequence as follows:

Forward:AATGATACGGCGACCACCGAGATCTACAC <i5><pad><link><16Sf>

Reverse: CAAGCAGAAGACGGCATACGAGAT <i7><pad><link><16Sr>

Table 6.1 Barcodes for Illumina Miseq sequencing

Barcode name	Barcode sequence	F or R
SA503	TAGCGAGT	Forward
SD503	CGATCTAC	Forward
SA505	TCATCGAG	Forward
SC503	CGTCGCTA	Forward
SB507	GATCGTGT	Forward
SC502	ATATACAC	Forward
SB505	ACGTCTCG	Forward
SB508	GTCAGATA	Forward
SC501	ACGACGTG	Forward

SD504	TGCGTCAC	Forward
SA712	TCGCTATA	Reverse
SC702	AGCGCTAT	Reverse
SA703	AGTAGCGT	Reverse
SA711	TCATAGAC	Reverse
SA708	GTCGCTCG	Reverse
SB704	CATAGAGA	Reverse
SB706	CTCGTTAC	Reverse
SB707	GCGCACGT	Reverse
SC705	CTAGCTCG	Reverse
SC712	TCGAGCTC	Reverse
SA701	AACTCTCG	Reverse
SA709	GTCGTAGT	Reverse
SA710	TAGCAGAC	Reverse
SB705	CGTAGATC	Reverse

Each well contained 17 ul of Accuprime Pfx Supermix, 1 ul of template DNA, and 2 ul of each paired set of index primers. Next, 1 ul of PCR grade H$_2$O was added to the negative control, and 1 ul of Mock Community (BEI Resources, Virginia, USA) was added to the positive control. The following programme was used for the thermal cycling: an initial 2 mins at 95 °C; 30 cycles of 20 sec at 95 °C, 15 sec at 55 °C and 5 mins at 72 °C; and a final step of 72 °C for 10 mins.

6.2.7 High-throughput amplicon sequencing (Illumina MiSeq)

In total, 12 DNA samples were analysed using Illumina sequencing (Illumina, San Diego, CA, USA). Illumina sequencing was performed at the Institute of Medical Genetics on the Cardiff University Heath Campus using 2 bp × 250 bp paired-end flow cells and reagent cartridges. The data generated from the Illumina sequencing was analysed using Mothur v1.38.1 (Schloss et al., 2009) in accordance with the MiSeq standard operating procedure (Kozich et al. 2013). In summary, the analysis

process started with the contigs formation, and then sequences filtration to remove ambiguous reads shorter than 245 bp and longer than 275 bp. The resulted sequences were reduced using the command (unique.seqs) to generate a unique set of sequences and then aligned with the SILVA database. The command (chimera.uchime) was used to remove chimeric sequences. The sequences were assigned to the taxonomy using the 'classify.seqs' command (Wang approach). Then, the (dist.seqs) command was used to generate a distance matrix between the aligned sequences. Finally, these sequences were clustered to operational taxonomic units (OTUs).

6.2.8 Statistical analysis

Statistical analysis was performed to understand the microbial community and the difference between MFCs and MECs. Shannon index and Chao1 were used to identify the species diversity and richness for each sample. In addition, weighted UniFrac analysis was performed to compute the difference between the microbial communities based on phylogenetic information. Principal coordinates analysis (PCoA) was used to visualise the similarities in the microbial community relationships based on the distance matrix. After clustering, the heat map was generated via R studio software to reflect any similarities and differences in the community composition among bacterial samples at the family level. A Venn diagram with shared and unique OTUs was used to depict the similarities and differences between the two communities.

6.3 Results and discussion:

6.3.1 Diversity of microbial community and composition

In total, 12 samples were analysed from water and electrode samples in the MFCs and the MECs. After removing the low-quality reads, there were 29362- 88108 effective reads in all samples. The sequencing obtained 230 and 383 operational taxonomic units (OTUs) from the samples, each with 95% similarity. Chao1 estimator ranged from 240 to 300 for the MFC and from 195 to 280 for the MECs, indicating that the MFCs had greater richness than the MECs. The Shannon diversity index was used to determine community diversity, and it varied between (3.1-3.6) for the MFCs and (2-3) in the MECs. Similar values of the Shannon index for the anode communities were obtained by Kiely et al. (2011). The Shannon index shows that the

microbial diversity in anode MFCs is greater than in anode MECs. The sequencing results indicated that microorganism communities in MFCs are more diverse than in MECs. Similarly, Chae et al. (2008) confirmed that lower species richness of bacteria was found in MECs compared to MFCs, and the Shannon index of MECs was lower than for MFCs.

Each system (MFC or MEC) was operated under certain operational conditions. Generally, the MFC was operated under aerobic cathode, whereas the MEC was operated under an anaerobic cathode and external power source. The operational conditions of these systems highly influenced the diversity and richness of the microorganisms. Operational conditions, such as applied voltage and pH, have demonstrated their impact on microbial communities in BESs (Patil et al., 2011; Ding et al., 2016). Applied voltage influences microbial activity in two ways; it either stimulates the microorganisms to grow and degrade organic matter, or it inhibits microorganisms if the current is too high. In addition, Chae et al. (2009) showed that using an external power source in an MEC can result in a change or damage to the biofilm. Furthermore, solution pH was demonstrated to have an impact on anode community structure (Patil et al., 2011).

6.3.2 Bacterial taxonomic identification

The sequences were assigned to identify the different communities in MFCs and MECs; the sequences were classified from phyla to genera. The relative abundance of a given bacteria group was set as the number of sequences affiliated with that group divided by the total number of sequences per sample.

In the MFCs, in total, 19 bacteria phyla were identified (19 phyla in MFC-1 and 17 phyla in MFC-2). The microbial populations belonged to 33 classes and 78 genera. The results showed that overall communities of the anodic biofilms in MFCs have the same species. As shown in Fig. 6.1, Synergistetes, Bacteroidetes, Proteobacteria and Firmicutes were the dominant phyla in the anode chambers of the MFCs. The sum of the four dominant phyla species accounted for 78.5% in MFC-1 (Synergistetes 27%, Bacteroidetes 27%, Proteobacteria 13% and Firmicutes 11.5%) of the total reads. Similarly in MFC-2, the same species were found to be the dominant species and accounted for 73.3 % (Synergistetes 32%, Bacteroidetes 19%, Proteobacteria 15.8% and Firmicutes 6.5%,) of the total reads, followed by other

major phyla, such as Chloroflexi 6%, Ignavibacteriae 2%. In addition, other minor phyla were found with low abundance in the community, such as Cloacimonetes 0.5% and Acidobacteria 0.2%. Around 11% of the total reads were not classified at the phylum level, which means that these bacteria are novel bacteria.

Similarly, in the MECs, 18 bacteria phyla were identified in MEC-1 (18 phyla) and MEC-2 (16 phyla), and the microbial populations belonged to 33 classes and 77 genera. The anodic biofilm in the MECs has been shown to have a similarity in bacteria species and structure. Proteobacteria, Firmicutes, and Bacteroidetes are the dominant phyla in the anode chambers of the MECs. This result is consistent with the composition that was found in the MEC study by Clauwaert et al. (2008), where Proteobacteria, Firmicutes, and Bacteroidetes phyla were found to be the dominant bacteria in MECs.

At phyla level, MEC-1 comprised Proteobacteria 24%, Firmicutes 20%, Bacteroidetes 6% and Synergistetes 6% of the total reads. Similarly, MEC-2 comprised Proteobacteria 41%, Firmicutes 15%, Bacteroidetes 6%, and Synergistetes 6% of the total reads. Other phyla with small quantities were found, such as Chloroflexi 0.6%, Spirochaetes 0.3%, and Actinobacteria 0.2%.

Bacteroidetes, Firmicutes, and Proteobacteria phyla are commonly found in MFC and MEC studies (Kan et al., 2010; Liu et al., 2012; Park et al., 2014). However, the microbial structure is not consistent in BES studies. Various phyla in the microorganism community have the ability to transfer electrons to the anode electrode. Bacteroidetes, Firmicutes, and Proteobacteria are the most common phyla in bio-electrochemical studies, and this result was consistent with previous research that used acetate as a main source of carbon (Park et al., 2014). A surprisingly high abundance of Synergistia phylum was found in the MFCs communities and less than 6% in the MECs communities. The Synergistia phylum was the dominant phylum in different MFC studies (Lesnik and Liu, 2014; Lee et al., 2016). The main source of this phylum might be the anaerobic digester sludge during the inoculation process (Ganesan et al., 2008). The Synergistetes phylum is commonly found in systems that were fed with acetate (Malvankar et al., 2012; Lee et al., 2016). In addition, the Synergistetes phylum is present in most BES microbial communities at a low percentage. To date, the role or function of the Synergistetes phylum in BESs is

unclear; it could be an amino acid fermenter, where it transforms amino acids into methane (Silva et al., 2013; Lee et al., 2016). Díaz et al. (2007) stated that the contribution of Synergistetes to overall MFC performance is unknown, and it could be linked to the ability of species such as *A. circumscriptus* to efficiently ferment a variety of amino acids. Similar to this study, a high abundance of Synergistetes (33%) was reported in MFCs fed with acetate (Lesnik and Liu, 2014).

The Bacteroidetes phylum was detected as the dominant phylum in the MFCs (19-27%), and in the MECs, the percentage of Bacteroidetes (6%) was low compared to in the MFCs. Bacteroidetes are fermentative bacteria that were induced in the anaerobic environment of the anode and are known to be capable of the biodegradation of organic pollutants (Sack et al., 2011).
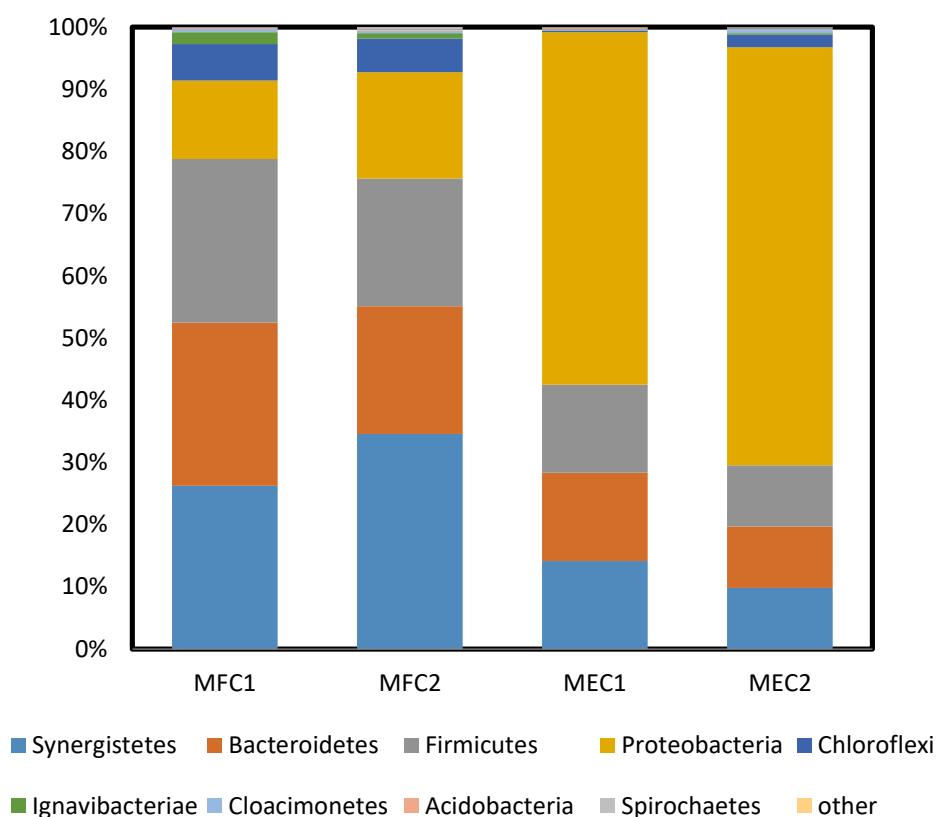
Figure 6.1 Taxonomic classification of bacterial 16s rRNA gene reads at phylum level.

In this study, electrochemically active bacteria, such as Proteobacteria, Firmicutes, and Acidobacteria, were present in the anodic chambers of both the MFCs and the MECs, and Proteobacteria and Firmicutes were found to be the dominant phyla.

Proteobacteria and Firmicutes phyla have been shown to have the ability to directly transfer the electrons to the anode electrode. Wrighton et al. (2008) stated that the functional role of Firmicutes in MFCs was current production. In addition, the Firmicutes phylum is commonly abundant in dual-chamber MFCs and is responsible for power production (Jung and Regan, 2007). The relative abundance of Firmicutes in the MECs was higher than in the MFCs, probably due to the operational conditions.

In MFC class level, 33 class levels were detected, and the results showed that MFC-1 and MFC-2 had similar classes with variations in the percentage. The majority of bacterial classes in the MFC-1 belonged to Synergistia 27%, Bacteroidetes_unclassified 17%, Clostridia 10%, Bacteroidia 8%, Betaproteobacteria 7%, and Deltaproteobacteria 5%. Similarly, the majority of bacterial classes in MFC-2 belonged to Synergistia 32%, Deltaproteobacteria 12%, Bacteroidetes_unclassified 11%, Clostridia 6%, Bacteroidia 4% and Betaproteobacteria 4%. Other classes with small quantities were found, such as Ignavibacteria 2%, Alphaproteobacteria 0.1%, and Gammaproteobacteria 0.1%.

In MEC class level, sequencing was able to detect 33 class levels in the MECs (Figure 6.2). The bacterial class in the MEC-1 belonged to Deltaproteobacteria 12%, Clostridia 7%, Synergistia 6%, and Negativicutes 4.5%, and MEC-2 composed of Negativicutes 20%, Deltaproteobacteria 17%, Clostridia 7%, and Synergistia 6%. Other minor classes were found in the composition, such as Firmicutes_unclassified 1%, Anaerolineae 0.5%, Alphaproteobacteria 0.4%, and Planctomycetia 0.3%.

The classes Synergistia, Clostridia, and Deltaproteobacteria were dominant in both systems (MFC and MEC). Those classes have been reported to be the dominant classes in BESs and are correlated with energy generation (Sun et al., 2012). Deltaproteobacteria are electrochemically active bacteria that play an important role in generating protons and electrons during their metabolism and are involved in energy generation (Logan, 2009). The Deltaproteobacteria class is commonly found in acetate-enriched MFCs, and it is responsible for the direct electron transfer to the electrode (Zhang et al., 2011b). The class Clostridia has been reported to play an important role in power generation and for being responsible for converting

fermentable substrate into simple organics (Jiang et al., 2016). The class Synergistia belongs to the Synergistetes phylum, which has been discussed earlier.

In genera level, 78 genera were observed in each MFC. The MFC-1 anodic community mainly comprised *Desulfovibrio* 4.5%, *Butyricicoccus* 4.5%, *Petrimonas* 4%, *Propionivibrio* 1.5%, *Desulfovirga* 1.5% and *Geobacter* 0.8%. In MFC-2, a similar trend of genera was observed in the anode community; the community contains *Petrimonas* 7%, *Butyricicoccus* 6.5%, *Thauera* 3.5%, *Ignavibacterium* 2%, *Desulfovibrio* 1.5%, and *Geobacter* 0.1%. Around 59% of the total composition was assigned as unclassified at the genus level, which indicates that it has not been possible to detect novel bacteria until now (Figure 6.3).
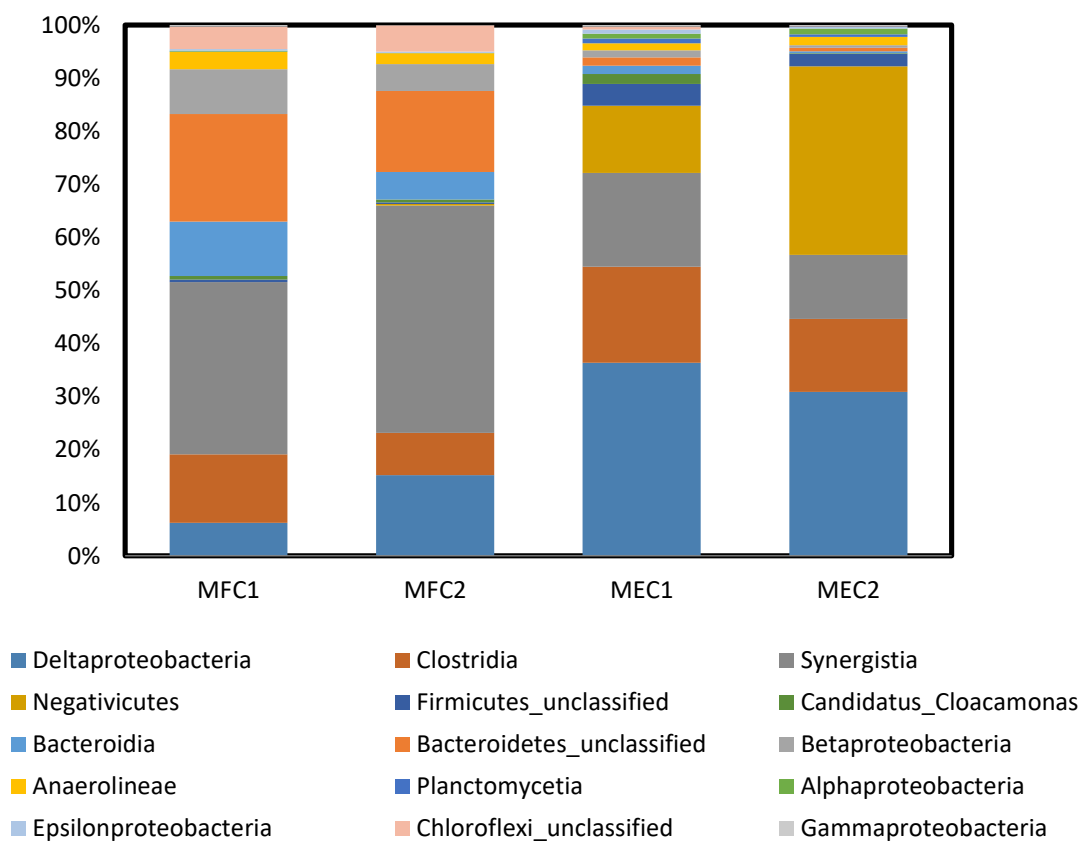
Figure 6.2 Taxonomic classification of bacterial 16s rRNA gene reads at class level

The community of MEC-1 mainly included *Desulfovibrio* 14%, *Acidaminococcus* 2%, *Desulfocapsa* 1.5%, *Acetobacterium* 1%, and *Cloacibacillus* 1%. MEC-2 included *Desulfovibrio* 12.5%, *Butyricicoccus* 5%, *Cloacibacillus* 0.7%, *Acidaminococcus* 0.5%, and *Desulfobulbus* 0.45%. More than 62% of the total

composition was not classified due to the complexity of the community. Different microorganism species can be found in the anode chamber, but not all of those species are involved in energy or current production. There are species that are involved only inorganic substance degradation.

In terms of electricity generation, *Desulfovibrio*, which belongs to the Deltaproteobacteria class, was the dominant gene among the classified genera in both systems. However, the presence of *Desulfovibrio* in the MECs (12 - 14 %) was greater than in the MFCs (1.5 - 4.5 %). In addition, the relative abundance of *Desulfovibrio* in MFC-1 was higher than in MFC-2. *Desulfovibrio* is an important genus in current production, and it was reported to be involved in both current production and organic degradation (Liu et al., 2012). *Desulfovibrio* was the common predominant exoelectrogen in the anodic biofilm in both systems, thus demonstrating that this genus was well adapted to the operating conditions and contributes to the current generation as a main exoelectrogen in the electrodes.

Desulfovibrio has been reported to be the dominant genus in different BES studies, and its role in electricity generation has been confirmed (Bond et al. 2002; Zhao et al. 2008). *Desulfovibrio* is responsible for transferring the electrons from the substrate to the electrode surface via the outer membrane cytochrome. Kang et al. (2014) stated that in mediator-less MFCs, *Desulfovibrio* was observed to enhance current generation and was able to transfer the electrons more efficiently than *Geobacter*. In addition to *Desulfovibrio* for electricity generation, *Geobacter* species are well-known exoelectrogenic bacteria; *Geobacter's* role is crucial in direct electron transfer without the aid of any mediators (Pant et al., 2010). *Geobacter* is one of the most important genera for electron transport between the bacteria and electrode. The percentages of *Geobacter* (< 1%) detected in both systems were low compared to previous studies, showing a higher percentage in single-chamber MFCs (Butler and Nerenberg, 2010; Yates et al., 2012). However, low percentages of exoelectrogens, such as *Geobacter* and *Shewanella*, have been reported in different studies (Kim et al., 2007; Miran et al., 2015).

The presence of these species is not a necessity for high power production (Aelterman et al., 2006). It has been reported that the performance of mixed-culture BESs was better than the pure culture due to the interaction of communities (Yates et al., 2012). Many species that are capable of generating electricity were found in the

anode biofilm; however, these species were not numerically abundant and accounted for (<0.2%). In addition, *Shewanella*, which is commonly present in BES, was not detected in either the MFCs or the MECs. *Shewanella* has been reported to grow in low nutrient environments (Thormann et al., 2004), but the synthetic wastewater in this study contains high concentrations of nutrients, which tends to inhibit the growth of *Shewanella*. Thormann et al. (2004) stated that the presence of oxygen with a high concentration of nutrients leads organisms to catabolize the nutrients aerobically rather than investing energy in the formation of the biofilm. *Shewanella* has not been detected in many MFC and MEC studies (Lu et al., 2012; Miran et al., 2015). *Butyricicoccus*, from the class Clostridia of the phylum Firmicutes, was found with approximately the same percentage in both systems. *Butyricicoccus* was reported to utilise acetate and produce butyrate, H_2 and CO_2 (Eeckhaut et al., 2008).

In terms of organic matter removal, the pathway of organic matter degradation in an MFC is similar to the anaerobic digestion process (hydrolysis and fermentation). As mentioned earlier, CE was low in this study, and the COD removal efficiency was over 70% in both systems. This suggests that there was competition for the substrate among exoelectogens and other microbial communities in the system, which means that most of the substrate was not involved in current generation. *Bacteroides* is one of fermentative bacteria responsible for producing metabolites for exoelectrogenes and hydrolysing complex organics (Rismani-Yazdi et al., 2013). *Bacteroides* is one of the dominant classes found in the MFCs; the presence of this genus is crucial for the good operation and organic matter degradation of the MFCs (Jia et al., 2013). In addition, fermentative bacteria (*Petrimonas*) are another genus that showed the ability to improve H_2 production in MECs (Khan et al., 2017).

Small quantities of fermentative bacteria were observed in the anode community (*Paludibacter, Petrimonas*, and *Anaerovorax*). These species were responsible for utilising sugars and amines to produce organic acids, which are subsequently metabolised by exoelectrogens for electricity generation (Lu et al., 2012). Furthermore, *Zoogloea* and *Dechloromonas*, which are responsible for wastewater treatment, were found in small percentages (<1%). In addition, some of the species that were observed in BESs have unclear functions, such as *Cloacibacillus*. *Cloacibacillus* was mainly found in the MEC bacteria community; this species might

reach the system during the inoculation process with anaerobic digester sludge (Zeng et al., 2015).
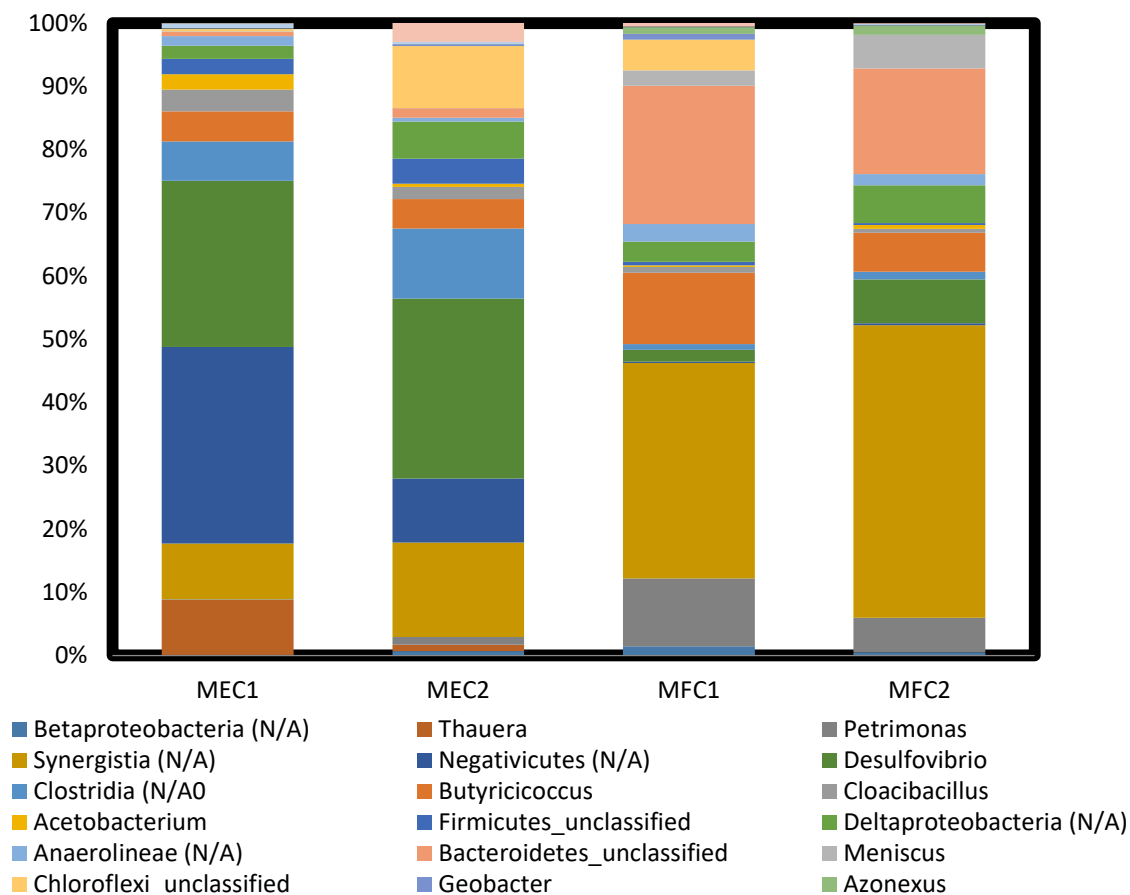
Figure 6.3 Taxonomic classification of bacterial 16s rRNA gene reads at genus level.

6.3.3 Difference and similarities

The microbial communities at the phylum level in MFC and MEC are significantly different. In MFCs, Synergistetes were the dominant phylum followed by Bacteroidetes, then Proteobacteria, Firmicutes, finally Chloroflexi. The order of the phyla in both MFCs was the same; however, the percentage was different. In MECs, Proteobacteria was the dominant phylum, followed by Firmicutes, Bacteroidetes, Synergistetes and Chloroflexi.

Proteobacteria in the MECs was observed in higher percentages (24 – 41 %) than in the MFCs (13 – 15 %), as Proteobacteria species are well known for their ability to produce and consume H_2 (Schaetzle et al., 2008). The presence of Chloroflexi in

MFCs and MECs is not unusual, as they are common in biological nutrient removal processes. Chloroflexi has been found as a dominant phylum in the anode biofilm in different MFC studies (De Schamphelaire et al., 2010); in this study, it was present in the MFCs (6 %) at higher percentages than in the MECs (< 1 %). Chloroflexi plays an important role in wastewater treatment (responsible for the degradation of carbohydrates) and nitrogen removal (Meng et al., 2013). Finally, the abundance of Synergistetes in the MFCs (27 – 32 %) was higher than in the MECs (5 – 6 %). Further studies are needed to understand the role of Synergistetes in BESs.

To provide a better understanding of the system, genera were analysed. A hierarchy cluster heat map highlighted the top 50 families, accounting for the most read sequences (Fig.6.4). The heat map showed clear distinctions in community structure between the anode of the MFCs and the anode of the MECs, despite the fact that they were inoculated with the same wastewater. In genus level analysis, the dominant genera in both systems were different. There were some genera present in the MFCs only and that could not be detected in the MECs. In total, 1037 OTUs were detected in both the MFCs and the MECs (Fig.6.5). Both systems were sharing 259 OTUs accounting for 25% of the total OTUs, and the majority of the shared OTUs were Proteobacteria and Bacteroidetes. In addition, 318 OTUs were detected only in the MFCs, whereas 201 OTUs were only detected in the MECs.

Proteobacteria and Bacteroidetes are commonly found as dominant phyla in BESs fed with artificial wastewater (Shimoyama et al., 2009), industrial wastewater (Kiely et al., 2011), and acetate (Ishii et al., 2008). Proteobacteria, which include Deltaproteobacteria species, were responsible for direct electricity production. Similarly, in the Bacteroidetes phylum, Shimoyama et al. (2009) stated that Bacteroidetes, which is correlated with electricity generation from artificial wastewater, was an abundant phylum in a continuous-flow cassette-electrode MFC. Therefore, Proteobacteria and Bacteroidetes phyla are the most important phyla in BESs, as both MFCs and MECs contain those phyla.

At the genera level, statistical analysis was conducted to identify the difference in genus between the microbial communities in the MFCs and the MECs. There was a statistically significant difference (P<0.05) between the two communities, as some genus were found in one system but could not be found in the other. The *Bacteroides*

gene, which is known to be able to produce H$_2$ by fermentation and to produce electricity in MFCs (Kim et al., 2006), was found only in the MFCs in small quantities (< 1%). *Acidaminococcus* from the Firmicutes phylum was detected only in the MECs, which shows their importance in the operation of MECs. The role of *Acidaminococcus* in MECs is amino acid degradation, and it is involved in enhancing hydrogen productivity (Lay et al., 2010). The genes *Desulfocapsa* and *Telmatospirillum* from the Proteobacteria phylum were found in the MECs in higher abundance than in the MFCs.
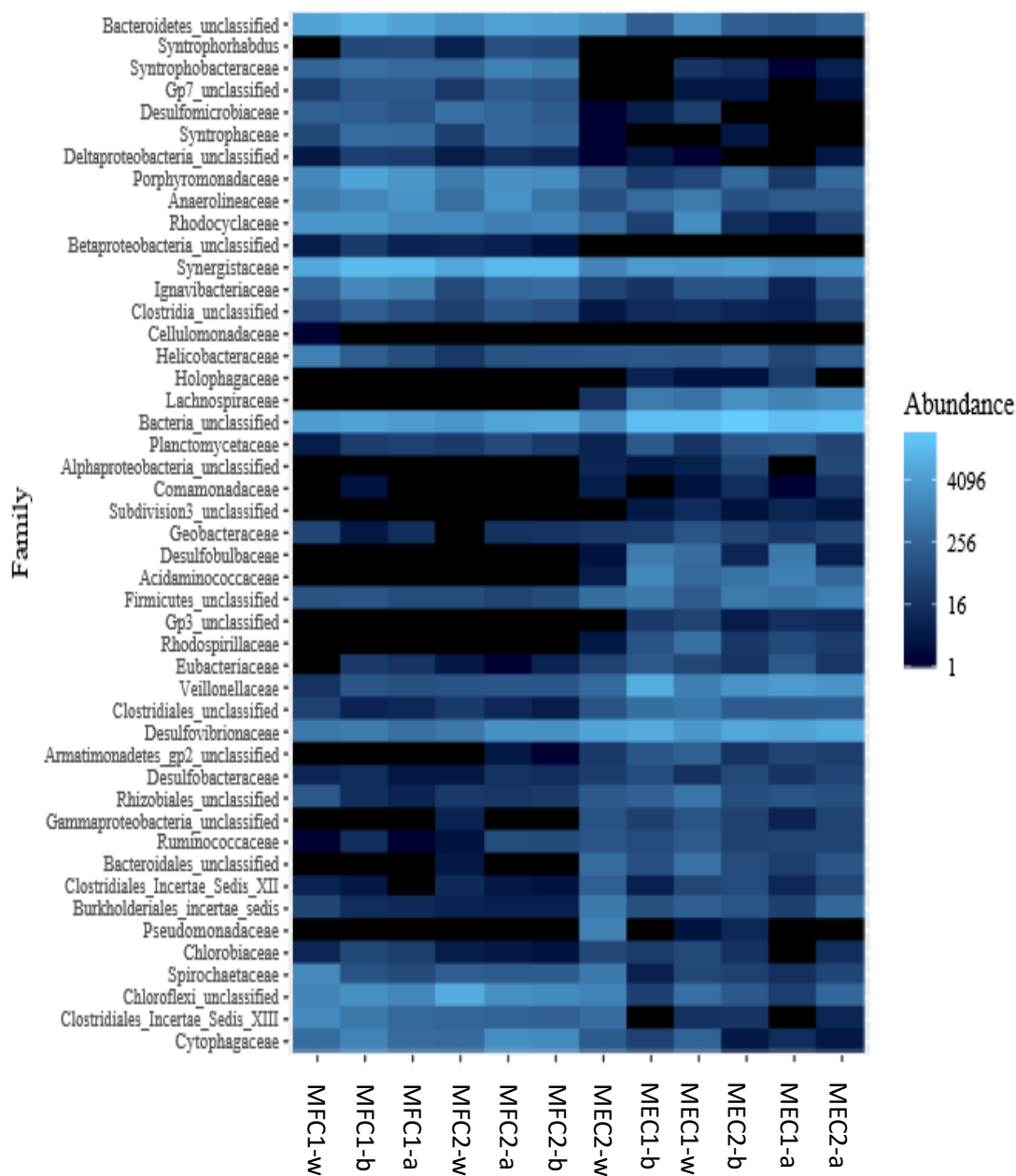
Figure 6.4 Heat map graph of hierarchy cluster for the top fifty families.

Desulfobulbus is a well-known gene that plays an important role in transferring electrons to the anode; it belongs to the sulphate reducers class, and it is involved in electricity generation in BESs (Lovley, 2006). It was observed in this study that the MFCs and the MECs contained a low percentage of *Desulfobulbus*. In addition, it has been reported that *Desulfobulbus* is able to produce electricity in an MFC, using the anode electrode as a direct electron acceptor (Holmes et al., 2004).

The *Pseudomonas* genus was found in both systems at a low percentage (<1 %); however, it was present in the MECs with a higher percentage than in the MFCs. *Pseudomonas* have commonly been found in MEC studies. The presence of *Pseudomonas* can support electricity generation by self-producing mediators to shuttle electrons outside the cell or between cells (Boon et al., 2008). In addition, *Pseudomonas* is responsible for organic matter degradation and metal resistance. The *Thauera* genus, which belongs to beta-proteobacteria, was observed in both MFCs (0.3 – 4 %); it is well known as a denitrifier that is able to degrade aromatic compounds (Liu et al., 2006). Different studies have reported the presence of *Thauera* in MFCs that are treating wastewater with high nitrogen concentration, where it has demonstrated the ability to degrade organic compounds in wastewater and enhance nitrogen removal (Sayess et al., 2013). *Propionivibrio*, which belongs to the class Betaproteobacteria, was detected in the MFCs only, so this bacteria could be used in bioenergy production (Wang et al., 2016a)
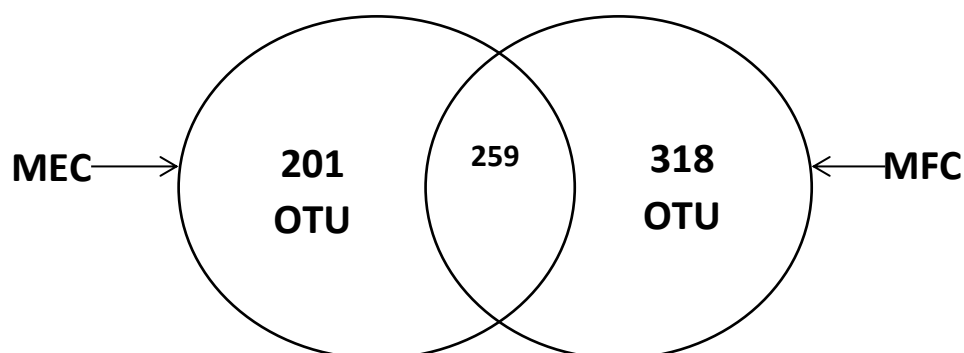
Figure 6.5 Venn diagram of bacterial communities with shared and unique OTUs among MFC and MEC anode biofilm

Acidaminococcus are fermentative bacteria responsible for amino acid degradation and are involved in enhancing hydrogen productivity (Lay et al., 2010). The

Acidaminococcus genus was detected only in the MECs, and the presence of this gene might be linked to the system operational conditions.

Cluster analysis of the anodic biofilm of both the MFCs and the MECs showed that the bacterial communities were different. As with the *Acidaminococcus* genus, the differences found between the communities in the MFCs and the MECs might be due to the differences in the system operational conditions. All the reactors had the same design, and the anode chambers were inoculated with the same wastewater and fed with same synthetic wastewater.

Principal Coordinates Analysis (PCoA) was used to visualise and compare the dissimilarity between two different systems (Fig 6.6). The two first ordination axes explained 41% of the variability found in the microbial community compositions. The duplicate reactors MFCs were clustered together, which means that the microbial communities were similar; the same observation was found with the MECs. PCoA showed a clear separation between the communities in the MFCs and those in the MECs. The analysis shows great diversity in the communities of the anode in the MFCs and in the MECs. These results showed the impact of the reactor operational conditions on the community structure.

In Figure 6.6, the green circles represent the anode electrodes from the MECs, and the green triangle represents the water sample from the anode chamber in the MECs. The red circles represent the anode electrodes from the MFCs, and the red triangle represents the water sample from the anode chamber in the MFCs. It can be seen clearly that the biofilm communities of the MECs are located in the top right corner, and the biofilm communities of the MFCs are located in the top left corner of the plot.
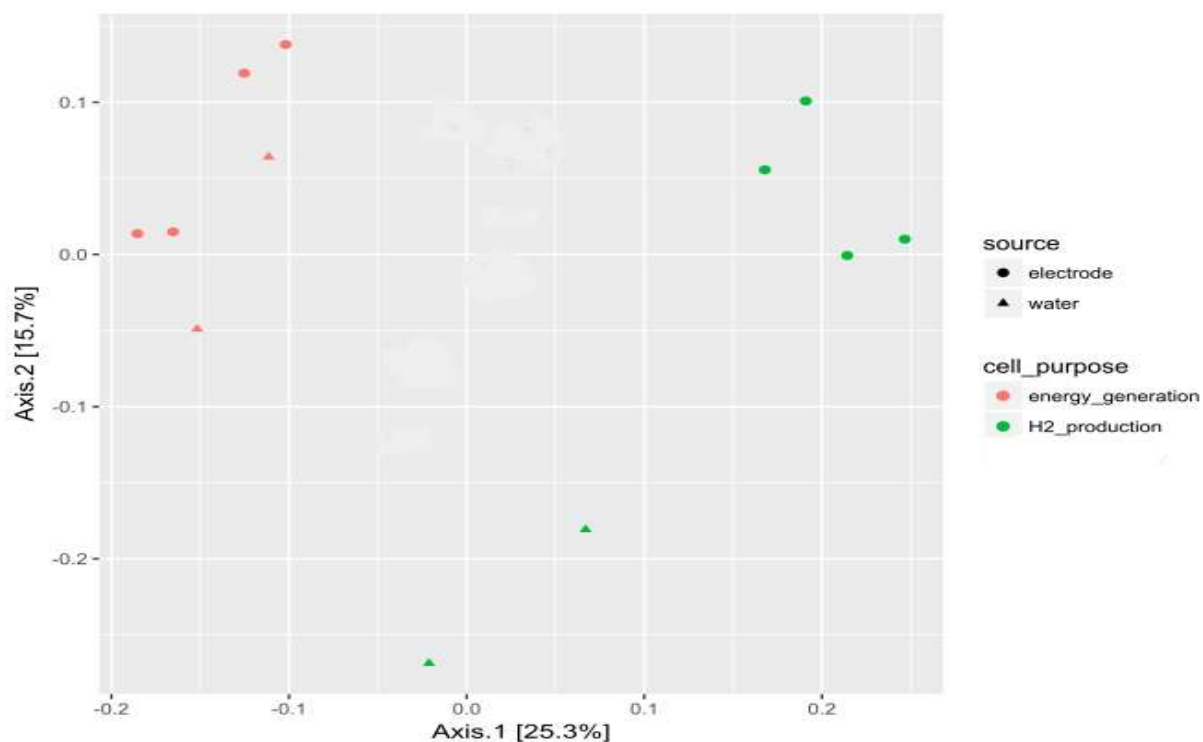
Figure 6.6 PCoA plot analysis based on the sequencing data. The axes are the percentages of variation explained by the components

6.3.4 The impact of operation conditions on microbial community in BES

The MFCs and MECs were operated with the same synthetic wastewater, and both systems had a similar design. However, as mentioned previously, the operational conditions, such as hydraulic retention time and pH, were different. Hydraulic retention time is an important factor that has an effect on microbial community. The change of hydraulic retention time might lead to changes in the cellular physiology and the community level. Some bacteria species can survive for a short hydraulic retention time, whereas some may disappear (JingRui et al., 2016). In the MFCs, the cycle duration was 48 hours, whereas in the MEC, the cycle duration was between 3-6 days. Thus, variations in microbial community could be observed between the MFCs and the MECs.

Furthermore, the power source that is mainly used in MECs to overcome the thermodynamic limit for hydrogen evolution has an effect on the microbial community. Ding et al. (2016) stated that applying high voltage to the circuit can be harmful to living organisms and might inhibit their existence. In addition, a high

voltage might reduce biofilm density on the anode electrode, and that would result in changes to the microbial community

In addition, pH is another important parameter that influenced the microbial community. Due to organic matter oxidation at the anode chamber, the pH around the anode decreased and reached 5 in some cases. Solution pH has a great influence on bacteria community and bacterial growth; thus, any change in the environmental pH could affect the microbial community (Chae et al., 2009). Low pH inhibits the microbial activity and biofilm formation, and reduces system performance. In addition, variations in solution pH may affect the distribution of bacteria on the electrode and, as a result, change the microbial structure (Gao et al., 2016). The growth of Exoelectrogenic *Geobacter* was observed to be inhibited at a pH below 6.4, and there was no growth below pH 5.5 (Kim and Lee, 2010). Thus, a low percentage of exoelectrogenic *Geobacter* was observed in this study.

Furthermore, cathode aeration had a great impact on the microbial community. The diffusion of oxygen from the cathode to the anode may affect the presence of different bacteria species. Thus, the diversity of the MFCs was greater than that of the MECs. El-Chakhtoura et al. (2014) confirmed that the presence of oxygen leads to higher phylogenetic diversity.

Many bacteria species can contribute significantly to energy generation, and the low presence of the exoelectrogenic microbes, such as *Geobacter*, in the system does not mean low system performance. The positive correlation between the key player microbes in the anode and electricity generation performance is not always observed (Kiely et al., 2010). Many minor bacteria communities may be involved in electricity production and enhance the performance. Among the 60% of unclassified genera, there could be an exoelectogens species that plays a role in electricity generation, but unfortunately, the electricity-producing ability of unclassified bacteria has not been ascertained (Lu et al., 2012).

6.4 Summary

- This chapter has illustrated the overall structure of the microbial community in the MFCs and MECs that were designed for concurrent energy generation / H$_2$ production and P recovery.

- The microbial community in the MFCs had greater richness than that in the MECs based on the Chao 1 estimator. The Shannon diversity index of the MFCs was higher than that of the MECs.

- In total, 19 phyla, 33 classes, and 78 genera were found in the MFCs, whereas in the MECs, 18 phyla, 33 classes, and 77 genera were found.

- The dominant phyla in MFCs were Synergistetes, Bacteroidetes, Proteobacteria, and Firmicutes, whereas the dominant phyla in MECs were Proteobacteria, Firmicutes, and Bacteroidetes.

- Bacteroidetes, Proteobacteria and Firmicutes were the main phyla in the BESs.

- *Desulfovibrio*, which belongs to the Deltaproteobacteria class, was the dominant gene among the classified genera in both systems, and it might be responsible for electricity generation.

6.5 Conclusion

The results in this chapter have investigated the composition and structure of microbial community in the MFCs and the MECs that were used for concurrent P recovery and energy generation/ H$_2$ production. In summary, the results from Illumina high-throughput sequencing showed that the microbial community structure of the MFCs was more diverse than that of the MECs. However, while the structure of the MFC community was different from that of the MEC community, both shared the same dominant species. The dominant phyla in both systems were in agreement with the findings of previous studies; however, direct comparison of microbial community structure between studies is not feasible. The results indicated remarkable differences in the diversity and structure of the bacterial communities. Principle coordinate analysis showed that the community of the MFCs was different from that of the MECs, and this variation might occur due to the differences in the operational conditions of the MFCs and the MECs. In addition, due to organic matter oxidation, hydraulic retention time, and applied voltage, anode pH had an influence on microbial community composition and structure.

Chapter 7

Conclusion

7.0 Conclusion

7.1 Summary

The main aim of this thesis was to study and understand the parameters for the optimisation of the design and performance of dual-chamber BES for concurrent phosphorus recovery, and energy generation/hydrogen production. The reactors were designed with dual-chamber reactors in order to overcome pH buffering in single-chamber bio-electrochemical systems and enhance P recovery and H_2 production. The systems were designed to concurrently treat wastewater, recover P, and generate energy (MFC) or produce hydrogen (MEC). In addition, the study aimed to understand and study the parameters for the optimisation of the design and the performance of BESs for concurrent P recovery and energy generation/H_2 production. The main conclusions from the investigations conducted to fulfil the main aim are presented in the following section.

7.2 Conclusion

The literature review identified that BESs represent a multi-functional promising technology that can be implemented in wastewater treatment plants to minimise energy consumption and protect global natural resources. Generally, single-chamber BESs have been widely used to improve energy generation. However, the single-chamber design limits P recovery and reduces H_2 production. Therefore, dual-chamber BESs were suggested as an important design to improve P recovery in BESs and H_2 production in MECs. To date, there has been no investigation of the parameters for the optimisation of the design and performance of BESs for concurrent phosphorus recovery and energy generation/hydrogen production.

Four lab-scale BESs (two MFCs and two MECs) were designed and set up at Cardiff University School of Engineering to experimentally assess P recovery in dual-chamber BESs and investigate the impacts of different operational conditions on P recovery and energy generation/H_2 production. System performances were evaluated by coulombic efficiency, power density, H_2 production and P precipitation rate.

The results presented in Chapter 3 demonstrated that P was recovered via precipitation due to the high pH in the cathode chamber, which resulted from

oxidation-reduction reactions. X-ray diffraction and SEM-EDS analysis were used to identify the main components of the precipitate, and the precipitate was determined to be magnesium ammonium phosphate hexahydrate (struvite). The MFCs achieved a maximum P precipitation efficiency of 90% with coulombic efficiency ranging from 1 to 10%. The MFCs achieved a low coulombic efficiency and deterioration in current generation was observed, that might be due to the P precipitation on the cathode surface and the membrane surface. In terms of treatment efficiency, MFCs achieved an average of 80% treatment efficiency, which confirms the ability of these systems to be used in wastewater treatment. The three operational parameters (COD concentration, cathode aeration flow rate, and external resistance) were found to have significant impacts on MFC performance and P recovery. The statistical analysis showed that COD concentration and cathode aeration flow rate are the key factors influencing P recovery and energy generation.

The results presented in Chapter 4 represent an optimisation study to enhance and optimise energy generation and P recovery through operational conditions (influent COD and cathode aeration flow rate) using full factorial design and central composite design. The statistical tools were adopted to identify any interaction between influent COD and cathode aeration flow rate, and any effects on power density, coulombic efficiency, COD removal, cathode pH, and P recovery. Energy generation and P recovery were highly affected by COD concentration and aeration flow rate. The effect of influent COD was greater than cathode aeration flow rate on all the responses. COD had a significant effect on all the responses, whereas cathode aeration had a significant effect on power density, CE, and P precipitation efficiency. The interaction effect between influent COD and cathode aeration was significant for cathode pH, which is the most important factor for P recovery. COD concentration had mixed effects on cathode pH at different levels of cathode aeration flow rate. Statistical analysis of the data obtained from the lab-scale MFCs was used to develop predictive models for P recovery and maximum power density that can be used in design stage. Furthermore, cathode pH was observed to have an impact on crystal size, as bigger crystals were found at a pH between 8-9. Fully understanding the impacts of and the interactions between factors such as COD concertation and cathode aeration flow rate for MFC performance will help to operate the system

under the optimal conditions, which in turn helps to reduce the operational costs and optimise the responses.

The results presented in Chapter 5 demonstrated the ability of MECs to concurrently produce H_2 and recover P. Similar to in MFCs, P was precipitated in the cathode chamber due to the consumption of protons at the cathode, which resulted in high pH. The precipitates were confirmed to be struvite. The MECs achieved a maximum H_2 production rate of 0.28 m^3-H_2/m^3/d (at applied voltage = 1.1 V, COD = 500 mg/L) and a maximum precipitate efficiency of 95% (at applied voltage =1.1 V, COD =1500 mg/L). In addition, the MECs achieved a maximum CE of 51%, and the overall energy recovery ranged from η_{E+S}= 25 ± 1 % to 37 ± 1.7 %. Applying high voltage to a circuit might decrease the COD removal and inhibit the microbial activity. The response surface methodology was used to identify the impact of each factor (applied voltage and COD concentration) on H_2 production and P recovery. In addition, the data obtained from the lab-scale MECs were used to develop predictive models for H_2 production and P recovery. A high applied voltage would result in higher H_2 production and high precipitation efficiency. It is important to consider the initial COD concentration if the system is to be used for H_2 production and P recovery. More importantly, this model can help in achieving the balance between P recovery and H_2 production.

Finally, the results presented in Chapter 6 analysed the microbial composition and structure in MFCs and MECs. The results demonstrated that the microbial community in the MFCs was richer and more diverse than that in the MECs. The structure of the MFC community was different from that of the MEC community; however, both shared the same dominant phyla. Bacteroidetes, Proteobacteria and Firmicutes were the main phyla in both the MFCs and the MECs. The *Desulfovibrio* genus was the dominate genus among the classified genera in both systems, and it was responsible for electricity generation. The percentage of *Geobacter* genus in both communities was low; however, the presence of this genus is not a necessity for high power production. The difference in microbial community and structure between the MFCs and the MECs might be attributed to the differences in operational conditions.

Chapter 8

Recommendations for further work

8.0 Recommendations for further work

- This study has demonstrated that dual-chamber BESs can be used for effective energy generation, H_2 production, and P recovery. However, electrode scaling due to struvite precipitation leads to high energy loss and minimises BES performance. Therefore, further studies should be conducted to find a way to minimise the amount of precipitates on the cathode surface. This could be achieved through finding a protective material that prevents particles from attaching to the electrode or designing the system in a way that the cathode electrode can be replaced automatically with a new electrode once the voltage starts to decrease.

- The precipitated struvite in BESs was pure struvite because the system was operated with synthetic wastewater. Therefore, it is possible that with the use of real wastewater, different phosphorus crystals may precipitate. More studies are needed to determine the impacts of using real wastewater on BES performance and P recovery.

- New modifications can be made to the BES to minimise ammonia volatilization due to the high pH at the BES cathode. This can be achieved by reintroducing NH_3 from the cathode into the anolyte and using ammonia as an electron shuttle.

- The low coulombic efficiency in BESs, especially in MFCs, should be improved to be scaled up and applied in the wastewater treatment industry. Low coulombic efficiency resulted from different parameters. Oxygen diffusion into the anode chamber is a major issue that reduces BES performance. However, biocathode systems can be used to reduce oxygen diffusion and operational costs. In addition, the growth of methanogenic bacteria that use the substrate for metabolism instead of current production is another issue that decreases coulombic efficiency.

- At high COD concentration, a BES requires a long batch cycle to fully degrade organic matter. Long cycle duration leads to a reduction in anolyte pH to below 6 and as a result, a reduction in power generation and microorganism inhibition may occur. To overcome this issue, continuous flow may be employed instead of the batch cycle or using a short batch cycle duration.

- Some operational conditions, such as solution conductivity and temperature, were kept constant during the BES experiment. These parameters are important and may have an influence on energy generation, P recovery, internal resistance, and electron transfer mechanism. Therefore, further studies are needed to determine the impacts of these parameters on system performance.

- The architecture of the BES improves the BES performance, where using dual chamber BES can increase the internal resistance. Increasing electrode distance leads to an increase in the internal resistance and, as a result, reduces the power output. Thus, the distance between the electrodes in future studies should be reduced.

- Microbial community is an important parameter in BES performance; more studies are required to enhance the presence of exoelectrogens, such as *Geobacter* and *Shewanella* in BES to improve current generation.

.

References

Aage, H. and Andersen, B. and Blom, A. and Jensen, I. 1997. The solubility of struvite. *Journal of Radioanalytical and Nuclear Chemistry* 223(1-2), pp. 213-215.

Abbasi, U. and Jin, W. and Pervez, A. and Bhatti, Z. A. and Tariq, M. and Shaheen, S. and Iqbal, A. and Mahmood, Q. 2016. Anaerobic microbial fuel cell treating combined industrial wastewater: Correlation of electricity generation with pollutants. *Bioresource technology* 200, pp. 1-7.

Abourached, C. and Lesnik, K. L. and Liu, H. 2014. Enhanced power generation and energy conversion of sewage sludge by CEA–microbial fuel cells. *Bioresource technology* 166, pp. 229-234.

Aboutalebi, H. and Sathasivan, A. and Krishna, K. B. and Kohpaei, A. J. 2011. Expediting COD removal in microbial electrolysis cells by increasing biomass concentration. *Bioresource technology* 102(4), pp. 3981-3984.

Adnan, A. and Koch, F. A. and Mavinic, D. S. 2003. Pilot-scale study of phosphorus recovery through struvite crystallization-II: Applying in-reactor supersaturation ratio as a process control parameter. *Journal of Environmental Engineering and Science* 2(6), pp. 473-483.

Aelterman, P. and Rabaey, K. and Pham, H. T. and Boon, N. and Verstraete, W. 2006. Continuous electricity generation at high voltages and currents using stacked microbial fuel cells. *Environmental science & technology* 40(10), pp. 3388-3394.

Aelterman, P. and Versichele, M. and Marzorati, M. and Boon, N. and Verstraete, W. 2008. Loading rate and external resistance control the electricity generation of microbial fuel cells with different three-dimensional anodes. *Bioresource Technology* 99(18), pp. 8895-8902.

Ahn, Y. and Hatzell, M. C. and Zhang, F. and Logan, B. E. 2014. Different electrode configurations to optimize performance of multi-electrode microbial fuel cells for generating power or treating domestic wastewater. *Journal of Power Sources* 249, pp. 440-445.

Almatouq, A. and Babatunde, A. O. 2016. Concurrent Phosphorus Recovery and Energy Generation in Mediator-Less Dual Chamber Microbial Fuel Cells: Mechanisms and Influencing Factors. *International Journal of Environmental Research and Public Health* 13(4), p. 375.

Amari, S. and Vahdati, M. and Ebadi, T. 2015. Investigation into effects of cathode aeration on output current characteristics in a tubular microbial fuel cell. *International Journal of Environmental Science and Technology* 12(12), pp. 4037-4042.

Asghar, A. and Abdul Raman, A. A. and Daud, W. M. A. W. 2014. A comparison of central composite design and Taguchi method for optimizing Fenton process. *The Scientific World Journal* 2014.

Babić-Ivančić, V. and Kontrec, J. and Kralj, D. and Brečević, L. 2002. Precipitation diagrams of struvite and dissolution kinetics of different struvite morphologies. *Croatica Chemica Acta* 75(1), pp. 89-106.

Behera, M. and Ghangrekar, M. 2016. Optimization of Operating Conditions for Maximizing Power Generation and Organic Matter Removal in Microbial Fuel Cell. *Journal of Environmental Engineering*, p. 04016090.

Blöcher, C. and Niewersch, C. and Melin, T. 2012. Phosphorus recovery from sewage sludge with a hybrid process of low pressure wet oxidation and nanofiltration. *Water research* 46(6), pp. 2009-2019.

Boon, N. and Aelterman, P. and Clauwaert, P. and De Schamphelaire, L. and Vanhaecke, L. and De Maeyer, K. and Höfte, M. and Verstraete, W. and Rabaey, K. 2008. Metabolites produced by Pseudomonas sp. enable a Gram-positive bacterium to achieve extracellular electron transfer. *Applied Microbiology and Biotechnology* 77(5), pp. 1119-1129.

Butler, C. S. and Nerenberg, R. 2010. Performance and microbial ecology of air-cathode microbial fuel cells with layered electrode assemblies. *Applied microbiology and biotechnology* 86(5), pp. 1399-1408.

Call, D. and Logan, B. E. 2008. Hydrogen production in a single chamber microbial electrolysis cell lacking a membrane. *Environmental science & technology* 42(9), pp. 3401-3406.

Call, D. F. and Merrill, M. D. and Logan, B. E. 2009a. High surface area stainless steel brushes as cathodes in microbial electrolysis cells. *Environmental science & technology* 43(6), pp. 2179-2183.

Call, D. F. and Wagner, R. C. and Logan, B. E. 2009b. Hydrogen production by Geobacter species and a mixed consortium in a microbial electrolysis cell. *Applied and environmental microbiology* 75(24), pp. 7579-7587.

Çelen, I. and Buchanan, J. R. and Burns, R. T. and Robinson, R. B. and Raman, D. R. 2007. Using a chemical equilibrium model to predict amendments required to precipitate phosphorus as struvite in liquid swine manure. *Water Research* 41(8), pp. 1689-1696.

Cercado-Quezada, B. and Delia, M.-L. and Bergel, A. 2010. Testing various food-industry wastes for electricity production in microbial fuel cell. *Bioresource technology* 101(8), pp. 2748-2754.

Çetinkaya, A. Y. and Köroğlu, E. O. and Demir, N. M. and Baysoy, D. Y. and Özkaya, B. and Çakmakçı, M. 2015. Electricity production by a microbial fuel cell fueled by brewery wastewater and the factors in its membrane deterioration. *Chinese Journal of Catalysis* 36(7), pp. 1068-1076.

Chae, K.-J. and Choi, M.-J. and Lee, J.-W. and Kim, K.-Y. and Kim, I. S. 2009. Effect of different substrates on the performance, bacterial diversity, and bacterial viability in microbial fuel cells. *Bioresource technology* 100(14), pp. 3518-3525.

Chae, K.-J. and Choi, M.-J. and Lee, J. and Ajayi, F. and Kim, I. S. 2008. Biohydrogen production via biocatalyzed electrolysis in acetate-fed bioelectrochemical cells and microbial community analysis. *International Journal of Hydrogen Energy* 33(19), pp. 5184-5192.

Chaudhuri, S. K. and Lovley, D. R. 2003. Electricity generation by direct oxidation of glucose in mediatorless microbial fuel cells. *Nature biotechnology* 21(10), pp. 1229-1232.

Chen, G.-W. and Choi, S.-J. and Lee, T.-H. and Lee, G.-Y. and Cha, J.-H. and Kim, C.-W. 2008. Application of biocathode in microbial fuel cells: cell performance and microbial community. *Applied microbiology and biotechnology* 79(3), pp. 379-388.

Chen, S. and He, G. and Liu, Q. and Harnisch, F. and Zhou, Y. and Chen, Y. and Hanif, M. and Wang, S. and Peng, X. and Hou, H. 2012. Layered corrugated electrode macrostructures boost microbial bioelectrocatalysis. *Energy & Environmental Science* 5(12), pp. 9769-9772.

Cheng, S. and Liu, H. and Logan, B. E. 2006. Increased power generation in a continuous flow MFC with advective flow through the porous anode and reduced electrode spacing. *Environmental science & technology* 40(7), pp. 2426-2432.

Cheng, S. and Logan, B. E. 2007. Ammonia treatment of carbon cloth anodes to enhance power generation of microbial fuel cells. *Electrochemistry Communications* 9(3), pp. 492-496.

Cheng, S. and Logan, B. E. 2011a. High hydrogen production rate of microbial electrolysis cell (MEC) with reduced electrode spacing. *Bioresource technology* 102(3), pp. 3571-3574.

Cheng, S. and Logan, B. E. 2011b. Increasing power generation for scaling up single-chamber air cathode microbial fuel cells. *Bioresource technology* 102(6), pp. 4468-4473.

Clauwaert, P. and Toledo, R. and van der Ha, D. and Crab, R. and Verstraete, W. and Hu, H. and Udert, K. and Rabaey, K. 2008. Combining biocatalyzed electrolysis with anaerobic digestion. *Water Science and Technology* 57(4), pp. 575-579.

Cooper, J. and Lombardi, R. and Boardman, D. and Carliell-Marquet, C. 2011. The future distribution and production of global phosphate rock reserves. *Resources, Conservation and Recycling* 57, pp. 78-86.

Cord-Ruwisch, R. and Law, Y. and Cheng, K. Y. 2011. Ammonium as a sustainable proton shuttle in bioelectrochemical systems. *Bioresource technology* 102(20), pp. 9691-9696.

Cusick, R. D. and Logan, B. E. 2012. Phosphate recovery as struvite within a single chamber microbial electrolysis cell. *Bioresource technology* 107, pp. 110-115.

Cusick, R. D. and Ullery, M. L. and Dempsey, B. A. and Logan, B. E. 2014. Electrochemical struvite precipitation from digestate with a fluidized bed cathode microbial electrolysis cell. *water research* 54, pp. 297-306.

Das, S. and Mangwani, N. 2010. Recent developments in microbial fuel cells: a review. *J. Sci. Ind. Res* 69, pp. 727-731.

De Schamphelaire, L. and Cabezas, A. and Marzorati, M. and Friedrich, M. W. and Boon, N. and Verstraete, W. 2010. Microbial community analysis of anodes from sediment microbial fuel cells powered by rhizodeposits of living rice plants. *Applied and environmental microbiology* 76(6), pp. 2002-2008.

Desmidt, E. and Ghyselbrecht, K. and Zhang, Y. and Pinoy, L. and Van der Bruggen, B. and Verstraete, W. and Rabaey, K. and Meesschaert, B. 2015. Global phosphorus scarcity and full-scale P-recovery techniques: a review. *Critical Reviews in Environmental Science and Technology* 45(4), pp. 336-384.

Díaz, C. and Baena, S. and Fardeau, M.-L. and Patel, B. 2007. Aminiphilus circumscriptus gen. nov., sp. nov., an anaerobic amino-acid-degrading bacterium from an upflow anaerobic sludge reactor. *International journal of systematic and evolutionary microbiology* 57(8), pp. 1914-1918.

Ding, A. and Yang, Y. and Sun, G. and Wu, D. 2016. Impact of applied voltage on methane generation and microbial activities in an anaerobic microbial electrolysis cell (MEC). *Chemical Engineering Journal* 283, pp. 260-265.

Ditzig, J. and Liu, H. and Logan, B. E. 2007. Production of hydrogen from domestic wastewater using a bioelectrochemically assisted microbial reactor (BEAMR). *International Journal of Hydrogen Energy* 32(13), pp. 2296-2304.

DouglasC, M. 2009. Design and analysis of experiments. Douglas C. Montgomery. Wiley, London.

Doyle, J. D. and Parsons, S. A. 2002. Struvite formation, control and recovery. *Water research* 36(16), pp. 3925-3940.

Durrant, A. and Scrimshaw, M. and Stratful, I. and Lester, J. 1999. Review of the feasibility of recovering phosphate from wastewater for use as a raw material by the phosphate industry. *Environmental Technology* 20(7), pp. 749-758.

Eeckhaut, V. and Van Immerseel, F. and Teirlynck, E. and Pasmans, F. and Fievez, V. and Snauwaert, C. and Haesebrouck, F. and Ducatelle, R. and Louis, P. and Vandamme, P. 2008. Butyricicoccus pullicaecorum gen. nov., sp. nov., an anaerobic, butyrate-producing bacterium isolated from the caecal content of a broiler chicken. *International journal of systematic and evolutionary microbiology* 58(12), pp. 2799-2802.

El-Chakhtoura, J. and El-Fadel, M. and Rao, H. A. and Li, D. and Ghanimeh, S. and Saikaly, P. E. 2014. Electricity generation and microbial community structure of air-cathode microbial fuel cells powered with the organic fraction of municipal solid waste and inoculated with different seeds. *Biomass and bioenergy* 67, pp. 24-31.

Escapa, A. and Lobato, A. and García, D. and Morán, A. 2013. Hydrogen production and COD elimination rate in a continuous microbial electrolysis cell: the influence of hydraulic retention time and applied voltage. *Environmental Progress & Sustainable Energy* 32(2), pp. 263-268.

Fang, F. and Zang, G.-L. and Sun, M. and Yu, H.-Q. 2013. Optimizing multi-variables of microbial fuel cell for electricity generation with an integrated modeling and experimental approach. *Applied Energy* 110, pp. 98-103.

Fattah, K. P. and Mavinic, D. S. and Koch, F. A. and Jacob, C. 2008. Determining the feasibility of phosphorus recovery as struvite from filter press centrate in a secondary wastewater treatment plant. *Journal of Environmental Science and Health, Part A* 43(7), pp. 756-764.

Fischer, F. and Bastian, C. and Happe, M. and Mabillard, E. and Schmidt, N. 2011. Microbial fuel cell enables phosphate recovery from digested sewage sludge as struvite. *Bioresource Technology* 102(10), pp. 5824-5830.

Forrestal, C. and Huang, Z. and Ren, Z. J. 2014. Percarbonate as a naturally buffering catholyte for microbial fuel cells. *Bioresource technology* 172, pp. 429-432.

Freguia, S. and Rabaey, K. and Yuan, Z. and Keller, J. 2008. Sequential anode–cathode configuration improves cathodic oxygen reduction and effluent quality of microbial fuel cells. *Water Research* 42(6), pp. 1387-1396.

Ganesan, A. and Chaussonnerie, S. and Tarrade, A. and Dauga, C. and Bouchez, T. and Pelletier, E. and Le Paslier, D. and Sghir, A. 2008. Cloacibacillus evryensis gen. nov., sp. nov., a novel asaccharolytic, mesophilic, amino-acid-degrading bacterium within the phylum 'Synergistetes', isolated from an anaerobic sludge digester. *International journal of systematic and evolutionary microbiology* 58(9), pp. 2003-2012.

Gao, P. and Xu, W. and Sontag, P. and Li, X. and Xue, G. and Liu, T. and Sun, W. 2016. Correlating microbial community compositions with environmental factors in activated sludge from four full-scale municipal wastewater treatment plants in Shanghai, China. *Applied microbiology and biotechnology* 100(10), pp. 4663-4673.

Gil-Carrera, L. and Mehta, P. and Escapa, A. and Morán, A. and García, V. and Guiot, S. and Tartakovsky, B. 2011. Optimizing the electrode size and arrangement in a microbial electrolysis cell. *Bioresource technology* 102(20), pp. 9593-9598.

Gil, G.-C. and Chang, I.-S. and Kim, B. H. and Kim, M. and Jang, J.-K. and Park, H. S. and Kim, H. J. 2003. Operational parameters affecting the performannce of a mediator-less microbial fuel cell. *Biosensors and Bioelectronics* 18(4), pp. 327-334.

Gorby, Y. A. and Yanina, S. and McLean, J. S. and Rosso, K. M. and Moyles, D. and Dohnalkova, A. and Beveridge, T. J. and Chang, I. S. and Kim, B. H. and Kim, K. S. 2006. Electrically conductive bacterial nanowires produced by Shewanella oneidensis strain MR-1 and other microorganisms. *Proceedings of the National Academy of Sciences* 103(30), pp. 11358-11363.

Gude, V. G. 2016. Wastewater treatment in microbial fuel cells–an overview. *Journal of Cleaner Production* 122, pp. 287-307.

Güney, K. and Weidelener, A. and Krampe, J. 2008. Phosphorus recovery from digested sewage sludge as MAP by the help of metal ion separation. *Water research* 42(18), pp. 4692-4698.

Hallenbeck, P. C. and Benemann, J. R. 2002. Biological hydrogen production; fundamentals and limiting processes. *International Journal of Hydrogen Energy* 27(11), pp. 1185-1193.

Hamzeh, Y. and Ashori, A. and Mirzaei, B. and Abdulkhani, A. and Molaei, M. 2011. Current and potential capabilities of biomass for green energy in Iran. *Renewable and Sustainable Energy Reviews* 15(9), pp. 4934-4938.

Hao, X.-D. and Wang, C.-C. and Lan, L. and Van Loosdrecht, M. 2008. Struvite formation, analytical methods and effects of pH and Ca2+. *Water Science and Technology* 58(8), pp. 1687-1692.

Happe, M. and Sugnaux, M. and Cachelin, C. P. and Stauffer, M. and Zufferey, G. and Kahoun, T. and Salamin, P.-A. and Egli, T. and Comninellis, C. and Grogg, A.-F. 2016. Scale-up of phosphate remobilization from sewage sludge in a microbial fuel cell. *Bioresource technology* 200, pp. 435-443.

Harnisch, F. and Schröder, U. and Scholz, F. 2008. The suitability of monopolar and bipolar ion exchange membranes as separators for biological fuel cells. *Environmental science & technology* 42(5), pp. 1740-1746.

He, Z. and Huang, Y. and Manohar, A. K. and Mansfeld, F. 2008. Effect of electrolyte pH on the rate of the anodic and cathodic reactions in an air-cathode microbial fuel cell. *Bioelectrochemistry* 74(1), pp. 78-82.

He, Z. and Minteer, S. D. and Angenent, L. T. 2005. Electricity generation from artificial wastewater using an upflow microbial fuel cell. *Environmental science & technology* 39(14), pp. 5262-5267.

Heidrich, E. and Curtis, T. and Dolfing, J. 2010. Determination of the internal chemical energy of wastewater. *Environmental Science & Technology* 45(2), pp. 827-832.

Heidrich, E. S. and Edwards, S. R. and Dolfing, J. and Cotterill, S. E. and Curtis, T. P. 2014. Performance of a pilot scale microbial electrolysis cell fed on domestic wastewater at ambient temperatures for a 12month period. *Bioresource technology* 173, pp. 87-95.

Hirooka, K. and Ichihashi, O. 2013. Phosphorus recovery from artificial wastewater by microbial fuel cell and its effect on power generation. *Bioresource technology* 137, pp. 368-375.

Ho, P. I. and Kumar, G. G. and Kim, A. and Kim, P. and Nahm, K. S. 2011. Microbial electricity generation of diversified carbonaceous electrodes under variable mediators. *Bioelectrochemistry* 80(2), pp. 99-104.

Holmes, D. E. and Bond, D. R. and Lovley, D. R. 2004. Electron transfer by Desulfobulbus propionicus to Fe (III) and graphite electrodes. *Applied and Environmental Microbiology* 70(2), pp. 1234-1237.

Höök, M. and Li, J. and Johansson, K. and Snowden, S. 2012. Growth rates of global energy systems and future outlooks. *Natural Resources Research* 21(1), pp. 23-41.

Hosseinpour, M. and Vossoughi, M. and Alemzadeh, I. 2014. An efficient approach to cathode operational parameters optimization for microbial fuel cell using response surface methodology. *Journal of Environmental Health Science and Engineering* 12(1), p. 1.

Hu, D. and Zhou, Z. and Niu, T. and Wei, H. and Dou, W. and Jiang, L.-M. and Lv, Y. 2017. Co-treatment of reject water from sludge dewatering and supernatant from sludge lime stabilization process for nutrient removal: A cost-effective approach. *Separation and Purification Technology* 172, pp. 357-365.

Hu, H. and Fan, Y. and Liu, H. 2008. Hydrogen production using single-chamber membrane-free microbial electrolysis cells. *Water research* 42(15), pp. 4172-4178.

Huang, L. and Regan, J. M. and Quan, X. 2011. Electron transfer mechanisms, new applications, and performance of biocathode microbial fuel cells. *Bioresource Technology* 102(1), pp. 316-323.

Hussain, A. and Manuel, M. and Tartakovsky, B. 2016. A comparison of simultaneous organic carbon and nitrogen removal in microbial fuel cells and microbial electrolysis cells. *Journal of environmental management* 173, pp. 23-33.

Hutnik, N. and Piotrowski, K. and Wierzbowska, B. and Matynia, A. 2011. Continuous reaction crystallization of struvite from phosphate (V) solutions containing calcium ions. *Crystal Research and Technology* 46(5), pp. 443-449.

Ichihashi, O. and Hirooka, K. 2012. Removal and recovery of phosphorus as struvite from swine wastewater using microbial fuel cell. *Bioresource technology* 114, pp. 303-307.

IEA. 2007. Hydrogen Production & Distribution

IEA. 2016. *Key world energy statistics* [Online]. International Energy Agency Available at: https://www.iea.org/publications/freepublications/publication/KeyWorld2016.pdf [Accessed.

Ishii, S. i. and Suzuki, S. and Norden-Krichmar, T. M. and Wu, A. and Yamanaka, Y. and Nealson, K. H. and Bretschger, O. 2013. Identifying the microbial communities and operational conditions for optimized wastewater treatment in microbial fuel cells. *Water research* 47(19), pp. 7120-7130.

Ishii, S. i. and Watanabe, K. and Yabuki, S. and Logan, B. E. and Sekiguchi, Y. 2008. Comparison of electrode reduction activities of Geobacter sulfurreducens and an enriched consortium in an air-cathode microbial fuel cell. *Applied and environmental microbiology* 74(23), pp. 7348-7355.

Ivakin, Y. D. and Danchevskaya, M. and Muravieva, G. 2015. Induced formation of corundum crystals in supercritical water fluid. *Russian Journal of Physical Chemistry B* 9(7), pp. 1082-1094.

Jadhav, G. and Ghangrekar, M. 2009. Performance of microbial fuel cell subjected to variation in pH, temperature, external load and substrate concentration. *Bioresource Technology* 100(2), pp. 717-723.

Jaffer, Y. and Clark, T. and Pearce, P. and Parsons, S. 2002. Potential phosphorus recovery by struvite formation. *Water Research* 36(7), pp. 1834-1842.

Jia, J. and Tang, Y. and Liu, B. and Wu, D. and Ren, N. and Xing, D. 2013. Electricity generation from food wastes and microbial community structure in microbial fuel cells. *Bioresource technology* 144, pp. 94-99.

Jiang, H. and Luo, S. and Shi, X. and Dai, M. and Guo, R.-b. 2012. A novel microbial fuel cell and photobioreactor system for continuous domestic wastewater treatment and bioelectricity generation. *Biotechnology letters* 34(7), pp. 1269-1274.

Jiang, Y.-B. and Zhong, W.-H. and Han, C. and Deng, H. 2016. Characterization of Electricity Generated by Soil in Microbial Fuel Cells and the Isolation of Soil Source Exoelectrogenic Bacteria. *Frontiers in Microbiology* 7.

JingRui, Z. and Gefu, Z. and Xiaofang, P. and Ajay Kumar, J. and Lin, L. and Xu, H. and Chaoxiang, L. 2016. Effects of hydraulic retention time and influent alkalinity on the performance of bio-electrochemical system assisted anaerobic baffled reactor. *Desalination and Water Treatment* 57(53), pp. 25399-25410.

Juang, D.-F. and Yang, P.-C. and Chou, H.-Y. and Chiu, L.-J. 2011. Effects of microbial species, organic loading and substrate degradation rate on the power generation capability of microbial fuel cells. *Biotechnology letters* 33(11), pp. 2147-2160.

Juang, D. and Yang, P. and Kuo, T. 2012. Effects of flow rate and chemical oxygen demand removal characteristics on power generation performance of microbial fuel cells. *International Journal of Environmental Science and Technology* 9(2), pp. 267-280.

Jung, S. and Regan, J. M. 2007. Comparison of anode bacterial communities and performance in microbial fuel cells with different electron donors. *Applied microbiology and biotechnology* 77(2), pp. 393-402.

Kabdaşlı, I. and Tünay, O. and İşlek, Ç. and Erdinc, E. and Hüskalar, S. and Tatlı, M. 2006. Nitrogen recovery by urea hydrolysis and struvite precipitation from anthropogenic urine. *Water Science and Technology* 53(12), pp. 305-312.

Kadier, A. and Simayi, Y. and Abdeshahian, P. and Azman, N. F. and Chandrasekhar, K. and Kalil, M. S. 2016. A comprehensive review of microbial electrolysis cells (MEC) reactor designs and configurations for sustainable hydrogen gas production. *Alexandria Engineering Journal* 55(1), pp. 427-443.

Kalathil, S. and Lee, J. and Cho, M. H. 2011. Granular activated carbon based microbial fuel cell for simultaneous decolorization of real dye wastewater and electricity generation. *New biotechnology* 29(1), pp. 32-37.

Kan, J. and Hsu, L. and Cheung, A. C. and Pirbazari, M. and Nealson, K. H. 2010. Current production by bacterial communities in microbial fuel cells enriched from wastewater sludge with different electron donors. *Environmental science & technology* 45(3), pp. 1139-1146.

Kang, C. S. and Eaktasang, N. and Kwon, D.-Y. and Kim, H. S. 2014. Enhanced current production by Desulfovibrio desulfuricans biofilm in a mediator-less microbial fuel cell. *Bioresource technology* 165, pp. 27-30.

Karube, I. and Matsunaga, T. and Tsuru, S. and Suzuki, S. 1977. Biochemical fuel cell utilizing immobilized cells of Clostridium butyricum. *Biotechnology and Bioengineering* 19(11), pp. 1727-1733.

Katuri, K. P. and Scott, K. and Head, I. M. and Picioreanu, C. and Curtis, T. P. 2011. Microbial fuel cells meet with external resistance. *Bioresource technology* 102(3), pp. 2758-2766.

Kelly, P. T. and He, Z. 2014. Nutrients removal and recovery in bioelectrochemical systems: a review. *Bioresource technology* 153, pp. 351-360.

Khan, M. and Nizami, A. and Rehan, M. and Ouda, O. and Sultana, S. and Ismail, I. and Shahzad, K. 2017. Microbial electrolysis cells for hydrogen production and urban wastewater treatment: A case study of Saudi Arabia. *Applied Energy* 185, pp. 410-420.

Kiely, P. D. and Call, D. F. and Yates, M. D. and Regan, J. M. and Logan, B. E. 2010. Anodic biofilms in microbial fuel cells harbor low numbers of higher-power-producing bacteria than abundant genera. *Applied microbiology and biotechnology* 88(1), pp. 371-380.

Kiely, P. D. and Cusick, R. and Call, D. F. and Selembo, P. A. and Regan, J. M. and Logan, B. E. 2011. Anode microbial communities produced by changing from microbial fuel cell to microbial electrolysis cell operation using two different wastewaters. *Bioresource technology* 102(1), pp. 388-394.

Kim, G. and Webster, G. and Wimpenny, J. and Kim, B. and Kim, H. and Weightman, A. 2006. Bacterial community structure, compartmentalization and activity in a microbial fuel cell. *Journal of applied microbiology* 101(3), pp. 698-710.

Kim, J. R. 2006. *Development of Microbial Fuel Cells (MFCs) using Efficient Acclimation and Various Substrates.* ProQuest.

Kim, J. R. and Dec, J. and Bruns, M. A. and Logan, B. E. 2008. Removal of odors from swine wastewater by using microbial fuel cells. *Applied and environmental microbiology* 74(8), pp. 2540-2543.

Kim, J. R. and Jung, S. H. and Regan, J. M. and Logan, B. E. 2007. Electricity generation and microbial community analysis of alcohol powered microbial fuel cells. *Bioresource technology* 98(13), pp. 2568-2577.

Kim, K.-Y. and Yang, W. and Evans, P. J. and Logan, B. E. 2016. Continuous treatment of high strength wastewaters using air-cathode microbial fuel cells. *Bioresource Technology* 221, pp. 96-101.

Kim, M.-S. and Lee, Y.-j. 2010. Optimization of culture conditions and electricity generation using Geobacter sulfurreducens in a dual-chambered microbial fuel-cell. *International Journal of Hydrogen Energy* 35(23), pp. 13028-13034.

Kim, S.-C. 2016. Application of response surface method as an experimental design to optimize coagulation–flocculation process for pre-treating paper wastewater. *Journal of Industrial and Engineering Chemistry* 38, pp. 93-102.

Kim, Y. and Logan, B. E. 2013. Simultaneous removal of organic matter and salt ions from saline wastewater in bioelectrochemical systems. *Desalination* 308, pp. 115-121.

Kozich, J. J. and Westcott, S. L. and Baxter, N. T. and Highlander, S. K. and Schloss, P. D. 2013. Development of a dual-index sequencing strategy and curation pipeline for analyzing amplicon sequence data on the MiSeq Illumina sequencing platform. *Applied and environmental microbiology* 79(17), pp. 5112-5120.

Kozik, A. and Hutnik, N. and Gluzińska, J. and Piotrowski, K. 2011. Recovery of phosphate (V) ions from liquid waste solutions containing organic impurities. *CHEMIK nauka-technika-rynek* 1(65), pp. 675-686.

Kozik, A. and Hutnik, N. and Piotrowski, K. and Mazienczuk, A. and Matynia, A. 2013. Precipitation and Crystallization of Struvite from Synthetic Wastewater under Stoichiometric Conditions. *Advances in Chemical Engineering and Science* 3(04), p. 20.

Kyazze, G. and Popov, A. and Dinsdale, R. and Esteves, S. and Hawkes, F. and Premier, G. and Guwy, A. 2010. Influence of catholyte pH and temperature on hydrogen production from acetate using a two chamber concentric tubular microbial electrolysis cell. *international journal of hydrogen energy* 35(15), pp. 7716-7722.

Lay, C.-H. and Wu, J.-H. and Hsiao, C.-L. and Chang, J.-J. and Chen, C.-C. and Lin, C.-Y. 2010. Biohydrogen production from soluble condensed molasses fermentation using anaerobic fermentation. *International journal of hydrogen energy* 35(24), pp. 13445-13451.

Le Corre, K. S. and Valsami-Jones, E. and Hobbs, P. and Parsons, S. A. 2005. Impact of calcium on struvite crystal size, shape and purity. *Journal of Crystal Growth* 283(3), pp. 514-522.

Le Corre, K. S. and Valsami-Jones, E. and Hobbs, P. and Parsons, S. A. 2007. Impact of reactor operation on success of struvite precipitation from synthetic liquors. *Environmental technology* 28(11), pp. 1245-1256.

Le Corre, K. S. and Valsami-Jones, E. and Hobbs, P. and Parsons, S. A. 2009. Phosphorus recovery from wastewater by struvite crystallization: A review. *Critical Reviews in Environmental Science and Technology* 39(6), pp. 433-477.

Lee, D.-J. and Liu, X. and Weng, H.-L. 2014. Sulfate and organic carbon removal by microbial fuel cell with sulfate-reducing bacteria and sulfide-oxidising bacteria anodic biofilm. *Bioresource technology* 156, pp. 14-19.

Lee, J. and Rahman, M. and Ra, C. 2009. Dose effects of Mg and PO 4 sources on the composting of swine manure. *Journal of hazardous materials* 169(1), pp. 801-807.

Lee, Y.-Y. and Kim, T. G. and Cho, K.-S. 2016. Characterization of the COD removal, electricity generation, and bacterial communities in microbial fuel cells treating molasses wastewater. *Journal of Environmental Science and Health, Part A* 51(13), pp. 1131-1138.

Leong, J. X. and Daud, W. R. W. and Ghasemi, M. and Liew, K. B. and Ismail, M. 2013. Ion exchange membranes as separators in microbial fuel cells for bioenergy conversion: a comprehensive review. *Renewable and Sustainable Energy Reviews* 28, pp. 575-587.

Lesnik, K. L. and Liu, H. 2014. Establishing a core microbiome in acetate-fed microbial fuel cells. *Applied microbiology and biotechnology* 98(9), pp. 4187-4196.

Li, X. and Hu, B. and Suib, S. and Lei, Y. and Li, B. 2011. Electricity generation in continuous flow microbial fuel cells (MFCs) with manganese dioxide (MnO 2) cathodes. *Biochemical Engineering Journal* 54(1), pp. 10-15.

Liu, B. and Zhang, F. and Feng, X. and Liu, Y. and Yan, X. and Zhang, X. and Wang, L. and Zhao, L. 2006. Thauera and Azoarcus as functionally important genera in a denitrifying quinoline-removal bioreactor as revealed by microbial community structure comparison. *FEMS microbiology ecology* 55(2), pp. 274-286.

Liu, H. and Cheng, S. and Logan, B. E. 2005a. Power generation in fed-batch microbial fuel cells as a function of ionic strength, temperature, and reactor configuration. *Environmental science & technology* 39(14), pp. 5488-5493.

Liu, H. and Grot, S. and Logan, B. E. 2005b. Electrochemically assisted microbial production of hydrogen from acetate. *Environmental science & technology* 39(11), pp. 4317-4320.

Liu, T. and Yu, Y.-y. and Li, D. and Song, H. and Yan, X. and Chen, W. N. 2016. The effect of external resistance on biofilm formation and internal resistance in Shewanella inoculated microbial fuel cells. *RSC Advances* 6(24), pp. 20317-20323.

Liu, W. and Wang, A. and Sun, D. and Ren, N. and Zhang, Y. and Zhou, J. 2012. Characterization of microbial communities during anode biofilm reformation in a two-chambered microbial electrolysis cell (MEC). *Journal of biotechnology* 157(4), pp. 628-632.

Liu, Y. and Climent, V. and Berna, A. and Feliu, J. M. 2011. Effect of temperature on the catalytic ability of electrochemically active biofilm as anode catalyst in microbial fuel cells. *Electroanalysis* 23(2), pp. 387-394.

Logan, B. 2011. How to Innoculate your Cube MFC.

Logan, B. E. 2009. Exoelectrogenic bacteria that power microbial fuel cells. *Nature Reviews Microbiology* 7(5), pp. 375-381.

Logan, B. E. and Call, D. and Cheng, S. and Hamelers, H. V. and Sleutels, T. H. and Jeremiasse, A. W. and Rozendal, R. A. 2008. Microbial electrolysis cells for high yield hydrogen gas production from organic matter. *Environmental Science & Technology* 42(23), pp. 8630-8640.

Logan, B. E. and Hamelers, B. and Rozendal, R. and Schröder, U. and Keller, J. and Freguia, S. and Aelterman, P. and Verstraete, W. and Rabaey, K. 2006. Microbial fuel cells: methodology and technology. *Environmental science & technology* 40(17), pp. 5181-5192.

Logan, B. E. and Regan, J. M. 2006. Electricity-producing bacterial communities in microbial fuel cells. *TRENDS in Microbiology* 14(12), pp. 512-518.

Logan, B. E. and Wallack, M. J. and Kim, K.-Y. and He, W. and Feng, Y. and Saikaly, P. E. 2015. Assessment of microbial fuel cell configurations and power densities. *Environmental Science & Technology Letters* 2(8), pp. 206-214.

Longo, S. and d'Antoni, B. M. and Bongards, M. and Chaparro, A. and Cronrath, A. and Fatone, F. and Lema, J. M. and Mauricio-Iglesias, M. and Soares, A. and Hospido, A. 2016. Monitoring and diagnosis of energy consumption in wastewater treatment plants. A state of the art and proposals for improvement. *Applied Energy* 179, pp. 1251-1268.

Lovley, D. R. 2006. Bug juice: harvesting electricity with microorganisms. *Nature Reviews Microbiology* 4(7), pp. 497-508.

Lu, L. and Xing, D. and Ren, N. 2012. Pyrosequencing reveals highly diverse microbial communities in microbial electrolysis cells involved in enhanced H 2 production from waste activated sludge. *Water research* 46(7), pp. 2425-2434.

Luo, H. and Jenkins, P. E. and Ren, Z. 2010. Concurrent desalination and hydrogen generation using microbial electrolysis and desalination cells. *Environmental science & technology* 45(1), pp. 340-344.

Luo, H. and Liu, G. and Zhang, R. and Bai, Y. and Fu, S. and Hou, Y. 2014. Heavy metal recovery combined with H 2 production from artificial acid mine drainage using the microbial electrolysis cell. *Journal of hazardous materials* 270, pp. 153-159.

Luo, Q. and Wang, H. and Zhang, X. and Qian, Y. 2005. Effect of direct electric current on the cell surface properties of phenol-degrading bacteria. *Applied and environmental microbiology* 71(1), pp. 423-427.

Luo, S. and Sun, H. and Ping, Q. and Jin, R. and He, Z. 2016. A Review of Modeling Bioelectrochemical Systems: Engineering and Statistical Aspects. *Energies* 9(2), p. 111.

Madani, S. and Gheshlaghi, R. and Mahdavi, M. A. and Sobhani, M. and Elkamel, A. 2015. Optimization of the performance of a double-chamber microbial fuel cell through factorial design of experiments and response surface methodology. *Fuel* 150, pp. 434-440.

Malvankar, N. S. and Lau, J. and Nevin, K. P. and Franks, A. E. and Tuominen, M. T. and Lovley, D. R. 2012. Electrical conductivity in a mixed-species biofilm. *Applied and environmental microbiology* 78(16), pp. 5967-5971.

Martin, E. and Savadogo, O. and Guiot, S. and Tartakovsky, B. 2010. The influence of operational conditions on the performance of a microbial fuel cell seeded with mesophilic anaerobic sludge. *Biochemical Engineering Journal* 51(3), pp. 132-139.

Mashkour, M. and Rahimnejad, M. 2015. Effect of various carbon-based cathode electrodes on the performance of microbial fuel cell. *Biofuel Research Journal* 2(4), pp. 296-300.

Meng, F. and Wang, Y. and Huang, L. N. and Li, J. and Jiang, F. and Li, S. and Chen, G. H. 2013. A novel nonwoven hybrid bioreactor (NWHBR) for enhancing simultaneous nitrification and denitrification. *Biotechnology and bioengineering* 110(7), pp. 1903-1912.

Merino-Jimenez, I. and Celorrio, V. and Fermin, D. J. and Greenman, J. and Ieropoulos, I. 2017. Enhanced MFC power production and struvite recovery by the addition of sea salts to urine. *Water Research* 109, pp. 46-53.

Miles, R. 2009. United nations department of economic and social affairs.

Min, B. and Román, Ó. B. and Angelidaki, I. 2008. Importance of temperature and anodic medium composition on microbial fuel cell (MFC) performance. *Biotechnology letters* 30(7), pp. 1213-1218.

Miran, W. and Nawaz, M. and Kadam, A. and Shin, S. and Heo, J. and Jang, J. and Lee, D. S. 2015. Microbial community structure in a dual chamber microbial fuel cell fed with brewery waste for azo dye degradation and electricity generation. *Environmental Science and Pollution Research* 22(17), pp. 13477-13485.

Mohammed, Y. and Mustafa, M. and Bashir, N. and Ogundola, M. and Umar, U. 2014. Sustainable potential of bioenergy resources for distributed power generation development in Nigeria. *Renewable and Sustainable Energy Reviews* 34, pp. 361-370.

Molognoni, D. and Puig, S. and Balaguer, M. D. and Liberale, A. and Capodaglio, A. G. and Callegari, A. and Colprim, J. 2014. Reducing start-up time and minimizing energy losses of microbial fuel cells using maximum power point tracking strategy. *Journal of Power Sources* 269, pp. 403-411.

Montgomery, D. C. 2001. *Design and analysis of the experimental* New York: john Wiley &sons.

Moon, H. and Chang, I. S. and Kim, B. H. 2006. Continuous electricity production from artificial wastewater using a mediator-less microbial fuel cell. *Bioresource Technology* 97(4), pp. 621-627.

Morales, N. and Boehler, M. A. and Buettner, S. and Liebi, C. and Siegrist, H. 2013. Recovery of N and P from urine by struvite precipitation followed by combined stripping with digester sludge liquid at full scale. *Water* 5(3), pp. 1262-1278.

Moussa, S. B. and Maurin, G. and Gabrielli, C. and Amor, M. B. 2006. Electrochemical precipitation of struvite. *Electrochemical and solid-state letters* 9(6), pp. C97-C101.

Mulchandani, A. and Westerhoff, P. 2016. Recovery opportunities for metals and energy from sewage sludges. *Bioresource technology* 215, pp. 215-226.

Myers, R. H. and Montgomery, D. C. and Anderson-Cook, C. M. 2016. *Response surface methodology: process and product optimization using designed experiments*. John Wiley & Sons.

Najafpour, G. and Rahimnejad, M. and Ghoreshi, A. 2011. The enhancement of a microbial fuel cell for electrical output using mediators and oxidizing agents. *Energy Sources, Part A: Recovery, Utilization, and Environmental Effects* 33(24), pp. 2239-2248.

Nam, J.-Y. and Kim, H.-W. and Lim, K.-H. and Shin, H.-S. 2010. Effects of organic loading rates on the continuous electricity generation from fermented wastewater using a single-chamber microbial fuel cell. *Bioresource technology* 101(1), pp. S33-S37.

Nam, J.-Y. and Logan, B. E. 2012. Optimization of catholyte concentration and anolyte pHs in two chamber microbial electrolysis cells. *international journal of hydrogen energy* 37(24), pp. 18622-18628.

Nelson, N. O. and Mikkelsen, R. L. and Hesterberg, D. L. 2003. Struvite precipitation in anaerobic swine lagoon liquid: effect of pH and Mg: P ratio and determination of rate constant. *Bioresource Technology* 89(3), pp. 229-236.

Neset, T.-S. S. and Bader, H.-P. and Scheidegger, R. and Lohm, U. 2008. The flow of phosphorus in food production and consumption—Linköping, Sweden, 1870–2000. *Science of the Total Environment* 396(2), pp. 111-120.

Newton, G. J. and Mori, S. and Nakamura, R. and Hashimoto, K. and Watanabe, K. 2009. Analyses of current-generating mechanisms of Shewanella loihica PV-4 and Shewanella oneidensis MR-1 in microbial fuel cells. *Applied and environmental microbiology* 75(24), pp. 7674-7681.

Offei, F. and Thygesen, A. and Mensah, M. and Tabbicca, K. and Fernando, D. and Petrushina, I. and Daniel, G. 2016. A viable electrode material for use in microbial fuel cells for tropical regions. *Energies* 9(1), p. 35.

Oh, S. and Kim, J. and Joo, J.-H. and Logan, B. 2009. Effects of applied voltages and dissolved oxygen on sustained power generation by microbial fuel cells. *Water science and technology* 60(5), pp. 1311-1317.

Ohlinger, K. N. and PE and Young, T. M. and Schroeder, E. D. 1999. Kinetics effects on preferential struvite accumulation in wastewater. *Journal of Environmental Engineering* 125(8), pp. 730-737.

Pandit, S. and Ghosh, S. and Ghangrekar, M. and Das, D. 2012. Performance of an anion exchange membrane in association with cathodic parameters in a dual chamber microbial fuel cell. *international journal of hydrogen energy* 37(11), pp. 9383-9392.

Pant, D. and Van Bogaert, G. and Diels, L. and Vanbroekhoven, K. 2010. A review of the substrates used in microbial fuel cells (MFCs) for sustainable energy production. *Bioresource technology* 101(6), pp. 1533-1543.

Park, T.-J. and Ding, W. and Cheng, S. and Brar, M. S. and Ma, A. P. Y. and Tun, H. M. and Leung, F. C. 2014. Microbial community in microbial fuel cell (MFC) medium and effluent enriched with purple photosynthetic bacterium (Rhodopseudomonas sp.). *AMB Express* 4(1), p. 22.

Pastor, L. and Marti, N. and Bouzas, A. and Seco, A. 2008. Sewage sludge management for phosphorus recovery as struvite in EBPR wastewater treatment plants. *Bioresource Technology* 99(11), pp. 4817-4824.

Patil, S. A. and Harnisch, F. and Koch, C. and Hübschmann, T. and Fetzer, I. and Carmona-Martínez, A. A. and Müller, S. and Schröder, U. 2011. Electroactive mixed culture derived biofilms in microbial bioelectrochemical systems: the role of pH on biofilm formation, performance and composition. *Bioresource technology* 102(20), pp. 9683-9690.

Pham, C. A. and Jung, S. J. and Phung, N. T. and Lee, J. and Chang, I. S. and Kim, B. H. and Yi, H. and Chun, J. 2003. A novel electrochemically active and Fe (III)-reducing bacterium phylogenetically related to Aeromonas hydrophila, isolated from a microbial fuel cell. *FEMS Microbiology Letters* 223(1), pp. 129-134.

Pham, T. H. and Aelterman, P. and Verstraete, W. 2009. Bioanode performance in bioelectrochemical systems: recent improvements and prospects. *Trends in Biotechnology* 27(3), pp. 168-178.

Pinto, R. and Srinivasan, B. and Guiot, S. and Tartakovsky, B. 2011. The effect of real-time external resistance optimization on microbial fuel cell performance. *Water research* 45(4), pp. 1571-1578.

Prywer, J. and Torzewska, A. and Płociński, T. 2012. Unique surface and internal structure of struvite crystals formed by Proteus mirabilis. *Urological research* 40(6), pp. 699-707.

Puig, S. and Serra, M. and Coma, M. and Cabré, M. and Balaguer, M. D. and Colprim, J. 2010. Effect of pH on nutrient dynamics and electricity production using microbial fuel cells. *Bioresource technology* 101(24), pp. 9594-9599.

Qin, B. and Luo, H. and Liu, G. and Zhang, R. and Chen, S. and Hou, Y. and Luo, Y. 2012. Nickel ion removal from wastewater using the microbial electrolysis cell. *Bioresource technology* 121, pp. 458-461.

Rabaey, K. and Verstraete, W. 2005. Microbial fuel cells: novel biotechnology for energy generation. *TRENDS in Biotechnology* 23(6), pp. 291-298.

Rahimnejad, M. and Adhami, A. and Darvari, S. and Zirepour, A. and Oh, S.-E. 2015. Microbial fuel cell as new technology for bioelectricity generation: a review. *Alexandria Engineering Journal* 54(3), pp. 745-756.

Rahimnejad, M. and Bakeri, G. and Ghasemi, M. and Zirepour, A. 2014. A review on the role of proton exchange membrane on the performance of microbial fuel cell. *Polymers for Advanced Technologies* 25(12), pp. 1426-1432.

Rahimnejad, M. and Najafpour, G. and Ghoreyshi, A. and Shakeri, M. and Zare, H. 2011. Methylene blue as electron promoters in microbial fuel cell. *international journal of hydrogen energy* 36(20), pp. 13335-13341.

Rahman, M. M. and Liu, Y. and Kwag, J.-H. and Ra, C. 2011. Recovery of struvite from animal wastewater and its nutrient leaching loss in soil. *Journal of hazardous materials* 186(2), pp. 2026-2030.

Rahman, M. M. and Salleh, M. A. M. and Rashid, U. and Ahsan, A. and Hossain, M. M. and Ra, C. S. 2014. Production of slow release crystal fertilizer from wastewaters through struvite crystallization–A review. *Arabian Journal of Chemistry* 7(1), pp. 139-155.

Ramachandran, R. and Chen, S.-M. and Kumar, G. p. G. 2015. Enhancement of different fabricated electrode materials for microbial fuel cell applications: An overview. *International Journal of Electrochemical Science* 10(9), pp. 7111-7137.

Rastegar, S. and Mousavi, S. and Shojaosadati, S. and Sheibani, S. 2011. Optimization of petroleum refinery effluent treatment in a UASB reactor using response surface methodology. *Journal of hazardous materials* 197, pp. 26-32.

Rathmell, A. R. and Wiley, B. J. 2011. The synthesis and coating of long, thin copper nanowires to make flexible, transparent conducting films on plastic substrates. *Advanced Materials* 23(41), pp. 4798-4803.

Reddy, L. V. and Kumar, S. P. and Wee, Y.-J. 2010. Microbial Fuel Cells (MFCs)-a novel source of energy for new millennium. *Current Research Technology and Education Topics in Applied Microbiology and Microbial Biotechnology* 2(13), pp. 956-964.

Rismani-Yazdi, H. and Carver, S. M. and Christy, A. D. and Tuovinen, O. H. 2008. Cathodic limitations in microbial fuel cells: an overview. *Journal of Power Sources* 180(2), pp. 683-694.

Rismani-Yazdi, H. and Carver, S. M. and Christy, A. D. and Yu, Z. and Bibby, K. and Peccia, J. and Tuovinen, O. H. 2013. Suppression of methanogenesis in cellulose-fed microbial fuel cells in relation to performance, metabolite formation, and microbial population. *Bioresource technology* 129, pp. 281-288.

Rismani-Yazdi, H. and Christy, A. D. and Carver, S. M. and Yu, Z. and Dehority, B. A. and Tuovinen, O. H. 2011. Effect of external resistance on bacterial diversity and metabolism in cellulose-fed microbial fuel cells. *Bioresource technology* 102(1), pp. 278-283.

Rivera, I. and Buitrón, G. and Bakonyi, P. and Nemestóthy, N. and Bélafi-Bakó, K. 2015. Hydrogen production in a microbial electrolysis cell fed with a dark fermentation effluent. *Journal of Applied Electrochemistry* 45(11), pp. 1223-1229.

Ronteltap, M. and Maurer, M. and Hausherr, R. and Gujer, W. 2010. Struvite precipitation from urine–influencing factors on particle size. *Water research* 44(6), pp. 2038-2046.

Rozendal, R. A. and Hamelers, H. V. and Buisman, C. J. 2006a. Effects of membrane cation transport on pH and microbial fuel cell performance. *Environmental science & technology* 40(17), pp. 5206-5211.

Rozendal, R. A. and Hamelers, H. V. and Euverink, G. J. and Metz, S. J. and Buisman, C. J. 2006b. Principle and perspectives of hydrogen production through biocatalyzed electrolysis. *International Journal of Hydrogen Energy* 31(12), pp. 1632-1640.

Rozendal, R. A. and Hamelers, H. V. and Molenkamp, R. J. and Buisman, C. J. 2007. Performance of single chamber biocatalyzed electrolysis with different types of ion exchange membranes. *Water Research* 41(9), pp. 1984-1994.

Rozendal, R. A. and Hamelers, H. V. and Rabaey, K. and Keller, J. and Buisman, C. J. 2008. Towards practical implementation of bioelectrochemical wastewater treatment. *Trends in biotechnology* 26(8), pp. 450-459.

Rozendal, R. A. and Leone, E. and Keller, J. and Rabaey, K. 2009. Efficient hydrogen peroxide generation from organic matter in a bioelectrochemical system. *Electrochemistry Communications* 11(9), pp. 1752-1755.

Sack, E. L. and van der Wielen, P. W. and van der Kooij, D. 2011. Flavobacterium johnsoniae as a model organism for characterizing biopolymer utilization in oligotrophic freshwater environments. *Applied and environmental microbiology* 77(19), pp. 6931-6938.

Sánchez-Monedero, M. and Roig, A. and Paredes, C. and Bernal, M. 2001. Nitrogen transformation during organic waste composting by the Rutgers system and its effects on pH, EC and maturity of the composting mixtures. *Bioresource Technology* 78(3), pp. 301-308.

Sayess, R. R. and Saikaly, P. E. and El-Fadel, M. and Li, D. and Semerjian, L. 2013. Reactor performance in terms of COD and nitrogen removal and bacterial community structure of a three-stage rotating bioelectrochemical contactor. *Water research* 47(2), pp. 881-894.

Schaetzle, O. and Barrière, F. and Baronian, K. 2008. Bacteria and yeasts as catalysts in microbial fuel cells: electron transfer from micro-organisms to electrodes for green electricity. *Energy & Environmental Science* 1(6), pp. 607-620.

Schloss, P. D. and Westcott, S. L. and Ryabin, T. and Hall, J. R. and Hartmann, M. and Hollister, E. B. and Lesniewski, R. A. and Oakley, B. B. and Parks, D. H. and Robinson, C. J. 2009. Introducing mothur: open-source, platform-independent, community-supported software for describing and comparing microbial communities. *Applied and environmental microbiology* 75(23), pp. 7537-7541.

Schröder, U. and Nießen, J. and Scholz, F. 2003. A generation of microbial fuel cells with current outputs boosted by more than one order of magnitude. *Angewandte Chemie International Edition* 42(25), pp. 2880-2883.

Sharma, T. and Reddy, A. L. M. and Chandra, T. and Ramaprabhu, S. 2008. Development of carbon nanotubes and nanofluids based microbial fuel cell. *International journal of hydrogen energy* 33(22), pp. 6749-6754.

Shimoyama, T. and Yamazawa, A. and Ueno, Y. and Watanabe, K. 2009. Phylogenetic analyses of bacterial communities developed in a cassette-electrode microbial fuel cell. *Microbes and environments* 24(2), pp. 188-192.

Silva, T. and Verde, L. and Neto, E. S. and Oliveira, V. 2013. Diversity analyses of microbial communities in petroleum samples from Brazilian oil fields. *International Biodeterioration & Biodegradation* 81, pp. 57-70.

Sleutels, T. H. and Darus, L. and Hamelers, H. V. and Buisman, C. J. 2011. Effect of operational parameters on Coulombic efficiency in bioelectrochemical systems. *Bioresource technology* 102(24), pp. 11172-11176.

Sleutels, T. H. and Hamelers, H. V. and Buisman, C. J. 2010. Reduction of pH buffer requirement in bioelectrochemical systems. *Environmental science & technology* 44(21), pp. 8259-8263.

Sleutels, T. H. and Hamelers, H. V. and Rozendal, R. A. and Buisman, C. J. 2009. Ion transport resistance in microbial electrolysis cells with anion and cation exchange membranes. *international journal of hydrogen energy* 34(9), pp. 3612-3620.

Stratful, I. and Scrimshaw, M. and Lester, J. 2001. Conditions influencing the precipitation of magnesium ammonium phosphate. *Water Research* 35(17), pp. 4191-4199.

Sun, H. and Xu, S. and Zhuang, G. and Zhuang, X. 2016. Performance and recent improvement in microbial fuel cells for simultaneous carbon and nitrogen removal: A review. *Journal of Environmental Sciences* 39, pp. 242-248.

Sun, Y. and Wei, J. and Liang, P. and Huang, X. 2012. Microbial community analysis in biocathode microbial fuel cells packed with different materials. *AMB express* 2(1), p. 1.

Tao, Q. and Luo, J. and Zhou, J. and Zhou, S. and Liu, G. and Zhang, R. 2014. Effect of dissolved oxygen on nitrogen and phosphorus removal and electricity production in microbial fuel cell. *Bioresource technology* 164, pp. 402-407.

Thormann, K. M. and Saville, R. M. and Shukla, S. and Pelletier, D. A. and Spormann, A. M. 2004. Initial phases of biofilm formation in Shewanella oneidensis MR-1. *Journal of bacteriology* 186(23), pp. 8096-8104.

Thorndahl, U. 1993. Nitrogen removal from returned liquors. *Water and Environment Journal* 7(5), pp. 492-496.

Torres, C. I. and Kato Marcus, A. and Rittmann, B. E. 2008. Proton transport inside the biofilm limits electrical current generation by anode-respiring bacteria. *Biotechnology and Bioengineering* 100(5), pp. 872-881.

Valle, A. and Zanardini, E. and Abbruscato, P. and Argenzio, P. and Lustrato, G. and Ranalli, G. and Sorlini, C. 2007. Effects of low electric current (LEC) treatment on pure bacterial cultures. *Journal of applied microbiology* 103(5), pp. 1376-1385.

Velasquez-Orta, S. and Head, I. and Curtis, T. and Scott, K. 2011. Factors affecting current production in microbial fuel cells using different industrial wastewaters. *Bioresource technology* 102(8), pp. 5105-5112.

Venkata Mohan, S. and Velvizhi, G. and Annie Modestra, J. and Srikanth, S. 2014. Microbial fuel cell: Critical factors regulating bio-catalyzed electrochemical process and recent advancements. *Renewable and Sustainable Energy Reviews* 40(C), pp. 779-797.

Wang, C.-C. and Hao, X.-D. and Guo, G.-S. and Van Loosdrecht, M. 2010. Formation of pure struvite at neutral pH by electrochemical deposition. *Chemical Engineering Journal* 159(1), pp. 280-283.

Wang, H. and Heil, D. and Ren, Z. J. and Xu, P. 2015. Removal and fate of trace organic compounds in microbial fuel cells. *Chemosphere* 125, pp. 94-101.

Wang, J. and Burken, J. G. and Zhang, X. and Surampalli, R. 2005. Engineered struvite precipitation: Impacts of component-ion molar ratios and pH. *Journal of Environmental Engineering* 131(10), pp. 1433-1440.

Wang, J. and Song, X. and Wang, Y. and Abayneh, B. and Ding, Y. and Yan, D. and Bai, J. 2016a. Microbial community structure of different electrode materials in constructed wetland incorporating microbial fuel cell. *Bioresource technology* 221, pp. 697-702.

Wang, X. and Cheng, S. and Feng, Y. and Merrill, M. D. and Saito, T. and Logan, B. E. 2009. Use of carbon mesh anodes and the effect of different pretreatment methods on power production in microbial fuel cells. *Environmental science & technology* 43(17), pp. 6870-6874.

Wang, X. and Li, J. and Wang, Z. and Tursun, H. and Liu, R. and Gao, Y. and Li, Y. 2016b. Increasing the recovery of heavy metal ions using two microbial fuel cells operating in parallel with no power output. *Environmental Science and Pollution Research* 23(20), pp. 20368-20377.

Wei, L. and Han, H. and Shen, J. 2013. Effects of temperature and ferrous sulfate concentrations on the performance of microbial fuel cell. *International Journal of Hydrogen Energy* 38(25), pp. 11110-11116.

Wrana, N. and Sparling, R. and Cicek, N. and Levin, D. B. 2010. Hydrogen gas production in a microbial electrolysis cell by electrohydrogenesis. *Journal of Cleaner Production* 18, pp. S105-S111.

Wrighton, K. C. and Agbo, P. and Warnecke, F. and Weber, K. A. and Brodie, E. L. and DeSantis, T. Z. and Hugenholtz, P. and Andersen, G. L. and Coates, J. D. 2008. A novel ecological role of the Firmicutes identified in thermophilic microbial fuel cells. *The ISME journal* 2(11), pp. 1146-1156.

Wu, X. and Modin, O. 2013. Ammonium recovery from reject water combined with hydrogen production in a bioelectrochemical reactor. *Bioresource technology* 146, pp. 530-536.

Xia, A. and Cheng, J. and Song, W. and Su, H. and Ding, L. and Lin, R. and Lu, H. and Liu, J. and Zhou, J. and Cen, K. 2015. Fermentative hydrogen production using algal biomass as feedstock. *Renewable and Sustainable Energy Reviews* 51, pp. 209-230.

Xu, J. and Sheng, G.-P. and Luo, H.-W. and Li, W.-W. and Wang, L.-F. and Yu, H.-Q. 2012. Fouling of proton exchange membrane (PEM) deteriorates the performance of microbial fuel cell. *water research* 46(6), pp. 1817-1824.

Yahya, A. M. and Hussain, M. A. and Wahab, A. and Khairi, A. 2015. Modeling, optimization, and control of microbial electrolysis cells in a fed-batch reactor for production of renewable biohydrogen gas. *International Journal of Energy Research* 39(4), pp. 557-572.

Yanuka-Golub, K. and Reshef, L. and Rishpon, J. and Gophna, U. 2016. Community structure dynamics during startup in microbial fuel cells—The effect of phosphate concentrations. *Bioresource technology* 212, pp. 151-159.

Yates, M. D. and Kiely, P. D. and Call, D. F. and Rismani-Yazdi, H. and Bibby, K. and Peccia, J. and Regan, J. M. and Logan, B. E. 2012. Convergent development of anodic bacterial communities in microbial fuel cells. *The ISME journal* 6(11), pp. 2002-2013.

Ye, Y. and Wang, L. and Chen, Y. and Zhu, S. and Shen, S. 2010a. High yield hydrogen production in a single-chamber membrane-less microbial electrolysis cell. *Water Science and Technology* 61(3), pp. 721-727.

Ye, Z.-L. and Chen, S.-H. and Wang, S.-M. and Lin, L.-F. and Yan, Y.-J. and Zhang, Z.-J. and Chen, J.-S. 2010b. Phosphorus recovery from synthetic swine wastewater by chemical precipitation using response surface methodology. *Journal of Hazardous Materials* 176(1), pp. 1083-1088.

Yetilmezsoy, K. and Sapci-Zengin, Z. 2009. Recovery of ammonium nitrogen from the effluent of UASB treating poultry manure wastewater by MAP precipitation as a slow release fertilizer. *Journal of Hazardous Materials* 166(1), pp. 260-269.

Yossan, S. and Xiao, L. and Prasertsan, P. and He, Z. 2013. Hydrogen production in microbial electrolysis cells: choice of catholyte. *international journal of hydrogen energy* 38(23), pp. 9619-9624.

You, J. and Greenman, J. and Melhuish, C. and Ieropoulos, I. 2015. Electricity generation and struvite recovery from human urine using microbial fuel cells. *Journal of Chemical Technology and Biotechnology*.

Yu, J. and Seon, J. and Park, Y. and Cho, S. and Lee, T. 2012. Electricity generation and microbial community in a submerged-exchangeable microbial fuel cell system for low-strength domestic wastewater treatment. *Bioresource technology* 117, pp. 172-179.

Zeng, K. and Zhang, D. 2010. Recent progress in alkaline water electrolysis for hydrogen production and applications. *Progress in Energy and Combustion Science* 36(3), pp. 307-326.

Zeng, X. and Borole, A. P. and Pavlostathis, S. G. 2015. Biotransformation of furanic and phenolic compounds with hydrogen gas production in a microbial electrolysis cell. *Environmental science & technology* 49(22), pp. 13667-13675.

Zhang, F. and Ahn, Y. and Logan, B. E. 2014. Treating refinery wastewaters in microbial fuel cells using separator electrode assembly or spaced electrode configurations. *Bioresource technology* 152, pp. 46-52.

Zhang, F. and He, Z. 2012. Simultaneous nitrification and denitrification with electricity generation in dual-cathode microbial fuel cells. *Journal of Chemical Technology and Biotechnology* 87(1), pp. 153-159.

Zhang, F. and Jacobson, K. S. and Torres, P. and He, Z. 2010. Effects of anolyte recirculation rates and catholytes on electricity generation in a litre-scale upflow microbial fuel cell. *Energy & Environmental Science* 3(9), pp. 1347-1352.

Zhang, J.-N. and Zhao, Q.-L. and Aelterman, P. and You, S.-J. and Jiang, J.-Q. 2008. Electricity generation in a microbial fuel cell with a microbially catalyzed cathode. *Biotechnology letters* 30(10), pp. 1771-1776.

Zhang, L. and Li, C. and Ding, L. and Xu, K. and Ren, H. 2011a. Influences of initial pH on performance and anodic microbes of fed-batch microbial fuel cells. *Journal of Chemical Technology and Biotechnology* 86(9), pp. 1226-1232.

Zhang, T. and Ding, L. and Ren, H. 2009a. Pretreatment of ammonium removal from landfill leachate by chemical precipitation. *Journal of Hazardous Materials* 166(2), pp. 911-915.

Zhang, X. and Cheng, S. and Wang, X. and Huang, X. and Logan, B. E. 2009b. Separator characteristics for increasing performance of microbial fuel cells. *Environmental Science & Technology* 43(21), pp. 8456-8461.

Zhang, X. and He, W. and Ren, L. and Stager, J. and Evans, P. J. and Logan, B. E. 2015. COD removal characteristics in air-cathode microbial fuel cells. *Bioresource technology* 176, pp. 23-31.

Zhang, Y. and Min, B. and Huang, L. and Angelidaki, I. 2011b. Electricity generation and microbial community response to substrate changes in microbial fuel cell. *Bioresource technology* 102(2), pp. 1166-1173.

Zhang, Y. and Noori, J. S. and Angelidaki, I. 2011c. Simultaneous organic carbon, nutrients removal and energy production in a photomicrobial fuel cell (PFC). *Energy & Environmental Science* 4(10), pp. 4340-4346.

Zheng, Z.-m. and Hu, Q.-l. and Hao, J. and Xu, F. and Guo, N.-n. and Sun, Y. and Liu, D.-h. 2008. Statistical optimization of culture conditions for 1, 3-propanediol by Klebsiella pneumoniae AC 15 via central composite design. *Bioresource technology* 99(5), pp. 1052-1056.

Zhi, W. and Ge, Z. and He, Z. and Zhang, H. 2014. Methods for understanding microbial community structures and functions in microbial fuel cells: a review. *Bioresource technology* 171, pp. 461-468.

Zhou, S. and Wu, Y. 2012. Improving the prediction of ammonium nitrogen removal through struvite precipitation. *Environmental Science and Pollution Research* 19(2), pp. 347-360.

Zuo, Y. and Logan, B. 2011. Power generation in MFCs with architectures based on tubular cathodes or fully tubular reactors. *Water Science and Technology* 64(11), pp. 2253-2258.